JOURNAL OF THE

Electrochemical Society

l. 108, No. 5 May 1961

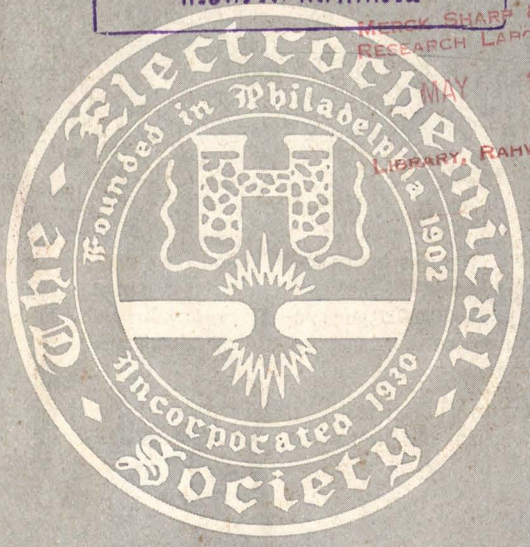

GLC Anodes Are CUSTOM MADE

for

Hooker Chemical Corporation

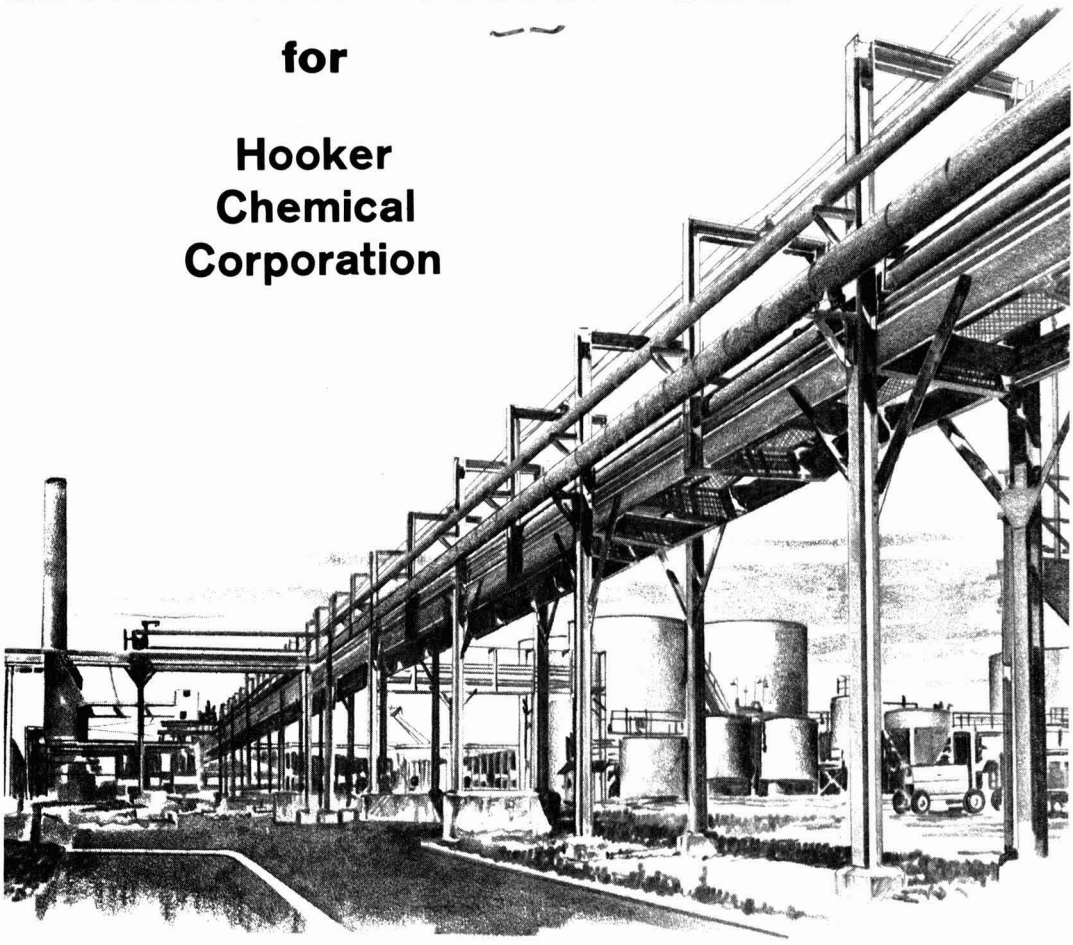

The Hooker Chlor-Alkali Plant at Montague, Mich.

Longer anode life, longer diaphragm life, reduced power consumption and reduced labor costs are the goals of the GLC program of technical exchanges between our engineers and those of our chlor-alkali customers.

GLC anodes now in use are achieving greater records of performance than ever before.

And as a result of our continuing technical exchange program, GLC customers can look forward to still better anode performance in the future.

Are your chlor-alkali operations experiencing the cost-saving advantages of GLC anodes, custom made to your special requirements?

PRODUCTS ELECTRODE GLC DIVISION YOU CAN TRUST ®

GREAT LAKES CARBON CORPORATION

18 EAST 48TH STREET, NEW YORK 17, N.Y. OFFICES IN PRINCIPAL CITIES

Manuscripts submitted to the Journal should be sent, in triplicate, to the Editorial Office at 1860 Broadway, New York 23, N. Y. They should conform to the revised Instructions to Authors, last published on pp. 46C-47C of the March 1961 issue. Manuscripts so submitted become the property of The Electrochemical Society and may not be published elsewhere, in whole or in part, unless permission is requested of and granted by the Editor.

The Electrochemical Society does not maintain a supply of reprints of papers appearing in its Journal. A photoprint copy of any particular paper, however, may be obtained by corresponding directly with the Engineering Societies Library, 29 W. 39 St., New York 18, N. Y.

Inquiries re positive microfilm copies for volumes should be addressed to University Microfilms, Inc., 313 N. First St., Ann Arbor, Mich.

Walter J. Johnson, Inc., 111 Fifth Ave., New York 3, N. Y., have reprint rights of out-of-print volumes of the Journal, and also have available for sale back volumes and single issues, with the exception of the current calendar year. Anyone interested in securing back copies should correspond direct with them.

Journal of the Electrochemical Society

MAY 1961 **VOL. 108 • NO. 5**

CONTENTS

Published monthly by The Electrochemical Society, Inc., from Manchester, N. H., **Executive Offices, Editorial Office** and **Circulation Dept.**, and **Advertising Office** at 1860 Broadway, New York 23, N. Y., combining the JOURNAL and TRANSACTIONS OF THE ELECTROCHEMICAL SOCIETY. Statements and opinions given in articles and papers in the JOURNAL OF THE ELECTROCHEMICAL SOCIETY are those of the contributors, and The Electrochemical Society assumes no responsibility for them. Subscription to members as part of membership service; subscription to nonmembers $24.00. Single copies $1.70 to members, $2.25 to nonmembers. Copyright 1961 by The Electrochemical Society, Inc. Entered as second-class matter at the Post Office at Manchester, N. H., under the act of August 24, 1912.

Editorial

What Are We Teaching Our Students?

RECENTLY a first-year student, with four full weeks of College Chemistry behind him, asked me some serious questions about the table of electronegativities of the elements. How far apart must the numbers be to insure a completely ionic compound? How close together for definite covalent bonding? What about the intermediate compounds? Was hydrogen omitted from the table by an oversight?

At about the same time, my class of juniors and seniors had an examination; one question was to trace the electrical conductance as stronger ammonia is dribbled into weaker copper sulfate solution. Not an easy question to answer in full, but a certain amount of pertinent information was available. There was demonstrated an appalling ignorance of the simple facts which would have made the available information useful.

The fact is that our undergraduate students are bombarded with so much information that many of them only succeed in becoming extremely confused. Recent "elementary" chemistry texts run 750 to 950 pages in length, and, while in general they contain excellent expositions of many phases of the subject, they are really suitable only for the mature, superior student who can grasp principles quickly and assimilate numerous details easily. The authors do not write for the students; they write for the professors. The text must contain as much theory as can be crowded in, at the most advanced level compatible with the author's conscience (one text has a 58-page chapter on Chemical Thermodynamics). If an attempt is made to include, with proper emphasis, a reasonable amount of descriptive chemistry, the book becomes a tome, a reference volume, not a text (the book mentioned above does not contain much systematic descriptive material).

A well-known physicist, a Nobel Prize winner, has told of his experience with college courses. He did not wish to become a chemist, but he saw a golden opportunity to learn a maximum amount of chemistry with a minimum of time and effort. He did not bother with textbooks—there were more important books to read. However, he paid careful attention to everything the professor said, because surely the lectures would cover all the important material. Also, he took good notes, which he studied diligently before the examinations, at the same time appraising carefully the type of questions most likely to be asked. In this way, he says, he could "walk into the examination and get a decent gentleman's grade." To get an *A* would be harder; you must study the professor and his whimseys.

I cannot recommend that students in general follow similar methods, but I do believe that the text should contain not much more than the professor can reasonably lecture about in the allotted time. The student should be able to study leisurely, without a feeling of futility, and he should be stimulated to ask, Where can I find more about this or that? In the great push to train more scientists more quickly, perhaps we actually are discouraging potential scientists. Possibly, superior students can be turned into Ph.D.'s in six years; maybe it is equally important to convince many others that we have something worth studying for eight years, or for a lifetime.

—CVK

NEW BELL LABORATORIES RESEARCH FORESHADOWS COMMUNICATIONS AT OPTICAL FREQUENCIES

A revolutionary new device, the continuously operating Optical Gas Maser, now under investigation at Bell Telephone Laboratories, foreshadows a whole new medium for communications: light.

Light waves vibrate at frequencies tens of millions of times higher than broadcast radio waves. Because of these high frequencies, a beam of light has exciting potentialities for handling enormous amounts of information.

Now for the first time, Bell Laboratories' new Optical Gas Maser continuously generates light waves that are "coherent." That is, the light waves move in phase as seen looking across the beam.

With further research, it is expected that such beams can be made to carry large amounts of information. The beams can be transmitted through long pipes. They can be projected very precisely through space, and might be used for communications between space vehicles.

Research with coherent light is another example of how Bell Laboratories prepares ahead for communications needs.

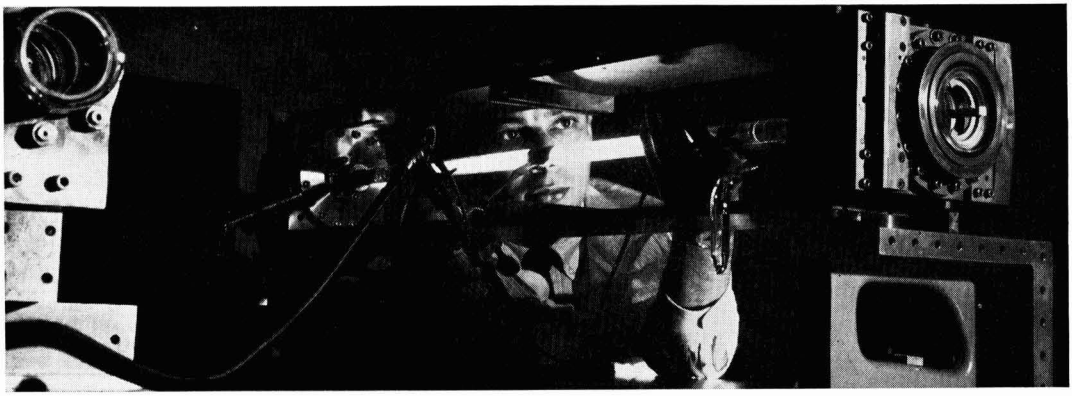

The Optical Gas Maser (above) was first demonstrated at Bell Telephone Laboratories. Heart of unit is a 40-inch tube containing helium and neon. Interaction between gas atoms produces a continuous, coherent beam of infrared light that may one day be used in communications.

BELL TELEPHONE LABORATORIES

WORLD CENTER OF COMMUNICATIONS RESEARCH AND DEVELOPMENT

A new idea in plating

ANACONDA

announces

"PLUS-4"

phosphorized copper anodes

in a new form

CURVED ANODES

for plating cylinders faster and more uniformly

To make anode surfaces parallel the rotogravure cylinder being plated, and to fit the curve of the current-carrying slings, Anaconda "Plus-4" phosphorized copper anodes are now extruded to precisely curved shapes.

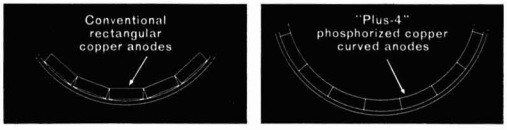

This design gives both cost savings and improved cylinder quality:

1. A more evenly plated cylinder. Because the distance between the cylinder and the anode surface is more uniform, the copper deposit is smoother and more uniform.

2. Finishing operations in most cases are reduced, as much as 50%, because of the uniform copper deposit.

3. Less scrap because anodes corrode more evenly.

4. Improved electrical efficiency and faster plating because of better contact with sling.

For more information, write: Anaconda American Brass Company, Waterbury 20, Conn. In Canada: Anaconda American Brass Ltd., New Toronto, Ont.

60107 L

Note: When you request information, please specify inside radius of anode.

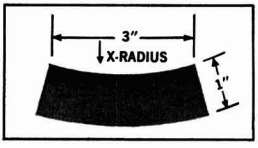

"PLUS-4"® phosphorized copper anodes

products of

ANACONDA®

Anaconda American Brass Company

The Silver-Silver Oxide Electrode

I. Anodic Oxidation in Alkaline Solutions

Charles P. Wales

U. S. Naval Research Laboratory, Washington, D. C.

ABSTRACT

Silver electrodes were oxidized anodically at 25°C in 35 or 50% KOH at constant charge currents that ranged from the ½ to 40 hr rates. The electrodes were given both partial and complete charges. Except at a low charging rate the capacity was higher in 35% KOH than at 50% KOH. Oxidation was highly efficient at the first two potential plateaus. During a charge at the Ag_2O/AgO plateau initially Ag_2O oxidizes to AgO and then the prevailing reaction is Ag oxidizing to AgO. Simultaneously some AgO reacts with Ag to give Ag_2O. Under certain discharge conditions AgO may reduce directly to Ag, with Ag_2O forming as a secondary product.

The silver oxide electrode has proved to be a useful electrode at high rates of discharge current, especially when coupled with Zn in a Ag-Zn battery. As more reliable Ag-Zn batteries have become available in recent years, they have been put to increasingly wider uses for special purposes requiring light weight or the ability to discharge at high rates. Experience has shown, however, that the Ag electrode is not charged easily, except at relatively low rates of current. The manufacturers usually specify a 12 to 24 hr rate of charge for commercial Ag-Zn batteries, which contain a 30-45% KOH solution as the electrolyte.

Published reports that give appreciable data on the charging of Ag electrodes usually indicate that the electrodes decreased continually in capacity, and thus results were not reproducible (1-3). While there have been many tests on Ag-Zn storage batteries, the results are not widely available and often have not clearly differentiated between effects taking place at the Ag electrode and those at the Zn electrode.

For these reasons there is need for an over-all study of the effect of charge rates and electrolyte concentration on the anodic oxidation of Ag. It is proposed to study the chargeability of the Ag electrode under various rates of current, electrolyte concentrations, and temperatures. An attempt will be made to determine the cause of these variations in chargeability and to find a method of improving the charge characteristics.

Experimental Procedure

The Ag electrodes were made by cutting in half Ag plates taken from a commercial Ag-Zn storage battery. The test electrodes measured about 28 x 66.5 x 0.7 mm and had a capacity of about 1.7 amp-hr. Each electrode was wrapped in several layers of the separator material normally used in Ag-Zn batteries. These electrodes served as both positive and negative electrodes and were assembled in pairs in closed plastic containers with an excess of electrolyte, together with a Ag, Ag_2O/OH^- reference electrode. The instrumentation and techniques previously described were used to control the charge and discharge current (4). A stabilized vacuum tube voltmeter having a 22-megohm input resistance was used as an aid in continuously recording potentials without drawing appreciable current from the cell or reference electrode. A simpler type of vacuum tube voltmeter, also having a 22-megohm input resistance, powered the current-sensitive relay used as the voltage cutoff for the discharge.

The basic charge rate was chosen arbitrarily to be 100 ma. The characteristics of a silver electrode were determined first at 100 ma in 35% KOH and then the charge rate was increased by doubling until the capacity was reduced appreciably. Other electrodes were put in 50% KOH after the initial cycling in 35% KOH. The cells were given both partial and complete charges at each of the charge rates and were always discharged at 100 ma (the 15 to 18 hr rate) to −300 mv without any appreciable open-circuit period. A few charges were made at 50 ma (the 40-hr rate), but this rate was not studied in detail due to the excessive length of time required for a cycle. All work was done at 25°C. It is proposed to study 20 and 5% KOH in the future, as well as temperatures of 50°, 0°, and −25°C.

Results and Discussion

The capacity decreased as the charge rates were increased (Fig. 1). The electrode capacity was pro-

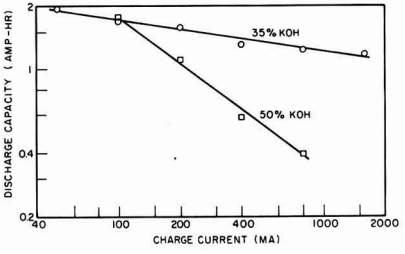

Fig. 1. Dependence of discharge capacity on charging current

portional to a negative exponential function of the charge current in the range of current that was studied. Kinoshita reported a similar result for charges at the 0.9-4.8 hr rates in 20% KOH, but at the 7-16 hr charge rates he found the capacity was less than would be expected from this exponential relationship (2). This may have been due to relatively large amounts of active material going into solution under his experimental conditions during the longer charge periods.

The capacity decreased much more rapidly in 50% KOH than in 35% KOH, indicating that the electrolyte concentration affects the charge acceptance. Dirkse and De Vries reported that the anodic formation of both Ag_2O and AgO have the same dependence on hydroxyl ion concentration in KOH (5). According to the mechanism for the formation of silver oxides proposed by Dirkse, the mobility of the OH^- ions is an important factor (6). Therefore as either the current density or KOH concentration is increased, a point may be reached at which the amount of oxide that can form before gassing takes place will be decreased, since these conditions impair the mobility of the OH^- ion.

The charge efficiency did not drop off at the higher rates of current (Table I). This table includes all complete cycles that did not reach gassing and in which there were no periods of stand between charge and discharge. Very short charges tended to give over 100% efficiency, probably due to the fact that after a cell is discharged to the endpoint a short additional discharge can be obtained after a stand period. For this reason, and since slight errors in measuring time affect the calculated efficiencies of short charges more than longer ones, the efficiencies calculated for the longer charges are believed to be more accurate. Therefore the arithmetic mean of the efficiencies weighted by the length of charge gives a more representative average than the simple arithmetic mean.

It has been reported that the charge efficiency is low at the AgO/Ag_2O potential plateau, at least under certain conditions (7, 8). In the present work there was no indication of a decrease in efficiency

Table I. Efficiency of charge-discharge cycles in 35% and 50% KOH at 25° using various rates of charge current and ending the charge before the potential rises to the gassing point

Charge rate, ma	No. of cycles	Efficiency, % Arithmetic mean	Efficiency, % Weighted* arithmetic mean
	35% KOH		
100	44	99.8	99.7
200	23	100.0	100.0
400	13	100.3	100.1
800	19	101.2	101.0
1600	11	100.8	99.8
	50% KOH		
100	30	99.6	99.7
200	14	100.4	100.3
400	12	100.1	100.2
800	9	100.5	100.5

* Weighted by the length of charge.

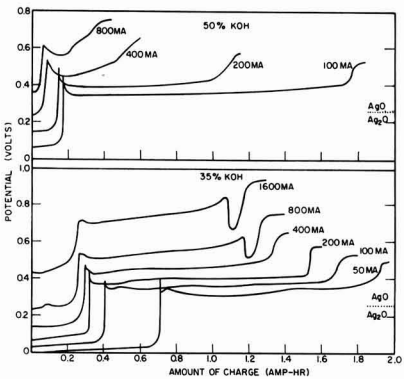

Fig. 2. Typical constant current charges in 50% and 35% KOH at 25°C. Potentials are given with respect to a Ag/Ag_2O reference electrode.

at this plateau near the end of the charge with the possible exception of the 1600 ma charge rate in 35% KOH. Even here the worst efficiency of any individual cycle among the 11 cycles that were believed to have been stopped short of gassing was 98.5%.

Charge Characteristics of the Electrodes

Varying the charge current gave a family of charge curves (Fig. 2). This clearly shows why low, time-consuming charge rates are used in Ag-Zn batteries, even though it would be much more convenient to shorten the charging time. When the cell was charged in 35% KOH at high rates (2 hr or less for a full charge) the potential often dropped just as gassing was reached. This is probably due to a temporary breaking open of the oxide layer which was preventing the remainder of the silver from being oxidized. Stresses may be set up as a result of fast formation of the film or layer due to the high current, and then be relieved by cracking. At the lower charging rates there is more time for both diffusion of the electrolyte into the electrodes, and reaction of the divalent Ag with metallic Ag according to

$$AgO + Ag \rightarrow Ag_2O \qquad [1]$$

Since the electrode is oxidized more completely before the barrier layers are formed, the lower charging rates are more effective.

After steady gassing was reached at the higher currents, the potential often fluctuated over a range of a few millivolts. Potential fluctuations could result from several causes: breaking of the surface film, varying O_2 pressure, and change of effective surface area due to the gas mechanically covering part of the surface. Relatively little additional charge was accepted at the gassing plateau, except at the higher charge rates where the electrodes normally had low capacity.

Charging became increasingly difficult at the higher currents in the more concentrated KOH solution and the potential tended to lack the sharp rise to the final gassing plateau. The electrode could be given a much greater total charge when stands were

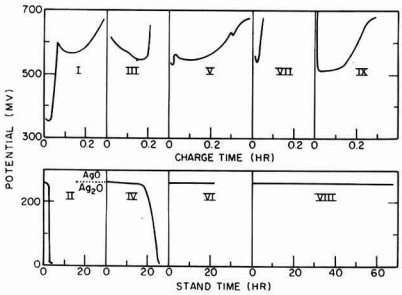

Fig. 3. Effect of stand periods on an 800-ma charge in 50% KOH at 25°C. The Roman numerals indicate the order in which periods of stand or charge took place. Potentials are given with respect to a Ag/Ag_2O reference electrode.

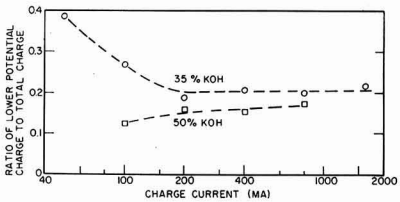

Fig. 4. Relationship between charging current and the portion of a charge that took place at the Ag/Ag_2O plateau.

interspersed between periods of high-rate charges. Figure 3 shows an electrode accepting about three times the normal 800-ma charge. The following discharge gave 95.8% of this charge, indicating that some gassing occurred at the higher potentials. This rapid charging rate combined with lowered ionic mobility due to concentrated KOH only allows the Ag which is near the surface to charge to AgO. This AgO reacts according to Eq. [1] during a stand, and at the same time the electrolyte within the plate has an opportunity to come to equilibrium with the bulk of the electrolyte in the cell. Stands in which the potential fell to the Ag_2O/Ag plateau (*i.e.*, in which all or almost all AgO had reacted) were much more effective in promoting further charging than were stands which remained at the AgO/Ag_2O level. It is interesting to note that the charge acceptance of charge V (Fig. 3) was greater than that of the initial charge. Perhaps the deeper formation of Ag_2O, which is assumed to take place during the stands, is accompanied with an opening of better electrolyte paths into the interior of the electrode.

The chargeability of these Ag electrodes varied from cycle to cycle, and is similar to the erratic performance often observed in Ag-Zn storage batteries (9). It was noted that when the lower potential plateau of a charge is shorter than normal, the total charge probably will also be shorter. This makes it possible to predict how much of a charge the cell is going to accept. When a cell was allowed to stand discharged for two or more days the next charge was usually either very long or very short at the lower plateau; seldom was it of average length. Apparently the initial condition of the electrode surface is a controlling factor in determining the charge acceptance. The effect of porosity or surface of the plate seems to be important and merits further study.

The portion of a charge which took place at the Ag/Ag_2O potential plateau varied with current density (Fig. 4). The ratio remained at about 0.20 from 200 to 1600 ma in 35% KOH, although it was higher at lower currents. The ratio seemed to increase with current in 50% KOH, but considering the variation between individual charges it is possible that this ratio was steady at about 0.17 in the 200 to 800 ma range of current. The fact that the portion of a charge occurring at the Ag/Ag_2O potential is lower in 50% KOH than it is in 35% KOH suggests that the electrolyte enters the reaction differently when Ag_2O is forming than it does when AgO forms. Dirkse however reported more Ag converted to Ag_2O in 42% KOH than in 8% KOH (6).

The charge length at the lower potential tended to increase with repeated cycling at any given current in 35% KOH, but decreased with cycling in 50% KOH. This probably resulted from changes in plate capacity since the capacity tended to decline in 50% KOH with cycling and to increase in 35% KOH. For example one plate in 35% KOH gained 25% in capacity after 111 cycles, while another plate in 50% KOH had lost 29% of its original capacity after 116 cycles. Replacing older KOH solutions with fresh ones had no noticeable effect on the length of the lower charge plateaus. Although doubling the charge current always decreased the electrode capacity, it was normal for the capacity to increase during the first 10-15 cycles at any given rate of charge in 35% KOH (but not in 50% KOH) with the largest increases occurring at the higher charge currents. As a result, capacity losses at the higher charge rates were not as large as they first appeared to be. André reported a somewhat similar effect: Ag electrodes seem to acquire a greater activity when used at high discharge rates (10). This may be due to the roughness of the electrode surface changing under different operating conditions.

Considerable interest has been expressed in the potential peak which occurs on charge when going from the Ag/Ag_2O to Ag_2O/AgO plateaus. It was reported by Hickling and Taylor that this peak corresponds to formation of an unstable higher oxide (11), but later work seems unanimously opposed to this view (8, 12-14). Jones, *et al.*, attributed the peak to the difficulty in forming AgO nuclei in the Ag_2O lattice (8). Dirkse and Werkema suggested that difficulty in nucleation does not explain the peak sometimes observed during a discharge and interpreted both peaks as being due to resistance of the Ag_2O layer (12). Cahan, *et al.*, measured the resistance during oxidation and reduction and showed that the peak was much higher than would be produced by resistance (14). They state that the charge peak is due to passivation, forcing the currents to small areas and producing a high overvoltage. Göhr and Lange report that most of the current in the formation of Ag_2O takes place by the tranference of the Ag^+ ion through the Ag_2O layer (15). They noted that usually the electrical conductivity of ions does

not obey Ohm's law, but instead there is an exponential relationship between current and voltage E. With a constant applied E the effective E drops as the Ag_2O layer thickens, with current dropping more rapidly. If one applies this reasoning to constant current conditions, instead of constant E, it can be seen that E must rise sharply to maintain a constant current. It was reported by Vidovich, *et al.*, that the high resistance found in this period probably characterizes one of the stages in the $Ag \rightarrow Ag_2O$ process, perhaps electrochemical adsorption of O on the Ag surface (16).

This peak is less pronounced at the higher rates of charge and has greater apparent ampere-hour capacity in the the more concentrated KOH (Fig. 2). Under higher current densities, less Ag_2O forms on the electrode surface before the AgO/Ag_2O plateau is reached, and resistance is lower so little or no peak would be expected if the peak were due to ohmic resistance. However the results shown, particularly in 50% KOH, indicate that polarization is the likely cause as suggested by Cahan, *et al.* (14). Ag_2O may continue to form on the surface for a time at the higher currents, either directly from anodic oxidation of Ag or from reaction [1], thus causing a longer but less sharp potential peak.

Reduction of the Electrodes

The discharge became shorter as the rate of the preceding charge increased, especially in 50% KOH, since the electrodes did not charge well at high rates of current (Fig. 5). The potentials of both plateaus were lower in 50% KOH than in 35% KOH. The Ag_2O/Ag plateau had a tendency to be 5-10 mv more negative during discharges that followed complete or nearly complete low-rate charges. This was due probably to decreased conductivity after most of the metallic Ag was oxidized. At the beginning of this plateau the potential normally reached a minimum value about 5-7 mv below the plateau, although this minimum usually was lacking after high-rate charges in 50% KOH when there would be less polarization since there was less charged active material. After an incomplete charge with all of the charge below the AgO/Ag_2O potential, the discharge often began at the minimum value and then increased.

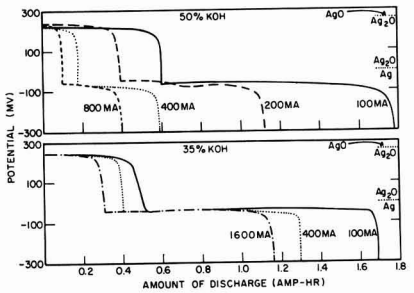

Fig. 5. Typical 100-ma discharges in 50% and 35% KOH at 25°C following charges to gas evolution at various rates. Numbers on curves give the charging current. Potentials are given with respect to a Ag/Ag_2O reference electrode.

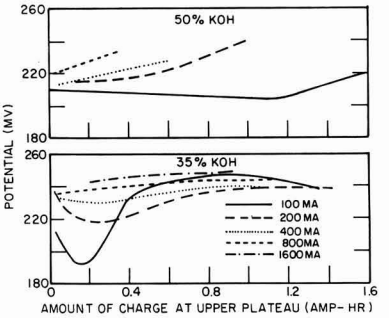

Fig. 6. Dependence of initial discharge potential on the amount of charge at the upper potential plateau. Potentials were measured after 0.01 hr of 100-ma discharge and are given with respect to a Ag/Ag_2O reference electrode. Individual measurements are not shown.

The potentials measured at 0.01 hr of discharge exhibited the AgO/Ag_2O potential after the electrodes were given only a short charge above this potential (Fig. 6). Figure 6 omits the 187 individual measurements, but shows curves that seemed to fit these measurements. The average deviation of the measurements from these curves was 3.3 mv. Two factors that may increase these potentials are the decreased electrode resistance as the amount of Ag_2O decreases, and the decreased current density on the AgO as the quantity of AgO increases. Opposing these is the increased resistance as the metallic Ag is oxidized. The minimums in the curves of Fig. 6 for 35% KOH at the lower charging currents may be due to consumption of AgO according to reaction [1]. This reaction may not take place readily after only small amounts of AgO are formed, if the initial AgO formation is surrounded by Ag_2O, but the lower charging rates allow more time for reaction [1] to take place.

The AgO/Ag_2O potential portion of a discharge curve often showed signs of an intermediate potential plateau when an electrode was only partially charged before the discharge (Fig. 7). In Fig. 7, 100% is defined as the average capacity obtained from the electrode after it was charged to gassing at a particular charge rate. The intermediate potential plateau was rare after the higher rates of charge, but occurred often when the cells were charged partially at the lower rates. For example, the intermediate potential level almost always was observed in 35% KOH during a discharge after a partial charge at 100 ma. With 200 ma charges this level usually was found when an electrode was 50-90% charged, but at 400 ma this level seldom was found, although there were some indications of it when an electrode was 70-90% charged. This intermediate level often was found when an electrode was 60-90% charged in 50% KOH with 100-ma partial charges, and on several occasions after the electrode was about 90% charged all of the higher discharge plateau took place at this intermediate potential.

This intermediate plateau indicates that the generally accepted theory of AgO reducing first to Ag_2O,

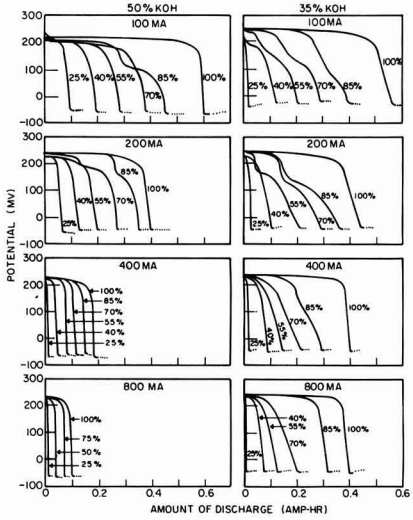

Fig. 7. Upper potential portion of 100-ma discharges following constant current charges of various lengths. Percentage values give charge lengths, where a charge that reaches gassing is defined as 100% at a particular rate. Potentials are given with respect to a Ag/Ag_2O reference electrode.

and then Ag_2O reducing to Ag, may not represent the entire picture of the discharge reactions. It may be that AgO also can discharge directly to Ag, in a reaction something like

$$AgO + H_2O + 2\,e \rightarrow Ag + 2\,OH^- \qquad [2]$$

Reaction [1] would be expected to take place simultaneously. The calculated potential for reaction [2] is midway between the equilibrium potentials of the lower and higher oxides and would be at 131 mv on the scale used in Fig. 7 if one assumes unit activity. However Ag would not be expected to have an activity of one under these conditions, since the little Ag forming this way may react with AgO very rapidly, perhaps even before the Ag can form into a crystal lattice.

Oxidation of the Electrodes

There is an almost linear dependence between the amount of discharge capacity that is obtained at the upper potential plateau following an incomplete charge and the amount of charge at this plateau (Fig. 8). The results of charges at 200 and 400 ma resembled the 100-ma curve of Fig. 8, and 800-ma charges were intermediate between the 100 and 1600 ma curves. These curves tend to become linear after

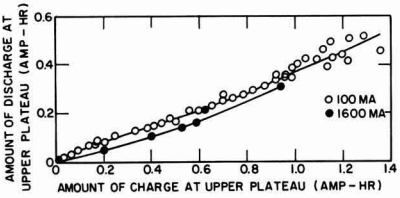

Fig. 8. Comparison of the amount of charge and discharge at the Ag_2O/AgO plateau in 35% KOH at 25°C.

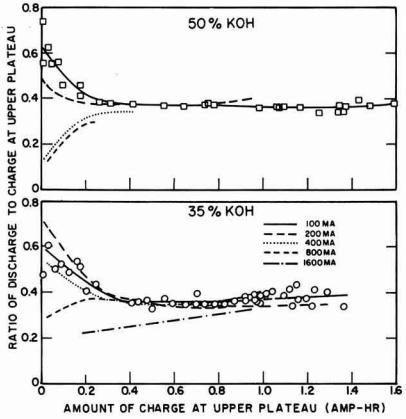

Fig. 9. Relationship between the amount of charge and the ratio (amount of discharge)/(amount of charge) at the Ag_2/AgO plateau. For clarity individual points are shown only for the 100-ma curves.

0.10-0.15 amp-hr of charge and may rise slightly near the end. The results in 50% KOH were more linear, but still quite similar to these shown in Fig. 8.

The ratio of the amount of discharge at the upper potential plateau to the amount of charge at this plateau is approximately the same as the slope of the curves in Fig. 8. If this ratio is plotted against the amount of charge, it can be seen more clearly that the curves of Fig. 8 are not linear (Fig. 9). The ratio is comparatively large initially at the lower charging currents and then it decreases; at high charge currents the ratio increases. Since the upper potential plateau is reached when the electrode is covered with Ag_2O, but still has much Ag in the interior, the initial charging reaction at this plateau is probably

$$Ag_2O + 2\,OH^- \rightarrow 2AgO + H_2O + 2\,e \qquad [3]$$

and a ratio of 1.0 would be expected for electrodes charged only a short time at this plateau, but this high a ratio was never found. After most or all of the Ag_2O is oxidized to AgO, a second reaction, probably the reverse of Eq. [2], takes over (13). This is a 2-electron reaction per atom of Ag, and therefore a ratio of 0.5 would describe it, but the measured ratio was always less than 0.5 when this 2-electron reaction was supposed to be occurring. There is also the possibility of a third reaction, some higher oxide which might be able to form, but there was no indication of this. Much of the evidence reported for an oxidation state of Ag higher than +2 can be interpreted in other ways, and if higher valence Ag does exist, it has little significance in alkaline batteries (9, 13, 17).

It is believed that reaction [3] takes place initially on Ag electrodes at the second charge plateau, and then the reverse of reaction [2]. The fact that the initial ratio at low charging currents is about twice as large at the later ratios (Fig. 9) is an indication of changing from a 1-electron to a 2-electron reaction. Another reaction seems to take place simultaneously, with the result that 20-30% of the AgO

does not appear during a discharge judging by the amount of discharge at potentials above the Ag_2O/Ag plateau, although there is no loss in the total amp-hr capacity. This probably is due mainly to reaction [1] taking place both during the charge and during the discharge. It is known that Ag and AgO can react in Ag electrodes (3, 13, 18), but it was thought to be a slow reaction under the conditions found here. However Cahan, *et al.*, report that this reaction should proceed rapidly, since the oxidation of Ag and reduction of AgO are both fast reactions (14). The rise in the ratio curves of Fig. 9 as the electrode nears a full charge may be due to a comparative lack of Ag available for [1].

The low ratios found initially at the higher currents may be due to some Ag still charging to Ag_2O when the electrode is first polarized to the AgO potential plateau. In addition reaction [1] will take place more readily with high rate charges, since more Ag will remain in the electrode and the Ag_2O layer will be thinner and less concentrated. On the other hand there would be less time for this reaction at the higher charge rates. In addition there is little sign of a decrease in this reaction rate as the amount of Ag that is present decreases. These are both indications that reaction [1] is fairly rapid. Perhaps the surface of a silver particle becomes AgO, which then reacts with the inner Ag. The resulting Ag_2O layer separates the Ag from the outer AgO layer. This AgO may prevent the Ag_2O from contacting the electrolyte, thus making further oxidation more difficult. If such a layer does form it is doubtful whether much of the remaining Ag would be oxidized. Since Ag would not be in contact with the electrolyte, unless cracks form in the layers, further charging would be restricted to ionic conduction of Ag^+ or $O^=$ through the solid lattice. This relatively slow process is probably efficient only at very low rates of current.

Conclusions

The capacity of the Ag electrodes decreased proportionally to a negative exponential function of charge current, with the decrease greater in 50% KOH than in 35% KOH. Although the capacity gradually declined with cycling in 50% KOH, it increased in 35% KOH, indicating that short cycle life is not necessarily a basic characteristic of Ag electrodes. Even at high rates of current the electrode charged with about 100% efficiency at the first two potential plateaus. The electrode accepted a greater total charge at the higher current densities when periods of charge alternated with open-circuit stands of sufficient length to allow much of the AgO to react with Ag. Variations in chargeability were an effect of surface condition.

When conditions are suitable AgO may reduce directly to Ag with Ag_2O being formed as a secondary product from the reaction between AgO and Ag. The main charge reaction at the Ag_2O/AgO plateau initially is Ag_2O oxidizing to AgO. Then the prevailing reaction changes to Ag oxidizing to AgO. Simultaneously with both of these reactions, part of the AgO that is formed reacts with Ag to give Ag_2O.

Manuscript received Sept. 12, 1960. This paper was prepared for delivery before the Houston Meeting, Oct. 9-13, 1960.

Any discussion of this paper will appear in a Discussion Section to be published in the December 1961 JOURNAL.

REFERENCES

1. F. Jirsa, *Z. Elektrochem.*, **33**, 129 (1927).
2. K. Kinoshita, *Bull. Chem. Soc. Japan*, **12**, 366 (1937).
3. I. A. Denison, *Trans. Electrochem. Soc.*, **90**, 387 (1946).
4. G. W. Work and C. P. Wales, *This Journal*, **104**, 67 (1957).
5. T. P. Dirkse and D. B. DeVries, *J. Phys. Chem.*, **63**, 107 (1959).
6. T. P. Dirkse, *This Journal*, **106**, 920 (1959).
7. A. P. Rollet, *Ann. Chim.*, (10) **13**, 137(1930).
8. P. Jones, H. R. Thirsk, and W. F. K. Wynne-Jones, *Trans. Faraday Soc.*, **52**, 1003 (1956).
9. C. P. Wales, NRL Report 5167, Aug. 11, 1958, Naval Research Laboratory, Washington, D. C.
10. H. G. André, *Bull. Soc. franc. élec.*, **1**, 132 (1941).
11. A. Hickling and D. Taylor, *Discussions Faraday Soc.*, No. 1, 277 (1947).
12. T. P. Dirkse and G. J. Werkema, *This Journal*, **106**, 88 (1959).
13. C. P. Wales and J. Burbank, *ibid.*, **106**, 885 (1959).
14. B. D. Cahan, J. B. Ockerman, R. F. Amlie, and P. Rüetschi, *ibid.*, **107**, 725 (1960).
15. H. Göhr and E. Lange, *Z. Phys. Chem.* (N. F.), **17**, 100 (1958).
16. G. L. Vidovich, D. I. Leikis, and B. N. Kabanov, *Doklady Akad. Nauk SSSR*, **124**, 855 (1959).
17. T. P. Dirkse, *This Journal*, **106**, 453 (1959).
18. T. P. Dirkse and B. Wiers, *ibid.*, **106**, 284 (1959).

Brief Communications

The JOURNAL accepts short technical reports having unusual importance or timely interest, where speed of publication is a consideration. The communication may summarize results of important research justifying announcement before such time as a more detailed manuscript can be published. Consideration also will be given to reports of significant unfinished research which the author cannot pursue further, but the results of which are of potential use to others. Comments on papers already published in the JOURNAL should be reserved for the Discussion Section published biannually.

Submit communications in triplicate, typewritten double-spaced, to the Editor, Journal of The Electrochemical Society, 1860 Broadway, New York 23, N. Y.

Some Important Factors That Influence the Composition of the Positive Plate Material in the Lead-Acid Battery

Vance H. Dodson[1]

The Electric Autolite Company, Toledo, Ohio

ABSTRACT

The composition of positive plate material formed (*a*) from positive pastes of various densities, (*b*) in aqueous sulfuric acid solutions of various specific gravities, (*c*) at various rates (current densities), and (*d*) at various temperatures has been studied. Variations in these conditions not only influence the total PbO_2 content of the formed material, but also the ratio of α-PbO_2 to β-PbO_2 in the formed material. The presence of α-PbO_2 in the positive plate material is attributed to the pH of the electrolyte within the paste during its development. A method for estimating the amounts of α -PbO_2 and β-PbO_2 in mixtures of the two is also described.

Lead-acid battery manufacturers are very much aware of the fact that the composition of formed positive plate material can vary from one batch to another, from one day to another, and from one plant to another. The differences in composition may be only minor in some cases, but in other instances they may be quite significant. While a multitude of factors can influence the composition of the developed positive material, only those which have been found to exert a major influence are discussed in this paper.

The lead dioxide formed in the positive plate is a mixture of two crystallographic modifications of PbO_2, α-PbO_2 and β-PbO_2 (1-6). Evidence has been presented in these earlier works which indicates that α-PbO_2 is formed by the direct oxidation of metallic lead above the $PbO_2/PbSO_4$ potential, and that β-PbO_2 is formed from $PbSO_4$ at the $PbO_2/PbSO_4$ potential. Most of the earlier studies of α-PbO_2 were carried out by anodizing pure lead and certain of its alloys in aqueous sulfuric acid at various potentials. Very little work has been reported in which these findings are related to actual battery plate manufacture. The influence of several manufacturing variables, such as positive paste density, developing acid concentration, rate of electroformation, and temperature of electroformation on the total PbO_2, α-PbO_2, and β-PbO_2 content of the positive plate material is reported in this paper.

Experimental

The positive pastes described in this work were prepared by blending a mixture of 70% lead oxide and 30% lead with water and sulfuric acid in a Baker-Perkins mixer. The density of the pastes was measured by the method of Dittmann and Harner after the pastes had been applied to the supporting grid and cured (7). All of the pastes were cured at room temperature, or slightly above, during which time most of the free water was lost by evaporation and most of the free lead in the paste was converted to lead oxide. After curing, the pastes contained 3-5% free lead.

All of the positive plate samples were thoroughly washed in water and dried at 110°C in a vacuum oven prior to their chemical analysis. The total per cent PbO_2 was determined iodometrically (8). The relative amounts of α-PbO_2 and β-PbO_2 were determined by x-ray diffraction. Three diffraction lines were chosen for analytical purposes, the 3.49 and the 2.79 lines of β-PbO_2 and the 2.61 line of α-PbO_2. A plot of the ratio of the average intensities of the first two lines to the intensity of the third *vs.* the composition of standard mixtures of pure α-PbO_2 and β-PbO_2, which approximates a straight line on a semi-log scale, was used as a yardstick for estimating the composition of the mixtures of the two dioxides prepared in this work (Fig. 1). This method gave reproducible results, within 5%, in repeated analyses of the standard mixtures and of the various samples of positive plate material. Each sample of positive material was thoroughly digested in ammonium acetate solution, washed with hot water, and vacuum dried at 110°C before being subjected to x-ray diffraction analysis. A Norelco x-ray diffraction unit equipped with a goniometer, Geiger counter, and recorder was used in this investigation. Copper K-alpha radiation was used in all of the analyses.

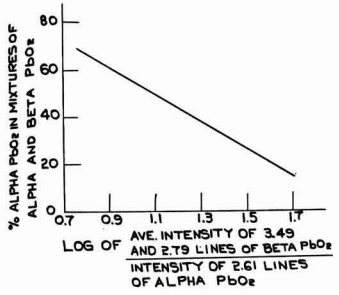

Fig. 1. X-ray diffraction data for mixtures of α- and β-PbO_2

[1] Present address: Dewey and Almy Chemical Division, W. R. Grace Co., Cambridge, Massachusetts.

The pure α-PbO_2 used in the standard mixtures was prepared by electrolyzing 2*N* solutions of sodium hydroxide saturated with lead oxide. Platinum electrodes and current densities in the range 0.8-1.6 ma/cm^2 were employed. The anodic deposits were washed successively with water, hot saturated solution of ammonium acetate and water, then vacuum dried at 110°C. The x-ray diffraction patterns of all of the preparations were in good agreement with those given in the literature for α-PbO_2 (5, 9). The pure β-PbO_2 used in the standard mixtures was Fisher Certified Reagent β-PbO_2.

The various aqueous solutions of sulfuric acid were prepared from commercial grade sulfuric acid whose specific gravity was 1.400. The concentrations of the acid solutions are expressed in terms of specific gravity, and these values have been corrected to 27°C.

The positive pastes were applied by hand pasting to 7% antimonial lead alloy grids, and the positive plates were then assembled into standard battery elements. Negative plates, chosen from the same production lot and containing negative paste of the same dry density, and resin coated cotton linter separators were used in the construction of the elements. Each element was formed in a one-cell battery container in a constant temperature bath. Positive plate potentials were measured against cadmium during electroformation. A pulsating, 60-cycle, current technique was employed in the measurements to eliminate the *IR* drop component of the positive plate potential (10). Unless otherwise stated, each of the cells was allowed to stand in its developing electrolyte for a period of 2 hr then subjected to 200 amp-hr of electroformation. The electroformation current density values cited in this work are based on the apparent surface area of the positive plates in the test cells.

Results and Discussion

Influence of positive paste density.—The composition of positive material formed from pastes of nine different densities is shown in Table I. The per cent α-PbO_2 in the positive plate material increases as the density of the positive paste increases. The density of the paste was raised by increasing the ratio of water to acid in the paste formula and lowered by decreasing that ratio. Therefore, as the density of the paste is increased, the amount of lead oxide in the paste either free or combined as one of the basic lead sulfates increases. Data in Table I indicate that there is a direct relationship between the amount of α-PbO_2 formed in the positive material and the amount of lead oxide in the cured positive paste.

Table I. Composition of positive material formed from pastes of several densities at 60°C, 7.2 ma/cm^2 current density and in 1.135 specific gravity electrolyte

Test Cell No.	Density of positive paste, g/cc	Composition of positive active material Total % PbO_2	% α-PbO_2	% β-PbO_2
1	3.81	93.1	17.5	75.6
2	3.98	90.5	23.0	67.5
3	4.08	90.5	29.5	61.0
4	4.13	88.7	34.5	54.2
5	4.18	89.2	32.5	56.7
6	4.23	86.2	37.0	49.2
7	4.28	86.8	39.0	47.8
8	4.56	84.5	49.5	35.0
9	4.60	84.5	55.5	29.0

In this study positive plate materials containing up to 55% α-PbO_2 were prepared from pastes having only 2-5% free lead. Positive material containing up to 70% α-PbO_2 has been prepared from similar pastes in other experiments. It is difficult to imagine that such large amounts of α-PbO_2 could originate from the pure lead either in the paste or in the grid. It has been suggested that small crystals of α-PbO_2 which form from free lead in the grid metal and/or the paste act as nuclei on which more α-PbO_2 can form (6). There are two arguments against this concept. First, if this nucleation is an important factor, then it is reasonable to expect that all positive pastes, regardless of density, would produce a positive material of about the same α-PbO_2 content. Second, if free lead must be converted to α-PbO_2 which then acts as nuclei for further formation of α-PbO_2, then α-PbO_2 would not start to appear in the positive plate material until late in the developing process when the potential of the positive plate had risen above the $PbO_2/PbSO_4$ potential. Evidence will be presented later in this paper which shows that the major portion of the α-PbO_2 found in the positive plate is formed during the early stages of development.

The total per cent PbO_2 in the positive material decreases as the density of the positive paste is increased. The number of ampere-hours of electroformation employed in this work was in sufficient excess so that any increase in weight of positive paste per cell with increase in paste density should not have influenced the total percentage of PbO_2 that was formed. The amounts of $PbSO_4$ found in the positive material formed from the paste of the lowest density and from the paste of the highest density were essentially the same. Neither α-PbO_2 nor β-PbO_2, as they are formed in the positive plate, are stoichiometric dioxides, and α-PbO_2 contains less oxygen than β-PbO_2. The calculated formula for α-PbO_2 found in forty different dry charged positive plate materials averages $PbO_{1.85}$ (11). Because of its lower oxygen content, positive material rich in α-PbO_2 would exhibit a lower total per cent PbO_2 by virtue of the method of analysis used in this work.

Influence of the initial concentration of the developing acid.—The composition of positive material formed from pastes of three densities in electrolyte of three different initial specific gravities is shown in Table II. The amount of α-PbO_2 in the positive material formed from a paste of a given density decreases as the initial specific gravity of the developing electrolyte increases. As the density of the paste is decreased, the amount of α-PbO_2 formed in the positive material decreases at all three specific gravity levels. These relationships can be accounted for if it is assumed that the lead oxide in the paste is in some way responsible for the major portion of the α-PbO_2 found in the positive material. The

Table II. α-PbO_2 content of positive material formed from pastes of different densities in electrolyte of different specific gravities at 60°C and 5.7 ma/cm² current density

Test Cell No.	Density of positive paste, g/cc	Initial sp gr of electrolyte	% α-PbO_2 in positive active material
10	4.15	1.100	40.0
11	4.15	1.150	25.0
12	4.15	1.250	9.0
13	4.46	1.100	48.0
14	4.46	1.150	33.0
15	4.46	1.250	20.0
16	4.88	1.100	54.0
17	4.88	1.150	40.0
18	4.88	1.250	30.0

amount of lead oxide, both as free oxide and as combined oxide in the basic lead sulfates, in the positive paste can be estimated from the amount and composition of the original paste ingredients. In the electrolyte whose specific gravity is 1.250 (Table II, test cell No. 18) there is sufficient sulfuric acid present in the cell to convert about three-fourths of the lead oxide to lead sulfate prior to electroformation. In the electrolyte whose specific gravity is 1.100 (Table II, test cell No. 16) there is only enough acid in the cell to convert about one-third of the lead oxide in the paste to lead sulfate prior to electroformation.

The total per cent PbO_2 in the positive materials formed from paste of the same density but in electrolyte of different specific gravities does not vary appreciably over the range of specific gravities studied here. However, the amount of $PbSO_4$ found in the positive materials increases as the initial specific gravity of the developing electrolyte is increased.

Influence of electroformation rate.—Positive paste of a fixed density (3.91 g/cc) was formed at three different rates in electrolyte of three different initial specific gravities. The composition of each of the positive plate materials is shown in Table III (test cell No. 22-30). The α-:β-PbO_2 ratio in the positive material appears to reach a maximum value somewhere near the 10 amp-20 hr (5.2 amp/cm²) electroformation rate. However, the data are not sufficient to establish the exact rate at which the maximum occurs. The reason or reasons for this maximum α-:β-PbO_2 ratio cannot be explained at this time, but some speculation is in order.

Table III. Composition of positive material formed at different rates in electrolyte of different specific gravities at 43°C

Test Cell No.	Density of positive paste, g/cc	Initial sp gr of electrolyte	Electro-development current density, ma/cm²	α-:β-PbO_2 ratio in positive material
22	3.91	1.150	10.4	0.32
23	3.91	1.150	5.2	0.67
24	3.91	1.150	2.6	0.49
25	3.91	1.200	10.4	0.09
26	3.91	1.200	5.2	0.45
27	3.91	1.200	2.6	0.33
28	3.91	1.250	10.4	0.06
29	3.91	1.250	5.2	0.11
30	3.91	1.250	2.6	0.06
31	4.70	1.150	10.4	1.17
32	4.70	1.150	5.2	1.32
33	4.70	1.150	2.6	1.93
34	4.70	1.200	10.4	0.78
35	4.70	1.200	5.2	1.07
36	4.70	1.200	2.6	1.43
37	4.70	1.250	10.4	0.61
38	4.70	1.250	5.2	0.70
39	4.70	1.250	2.6	0.96

In a separate experiment, positive paste of 4.39 g/cc density was formed at two different rates. Cells were withdrawn from the electroformation circuits at various intervals, and the positive plate material was analyzed. The composition of the positive material at various stages of electroformation is shown in Fig. 2. The α-PbO_2 content of the positive material rises rather sharply during the early stages of electroformation then levels off sometime after 100 amp-hr of formation. The β-PbO_2 content remains at a fairly low level during the early stages of electroformation then begins to rise after 50 amp-hr of formation. The differences in the α-PbO_2 levels finally attained during electroformation might be attributed to the potential of the positive plate during formation. It was noted that the positive plate potential approached the $PbO_2/PbSO_4$ potential more rapidly when the higher formation rate was employed. After 80 amp-hr of electroformation, the potential of the positive plates formed at the 40 amp rate was 100 to 150 mv higher than that of the plates formed at the 10 amp rate.

While the behavior of the positive plate potential might account for the decrease in the α-:β-PbO_2 ratio when the electroformation rate is increased from the 10 amp-20 hr rate to the 20 amp-10 hr rate, it does not account for the drop in the ratio that is experienced when the rate is decreased from the 10 amp-20 hr rate to the 5 amp-40 hr rate. In this case the rate of diffusion of the electrolyte may be an important factor. At a low electroformation rate, the electrolyte would have a greater opportunity to diffuse throughout the positive paste during the electroformation process and convert most of the lead oxide to sulfate before oxidation to β-PbO_2.

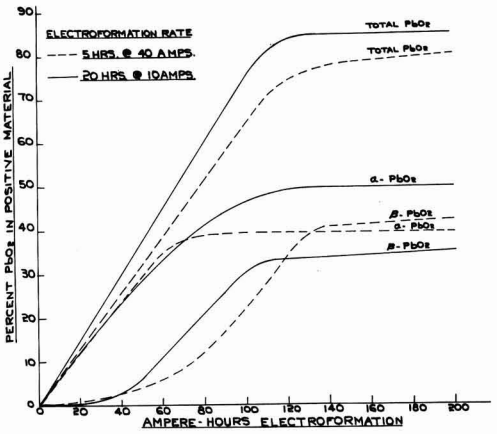

Fig. 2. Composition of positive material at various stages of electroformation. Positive paste density 4.39 g/cc formed in electrolyte of 1.135 initial sp gr at 50°C.

The composition of positive plate material formed from paste of a higher density (4.70 g/cc) at three different rates and in electrolyte of three different initial specific gravities is also shown in Table III (test cells No. 31-39). The α-:β-PbO_2 ratio in the formed positive material continues to increase as the electroformation rate is decreased and does not exhibit a maximum. Apparently, electrolyte diffusion is not a factor in determining the α-:β-PbO_2 ratio in positive material formed from a high density paste and the magnitude of the ratio is essentially the result of a progressively slower rate of increase of the positive plate potential with decreasing electroformation rate. It is interesting to note that when a paste of low density, such as that used in test cells No. 22-30 (Table III), is formed at temperatures below 10°C, the α-:β-PbO_2 ratio in the positive active material no longer exhibits a maximum, but continues to increase as the electroformation rate is decreased. Apparently at low temperatures diffusion of the electrolyte throughout the positive paste is not a factor in determining the ratio even though the paste is of a relatively low density.

Influence of electrolyte temperature.—Positive pastes of three densities were formed at three different temperatures at a rate of 5 amp (for 40 hr) in an electrolyte whose initial sp gr was 1.150. The composition of the positive plate material is shown in Table IV. The α-:β-PbO_2 ratio increases as the temperature of the electrolyte is raised, and the ratio is greater for the higher density pastes at all three of the temperatures investigated. The decrease in total PbO_2 with decrease in temperature, for a paste of a given density, agrees with the work of earlier investigators (12, 13). A more detailed analysis of positive material formed at three different temperatures is shown in Table V. The positive materials described in Table V are those produced at a rate of 5 amp (for 40 hr) in an electrolyte whose initial specific gravity was 1.200. The "% Remainder" listed in Table V is often referred to as "apparent" PbO. Even though only a part of this is really PbO, because both α- and β-PbO_2 are deficient in oxygen, the analytical data indicate that a decrease in the temperature of development results in an increase in the amount of lead oxide in the positive material at each paste density level. X-ray diffraction analysis of the positive materials are in agreement with the chemical analyses. The presence of PbO within the pellet of positive active material after electroformation is a strong indication that the degree of electrolyte diffusion throughout the paste is a function of both the paste density and temperature of the developing electrolyte.

Table IV. Composition of positive material formed from pastes of various densities at various temperatures in electrolyte of 1.150 sp gr at a 2.6 ma/in² current desnity

Test Cell No.	Density of positive paste, g/cc	Temp. of electrolyte, °C	Composition of positive material: Total % PbO_2	α-:β-PbO_2 ratio
40	4.03	4	80.5	0.12
41	4.03	24	86.0	0.25
42	4.03	43	90.9	0.47
43	4.39	4	70.0	0.25
44	4.39	24	84.5	0.66
45	4.39	43	90.9	1.19
46	4.70	4	63.7	0.47
47	4.70	24	80.8	1.00
48	4.70	43	89.8	1.93

Table V. Composition of positive material formed from pastes of various densities at various temperatures in electrolyte of 1.200 cm at a 2.6 ma/cm² current density

Temperature of formation, °C	Density of positive paste, g/cc	Composition of positive material: Total % PbO_2	% $PbSO_4$	% Free Pb	% Remainder
43	4.03	90.1	0.7	2.1	7.1
	4.39	90.6	0.3	2.4	6.7
	4.70	90.0	0.3	3.0	6.7
24	4.03	83.0	1.7	2.2	13.1
	4.39	78.6	1.0	2.4	18.0
	4.70	76.0	1.0	3.1	19.9
4	4.03	75.5	1.3	2.2	21.0
	4.39	67.7	0.7	2.5	29.1
	4.70	62.5	0.9	3.2	33.4

The relationship between the composition of positive plate material formed from pastes of two densities at two different rates and (*a*) the initial specific gravity of the electrolyte and (*b*) the temperature of the electrolyte during electroformation is illustrated in Fig. 3-6. The surface bounded by the solid lines in Fig. 3-6 represents the total per cent PbO_2 in the positive material. The surface bounded by the dotted lines represents the per cent α-PbO_2 in the positive material. The positive materials described in Fig. 3 and 4 were formed at the same rate but from paste of different densities. The higher α-PbO_2 plane in Fig. 4 is attributed to the higher density of the paste. The α-PbO_2 plane is generally lower in Fig. 5 than in Fig. 3, and this is attributed to the higher electroformation rate that was employed in preparing the positive materials shown in Fig. 5. The density of the positive paste from which the materials shown in Fig. 3 and 5 were prepared was the same. The effect of positive paste density on the α-PbO_2 content of the positive material is again illustrated in Fig. 5 and 6. The α-PbO_2 plane is lower in Fig. 6 than in Fig. 4 because a greater electrofor-

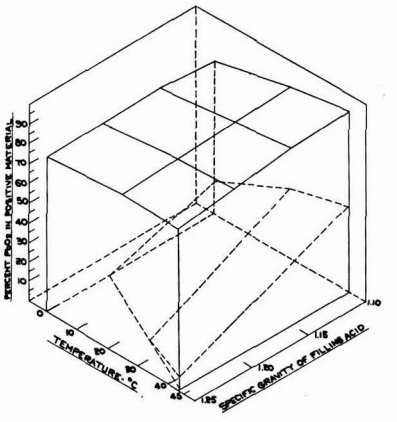

Fig. 3. Composition of positive material formed at a rate of 5 amp for 40 hr from paste of 4.03 g/cc density.

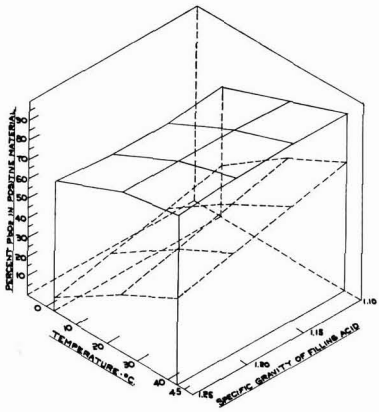

Fig. 4. Composition of positive material formed at a rate of 5 amp for 40 hr from paste of 4.70 g/cc density.

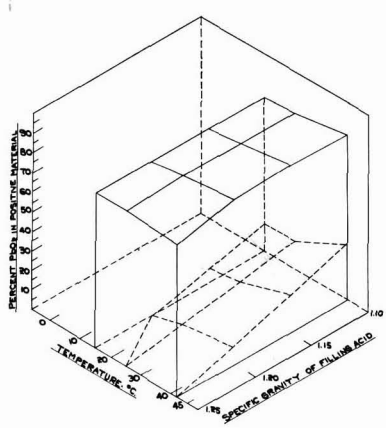

Fig. 5. Composition of positive material formed at a rate of 20 amp for 10 hr from paste of 4.03 g/cc density.

mation rate was employed in preparing the materials described in Fig. 6.

Conclusions

All of the data presented in this paper indicate that lead oxide is responsible for the major portion of the α-PbO_2 formed in the positive plate material. In the experiments described here, the amount of acid electrolyte added to each cell prior to its electroformation was not sufficient to convert completely all of the lead oxide present in the paste to lead sulfate. The interior of the positive plates should therefore be basic and remain basic until the acid, regenerated during development, has an opportunity to diffuse throughout the undeveloped paste.

The rate of diffusion of the electrolyte throughout the paste and the pH of the electrolyte in the pores of the paste are closely related. It has been shown recently that the electrode potential of α-PbO_2 is lower than that of β-PbO_2 in solutions whose pH is greater than 2 and that in such solutions, α-PbO_2 would be formed in preference to β-PbO_2 (14). In

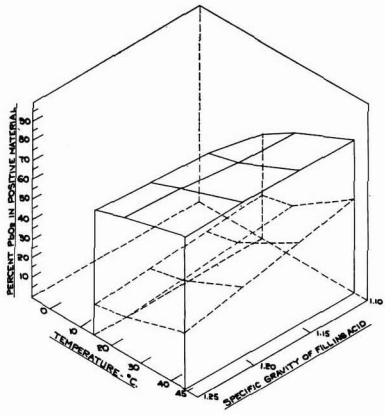

Fig. 6. Composition of positive material formed at a rate of 20 amp for 10 hr from paste of 4.70 g/cc density.

an extreme case where a high density paste, rich in PbO, is developed in a low gravity acid, the amount of unsulfated PbO present in the positive plate just prior to its development should be sufficient to maintain a fairly high pH within the paste during the first half of the developing period. This would favor the formation of large amounts of α-PbO_2. At the other extreme, where a low density paste is developed in a high gravity acid, there would be only enough lead oxide reserve in the plate to maintain a pH above 2 for a small portion of the developing period. Under these conditions only relatively small amounts of α-PbO_2 would be formed.

Manuscript received Oct. 27, 1960; revised manuscript received Jan. 12, 1961. This paper was prepared for delivery before the Houston Meeting, Oct. 9-13, 1960.

Any discussion of this paper will appear in a Discussion Section to be published in the December 1961 JOURNAL.

REFERENCES

1. N. Kameyama and T. Fukumato, *J. Soc. Chem. Ind., Japan*, **49**, 154 (1946).
2. J. J. Lander, *This Journal*, **98**, 213 (1951).
3. H. Bode and E. Voss, *Z. Elektrochem.*, **60**, 1053 (1956).
4. P. Ruetschi and B. D. Cahan, *This Journal*, **104**, 406 (1957).
5. J. Burbank, *ibid.*, **104**, 693 (1957).
6. P. Ruetschi and B. D. Cahan, *ibid.*, **105**, 369 (1958).
7. J. F. Dittmann and H. R. Harner, "Starting and Lighting Batteries," No. 7 in a Series, "Paste Preparation and Plate Control," The Eagle-Picher Company (1956).
8. K. Topf, *Z. Anal. Chem.*, **26**, 296 (1944).
9. A. I. Zaslovsky, Y. D. Kondrashov, and S. S. Tolkachev, *Doklady, Akad. Nauk, SSSR.*, **75**, 559 (1950).
10. K. Kordesch and A. Marko, *This Journal*, **107**, 481 (1960).
11. V. Dodson, ED-6254, Dec. 1959, The Electric Autolite Co., Toledo, Ohio.
12. R. H. Greenburg and B. P. Caldwell, *Trans. Electrochem. Soc.*, **80**, 71 (1941).
13. J. E. Hatfield and O. W. Brown, *ibid.*, **72**, 361 (1937).
14. P. Ruetschi, R. T. Angstadt, and B. D. Cahan, *This Journal*, **106**, 547 (1959).

The Composition and Performance of Positive Plate Material in the Lead-Acid Battery

Vance H. Dodson[1]

The Electric Autolite Company, Toledo, Ohio

ABSTRACT

The discharge capacities of α-PbO_2 and β-PbO_2 at various discharge current densities have been measured. The capacity of α-PbO_2 is considerably lower than that of β-PbO_2 over the range of discharge rates employed in this work. The change in composition of the positive plate material during (*a*) initial SAE 20-hr discharge, (*b*) successive SAE 20-hr discharge tests, (*c*) high rate discharge at 26.7° and at —18°C, and (*d*) stand at 26.7°C has been studied. The performance of the positive plate under the conditions of these tests can be related to the relative amounts of α-PbO_2 and β-PbO_2 in the positive material.

The relationship between the composition of the positive plate material and some of its performance characteristics has been reported previously by several investigators (1-3). These earlier works were concerned with the total per cent PbO_2 and per cent "apparent" PbO and their influence on the discharge capacity and open-circuit reactions of the positive material.

Two forms of PbO_2 have been found in positive plate material, α-PbO_2 and β-PbO_2 (4-7). The former is the orthorhombic and the latter is the more common tetragonal modification. It has been shown previously that the amounts of α- and β-PbO_2 that are formed in the positive plate material vary with the (*a*) density of the positive paste, (*b*) specific gravity of the developing acid, (*c*) rate of development, and (*d*) temperature of development (8). Positive material containing α-PbO_2 in amounts ranging from traces to 70% have been prepared (8).

The work reported in this paper was carried out to determine the influence of α-PbO_2 on the performance of the positive plate. The change in the composition of the positive material, with respect to total PbO_2, β-PbO_2, and α-PbO_2, during discharge and stand was also investigated.

Experimental Procedure

Positive paste was prepared by blending a mixture of 70% lead oxide and 30% lead with water and sulfuric acid. The density of the pastes was measured by the method of Dittmann and Harner after the pastes had been applied to the supporting grid and cured (9). The pastes were cured at room temperature, or slightly above, during which time most of the free water was lost by evaporation and most of the free lead in the paste was converted to lead oxide. After curing, the pastes contained 3-5% free lead. The pastes were applied by hand pasting to 7% antimonial lead alloy grids. The grid alloy in the negative plates was the same as that in the positive plates. Resin coated cotton linter separators were used in the construction of the battery elements.

All of the positive plate samples were thoroughly washed in water and dried at 110°C in a vacuum oven prior to their chemical analysis. The total per cent PbO_2 was determined iodometrically (10). The relative amounts of α-PbO_2 and β-PbO_2 in the positive materials were determined by x-ray diffraction analysis (8). Each sample was digested in hot ammonium acetate solution, washed with hot water, and vacuum dried at 110°C before being subjected to x-ray diffraction analysis. A Norelco x-ray diffraction unit equipped with a goniometer, Geiger counter, and recorder was used in this investigation. Copper K-alpha radiation was employed in all of the analyses. The weight and composition of the positive material in a given plate or cell was assumed to be representative of that in the other plates or cells of that series in the same state of charge.

The various aqueous solutions of sulfuric acid were prepared from commercial grade sulfuric acid whose specific gravity was 1.400. The concentrations of the acid solutions are expressed in terms of specific gravity and these values have been corrected to 26.7°C. Alkaline electrolytes were prepared from Fisher Certified Reagent sodium hydroxide.

Most of the batteries were subjected to the SAE 20-hr test. In this test, the electrolyte in each cell is adjusted to a specific gravity of 1.285 and to a temperature of 26.7°C. The battery is then discharged at a rate equal to one-twentieth of its rated ampere-hour capacity in a water bath maintained at 26.7°C. The discharge is terminated when the voltage reaches 1.75 v/cell.

Specific Experiments and Results

Capacity of α- and β-PbO_2 at various discharge current densities.—One group of cured positive plates containing paste of 4.52 g/cc density was soaked in 1*N* NaOH for 2 hr then developed as positives in the alkaline electrolyte at a current density of 10 ma/cm^2 (apparent positive plate area) for 96 hr. The temperature of the electrolyte was maintained at 27° ± 2°C. Lead-antimony alloy grids were used as negatives in the developing process. The

[1] Present address: Dewey and Almy Chemical Co., W. R. Grace Co., Cambridge, Mass.

PbO_2 formed in the positive plate under these conditions was identified as α-PbO_2 by x-ray diffraction analysis (4, 7).

A second group of the positive plates was allowed to stand in acid of 1.400 sp gr for 18 hr, then developed as positives in 1.135 sp gr acid at a current density of 10 ma/cm² (apparent positive plate area) for 18 hr and at a current density of 3 ma/cm² for an additional 72 hr. The PbO_2 formed in the positive plate under these conditions was practically pure β-PbO_2. Traces of α-PbO_2 which appeared in the material were attributed to the oxidation of free lead in the grid metal and in the paste.

After electroformation, both groups of positive plates were washed and dried at 110°C in a vacuum oven. The positive material was removed from four of the plates prepared in the alkaline medium and from four of the plates prepared in the acid medium for chemical and x-ray diffraction analysis. Each of the remaining plates was weighed, soaked in acid of 1.260 sp gr for 1 hr and discharged in acid of the same specific gravity at 26.7°C. Two production dry charged negative plates which had been activated in 1.260 acid were used in the discharge of each of the positive plates, and the amount of negative material in each of the cells was in sufficient excess to cause the positive plate to limit the discharge. Each discharge was terminated when the voltage of the cell reached 1 v. After the discharge, each positive plate was stripped of its active material in hot mannitol solution, 10 g hydrazine dihydrochloride, 20 g mannitol, 100 g sodium hydroxide, per liter of solution, and the weight of the supporting grid was determined.

The discharge capacities of α-PbO_2 and of β-PbO_2, containing traces of α-PbO_2, at four different discharge current densities and at 26.7°C are listed in Table I. The current densities are based on the apparent area of the positive plate, and the capacities are in units of ampere-hours per 453 g of PbO_2 present in the positive material. Each of the capacities cited in Table I is the average of three determinations. The discharge capacity of α-PbO_2 is considerably lower than that of β-PbO_2 at all four current density levels. It was not ascertained in this work whether the difference between the discharge capacities of the two forms of PbO_2 is due to their different crystallographic forms or to a difference in the surface area and pore structure of the plates containing the two oxides.

Discharge capacity of α- and β-PbO_2 at the SAE 20-hr rate.—One series of six, 11 plate, 55 amp-hr capacity cells was developed in 1*N* NaOH. The positive plates were washed and dried and the plates from five of the cells were coupled with dry charged negative plates which had been activated in acid of 1.285 sp gr. The five elements were placed in their appropriate battery case and electrolyte of 1.285 sp gr was added to each cell. After standing for 2 hr in their electrolyte, each of the five cells was subjected to the SAE 20-hr test. The weight and composition of the positive material in the sixth cell was determined. The entire procedure was repeated with a second series of six cells.

Table I. Discharge capacities of α- and β-PbO_2 at 26.7°C

Form of PbO_2	Discharge rate, ma/cm²	Discharge capacity, amp-hr/453 g of PbO_2
α-PbO_2	174.1	16.4 ± 0.3
β-PbO_2	174.1	28.2 ± 0.2
α-PbO_2	122.0	18.1 ± 0.1
β-PbO_2	122.0	30.3 ± 0.2
α-PbO_2	52.3	22.6 ± 0.1
β-PbO_2	52.3	39.1 ± 0.3
α-PbO_2	17.4	34.0 ± 0.2
β-PbO_2	17.4	52.5 ± 0.1

A third series of six cells, of the same type and capacity, was developed in acid of 1.135 sp gr after standing over night in 1.400 sp gr acid. The positive plates were coupled with dry charged negatives which had been activated in acid of 1.285 sp gr. Five of the cells were subjected to the SAE 20-hr discharge test. The weight and composition of the positive material in the sixth cell was determined. The entire procedure was repeated with a fourth series of six cells.

The results of the discharges indicate that the capacity of α-PbO_2 is 50.0 ± 0.3 amp-hr/453 g of α-PbO_2 present in the cell and that the capacity of β-PbO_2, containing traces of α-PbO_2, is 78.0 ± 0.2 amp-hr/453 g of β-PbO_2 in the cell. Positive plates of 0.060 in. thickness were used in the comparison of PbO_2 capacitites at the SAE 20-hr rate, and all of the discharges were limited by the positive plate.

The measured SAE 20-hr capacities of α-PbO_2 and of β-PbO_2 can be used, with some accuracy, to calculate the SAE 20-hr capacity of a battery whose positive plate material contains a mixture of the two, assuming, of course, that the positive plate limits the discharge. Forty-four batteries, both 6-v and 12-v, of various ampere-hour capacities and containing positive plates whose thickness was in the range 0.060-0.080 in. were discharged according to SAE 20-hr discharge test specifications. One cell was removed from each battery prior to its discharge, and the weight and composition of the positive material in those cells was determined. Positive pastes of various densities were incorporated in the batteries and the batteries were developed in electrolyte of various initial specific gravities and at different temperatures in order to produce positive plate materials of different α- and β-PbO_2 contents (8). The average per cent deviation between the measured SAE 20-hr capacities and those calculated from the weights of α-PbO_2 and β-PbO_2 in the cells and their individual capacities is 2.8%. A comparison of the measured and calculated capacities of ten of the test batteries is shown in Table II.

It has been shown previously that the total per cent PbO_2 in the formed positive plate decreases as the temperature of electroformation is decreased (1, 2, 8). The ratio of α-:β-PbO_2 in the formed positive plate also decreases as the temperature is lowered (8). Hatfield and Brown have reported that the PbO_2 formed at the lower temperatures exhibits a greater initial capacity (1). When the relative capacities of α- and β-PbO_2 are considered it is not surprising that positive material formed at low tem-

Table II. Measured and calculated SAE 20-hr discharge capacities

Composition of positive plate material prior to SAE 20-hr discharge test at 26.7°C		SAE 20-hr discharge capacity at 26.7°C	
Wt of β-PbO_2, g/cell	Wt of α-PbO_2, g/cell	Measured, amp-hr	Calculated,[a] amp-hr
331	58	62.8	63.2
317	69	61.0	62.1
302	53	57.1	57.6
299	95	62.6	61.8
286	72	56.7	57.0
273	106	57.1	58.6
258	202	65.6	66.5
241	205	63.1	63.9
231	169	59.3	58.3
217	198	60.0	59.1

[a] Calculated on the basis, 50 amp-hr/453 g of α-PbO_2 and 78 amp-hr/453 g of β-PbO_2 in battery cell.

peratures and having a lower total PbO_2 and α-PbO_2 content has a greater capacity than positive material formed at high temperatures and having a higher total PbO_2 and α-PbO_2 content. The composition of positive material formed from the same paste but at two different temperatures and the measured and calculated SAE 20-hr capacities of batteries containing those positive materials are shown in Table III. While the positive material developed at 8°C contains less PbO_2 (total) than that developed at 45°C, its measured and calculated SAE 20-hr capacity is higher. The greater capacity, in terms of ampere-hours per 453 g of PbO_2, of positive material formed at low temperatures, as noted by Hatfield and Brown, is due to the reduced α-:β-PbO_2 ratio in the material.

Change in positive plate composition during the SAE discharge test.—A series of twelve 11 plate, 60 amp-hr capacity cells was assembled from mated positive and negative plates. The elements were placed in their appropriate battery cases and developed in acid whose initial specific gravity was 1.135. Development was carried out at an 11 amp rate for 18 hr at 60°C. Each cell was then made ready for the SAE 20-hr test. Cell No. 1 was removed from the test circuit 5 min before the discharge was started and cells No. 2 through No. 7 were removed from the discharge circuit at various time intervals during the test. Cell No. 8 was removed at the end of the discharge. The four remaining cells were fully charged and cell No. 9 was removed just before and cell No. 10 immediately after the second 20-hr discharge test. The two remaining cells were again fully charged. Cell No. 11 was removed just before and cell No. 12 immediately after a third 20-hr discharge. The positive plates were taken from each cell as it was removed from the test circuit, and the weight and composition of the positive material in the cell was determined.

Table III. Positive material formed from paste of 4.03 g/cc density in electrolyte of 1.200 sp gr at a current density of 5.2 ma/cm² and at 2 temperatures

Description of positive material	Positive material formed at 8°C	Positive material formed at 45°C
Wt of positive material g/cell	429	443
Wt of β-PbO_2 g/cell	335	259
Wt of α-PbO_2 g/cell	0	116
SAE 20-hr capacity measured amp-hr	58.1	57.6
Calculated amp-hr	57.6	57.3

The composition of the positive plate material at various stages of the SAE 20-hr discharge test is illustrated in Fig. 1. The data indicate that β-PbO_2 discharges at a greater rate and to a greater extent than does α-PbO_2. The difference could be due to the fact that the α-PbO_2 is located within the positive material pellet and its rate of discharge is retarded by the lack of available acid.

The composition of positive plate material before and after three successive SAE 20-hr discharge tests is illustrated in Fig. 2. Although the α-PbO_2 content of the positive material decreases during the first discharge, it remains essentially constant during the subsequent charges and discharges. The amount of β-PbO_2 in the positive material after the second charging operation is greater than that initially present, and the increase is comparable to the decrease in the α-PbO_2 content during the first discharge. Since β-PbO_2 is formed from $PbSO_4$ during charge (6, 7), the α-PbO_2 that is converted to $PbSO_4$ during a given discharge should fail to reappear on charging and should be replaced by a comparable amount of β-PbO_2.

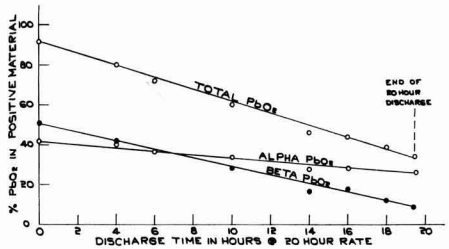

Fig. 1. Composition of positive material at various stages of the SAE 20-hr discharge test.

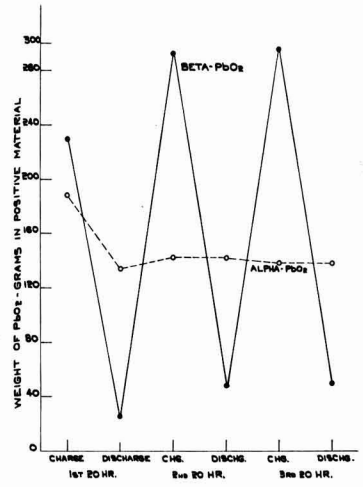

Fig. 2. Composition of positive material before and after successive SAE 20-hr discharge tests.

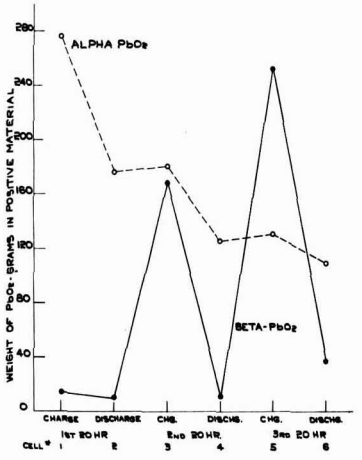

Fig. 3. Composition of positive material, originally rich in α-PbO_2, before and after successive SAE 20-hr discharge tests.

The change in the composition of positive material rich in α-PbO_2 during successive SAE 20-hr discharge tests is illustrated in Fig. 3. The positive plates employed in this work were formed in 1*N* NaOH, washed and dried prior to their assembly into 11 plate, 60 amp-hr capacity elements. The amount of α-PbO_2 that undergoes discharge decreases with each successive discharge. The α-PbO_2 content of the positive material does not change appreciably during the charging operations. The β-PbO_2 content increases with each successive charging operation, and each increase is roughly comparable to the decrease exhibited by the α-PbO_2 during the previous discharge. The small amount of β-PbO_2 found in the positive material before the first discharge is probably the result of the charge given the plates in the acid electrolyte prior to the test. X-ray diffraction analyses of positive plate material developed in alkaline solutions have always indicated that small amounts of PbO were present. It is reasonable to assume that during the charging of the plates in the acid electrolyte the PbO forms $PbSO_4$ and this in turn is converted to β-PbO_2.

The data in Fig. 2 and 3 indicate that the α-PbO_2 content eventually reaches a steady level during successive SAE 20-hr tests and that this level is dependent on the initial amounts of α-PbO_2 and β-PbO_2 in the positive material. It is common laboratory practice to subject a test battery to two, and sometimes three, successive SAE 20-hr discharge tests. Very often the capacity of the second discharge is greater than that of the first. In some cases there is very little difference between the first and second discharge capacities. In a few instances the second discharge capacity is lower than the first. Batteries containing positive material in which the initial α-:β-PbO_2 ratio is similar to or higher than that pictured in Fig. 2 should exhibit an increase in capacity during the second discharge. When the amount of α-PbO_2 in the positive material is low, the second discharge capacity is apt to be the same as the first. A loss in SAE 20-hr capacity with successive discharges cannot be accounted for on the basis of the α- and β-PbO_2 content of the positive plate material.

High rate discharge capacity of mixtures of α- and β-PbO_2.—Mated pairs of 11 plate, 60 amp-hr capacity, cells containing positive paste of two densities, 4.09 and 4.82 g/cc, were developed in electrolyte of three different initial specific gravities to produce positive material of various α- and β-PbO_2 content (8). The specific gravity of the electrolyte in each cell was adjusted to 1.260, and one cell of each pair was dismantled and the positive plate material was weighed and analyzed. The other cells were discharged at a 300 amp rate at 27° and at −18°C. Oversized negatives were used in each cell so that the discharges were limited by the positive plate.

The capacities of α-PbO_2 and β-PbO_2 when discharged at a 300 amp rate (156 ma/cm², apparent positive plate area) are listed in Table IV. The individual capacities of α- and β-PbO_2 were obtained by solving simultaneous equations containing the measured capacity of each cell and the amounts of α- and β-PbO_2 in each cell just prior to its discharge. The major portion of the total capacity of the positive plate is contributed by the β-PbO_2 during a high rate discharge. The discharge capacities of both α- and β-PbO_2 are lowered when the density of the paste from which the positive material is formed is increased. This is probably the result of the decrease in the porosity of the positive material with increase in its density. The effect of paste density on the capacities of α- and β-PbO_2 is not noticeable at the SAE 20-hr discharge rate. The capacities listed in the first line of Table IV are in good agreement with those presented in Table I. Capacities of 17 and 29 amp-hr for α- and β-PbO_2, respectively, would have been predicted by interpolating the data in Table I.

Change in positive plate composition during wet storage.—Fifteen plate, 105 amp-hr elements were asembled from mated positive and negative pasted plates. The elements were formed in their appropriate battery cases under identical conditions, temperature, initial specific gravity of electrolyte, and electroformation rate. The specific gravity of the electrolyte in each cell was adjusted to 1.280 and the cells were allowed to stand at 26.7°C. The weight and composition of the positive plate material was determined after various periods of stand and after recharge following the various periods of stand. The SAE 20-hr discharge capacities after 0, 10, 30, and 60 day stand periods and recharge were also measured.

Table IV. Discharge capacities of α-PbO_2 and β-PbO_2 at a 300 amp rate

Temperature of discharge, °C	Density of positive paste, g/cc	Discharge capacity amp-hr/453 g of PbO_2 in cell	
		β-PbO_2	α-PbO_2
27	4.09	28	15
	4.82	23	10
−18	4.09	18	8
	4.82	15	3.5

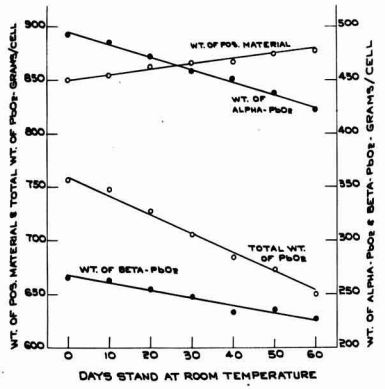

Fig. 4. Composition of positive material after various periods of stand at 26.7°C and in electrolyte of 1.280 initial sp gr.

The composition of positive plate material after various periods of stand at 26.7°C is shown in Fig. 4. The high α-PbO_2 content of the positive material is not surprising since the cells contained positive paste of high density (4.64 g/cc) and were formed in electrolyte of low initial specific gravity (1.050) (8). The measured decrease in amount of total PbO_2 in the positive material was 108 g over the 60-day period. If it is assumed that the PbO_2 was converted to $PbSO_4$, the weight of the positive plate material should have increased by 29 g. The measured gain in weight of the positive material was 27 g. Of the 108 g of PbO_2 that was converted to $PbSO_4$ during the 60-day stand period, 72 g was α-PbO_2 and 36 g was β-PbO_2. The rate of conversion of α-PbO_2 to $PbSO_4$ in aqueous sulfuric acid has been observed to be approximately twice that of pure β-PbO_2 at 26.7°C, and the reactions appear to be first order with respect to the concentration of the sulfate ion (11). Greenburg and Caldwell have shown that the rate of self-discharge of the positive plate, at 24°C and in 1.280 sp gr electrolyte, decreases with increasing temperature of formation (2). As the temperature of formation is lowered from 27° to 7°C one might expect an increase in the self-discharge rate because of the increasing amounts of PbO that appear in the formed positive material (2, 8). However, there is a conflict between the earlier data (2) and that presented here, when the formation temperature range of 27°-49°C is considered. The rate of sulfation would be expected to increase as the temperature is raised from 27°C to 49°F. Although the amount of PbO in the formed plate is small in this range of formation temperatures, the amount of α-PbO_2 that is formed increases steadily (8).

Ruetschi and Angstadt have shown that a positive plate that has been given a single discharge and recharge undergoes self-discharge at a lower rate than one that has not been given such a cycle (3). As a result of the one cycle, the total per cent PbO_2 in the positive plate increased from 92% to 94%. The difference in self-discharge rate can be attributed to the cycling operation which would reduce the α-PbO_2 and increase the β-PbO_2 content of the positive plate. The reported increase in the total per cent PbO_2 after the one cycle tends to substantiate this. Alpha-PbO_2, as it is formed in the positive plate, is more deficient in oxygen than β-PbO_2 (11). As the α-PbO_2 is replaced by β-PbO_2, the total PbO_2 content rises.

The fact that α-PbO_2 undergoes discharge at a slower rate than β-PbO_2 during the SAE 20-hr test (Fig. 1) and the fact that α-PbO_2 undergoes self-discharge at a faster rate than β-PbO_2 are not necessarily contradictory. Since α-PbO_2 is located within the pellet of the positive material, its rate of discharge will be retarded because of the limited amount of acid available for discharge. The self-discharge test is conducted over a long period of time, and the availability of the electrolyte for reaction is not a problem.

The composition of the positive plate material that had been on stand for various periods of time at 26.7°C then recharged is illustrated in Fig. 5. The total PbO_2 exhibits a gradual increase as the time of stand, prior to recharge, increases. The weight of β-PbO_2 in the recharged positive plate also rises linearly with time of stand, prior to recharge. The weight of α-PbO_2 in the recharged material decreases with time of stand. The amount of α-PbO_2 in the positive material after each period of stand was not altered appreciably by the subsequent charging operation.

It is well known that wet and charged batteries exhibit a better SAE 20-hr discharge capacity if they are fully charged, allowed to stand for several days, then recharged, prior to the discharge test. The SAE 20-hr capacities of cells that had been on stand at 26.7°C for 0, 10, 30, and 60 day periods, and recharged, steadily increased as the time of

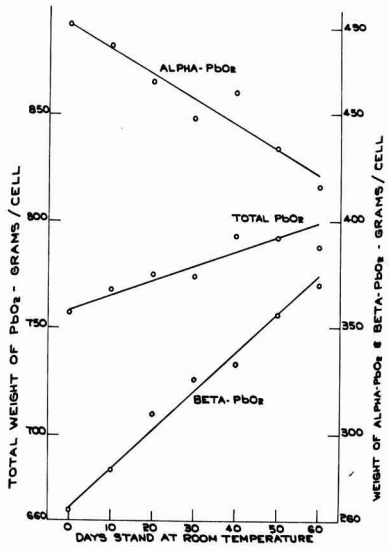

Fig. 5. Composition of positive material which had been allowed to stand for various periods of time at 26.7°C and which had been fully charged following the stand periods. Initial specific gravity of electrolyte, 1.280.

stand increased. This increase appears to be the direct result of the positive plate gaining capacity by way of increasing its β-PbO_2 content. The increase in capacity which occurs as a result of storage has been attributed previously to the decrease in density of the positive plate material (12).

Effect of positive plate composition on SAE overcharge and cycle life performance.—Six volt, 15 plate, 105 amp-hr capacity batteries were assembled from mated positive plates that had been developed in 1*N* NaOH, washed and dried and mated dry charged negative plates. The cells were filled with 1.265 sp gr acid and allowed to stand 1 hr. Two of the batteries were placed on SAE Overcharge Life Test and two were placed on SAE Cycle Life Test.

The performance during SAE overcharge life of two batteries (No. 5 and No. 6) which contained positive material developed in 1*N* NaOH is shown in Fig. 6. Both batteries far exceeded the SAE overcharge life requirement for the particular type of battery as well as the average overcharge life of six, acid developed, production batteries (Fig. 6). Battery No. 5 failed earlier in the test than did No. 6 because of a premature separator breakdown. During the course of their SAE overcharge life test, the batteries were discharged once a week for a period of 30 sec at a 300 amp rate. When the 30 sec voltage fell below the required value of 3.60 v, the batteries were said to have failed. Each weekly discharge removed 2.5 amp-hr capacity. During the first few discharges and recharges the α-PbO_2 content of the positive plate should decrease and the β-PbO_2 content should increase. However, as the amount of β-PbO_2 increases it should take on more of the burden of the discharge, especially when the discharge rate is high. It is conceivable that the α-:β-PbO_2 ratio in the positive material could become fairly constant and that the amount of α-PbO_2 could remain at a rather high level.

It has been reported previously that positive grid corrosion during overcharge is greatly influenced by the potential of the positive plate (13). The positive plate potential of batteries No. 5 and No. 6 (Fig. 6) were measured periodically during the first five weeks of the overcharge test and averaged 2.42 v/cell (*vs.* cadmium). The positive plate potential of the six production batteries which were on test at the same time averaged 2.47 v/cell (*vs.* cadmium). Lander's data show that this difference in positive plate potential can reduce the corrosion rate of the positive grid by as much as 80% during SAE overcharge life (13). The exceptionally long overcharge life of the two test batteries (No. 5 and No. 6, Fig. 6) can be attributed, in part at least, to the lower rate of positive grid corrosion resulting from the lower positive plate potential. It has been shown that the oxygen overvoltage on α-PbO_2 is lower than that on β-PbO_2 (14). During corrosion studies of lead and certain of its alloys the oxygen overvoltage has been observed to decrease as the amount of α-PbO_2 in the corrosion layer increases (15). The high concentration of α-PbO_2 in the positive plate material in batteries No. 5 and No. 6 could be responsible for the lower positive plate potential. In actual laboratory practice a battery is subjected to two or more SAE 20-hr discharge tests before it is placed on the SAE overcharge life test. This type of cycle (or cycles) is deep enough to reduce the α-PbO_2 content to a level where its effect on the positive plate potential is difficult to measure.

The SAE cycle life performance of batteries No. 7 and No. 8 which contained positive material rich in α-PbO_2 is shown in Fig. 7. Since the performance of battery No. 7 was very similar to that of No. 8, it was excluded from Fig. 7. The discharge capacities cited in Fig. 7 are those obtained by periodically discharging the batteries at a 40 amp rate to an out voltage of 5.10 v. Each SAE life cycle includes a discharge at a 40 amp rate for 1 hr and a charge at a 10 amp rate for 5 hr. The rise in capacity of battery No. 8 (and No. 7) early in the test can be attributed to the conversion of α-PbO_2 to β-PbO_2 by the repeated discharge and charge processes. Since the discharges during the test are not as deep as the 20-hr discharge and since the rate of discharge is considerably higher than that of the SAE 20-hr test, the conversion of α-PbO_2 to β-PbO_2 is relatively slow and a large number of cycles is required before a stable α-:β-PbO_2 ratio is attained in the positive plate material.

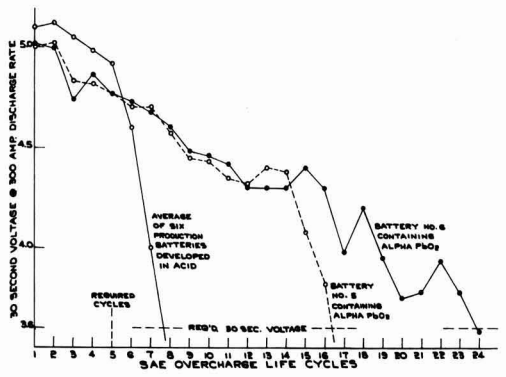

Fig. 6. SAE overcharge life performance of standard production batteries and of batteries containing large amounts of α-PbO_2.

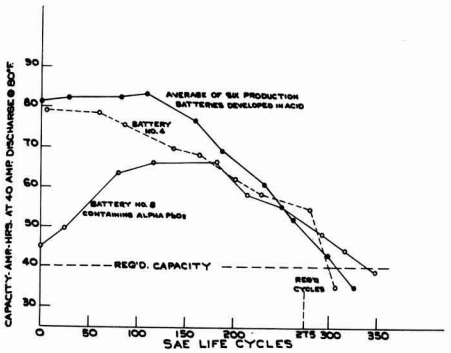

Fig. 7. SAE life cycle performance of standard production batteries and of batteries containing large amounts of α-PbO_2.

Battery No. 4 (Fig. 7) was originally rich in α-PbO_2 but given two successive SAE 20-hr discharge tests before being placed on test. The preliminary treatment apparently reduced the α-PbO_2 content of the positive material to a level comparable to that in the acid developed production batteries. The six production batteries, the performances of which are averaged in Fig. 7, were also subjected to two SAE 20-hr discharges before being placed on the SAE cycle life test. Battery No. 8 (and No. 7) exhibited a slightly longer life than the average life of the six production batteries and the life of battery No. 4. This could be due to a lower rate of positive grid corrosion during the overcharge portion of the first 25-50 life cycles, when α-PbO_2 was the predominant species of PbO_2 in the positive plate material of battery No. 8.

Manuscript received Nov. 10, 1960; revised manuscript received Jan. 17, 1961. This paper was prepared for delivery before the Houston Meeting, Oct. 9-13, 1960.

Any discussion of this paper will appear in a Discussion Section to be published in the December 1961 JOURNAL.

REFERENCES

1. J. E. Hatfield and O. W. Brown, *Trans. Electrochem. Soc.*, **72**, 361 (1937).
2. R. H. Greenburg and B. P. Caldwell, *ibid.*, **80**, 71 (1941).
3. P. Ruetschi and R. T. Angstadt, *This Journal*, **105**, 555 (1958).
4. A. I. Zaslavsky, Y. D. Kondrashov, and S. S. Tolkachev, *Doklady Akad. Nauk. SSSR.*, **75**, 559 (1950).
5. R. Bode and E. Voss, *Z. Elektrochem.*, **60**, 1053 (1956).
7. P. Ruetschi and B. D. Cahan, *This Journal*, **104**, 406 (1957).
7. J. Burbank, *ibid.*, **104**, 693 (1957).
8. V. H. Dodson, *ibid.*, **108**, 401 (1961).
9. J. F. Dittmann and H. R. Harner, "Starting and Lighting Batteries," No. 7 in a series, "Paste Preparation and Plate Control," Eagle-Picher Co. (1956).
10. K. Topf, *Z. anal. Chem.*, **26**, 296 (1944).
11. V. H. Dodson, ED-6161, June, 1960, The Electric Autolite Company, Toledo, Ohio.
12. J. F. Dittmann, and J. F. Sams, *This Journal*, **105**, 553 (1958).
13. J. J. Lander, *ibid.*, **105**, 289 (1958).
14. P. Ruetschi and B. D. Cahan, *ibid.*, **105**, 289 (1958).
15. P. Ruetschi and B. D. Cahan, *ibid.*, **105**, 369 (1958).

Inhibition by Ferric Sulfate of the Dissolution of Iron and Stainless Steel

A. C. Makrides[1]

Metals Research Laboratories, Union Carbide Metals Company, Niagara Falls, New York

ABSTRACT

Potentiostatic polarization experiments with type 410 stainless steel in ferric sulfate solutions show that the reduction curve for inhibitor and the oxidation curve of the metal can be superimposed without distortion from the corrosion potential to the mixed potential established by the inhibitor. The inhibitor concentration required to produce passivity is determined by the critical current density of the metal; it exceeds the concentration required to maintain passivity by about two orders of magnitude. Ferric ion does not protect pure iron in acid solution because of the very large critical current density of this metal. However, an iron electrode first made passive with impressed anodic current remains passive in ferric sulfate solutions after the current is discontinued. In this sense ferric ion is an inhibitor for pure iron as well as for stainless steel.

Stern (1) discussed inhibition of metal dissolution by oxidizing substances on the simple assumption that the (anodic) polarization curve of the metal and the reduction curve of the inhibitor are superimposed without distortion. Makrides and Stern (2) showed this assumption to be valid for inhibition by ferric sulfate of the dissolution of type 410 stainless steel in N H_2SO_4. In the active potential region, *i.e.*, at potentials more negative than the primary passive potential (E_{pp}), ferric ion is reduced at a diffusion-limited rate. It increases consequently the dissolution rate of a freely corroding electrode by providing an additional cathodic reaction besides hydrogen evolution. The dissolution rate increases with ferric ion concentration and flow velocity until some equivalent current is exceeded beyond which the electrode becomes passive. This current is the same as the critical current found by anodic polarization. The anodic polarization curve of the stainless steel in the active region is not affected by ferric ion. The primary passive potential is unaffected also (2).

The potential assumed by the electrode in the passive state is a mixed potential involving the couples Fe^{+++}/Fe^{++} and M^{n}/M. It approaches the reversible potential of the ferric couple when the corrosion current in the passive state is negligible in comparison to the Fe^{+++}/Fe^{++} exchange current (2).

The potential region between the active and the passive states was not examined in any detail pre-

[1] Present address: Field Research Laboratory, Socony Mobil Oil Company, Dallas, Texas.

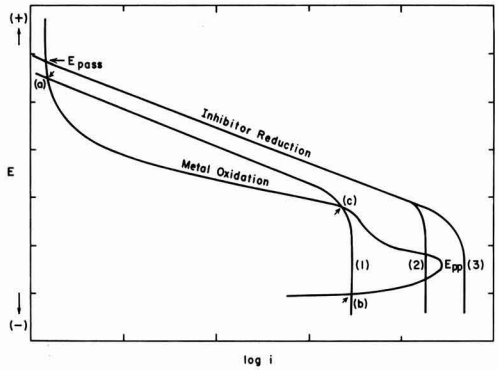

Fig. 1. Superposition of inhibitor reduction curves on the anodic curve of the metal. The potential corresponding to the current maximum of the anodic polarization curve is the primary passive potential, E_{pp}. The vertical lines give diffusion-limited reduction currents. Curves 1 and 2 are for the same flow velocity but for different inhibitor concentrations, $C_2 > C_1$. Curves 2 and 3 are for the same concentration but for different flow velocities, $V_3 > V_2$. The mixed potential in the passive region is given by the point of intersection of the inhibitor reduction curve and the anodic metal oxidation curve. It is generally more negative than the reversible potential of the inhibitor redox couple, but may coincide with it if the metal oxidation current is negligible compared with the exchange current of the redox couple.

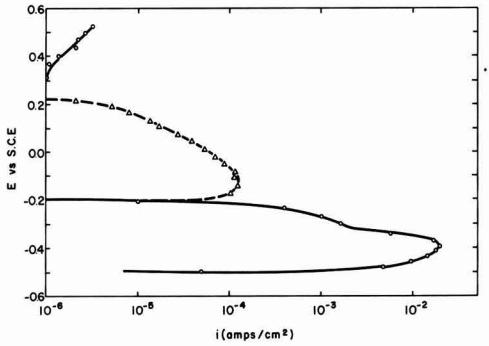

Fig. 2. A potentiostatic polarization curve for type 410 stainless steel in 0.52N H_2SO_4 + 0.08M Na_2SO_4 + 0.014N $Fe_2(SO_4)_3$ at 30°C and a linear flow velocity of 50 cm/sec. At potentials indicated by open circles the electrode was an anode while at those shown by triangles (dashed curve) it functioned as a cathode.

viously. In constructing a diagram similar to that in Fig. 1, it was assumed that the reduction curve for ferric ion was the same down to potentials close to E_{pp}. However, it was recognized that this assumption might not be rigorously correct if the nature of the passive film changed in a major way in this region. The previous extrapolation to potentials close to E_{pp} is shown here to be justified. It also is shown that ferric ion has no specific effect on the anodic polarization curve of the metal in this potential range. Similar work with pure iron showed that it is protected also by ferric ion under certain conditions. This result suggests that differences in the interaction of pure iron and type 410 stainless steel with ferric ion are caused mainly by the widely different critical current densities of the two metals.

Results and Discussion

The experimental arrangement has been reported (2, 3).

To study the effect of ferric ion on the transition between the active and the passive states, conditions were chosen corresponding to curve 1 in Fig. 1. In this case, a potentiostatic curve traced from $E > E_{pass}$ to the corrosion potential should exhibit a "negative loop," *i.e.*, the electrode should be a cathode between E_{pass} and the potential corresponding to point c.

The diffusion-limited current density for ferric ion reduction changes with concentration and flow velocity according to

$$i_d = n\mathbf{F}kc$$

where n is the number of equivalents per mole of oxidant, $\mathbf{F}$ is Faraday's constant, and k a rate constant which depends on flow velocity. The desired conditions can be obtained therefore by adjusting the flow velocity and the concentration.

The critical current density of type 410 stainless steel in 0.5*N* H_2SO_4 without ferric ion is $18 - 20 \times 10^{-3}$ amp/cm². Selecting a linear velocity of 50 cm/sec ($k = 2.0 \times 10^{-3}$ cm/sec) and a ferric ion concentration of 0.014 equiv/l, we find $i_d = 2.7 \times 10^{-3}$ amp/cm². These conditions are similar to those depicted in curve 1 of Fig. 1.

After a potential of +0.55 v *vs.* S.C.E. was reached in the anodic potentiostatic run, ferric ion was added to the concentration noted above, and the polarization curve was traced from $E = 0.55$ v to E_{corr}. In the potential region +0.260 to −0.205 v the electrode was a cathode as anticipated (Fig. 2).

A cathodic polarization curve for reduction of ferric ion can be derived from the data in Fig. 2. At any potential,

$$i_c = i_{ox} - i_{appl}$$

where i_c is the reduction current for Fe^{+++}, and i_{ox} the (anodic) oxidation current of the alloy. The applied current, i_{appl}, is taken to be negative when the electrode is a cathode and positive when an anode. The oxidation current at any given potential is given from the anodic curve traced in the absence of ferric ion [see Fig. 9, ref. (2)]. Using these values, we find that the Tafel curve for ferric ion reduction (Fig. 3) is given by

$$\eta = -0.16 \log \frac{i_c}{2 \times 10^{-7}}$$

with i_c in amp/cm². Here $\eta = E - E^{rev}$ is the overpotential and 2×10^{-7} is the exchange current ($i_c = i_o = 2 \times 10^{-7}$ at $\eta = 0$). We can compare this result with previous measurements (2) on type 410 stainless steel electrodes which were passive in ferric solutions for about two weeks. During this period the oxidation current in the upper section of the anodic polarization curve decayed to a small value ($\sim 10^{-6}$ amp/cm²). Consequently, i_{ox} was negligible in the potential region 0.5 to 0.2 v and i_c was equal to $-i_{appl}$. The polarization curve obtained for sub-

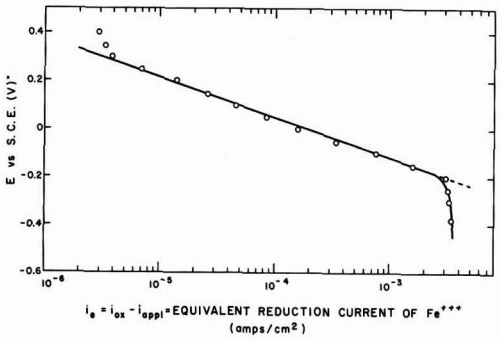

Fig. 3. Polarization curve for reduction of ferric ion on type 410 stainless steel derived from data given in Fig. 4. The Tafel equation is $\eta = -0.16 \log (i_c/2 \times 10^{-7})$.

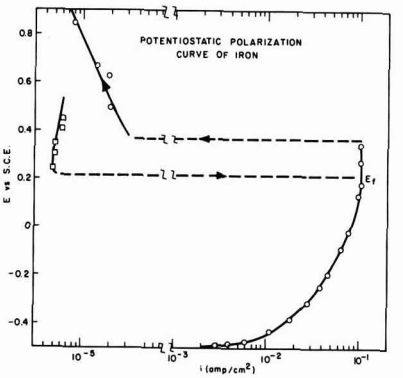

Fig 4. Potentiostatic polarization curve for iron in stagnant 0.1N H_2SO_4 + 0.3M Na_2SO_4 at 0°C. The hysteresis loop is probably due to concentration and ohmic overpotentials which are significant on the ascending branch. The apparent critical current density, here 10^{-1} amp/cm², increases with stirring.

stantially the same Fe^{+++} and Fe^{++} concentrations was

$$\eta = -0.155 \log \frac{i_c}{3 \times 10^{-7}}$$

in good agreement with our present result. Thus, the electrochemical parameters for ferric ion reduction are the same down to potentials close to E_{pp}. Therefore extrapolation of reduction curves to such potentials is justified (2). This agreement shows also that the anodic polarization curve of the metal is not changed by ferric ion in this potential region.

Deviations from Tafel behavior occur at both ends of the plot in Fig. 3. At small currents and positive potentials these are probably due to a relatively rapid decay of the (anodic) oxidation current with time (4). Since we assumed that the anodic curve did not change appreciably during our measurement, the actual cathodic current is probably less than calculated. Positive deviations from the Tafel line therefore are expected as observed.

Deviations at large current densities are caused by concentration polarization. When ferric ion reduction approaches its diffusion-limited value (potentials close to −0.2 v) concentration overvoltage becomes appreciable. The diffusion-limited current is independent of potential. It is estimated from the vertical section of Fig. 5 as 3.2×10^{-3} amp/cm² in fair agreement with 2.7×10^{-3} amp/cm² calculated from the rate constant and the ferric ion concentration (see above).

These results confirm and extend our previous conclusion (2) that ferric ion has no specific effect on the anodic polarization curve. Therefore, the minimum inhibitor concentration required to induce passivity as well as that to maintain it can be calculated from the anodic polarization curve. The first is the concentration at which the equivalent reduction current exceeds the critical current (1, 2), while the second is the minimum concentration at which a mixed potential in the passive region is stable ($i_{red} = i_{ox}$ at $E > E_{pp}$). The large difference between these current requirements suggests that protection may be achieved at very small oxidant concentrations provided the electrode is made passive first by anodic polarization. We found that the concentrations necessary to maintain and to produce a passive state with type 410 stainless steel in 0.5N H_2SO_4 were approximately in the ratio 1:100.[2] The possibility then suggested itself that, although ferric ion does not passivate pure iron, it may maintain an iron electrode passive if the electrode were polarized first anodically to a passive potential. This expectation was borne out by the experiments reported below.

Inhibition of iron dissolution.—Iron shows an abrupt transition to a passive state at a potential about +0.2 to +0.3 v *vs.* S.C.E. The potentiostatic polarization curve for iron in stagnant 0.1N H_2SO_4 + 0.3M Na_2SO_4 at 0°C is given in Fig. 4. The solution composition and temperature were selected to reduce the critical current density to an experimentally convenient value. The critical current density for type 410 stainless steel under the same conditions is only 1.3×10^{-3} amp/cm², while its primary passive potential is −0.420 v *vs.* S.C.E.

The hysteresis loop is probably due to concentration and ohmic overpotentials. These are appreciable at the high current densities of the ascending branch but negligible on the descending branch. The primary passive potential obtained from the descending branch, +0.22 v *vs.* S.C.E., coincides with the potential arrest (Flade potential) found on open-circuit decay from the passive to the active state.

Figure 4 demonstrates why it is difficult, if not impossible, to passivate pure iron with ferric ion. The rate constant for diffusion in stagnant solutions is $k \sim 10^{-5}$ cm/sec; to exceed 10^{-1} amp/cm² we require a ferric ion concentration of about 10^{2} M/1. Even at this concentration, were it attainable, it is unlikely that iron would become passive. Anodic passivation of iron in sulfuric acid solutions of moderate concentration is preceded by precipitation of a nonconducting layer of ferrous sulfate which restricts the applied current to small pores in the layer (5). The actual current density at which the passive film is produced has been estimated at about

[2] Since the reduction current in the active region increases with flow velocity (diffusion-limited rate) while in the passive region it is independent of velocity (activation controlled rate) this ratio changes with flow conditions. In stagnant solutions it is about 1:1000.

17 amp/cm² (5). With ferric ion the maximum current density cannot exceed the equivalent diffusion current.[3] Thus, in reality, we require a current of about 2 x 10^1 amp/cm² in the pores of a sulfate layer where diffusion is bound to be considerably slower than for a bare surface.[4]

While it was unlikely that ferric ion could passivate iron, it was thought probable that it would maintain it passive. The Fe^{+++}/Fe^{++} reversible redox potential is about 0.2 v more positive than the potential at which passivity of iron breaks down. All that is required here is that the reduction current be at least equal to the metal oxidation current at potentials more positive than the Flade potential. This current is only about 10^{-5} amp/cm² (Fig. 4).

Experiments with a pure iron electrode in 0.1*N* H_2SO_4 + 0.1M Na_2SO_4 + 0.036M $FeSO_4$ at 40°C are shown in Fig. 5.[5] The potential was displaced in a positive direction on addition of ferric ion (0.36 equiv/1); however, the electrode remained active and dissolved at a high rate. It then was passivated by applying an anodic current, $i_a = 4.10^{-1}$ amp/cm², from a constant current source. The current was reduced subsequently to 10^{-5} amp/cm² and maintained at this value while the ferrous sulfate layer dissolved (~5 min). The current then was discontinued. The electrode remained passive at −0.08 v with respect to the reversible Fe^{+++}/Fe^{++} potential (+0.492 v *vs.* S.C.E.). The potential of the iron electrode slowly became more positive and was −0.010 v with respect to $E_{Fe^{+++}/Fe^{++}}^{rev}$ at the end of 280 hr. The corrosion current at this potential was about 10^{-5} amp/cm². The electrode then was activated by a cathodic current of 7 x 10^{-4} amp/cm². These data show that iron can be protected by ferric ion provided it is made passive first with impressed current from an external source. Thus, differences in the interaction of ferric ion with stainless steel and with iron are mainly the result of different critical current densities for the two metals.

[3] This argument does not imply that iron would not become passive in other oxidizing solutions. The difference is, of course, that the ferrous salt is stable in the solutions considered here while it is not in oxidizing solutions which spontaneously passivate iron, *e.g.*, concentrated nitric acid.

[4] The equivalent reduction rate of ferric ion is increased several-fold by stirring. The apparent critical current density for passivating iron also increases with stirring because of a higher rate of removal of ferrous ion from the interface. If at high velocities precipitation of ferrous ion is prevented, the apparent and actual critical current densities should coincide at about 17 amp/cm². This may be within the range of reduction currents obtainable at such velocities. For example, we estimate $k \sim 10^{-1}$ cm/sec at 1000 cm/sec, so that $i_c \sim 20$ amp/cm² at a ferric ion concentration of about 2 M/l. However, this conclusion is uncertain because of excessive surface roughening at these current densities [see ref. (6)]. In any case, velocities of this magnitude could not be obtained in our cell.

[5] The Fe^{+++}/Fe^{++} exchange current increases more rapidly with temperature than the dissolution current for passive iron. Higher temperatures consequently favor stability of the mixed potential established by ferric ion in the passive region.

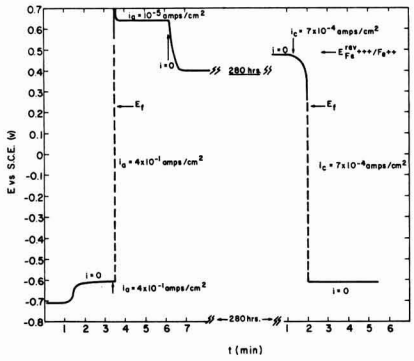

Fig. 5. Potential of an iron electrode in 0.1N H_2SO_4 + 0.1M Na_2SO_4 + 0.036M $FeSO_4$ + 0.36N $Fe_2(SO_4)_3$. The electrode was passivated by applying an anodic current $i_a = 4 \times 10^{-1}$ amp/cm². The current then was reduced to 10^{-5} amp/cm² and discontinued after 3 min. The electrode remained passive for the next 280 hr with a dissolution rate of about 10^{-5} amp/cm². It subsequently was activated by a cathodic current $i_c = 7 \times 10^{-4}$ amp/cm².

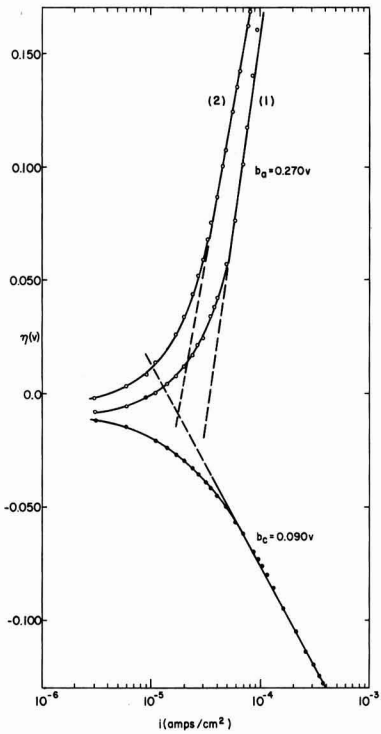

Fig. 6. Anodic and cathodic polarization curves on passive iron in 0.1N H_2SO_4 + 0.1M Na_2SO_4 + 0.036M $FeSO_4$ + 0.36N $Fe_2(SO_4)_3$ at 40°C. The anodic curve, 1, was obtained by increasing the current density relatively rapidly (1 min for each point). Curve 2 was the descending branch obtained after the electrode reached a steady potential at a current density of about 10^{-4} amp/cm².

Polarization measurements on passive iron are shown in Fig. 6. The cathodic curve follows a Tafel equation

$$\eta = -0.090 \log \frac{i}{1.4 \times 10^{-5}}$$

with i in amp/cm². The apparent[6] exchange current ($i_o' = 1.4 \times 10^{-5}$ amp/cm²) is larger than that given above for type 410 stainless steel since the Fe^{+++} and Fe^{++} concentrations were larger. The two exchange currents are of the same order when allowances are made for the difference in concentrations and temperature.

Two anodic curves are shown in Fig. 6. Curve 1 is for increasing and curve 2 for decreasing current

[6] "Apparent" because corrections for metal oxidation have not been made in calculating the Tafel constants. These are discussed below.

densities. The discrepancy between the two curves is due probably to changes of the dissolution rate of iron. Part of the applied current on anodic polarization goes into oxidation of iron so that a plot of i_{appl} *vs.* E does not give directly the polarization curve for Fe^{++} oxidation.[7] The passive film apparently thickens on anodic polarization and the metal oxidation current decreases. The potential at any fixed current density drifts therefore to more positive values. If relatively rapid measurements are made, curve 1 in Fig. 6 is obtained. Curve 2 of Fig. 6 is obtained by letting the potential reach its steady value at a relatively high anodic current density ($i \sim 10^{-4}$ amp/cm^2) and then *decreasing* the current stepwise. The drift of potential almost disappears (less than 1 mv/min).

Curve 2 probably refers to a thicker film than curve 1. The film thickness apparently does not change very much during run 2. Since the metal oxidation current decreases with film thickness, curve 2 should come closer to the oxidation curve for ferrous ion (shift to the left in Fig. 6). This argument is supported by the displacement of the resting potential, E_{pass}, to more positive values. The difference $E^{rev} - E_{pass}$ is a measure of the metal oxidation current and its decrease reflects the decrease in metal oxidation.[8] Fairly accurate polarization curves for both Fe^{+++} reduction and Fe^{++} oxidation can be derived from these data if corrections are made for metal oxidation along the lines suggested above. This analysis is, however, outside the scope of this paper and will not be pursued further here.

General Discussion

The results above demonstrate that if the inhibitor reduction current is less than the critical current, mixed potentials are stable in both the active and the passive region. The electrode assumes one or the other depending on circumstances. For example, if the metal is initially active, addition of inhibitor to a concentration C_1 (Fig. 1) gives a stable potential in the active region and an increased corrosion rate [point (a)]. If an anodic current is impressed through an auxiliary electrode so that the sum of the inhibitor reduction current and the applied current exceeds the critical current, the metal becomes passive and remains passive at point (b) when the current is discontinued.

There is a third point of intersection of anodic and cathodic curves under these circumstances [point (c) of curve 1 in Fig. 1] at which the anodic and cathodic partial currents are equal. However, the corresponding potential is unstable relative to small displacements in either direction. For example, if there is small positive fluctuation to $c + \delta c$, the anodic rate decreases while the cathodic rate remains about the same.[9] The resulting inequality in rates makes the potential even more positive since it produces a net deficiency of electrons in the electrode. The potential becomes increasingly positive until a stable mixed potential at (a) is reached. Similar remarks apply to a fluctuation of potential in the negative direction. If the cathodic reaction is under activation rather than diffusion control, the mixed potential at (c) is again unstable if the (absolute) slope, $\delta E/\delta i$, of the cathodic reaction exceeds that of the anodic reaction. If the reverse is true, the first intersection of the two partial curves falls on the section of the anodic curve which has a negative slope. The resulting mixed potential is probably stable, but protection is marginal since the dissolution rate in this region is still considerable.

Diagrams like Fig. 1 are useful in determining (*a*) the minimum inhibitor concentration required for protection at some specified acid concentration, temperature, and flow velocity; (*b*) the minimum inhibitor concentration required for maintaining protection once passivity is achieved; and (*c*) the response of the passive system to changes in inhibitor concentration or to an impressed transient cathodic current. A complete diagram for a real system can be obtained from the relevant electrochemical parameters determined in the presence of inhibitor (2). For practical purposes, it is sufficient to measure the potentiostatic polarization curve of the metal in the solution of interest (without inhibitor) and the Tafel constants for inhibitor reduction in the passive region. We then may give a reasonable accurate description of the system by extrapolating the reduction curve to the diffusion-limited current density which may be determined independently from the flow conditions and the inhibitor concentration.

Conclusions

1. The Tafel constants for reduction of ferric ion on type 410 stainless steel are the same from the mixed potential in the passive region to potentials close to the primary passive potential of the steel.
2. The ferric ion concentration required to induce passivity of type 410 stainless steel in 0.5*N* H_2SO_4 is at least two orders of magnitude greater than the concentration required to maintain it.
3. Although ferric ion does not passivate pure iron, it will maintain an iron electrode passive if the electrode is first anodically polarized to a passive potential. In this sense ferric ion is an inhibitor for pure iron as well as for stainless steel.

Acknowledgment

The author thanks Mr. R. Aikin who assisted skillfully in the experimental part of the work. Several valuable discussions with Dr. M. Stern are gratefully acknowledged.

Manuscript received Nov. 14, 1960.

Any discussion of this paper will appear in a Discussion Section to be published in the December 1961 JOURNAL.

REFERENCES

1. M. Stern, *This Journal* **105**, 638 (1958).
2. A. C. Makrides and M. Stern, *ibid.*, **107**, 877 (1960).
3. A. C. Makrides, *ibid.*, **107**, 869 (1960).
4. M. Stern, *ibid.*, **106**, 376 (1959).
5. U. F. Frank, *Z. Naturw.*, **4A**, 378 (1949).
6. A. C. Makrides and N. Hackerman, *This Journal*, **105**, 156 (1958).

[7] The metal oxidation current (corrosion current) at the resting potential is approximately equal to the (anodic) applied current necessary to displace the mixed potential to $\eta = 0$. It is estimated to be 10 to 20 μa/cm^2.

[8] The resting potential reverts eventually to its original value as the film returns to its steady-state thickness.

[9] It actually decreases somewhat which contributes further to electron deficiency in the electrode.

The Isolation of Surface Films from Copper

A. F. Beck and M. J. Pryor

Metallurgical Laboratories, Olin Mathieson Chemical Corporation, New Haven, Connecticut

ABSTRACT

A method for the isolation of oxide and sulfide films from copper has been developed. This depends on selective attack at the film-metal interface by a solution containing 3% ammonium acetate and 0.25% bromine in dried methanol. When stripping was performed in contact with dry air, no film dissolution or contamination was detected.

The isolation of surface films from metals frequently has permitted their detailed study by a variety of techniques such as transmission electron diffraction. In these cases the additional studies have assisted in clarifying the mechanism of surface reactions of metals.

Satisfactory methods for isolating surface films currently are confined to relatively few metals (1). The iodine-anhydrous methanol method (2) has been used extensively for the isolation of oxide films from iron. This solution selectively attacks the film-metal interface, thereby rapidly detaching the film. This technique has contributed materially to the understanding of the structure of passive films on iron (3-5). Similarly, the anhydrous bromine-methanol method is effective for stripping surface oxides from stainless steel (6). Both the bromine-methanol and iodine-methanol techniques have been used for the successful isolation of uncontaminated surface films from aluminum and some of its alloys (7, 8). However, these solutions do not preferentially attack the film-aluminum interface and so, unlike film stripping from ferrous materials, the whole of the metal must be dissolved.

It has so far proved difficult to develop satisfactory film stripping techniques for copper and its alloys. Although thick surface films can be removed by amalgamation, invariably these are contaminated badly. Aqueous potassium cyanide solution also will isolate films from copper, but the films so removed undergo structural modification during stripping (13). The anodic film stripping method originally developed by Evans and Stockdale (9) has been used for the isolation of oxides from copper (10) and has been modified recently by Harris, *et al.* (11). Their method consisted of anodic treatment (5-10 v) in deaerated aqueous saturated potassium chloride solution. Contamination generally can be avoided by careful pH control, but on occasion residual particles of copper will remain attached to thin oxide films (12). This is a consequence of the need for complete retention of metallic contact during anodic stripping so that the last traces of metal can be removed. Accordingly, there is a definite need for an alternate simple film stripping method whereby surface films may be detached from copper by selective interfacial corrosion in the absence of applied current.

This paper describes the development of a suitable alternative film stripping method. Reflection and transmission electron diffraction examinations were performed as part of this investigation to insure the absence of contamination and of any structural changes during stripping.

Experimental and Results

Materials and specimen preparation.—All chemicals used in the investigation were of C. P. grade. The 5 x 1 cm copper specimens were cut from annealed 0.025 cm thick sheet having a purity greater than 99.95%.

The specimens were degreased in benzene, washed in absolute methanol, and dried in air. They then were etched in 1.0*N* HCl for 2 min, followed by washing in methanol.

Oxide films were formed on these specimens by heating in dry air for the times and temperatures subsequently specified. Sulfide films were formed by exposing the specimens above a 1:1 solution of ammonium sulfide for 30 sec. All specimens were scored on one side into squares so that any film detached by the stripping solution was of suitable size for mounting on nickel grids for transmission electron diffraction examination.

The films were examined before stripping by reflection electron diffraction in order to determine their outer layer structure and by transmission electron diffraction after stripping to determine whether contamination or phase changes had occurred. These investigations were carried out with a Metropolitan-Vickers electron diffraction camera modified by the addition of a reducing lens ahead of the focusing lens. This gave a source reduction factor of 10 at 50 kv and 20 at 100 kv. Electron diffraction was carried out at 100 kv where the instrument exhibits an inherent resolving power of 1 in 3000, together with maximum resolution and contrast.

Preliminary procedures and results.—Films for the initial investigation were formed by heating copper in dry air for 10 min at 290°C and consisted mainly of Cu_2O with minor amounts of CuO concentrated at the film-air interface.

It became apparent that the range of solutions available for stripping films from copper was quite limited. Even mildly acidic and alkaline aqueous solutions rapidly dissolved the oxide films as did efficient complexing agents such as diacetyl and aqueous solutions of $\alpha\alpha'$ dipyridyl and sulfosalicylic acid.

Since nonaqueous film stripping solutions such as bromine-methanol also dissolved the oxide films rapidly, it was decided to investigate aqueous solutions of some of the less powerful complexing agents for copper. Of the several possibilities investigated it was found that aqueous solutions both of ammonium acetate and of ammonium citrate would detach grossly contaminated film fragments by selective attack at the film-metal interface. Further investigation was concentrated on the more effective ammonium acetate solutions.

In order to minimize gross contamination, the stripping action of various concentrations of ammonium acetate dissolved in absolute methanol was checked. These solutions stripped films by interfacial attack, the time required for stripping increasing with decreasing solute concentration. Times of the order of 12-24 hr were required for stripping under the better conditions (3% ammonium acetate). Although the solutions became colored blue-violet, at no time in these and in subsequent experiments was the coloration so intense as to prevent visual observation of stripping.

The screening experiments described above were carried out in solutions initially containing dissolved air (and traces of water) and which remained in contact with the atmosphere. A separate experiment was carried out in a closed oxygen-free system in which the solution was deaerated by purging with argon. In the absence of dissolved oxygen a solution containing 3 g ammonium acetate per 100 ml of absolute methanol did not attack copper in one day. This experiment implies that dissolution of copper in ammonium acetate-absolute methanol solutions containing dissolved air is oxygen depolarized. Therefore, inclusion of other oxidizing agents in the solution should accelerate stripping. Addition of 0.25% by weight of bromine materially hastened film stripping which occurred by selective attack at the film-metal interface in periods as short as 3 hr.

Transmission electron diffraction examination of films so stripped indicated partial dissolution of Cu_2O together with some contamination during the stripping. Contamination appeared as two phases, a light blue-gray precipitate mainly attached to the specimen and blue crystals forming both on the specimen and throughout the solution. The blue crystals were analyzed chemically and by x-ray diffraction. They appeared to consist of a cuprammonium(II) acetate coprecipitated with ammonium acetate. Chemical analysis suggested that each molecule of the complex contained only 2 molecules of ammonia. The light blue-gray precipitate was primarily $Cu(OH)_2$. No trace of methoxides or bromides was found. Transmission electron diffraction analysis of the film showed additional contamination which could not be identified accurately.

The presence of $Cu(OH)_2$ as a contaminant suggests that water, always present initially in absolute methanol and also absorbed rapidly from the atmosphere, was contributing to the formation of the blue-gray precipitate. Accordingly, an apparatus (Fig. 1) was constructed for performing film stripping under initially anhydrous conditions. The design of the apparatus was sufficiently flexible that film stripping also could be attempted in an inert, oxygen free atmosphere.

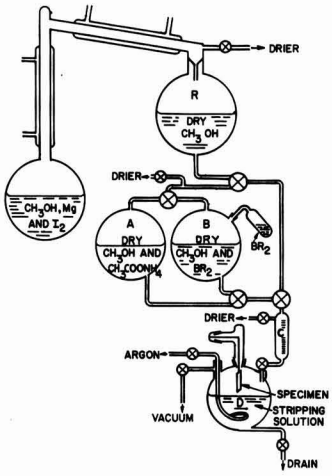

Fig. 1. Film stripping apparatus

The entire system first was alternately evacuated and flushed eight times with either air or argon dried by passing through anhydrous calcium sulfate. Absolute methanol was dried by refluxing with magnesium turnings and a trace of iodine after which it was distilled into the reservoir (R). Stock ammonium acetate-methanol and bromine-methanol solutions next were prepared by running the appropriate volumes of dried methanol from (R) into the storage flasks (A) and (B) which contained fixed weights of vacuum dried ammonium acetate and bromine respectively. The stock solutions were stirred magnetically to facilitate dissolution and could be used for periods up to two weeks after which their effectiveness decreased due to loss of ammonia from (A) and due to interaction of bromine with the methanol in (B). Ammonium acetate-bromine-methanol mixtures of various concentration were prepared by mixing the stock solutions in the graduated cylinder (C) after which they were transferred to reaction flask (D).

The reaction flask (D) was constructed so that copper specimens could be lowered into or raised from the stripping solution by means of a glass windlass. All stripping experiments described subsequently were carried out at room temperature. After stripping was complete the reaction flask was drained and the specimen washed with dried methanol from (R). The film could be left loosely attached to the specimen or shaken free for mounting for electron diffraction examination. Several strippings could be performed with the relatively large volumes of stock solution since the reaction flask could be isolated from the apparatus for the insertion of new specimens and flushed out with dried air prior to each new stripping.

Development of stripping method.—The apparatus (Fig. 1) enabled investigation of the stripping action of ammonium acetate-bromine-methanol solutions

under a wide variety of conditions. The remaining part of the investigation was concerned with defining the stripping conditions which resulted in best adherence to the ideal requirements summarized later. Detailed investigation was concentrated largely on Cu_2O films.

Stripping of oxide films formed by heating for 15 min at 200°C.—Oxide films formed under the foregoing conditions are reported to consist almost entirely of Cu_2O (14, 15). Using 120 ml of a solution containing 3.0% ammonium acetate and 0.25% bromine in dehydrated methanol, containing and in equilibrium with dried air at atmospheric pressure, the films were largely separated and remained only loosely attached to the specimen after 3 hr. When the bromine concentration was halved, the stripping time was approximately doubled. The oxide films were stripped intact with little or no tendency to curl and did not require supporting for mounting on 100 mesh grids for electron diffraction analysis. No precipitate was observed either on the specimen or in the bulk of the solution for as long as three days.

A transmission electron diffraction pattern of the stripped film is shown in Fig. 2. The pattern measurements from Fig. 2 are shown in Table I and correspond extremely well with cubic Cu_2O. No additional lines which might indicate the presence of contamination can be found.

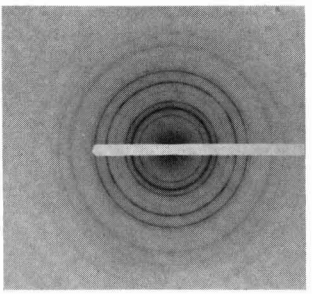

Fig. 2. Transmission electron diffraction pattern of stripped film formed by heating copper at 200°C for 15 min. Only Cu_2O reflections are found.

Additional experiments were carried out to check film stability and contamination by leaving specimens with loosely attached film in the solution for two weeks. With the longer times of immersion, blue crystals were precipitated. On diluting the solution with dehydrated methanol not only did the crystals

Table I. Electron diffraction results obtained by reflection and transmission techniques from oxide films on copper

hkl		Oxide films formed at					
		200°C Transmission		290°C Transmission		290°C Reflection	
Cu_2O cubic	CuO monoclinic	d	i/i_o	d	i/i_o	d	i/i_o
110		3.020	30	3.022	40		
	110			2.750	20	2.73	30
	$\bar{1}11$			2.521	25	2.52	100
111		2.462	100	2.467	100		
	111			2.320	20	2.31	90
200		2.135	30	2.134	40		
	112			1.959	5	1.96	15
	$\bar{2}02$			1.864	6	1.86	20
	112					1.77	15
211		1.743	15	1.742	20		
	020					1.71	15
	202					1.58	25
220	$\bar{1}13$	1.508	35	1.508	20	1.51	25
	022			1.418	6	1.42	70
	220, 113			1.380	4	1.38	40
310		1.349	6	1.350	10		
	311, $\bar{3}12$, 221					1.30	20
311		1.287	30	1.287	15		
	$\bar{2}22$					1.262	20
222		1.233	10	1.233	10		
	204, $\bar{1}14$			1.187	4	1.19	6
	222					1.16	15
321		1.140	6	1.140	10		
	$\bar{1}31$					1.09	17
400		1.066	6	1.066	15		
	204			1.040	10	1.04	2
411, 330	313	1.006	2	1.006	10	1.01	15
331	$\bar{2}24$, $\bar{1}15$	0.979	13	0.979	20	0.980	12
	420					0.956	2
420		0.954	11	0.953	15		
	$\bar{4}22$					0.937	5
	115, $\bar{3}31$					0.918	10
	224, 331					0.887	15
422		0.871	12	0.871	10		
	040, 225, 511					0.856	8
	$\bar{3}33$					0.840	4
511		0.821	8	0.821	10		

dissolve but also the oxide film was still found loosely attached to the specimen with no indications of thinning or contamination as judged by electron shadow microscopy and diffraction.

The relatively rapid stripping of Cu_2O is attributable to the addition of bromine which is believed to act as a cathodic depolarizer. However, previous experiments indicate that dissolved oxygen can serve the same purpose but permits film stripping at a slower rate. It became pertinent to determine whether oxygen was being reduced simultaneously with bromine in the previous successful film stripping since this reduction would produce traces of water. Accordingly, the previous experiment was repeated using identical experimental conditions except that the solution was deaerated with dried argon and stripping was performed in an argon atmosphere. Under deaerated conditions, cuprous oxide films rapidly dissolved. The rate of appearance of the cuprammonium complex in solution was decreased even though attack occurred on the specimen.

This result prompted investigation of the action of a wide variety of ammonium acetate bromine-methanol solutions under dehydrated and deaerated conditions. In all cases the cuprous oxide film dissolved quite readily even when bromine was excluded from the system. However, in the absence of bromine the copper itself was not attacked.

The foregoing results led to a more intensive study of the stability of Cu_2O films in ammonium acetate-bromine-methanol solutions. This study was performed by stripping films in an initially dried solution containing 3% ammonium acetate and 0.25% by weight of bromine in the presence of dry air. When the film was only loosely adherent to the specimen, it was washed carefully in dry methanol. The specimen then was transferred to a side arm in the reaction flask. Solutions of various compositions then were run into the flask after which the specimen was replaced. Gentle agitation was used to detach only a few squares of film. The specimen was raised again into the side arm for subsequent experiments. The rate of film dissolution, if any, was judged by the times required for complete dissolution of the film.

The results of this investigation are contained in Table II and demonstrate that Cu_2O is inert in dry methanol and methanol containing a minimum of 0.1% water, but is attacked to different degrees when detached from the metal by the other solutions used in this investigation. Dissolved oxygen does not affect the dissolution rate in ammonium acetate-methanol solutions. Accumulation of the cuprammonium complex reduces but does not stop dissolution of the film.

In comparing the results in Table II with the stability results described earlier in which the Cu_2O film remained loosely attached to the copper substrate, it is evident that protection against dissolution occurs only when the solutions contain dissolved air and when electrical contact between the film and the metal substrate is maintained.

Since Cu_2O films dissolve in 1 hr in a "spent" stripping solution when detached from the copper,

Table II. Stability of isolated Cu_2O films, detached from copper, in different nonaqueous solutions

Solution	Average time required for complete dissolution of the film
Dry methanol saturated with dry dissolved air	No detectable dissolution in 2 weeks
Absolute methanol in contact with moist air	No detectable dissolution in 2 weeks
3% ammonium acetate in dry methanol saturated with dry dissolved air	15 min
3% ammonium acetate in dry deaerated methanol	15 min
3% ammonium acetate, 0.25% bromine in dry methanol saturated with dry dissolved air	15 min
3% ammonium acetate, 0.25% bromine in dry deaerated methanol	30 min
3% ammonium acetate, 0.25% bromine dissolved in dry methanol containing dry dissolved air and $Cu(NH_3)_2(CH_3COO)_2$ resulting from immersion of a Cu specimen for 3 hr	60 min

and since the stripping itself takes 3 hr, it becomes important to determine whether limited film dissolution occurs early in the stripping process when the film is in electrical contact with the copper. Accordingly, a cuprous oxide film was well loosened but not detached from copper and repeatedly immersed into fresh stripping solution for 3-hr periods. The cycle was repeated six times with film fragments being detached after each cycle for electron diffraction and electron shadow microscope examination. No change of film structure or thickness was detected.

These experiments indicated that dissolution of Cu_2O during stripping can be prevented if the specimen is removed from solution when the film adheres loosely but still maintains electrical contact with the copper. Final detachment of the film for subsequent examination is best achieved by gentle agitation in methanol in which detached Cu_2O films are completely inert.

The procedure described above finally was checked to determine its suitability for stripping mixed cuprous-cupric oxide films and sulfide films. Less problem was anticipated with these films since both CuO and sulfide films are more inert to the film stripping solution than Cu_2O.

Stripping of oxide films formed by heating for 10 min at 290°C.—It has been reported that oxide films formed under these conditions consist mainly of Cu_2O with some CuO at the film-air interface (15, 16). Figure 3a shows a reflection diffraction pattern from the film before stripping. The lines are characteristic of CuO only (Table I) since the limited depth of penetration of the electron beam in reflection is not sufficient to obtain reflections from the underlying Cu_2O. The films formed at 290°C were stripped successfully in 5.5 hr without dissolution or contamination. Figure 3b is a transmission electron diffraction pattern of the stripped film. Relative intensity measurements indicate that it contains

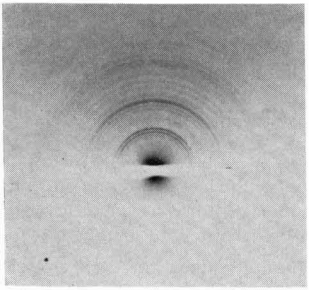

Fig. 3a. Reflection electron diffraction pattern of film formed by heating copper for 10 min at 290°C. Only CuO reflections are found.

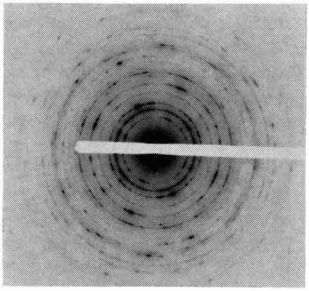

Fig. 3b. Transmission electron diffraction pattern of film shown in Fig. 3a stripped from the metal. The film contains approximately 95% Cu_2O and 5% CuO.

around 95% Cu_2O and 5% CuO. This composition was confirmed by chemical analysis and by x-ray analysis of portions of the stripped film too thick for transmission electron diffraction.

Stripping of sulfide films formed at 25°C.—Sulfide films, formed by the method described earlier, were stripped in 6 hr by the technique described above. The films were much more stable than oxide films in that they were not dissolved in 24 hr when detached from the copper and exposed either to fresh or "spent" stripping solution. Figure 4 shows a transmission electron diffraction pattern of a typical sulfide film. This appears to be duplex, consisting primarily of cubic Cu_2S with a smaller proportion of hexagonal CuS. Reflection diffraction gives primarily the hexagonal structure. The lines agree well with those in the transmission pattern except for several intensity misfits due to preferred orientation.

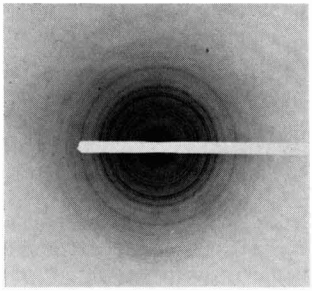

Fig. 4. Transmission electron diffraction pattern of stripped film formed by exposure of copper to the fumes of diluted ammonium sulfide. The film is composed primarily of cubic Cu_2S with a smaller amount of hexagonal CuS.

Discussion

Mechanism of film stripping.—The foregoing investigation indicates that a solution containing 3% ammonium acetate and 0.25% bromine dissolved in dried methanol will effectively isolate Cu_2O films, mixed Cu_2O-CuO films, and mixed Cu_2S-CuS films from copper without detectable contamination and film thinning provided that the stripping is performed in contact with dry air. In all cases stripping occurs by selective attack at the film-metal interface. However, if oxygen is excluded, Cu_2O films dissolve irrespective of the presence or absence of bromine. In deaerated ammonium acetate solutions containing bromine, the copper is attacked, whereas in deaerated solutions free from bromine no attack on the copper other than film dissolution can be detected. These experiments are pertinent to film stripping only and are not such as to permit detailed clarification of the chemistry of this system. Accordingly, the subsequent discussion is intended only to clarify the rather specific conditions required for successful film stripping.

The experimental observations argue that the stripping reaction is similar, in many respects, to an aqueous electrochemical reaction. The primary anodic reaction is believed to be the anodic dissolution of copper in the divalent[1] state at the film-metal interface

$$Cu = Cu^{++} + 2e \qquad [1]$$

During slow stripping in bromine free ammonium acetate-methanol solutions containing dissolved air the local cell cathodic reaction is likely to be

$$O_2 + 4H^+ + 4e = 2H_2O \qquad [2]$$

If this reaction is suppressed by deaeration, attack on the copper is prevented since oxygen reduction is the only possible cathodic reaction. Similar behavior has been observed previously during the dissolution of copper in aqueous ammoniacal solutions (16).

When bromine is added to solutions containing dissolved oxygen, the stripping rate is increased substantially probably because of the additional cathodic reaction

$$Br_2 + 2e = 2Br' \qquad [3]$$

It is believed that reactions [2] and [3] occur on the surface of the film since Cu_2O and sulfides of copper possess relatively good electronic conductivity. Accordingly, the longer time required to strip the thicker duplex oxide films formed at 290°C is considered to be due to the higher electronic resistance of the film.

The interaction between the product of the anodic and cathodic reactions has not been defined completely in this study. However, a cuprammonium(II) acetate, containing two molecules of ammonia, was

[1] The present work does not distinguish anodic dissolution of copper in the divalent state from dissolution in a monovalent condition followed by oxidation in solution to the divalent state. This distinction is unimportant from the standpoint of a mechanism of film stripping; consequently reactions are presented on the basis of dissolution as cupric ions for greatest simplicity.

precipitated after prolonged reaction of copper with the film stripping solution. It will be assumed that this compound also is formed prior to precipitation.[2] Accordingly, anodically formed cupric ions should interact with ammonium acetate according to the equation

$$Cu^{++} + 2CH_3COONH_4 = Cu(NH_3)_2(CH_3COO)_2 + 2H^+ \quad [4]$$

An over-all equation may be written for the corrosion of copper in bromine-free alcoholic ammonium acetate containing dissolved air by combination of reactions [1], [2], and [4] and follows

$$Cu + \tfrac{1}{2}O_2 + 2CH_3COONH_4 = Cu(NH_3)_2(CH_3COO)_2 + H_2O \quad [5]$$

A similar equation may be written, as follows, for the corrosion of copper in a dry alcoholic ammonium acetate-bromine solution freed from dissolved air

$$Cu + Br_2 + 2CH_3COONH_4 = Cu(NH_3)_2(CH_3COO)_2 + 2HBr \quad [6]$$

Table II shows that detached cuprous oxide films are dissolved by ammonium acetate. Equation [6] shows that hydrobromic acid is a reaction product during film stripping. Although the buffering action of the ammonium acetate could well offset the acidity produced in Eq. [6], the experimental results indicate that other factors are the simultaneous presence of dissolved oxygen in the solution and electrical contact of the film with the copper.

It is considered likely at this time that these two factors give rise to the formation of traces of water (Eq. [2]) together with a locally higher pH at the cathode surface, *i.e.*, the film-solution interface. It is believed that this local rise in pH adjacent to the oxide effectively protects it against detectable dissolution for periods as long as two weeks.

These considerations do much to clarify the rather special experimental conditions required for successful film stripping. Furthermore, it is evident that the traces of water generated by reduction of dissolved oxygen are insufficient to cause film contamination. This appears to arise primarily when the methanol is undried originally and when it can absorb further moisture from the atmosphere.

Present method as related to ideal film stripping requirements.—An ideal film stripping method should satisfy the following requirements:

1. The surface film should be inert to the film stripping solution, to the subsequent reaction products, and to the solutions used to wash the film after the reaction is complete. Secondary or spurious film formation in the stripping solution also must be avoided.

2. The stripping action should not lead to practical contamination of the film, such as by inclusion or absorption of reaction products or residual parent metal. This usually requires that products of reaction be completely soluble in the stripping solution. Neither should the stripping action result in any phase or orientation changes in the film.

3. The stripping action should occur rapidly. The stripping time is usually short if the film is detached by preferential attack at the film-metal interface.

4. The method should preferably allow visual observation of the stripping process so that the reaction may be terminated once the film adheres only loosely to the metal.

Accordingly, the results obtained with the new method should be compared finally with the ideal requirements in order to determine the over-all success.

1. Cuprous oxide films are not chemically inert to ammonium acetate-bromine-methanol solutions since they will dissolve when detached from the metal (Table II). However, dissolution of cuprous oxide films cannot be detected in periods up to two weeks when they maintain electrical contact with the copper substrate and when the stripping is carried out in the presence of dry air. A stripping solution that has partly reacted has even less tendency to dissolve cuprous oxide than the original solution (Table II). Cuprous oxide is chemically inert to dry or "wet" methanol. Cupric oxide and the sulfides of copper exhibit much more inert behavior than cuprous oxide. Therefore, under the specific experimental conditions outlined in this paper, it must be concluded that the oxide and sulfide films are inert to the stripping solution, reaction products, and washing solutions and satisfy this stringent requirement. No secondary film formation was ever detected even in periods as long as two weeks.

2. Table I shows that detectable contamination of the stripped films does not occur. Using 120 ml of solution per 10 cm^2 of specimen, the reaction products in the initially dried system are soluble for a minimum of three days, which is 12-24 times as long as the average stripping time. Any precipitate forming after three days can be redissolved by methanol without contaminating the films. Since no trace of residual copper ever was found by electron diffraction, it is concluded that the practical requirement of freedom from contamination is amply satisfied. The additional requirement of freedom from phase and orientation changes is more difficult to answer since the reflection diffraction examination gave structural information only on the outer portion of the film. However, Fig. 2 shows that cuprous oxide films formed by heating for 15 min at 200°C are not oxidized to the cupric condition in the stripping solution (Fig. 2, Table I). Line breadth measurements from Fig. 2 and from the cuprous oxide lines in Fig. 3b show that the cuprous oxide consists mainly of small crystallites about 100-150Å in diameter using the Sherrer approximation. In both cases the cuprous oxide is oriented partially with its (111) planes lying parallel to the copper surface. Such an orientation has been previously reported (17) from reflection electron diffraction studies of very thin unstripped cuprous oxide films. Transmission patterns of the mixed oxide film formed in 10 min at 290°C indicate the presence of approximately 95% cuprous oxide and 5% cupric oxide (Fig. 3b, Table I). This result also was confirmed by x-ray and chemical analysis of the stripped film. The reflection

[2] The number of ammonia molecules in the complex is of minor importance only from the film stripping standpoint.

pattern only reveals the presence of the outermost cupric oxide layer (Fig. 3a, Table I). Dighton and Miley (14), using the cathodic reduction technique (18, 19), reported that the composition of oxide films formed at 277°C was 93% cuprous oxide and 7% cupric oxide. This compares well with the 95% cuprous oxide formed at 290°C in the present work. These facts imply that films stripped by the method described in this paper are also free from phase and orientation changes.

3. Film stripping was achieved in this work by preferential attack at the film-copper interface in periods from 3-6 hr with the longer times being required for the thicker films. This is somewhat longer than the 20-30 min required to detach thin oxide films from iron by the iodine-methanol technique (2). However, it is much quicker than the action of the widely accepted iodine-methanol (8) and bromine-methanol (7) techniques on aluminum.

4. Although the stripping solution assumes a more intense blue-violet color with increasing dissolution of copper, this never obscures clear observation of the specimen.

Therefore, it may be concluded that the new method meets ideal requirements more closely than many other techniques successfully and widely used on other metals.

Acknowledgments

The authors wish to thank the Olin Mathieson Chemical Corporation for their support of this work and for their permission to publish the results.

Manuscript received Oct. 4, 1960; revised manuscript received Jan. 6, 1961.

Any discussion of this paper will appear in a Discussion Section to be published in the December 1961 JOURNAL.

REFERENCES

1. R. T. Phelps, E. A. Gulbransen, and J. W. Hickman, *Ind. Eng. Chem., Anal Ed.*, **18**, 391 (1946).
2. W. H. J. Vernon, F. Wormwell, and T. J. Nurse, *J. Chem. Soc.*, **1939**, 621.
3. J. E. O. Mayne and M. J. Pryor, *ibid.*, **1949**, 1830.
4. J. E. O. Mayne, J. W. Menter, and M. J. Pryor, *ibid.*, **1950**, 3229.
5. J. E. O. Mayne and J. W. Menter, *ibid.*, **1954**, 103.
6. E. M. Mahla and N. A. Nielson, *J. (and Trans.) Electrochem. Soc.*, **93**, 1 (1948).
7. O. Werner, *Z. Anal. Chem.*, **121**, 385 (1941).
8. M. J. Pryor and D. S. Keir, *This Journal*, **102**, 370 (1955).
9. U. R. Evans and J. Stockdale, *J. Chem. Soc.*, **1929**, 2651.
10. J. A. Darbyshire, *Trans. Faraday Soc.*, **27**, 675 (1931).
11. W. W. Harris, F. L. Ball, and A. T. Gwathmey, *Acta Met.*, **5**, 574 (1957).
12. J. V. Cathcart, *Private communication.*
13. G. I. Finch, A. G. Quarrell, and H. Wilman, *Trans. Faraday Soc.*, **31**, 1051 (1935).
14. A. L. Dighton and H. A. Miley, *Trans. Electrochem. Soc.*, **81**, 321 (1942).
15. W. E. Campbell and U. B. Thomas, *ibid.*, **76**, 303 (1939.)
16. J. Halpern, *This Journal*, **100**, 421 (1953).
17. G. D. Preston and L. L. Bircumshaw, *Phil. Mag.*, **20**, 706 (1935).
18. H. A. Miley, *J. Am. Chem. Soc.*, **59**, 2626 (1937).
19. J. B. Dvess and H. A. Miley, *Trans. AIME*, **133**, 239 (1939).

The Relative Stabilities of Oxidation States of Transitional Metals

George W. Watt

Department of Chemistry, The University of Texas, Austin, Texas

ABSTRACT

Conditions favorable to the formation of metals of the 3, 4, and 5d transitional series in all of their possible oxidation states are summarized. Certain broad generalizations are made with respect to factors possibly responsible for the relative stabilities of the various states; particular emphasis is placed on the character of the metal-ligand bond.

Of the many situations in which the relative stability of oxidation states of transitional metals is of importance, two familiar and closely interrelated practical processes may be represented by

$$M^\circ \rightleftharpoons M^{n+} + ne^-$$

where the forward reaction represents the corrosion of a base metal M and the reverse reaction represents the cathodic reduction of the corresponding ion, M^{n+}. More realistically, Eq [1] should be written in the form,

$$M^\circ + xL \rightleftharpoons [ML_x]^{n+} + ne^-$$

where L represents ligands associated with the central metal ion in a number, x, that (for monofunctional ligands) is the so-called coordination number of the metal atom or ion. These ligands may be monodentate ions or neutral molecules such as F^-, Cl^-, H_2O, NH_3, or polydentate species such as CO_3^{2-}, $C_2O_4^{2-}$, $NH_2CH_2CH_2NH_2$ (*en*), etc. Regardless of whether we are interested in the forward or reverse process, establishment of the chemical identity of the initial and final states is usually a relatively simple problem.

The much more difficult problem is that of determining the identity and relative stability of the intermediate oxidation state species and their mode of involvement in the rate-determining process. We may at once invoke a purely thermodynamic approach (1, 2), but thereby succeed in doing little more than proving that which is already obvious. If, for example, we are concerned with the relative stabilities of two oxidation states of a particular metal ion, n+ and n'+ (where $n > n'$) in an en-

vironment that provides potentially stabilizing ligands, it is at once apparent from the Nernst equation

$$E = E^\circ + \frac{RT}{nF} \ln \frac{[M^{n+}]}{[M^{n'+}]}$$

that changes in the electrode potential reflect the relative stabilities of the ions M^{n+} and $M^{n'+}$ in combination with the available ligands. Thus, if $[ML_x]^{n'+}$ is more stable than $[ML_x]^{n+}$ the value of E increases and M^{n+} is more readily reduced to $M^{n'+}$. Consider, for example, the relative stabilities of the ions Co^{3+} and Co^{2+} in the presence of the ligands H_2O and NH_3

$$Co^{2+} = Co^{3+} + e^- \quad E^\circ = -1.82 \text{ v}$$

In the presence of H_2O only, the high negative E° implies that $[Co(H_2O)_x]^{3+}$ is unstable with respect to reduction to Co^{2+}. In the presence of NH_3, however, the more stable $[Co(NH_3)_x]^{3+}$ predominates and is much more stable with respect to reduction to Co^{2+}. It is well known that, in the presence of ammonia, the oxidation of Co^{2+} to Co^{3+} in aqueous solution may be accomplished simply by bubbling air through the solution.

Although thermodynamic considerations are important and certainly cannot be ignored, this approach to the over-all problem of oxidation state stability has some rather severe limitations. In most practical situations, conditions of a fixed temperature with all species in their standard states usually do not obtain. Data for many of the couples of interest are commonly unavailable. The conclusion that a process is thermodynamically feasible does not preclude the possibility that it may proceed at near zero rate. Most importantly, this approach provides no information whatever as to why and how one ligand forms a preferentially stronger bond with a metal atom or ion.

Before we proceed with additional discussion of ligand properties in relation to oxidation state stabilization, certain items of terminology require clarification. The term "stability" is used in the sense of resistance to chemical change, irrespective of the nature thereof. The adoption of this usage carries with it the recognition that a given complex may be quite resistant to oxidation yet readily susceptible to hydrolysis. Thus, apparent contradictions may arise, but these are inescapable in the absence of a more absolute and universally applicable interpretation of the term in question. Also with respect to classes of oxidation states one must be equally arbitrary; terms such as abnormal, unusual, and unfamiliar (3) are useful but not very definitive. Here we will adopt the view (4) that the normal oxidation state of a transitional metal is that which is stable at room temperature in acidic aqueous solutions and that all others fall into the categories of lower and higher oxidation states. Examples of "normal" states therefore would be Ag^+, Fe^{3+}, and Pd^{2+}.

Next it is worthwhile to review briefly the conditions under which both very low and very high oxidation states may be produced. Although many of these species may not be of importance in connection with phenomena such as corrosion, they provide extremely important information bearing on the question of specific ligand properties in relation to oxidation state stabilization.

Methods for the Formation of Species Representative of Lower Oxidation States

Among the transitional elements, there are only a few examples of oxidation states < 0 and some of these are still subject to question. Hurd and coworkers (5) have produced Mn^{3-} in $H_3Mn(CO)_4$ by reducing manganese(II) iodide with Grignard reagent under pressure of carbon monoxide, while Hieber, *et al.* (6) have reported the apparent M^{2-} state in anions corresponding to the carbonyl hydrides of the type $H_2M(CO)_4$ where M = Fe, Ru, Os. A few examples of the 1- oxidation state are also found among the carbonyl hydrides such as $HCo(CO)_3$ (6); similar related compounds of Mn, Fe, Ni, Rh, Ir, and Re have also been reported, but are less well characterized. A hydrated Re^- ion has been reported to result from the reduction of potassium perrhenate with potassium in wet ethylenediammine (7) and the corresponding and reportedly pure Li^+Re^- is believed to result from the analogous reaction in aqueous solution (8). More recent work (9) however has questioned the character of this ion. Furthermore, efforts to produce K^+Re^- by the reduction of K_2ReBr_6 and other rhenium salts with solutions of potassium in liquid ammonia have been unsuccessful (10).

The classical example of a compound of a transitional element in the zero oxidation state is that of nickel carbonyl which is formed by direct union (11)

$$Ni + 4CO \rightarrow Ni(CO)_4$$

and hence without change in oxidation state of the metal; iron carbonyl, $Fe(CO)_5$, is formed similarly. The status of CO as a ligand that operates to stabilize metals in lower oxidation states is of particular interest. Owing to its strong reducing properties, this ligand is commonly employed as the primary reductant that produces the lower oxidation states, thus at 200° and 200 atm (6),

$$OsO_4 + 9CO \rightarrow Os(CO)_5 + 4CO_2$$

Other ligands that similarly serve to reduce and to stabilize the reduction product in lower oxidation states include C_6H_5NC and $(C_6H_5)_3P$. Somewhat stronger reducing conditions are necessary in some instances to produce species corresponding to the zero oxidation state; that most commonly employed consists of solutions of alkali metals in liquid ammonia at or below −33.5°. Typical examples involving ligands that might reasonably be expected to stabilize the zero state include,

$$K_2Ni(CN)_4 + 2K^+ + 2e^- \rightarrow K_4Ni(CN)_4 \quad [12]$$

$$K_2Pd(CN)_4 + 2K^+ + 2e^- \rightarrow K_4Pd(CN)_4 \quad [13]$$

$$K_2Ni(C \equiv CR)_4 + 2K^+ + 2e^- \rightarrow K_4Ni(C \equiv CR)_4 \quad [14]$$

Somewhat less stable species result when the ligands are NH_3 and $NH_2CH_2CH_2NH_2$ ("en"), thus

$$[Pt(NH_3)_4]Br_2 + 2K^+ + 2e^- \rightarrow [Pt(NH_3)_4] + 2KBr \quad [15]$$

$$[Ir(NH_3)_5Br]Br_2 + 3K^+ + 3e^- \rightarrow [Ir(NH_3)_5] + 3KBr \quad [16]$$

$$[Os(NH_3)_6]Br_3 + 3K^+ + 3e^- \rightarrow [Os(NH_3)_6] + 3KBr \quad [17]$$

and

$$[Pt(en)_2]I_2 + 2K^+ + 2e^- \rightarrow [Pt(en)_2] + 2KI \quad [18]$$

The other procedure most commonly employed is that of using a reducing agent (other than the ligand) in the presence of the ligand that stabilizes the zero state. These reactions can be carried out in a variety of media; they are perhaps best illustrated by the extensive work of Malatesta and his associates (19) on the synthesis and characterization of isonitrile complexes of transitional metals in the zero oxidation state, thus

$$2Ni(C_2H_3O_2)_2 + 8CH_3CN + N_2H_4 + 4KOH \rightarrow$$
$$2Ni(CNCH_3)_4 + 4KC_2H_3O_2 + N_2 + 4H_2O$$

$$2MoCl_3 + 12C_6H_5NC + 3Mg \rightarrow 2Mo(CNC_6H_5)_6 + 3MgCl_2$$

where the latter reaction is carried out in aqueous acetic acid. There are numerous variations on this approach that provide a wide variety of zero oxidation state complexes in which numerous types of ligands are incorporated (4).

The 1+ oxidation state is of course characteristic of Cu, Ag, and Au and is otherwise rather common also. There are numerous species in which this oxidation state appears to be reasonably well established for cobalt (20-24), *e.g.*, (25,26),

$$K_3Co(CN)_6 + 2K^+ + 2e^- \rightarrow K_4Co(CN)_4 + 2KCN$$

rhodium (23, 27, 28), ruthenium and osmium (29), and manganese and rhenium (30). Somewhat less stable species have also been detected (18),

$$[Pt(en)_2]I_2 + K^+ + e^- \rightarrow [Pt(en)_2]I + KI$$

The 1+ oxidation state of mercury is of course well known and there is recent evidence that is compatible with the view that Zn^+ and Cd^+ may be formed by the anodic oxidation of the corresponding metals (31). Since this approach to the formation of lower oxidation states is considered elsewhere (32), it is not discussed further here.

Methods for the Formation of Species Representative of Higher Oxidation States

The 2+ and 3+ oxidation states are for the most part to be considered as "normal" in the sense stated above. Accordingly, there remains to be considered the oxidation states > 3+; these may for present purposes be disposed of more simply and for two reasons. First, these are the oxidation states that, in processes such as corrosion, are more likely to represent the final states and are thus of less interest as intermediate species. Second, they have the common property of stabilization via combination with the two highly electronegative ligands, fluorine and oxygen.

Table I. Fluoro- and oxo-complexes of transitional metals

Fluoro-complexes

M^{3+}	M^{4+}	M^{5+}
K_3NiF_6	K_2TiF_6	KVF_6
K_3CuF_6	Cs_2MnF_6	$RbRuF_6$
$CsAgF_4$	Rb_2PdF_6	$LiIrF_6$
$CsAuF_4$	Na_2ReF_6	$CsNbF_6$

Oxo-complexes

M^{3+}	M^{4+}	M^{5+}	M^{6+}
Rb_5CuO_2	Ba_2CrO_5	$LiCrO_4$	Cs_2FeO_4
$Ba(CuO_2)_2 \cdot H_2O$	$SrFeO_4$	K_3FeO_4	Na_2CoO_4
	K_2NiO_3	$Ba_3(MnO_4)_2$	

The conditions under which stabilization of higher oxidation states may be realized has recently been reviewed by Klemm (33); this is largely a review of the work of Klemm, Scholder, and their students. It is sufficient here to list typical examples of fluoro and oxocomplexes of transitional metals in the 4+, 5+, and 6+ oxidation states, as well as the 3+ state for cases in which this is not to be considered as the "normal" oxidation state (Table I).

In addition to fluorine and oxygen, only a relatively few other ligands appear to be particularly effective in the stabilization of higher oxidation states. The paraperiodate, $(IO_6)^{5-}$, and orthotellurate, $(TeO_6)^{6-}$, anions have long been known to stabilize Ag^{3+} (34) and Cu^{3+} (34, 35). The 3+ oxidation state of nickel is stabilized in combination with triethylphosphine (36) and the 4+ with o-aminothiophenol (37). Both the 3+ and 4+ oxidation states of nickel are stabilized by the bidentate ligand (38, 39),

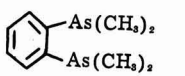

The foregoing all too brief account of the conditions under which both low and high oxidation states may be produced and stabilized should at least be sufficient to emphasize that recent years have witnessed a vast accumulation of information concerning some rather unusual chemical species. It is not much of an exaggeration to suggest that future work will provide examples of transitional metals stabilized in every reasonably conceivable oxidation state. This more extensive experimental background together with a more complete understanding of the nature of metal-ligand bonds should lead to that which is not now possible, *i.e.*, reliable predictions as to the conditions under which unusual oxidation states should be anticipated and their relative stabilities. Despite inadequate information, the paragraphs that follow represent efforts in the direction of generalization together with recognition of the inevitable exceptions.

Generalizations

Most of the complexes with which we are concerned involve bonds (interactions) between a metal atom or ion and a highly electronegative atom in the ligand molecule or ion; usually nitrogen or oxygen, less commonly sulfur, halide ions, phosphorus, or arsenic. In general, the early members of each transition series form somewhat more stable complexes with oxygen-containing ligands; in the 3d series this tendency is also exhibited by Mn^{2+} and Fe^{3+}. With increase in atomic number in each series, there is an increasing tendency toward preferential bonding to nitrogen; this tendency persists to and is indeed pronounced in the last two members of each series. Deductions of this kind arise from experimental observations commonly made during the course of synthesis under conditions that are competitive with respect to available ligands. While a beginning has been made toward a rationalization of such trends in terms of modern theory (40, 41), we are still far from achieving a complete understanding.

It is possible to generalize, also in a qualitative manner, with respect to the functionality of ligands. Thus, it is usually true that (for the same ligand atoms), complexes with bidentate ligands are more stable than those with monodentate ligands. This is the so-called "chelate effect" (42-45) which of course extends to tri and other polydentate ligands. Although there is an abundance of examples to support this generalization, there are also cases that emphasize that the increment of difference in stability may be quite small (15, 18). Such generalizations *per se*, however, are not very diagnostic with respect to the stabilization of high *vs.* low oxidation states.

A possibly more useful criterion, but one that involves important contradictions, is that of stability as a function of the electronegativity of ligand atoms. The most electronegative ligand atoms, fluorine and oxygen, are those most effective in stabilizing higher oxidation states. Furthermore, electronegativity increases among the halogens from iodine to fluorine and this parallels their effectiveness in the stabilization of higher oxidation states. On the other hand, carbon monoxide is also a highly electronegative ligand but it is essentially ineffectual in the stabilization of high oxidation states. Rather to the contrary, carbon monoxide is most effective in stabilizing lower oxidation states, notably the zero state in the metal carbonyls and their simple substitution products. Arguments may be advanced to show that the more highly electronegative ligands should be more effective in stabilizing lower oxidation states, and there is a considerable body of experimental evidence in support of this view (46). One inescapably reaches the conclusion, however, that the electronegativity of ligands is an important but by no means definitive factor.

Another type of correlation, also of limited utility, can be made on the basis of the old effective atomic number (E.A.N.) rule of Sidgwick. For spin-paired complexes, we consider that an atom or ion combines with ligands in a number such as to achieve the electronic configuration of the next inert gas. Thus, the nickel atom ($Z = 28$) should and does combine with four carbon monoxide ligands to achieve the krypton configuration ($Z = 36$). Similarly the stability of $[Pt(NH_3)_4]$ can be attributed to its correspondence to the radon configuration [*i.e.*, $Z_{Pt} = 78 + (4 \times 2e^-) = Z_{Rn} = 86$]. For most cases involving odd numbers of electrons, stability is achieved through dimerization. The deficiencies of this approach, however, are that (*a*) the E.A.N. rule generally does not apply to the early members of each transitional series, and (*b*) complexes are known that involve electrons in excess of the number corresponding to the anticipated inert gas configuration, and (*c*) the E.A.N. rules do not take into account the spatial requirements of specific ligands.

Finally, we come to the only basis that leads to any reasonable understanding of the reasons for stabilization of different oxidation states, *i.e.*, the detailed character of the metal-ligand bonds. Since these ideas have recently been elaborated by Chatt (4), they are presented in less detail here. The tentative conclusions that one reaches can be summarized as follows.

The availability of π-bonding orbitals on the ligand atom usually results in enhanced stability as compared with the case in which only σ bonds can be formed. Thus, complexes of the type $M(NR_3)_4$ are much less stable than $M(PR_3)_4$ and this is attributed to the available π-orbitals on the ligand phosphorus atom. If these π-type orbitals are vacant, electrons from the central metal atom or ion can occupy these relatively low energy orbitals. Thus addition of electrons to the d-orbitals of the metal ion is facilitated and the lower oxidation states are accordingly stabilized. If, on the other hand, the π-bonding ligand orbitals are filled, electrons from the central metal ion must occupy the higher energy antibonding π-orbitals. Consequently, the energy requirement for oxidation is less and the achievement of higher oxidation states is favored. This state of affairs is favorable to enhanced stability of higher oxidation states. In either of these situations the greater the electronegativity of the ligand atom the greater the stabilization should be. The ligand atoms of the elements of the first period in the periodic table, and more particularly the most electronegative ones, *i.e.*, N in NH_3, the primary amines, etc.; O in H_2O and OH^-, and F^- should thus be the most effective in stabilizing higher oxidation states. Ligands with vacant π-orbitals, *e.g.*, CO, NO, R_3P, R_3As, etc., should accordingly tend to stabilize lower oxidation states.

None of these generalizations however should be taken too literally in view of the exceptions that remain to be understood. It has recently been demonstrated, (47) for example, that the π-bonding ligand, $(C_6H_5)_2As\text{-}CH_2\text{-}CH_2\text{-}As(C_6H_5)_2$ is readily replaced by iodide ion which would be either σ-bonding or less strongly π-bonding. Similarly, the exclusively σ-bonding NH_3 ligand should not be expected to stabilize lower oxidation states and yet,

as shown above, ammines of Os, Ir, and Pt exhibit stabilities greater than would be predicted.

There is much more that could be included here with reference to more specific details of particular types of ligands and more especially those having intermediate properties (4). However, it seems sufficient for present purposes to emphasize that, under any practical circumstances, the metal oxidation state that achieves stability is very much a function of its environment in the sense of availability of specific types of ligands. Much remains to be learned before predictions can be made on other than a very qualitative basis.

Acknowledgments

Support of the writer's research program in this area by the U.S. Atomic Energy Commission, Contact AT-(40-1)-1639 and by The Robert A. Welch Foundation is gratefully acknowledged.

Manuscript received Oct. 17, 1960; revised manuscript received Jan. 13, 1961. This paper was prepared for delivery at a special symposium of the Corrosion Division on Unusual Valence States and the Difference Effect at the Houston Meeting, Oct. 9-13, 1960.

Any discussion of this paper will appear in a Discussion Section to be published in the December 1961 JOURNAL.

REFERENCES

1. J. Kleinberg, W. J. Argersinger, Jr., and E. Griswold, "Inorganic Chemistry," p. 128, D. C. Heath and Co., Boston (1960).
2. M. J. Copley, L. S. Foster, and J. C. Bailar, Jr., *Chem. Revs.*, **30**, 227 (1942).
3. J. Kleinberg, "Unfamiliar Oxidation States and Their Stabilization," University of Kansas Press (1950).
4. J. Chatt, *J. Inorg. Nuclear Chem.*, **8**, 515 (1958).
5. D. T. Hurd, G. W. Sentell, and F. J. Norton, *J. Am. Chem. Soc.*, **71**, 1899 (1949).
6. W. Hieber, "Fiat Review of German Science," Part II, p. 108 (1948).
7. J. B. Bravo, E. Griswold, and J. Kleinberg, *J. Phys. Chem.*, **58**, 18 (1954); *Science*, **115**, 375 (1952).
8. A. V. Grosse, *Z. Naturforsch.*, **8b**, 533 (1953); J. G. Floss and A. V. Grosse, *J. Inorg. Nuclear Chem.*, **9**, 318 (1959).
9. J. W. Cobble, *J. Phys. Chem.*, **61**, 727 (1957).
10. G. W. Watt and R. J. Thompson, Unpublished work.
11. L. Mond, C. Langer, and F. Quincke, *J. Chem. Soc.*, **57**, 749 (1890).
12. J. W. Eastes and W. M. Burgess, *J. Am. Chem. Soc.*, **64**, 1187 (1942).
13. J. J. Burbage and W. C. Fernelius, *ibid.*, **65**, 1484 (1943).
14. R. Nast. *Z. Naturforsch.*, **8b**, 381 (1953).
15. G. W. Watt, M. T. Walling, Jr., and P. I. Mayfield, *J. Am. Chem. Soc.*, **75**, 6175 (1953).
16. G. W. Watt and P. I. Mayfield, *ibid.*, **75**, 6178 (1953).
17. G. W. Watt and E. M. Potrafke, Unpublished work.
18. G. W. Watt, R. E. McCarley, and J. W. Dawes, *J. Am. Chem. Soc.*, **79**, 5163 (1957).
19. For references see, *e.g.*: L. Malatesta and L. Vallarino, *J. Chem. Soc.*, **1956**, 1867.
20. L. Malatesta, *Gazz. Chim. ital.*, **83**, 958 (1953).
21. A. A. Vleck, *Nature*, **180**, 753 (1957).
22. A. Sacco and M. Freni, *Ann. Chem. (Rome)*, **48**, 218 (1958).
23. B. Martin and G. M. Waind, *Proc. Chem. Soc.*, **1958**, 169.
24. N. Maki, J. Fujita, and R. Tsuchida, *Nature*, **183**, 458 (1959).
25. G. W. Watt, J. L. Hall, G. R. Choppin, and P. S. Gentile, *J. Am. Chem. Soc.*, **76**, 373 (1954).
26. G. W. Watt and R. J. Thompson, *J. Inorg. Nuclear Chem.*, **9**, 311 (1959).
27. J. Chatt and L. M. Venanzi, *J. Chem. Soc.*, **1957**, 4735.
28. W. Hieber, H. Heusinger, and O. Vohler, *Chem. Ber.*, **90**, 2425 (1957).
29. L. Vaska and E. M. Sloane, *J. Am. Chem. Soc.*, **82**, 1263 (1960).
30. D. Clauss and A. Lissner, *Z. anorg. u. allgem. Chem.*, **297**, 300 (1958).
31. D. T. Sorensen, A. W. Davidson, and J. Kleinberg, *J. Inorg. Nuclear Chem.*, **13**, 64 (1960).
32. A. W. Davidson, Paper presented at the Houston Meeting of the Electrochemical Society, October, 1960.
33. W. Klemm, *J. Inorg. Nuclear Chem.*, **8**, 532 (1958).
34. L. Malatesta, *Gazz. Chim. ital.*, **71**, 467, 580 (1941).
35. M. W. Lister, *Can. J. Chem.*, **31**, 638 (1953).
36. K. A. Jensen and B. Nygaard, *Acta Chem. Scand.*, **3**, 474 (1949).
37. W. Hieber and R. Bruck, *Naturwissenschaften*, **36**, 312 (1949).
38. R. S. Nyholm, *J. Chem. Soc.*, **1950**, 2061.
39. R. S. Nyholm, *ibid.*, **1951**, 2602.
40. F. Basolo and R. G. Pearson, "Mechanisms of Inorganic Reactions," p. 60, John Wiley & Sons, Inc., New York (1958).
41. J. Lewis and R. G. Wilkins, "Modern Coordination Chemistry," Interscience Publishers, Inc., New York (1960).
42. G. Schwarzenbach, *Helv. Chim. Acta*, **35**, 2344 (1952).
43. A. W. Adamson, *J. Am. Chem. Soc.*, **76**, 1578 (1954).
44. F. A. Cotton and F. E. Harris, *J. Phys. Chem.*, **59**, 1203 (1955).
45. R. W. Parry, "Chemistry of the Coordination Compounds," Edited by J. C. Bailar, Jr., p. 220-252, Reinhold Publishing Corp., New York (1956).
46. See, *e.g.*, S. Ahrland and J. Chatt, *J. Chem. Soc.*, **1957**, 1379.
47. G. W. Watt and R. Layton, Unpublished work.

Optical Properties of Anodic Oxide Films on Tantalum, Niobium, and Tantalum + Niobium Alloys, and the Optical Constants of Tantalum

L. Masing, J. E. Orme, and L. Young

British Columbia Research Council, University of British Columbia, Vancouver, British Columbia, Canada

ABSTRACT

The reflectivity of anodized electropolished tantalum was measured as a function of angle of incidence for 4358Å light polarized in the plane of incidence. The principal aim of these measurements was to obtain the refractive index of the oxide. This is needed to determine absolute thicknesses of oxide by the spectrophotometric method in which the wavelengths of minimum reflectivity due to interference at near normal incidence are determined. The measurements also provided a method of determining the optical constants of the metal, without assuming that the surface is perfectly flat or that an unanodized surface is free from oxide. It was found that films formed on tantalum in 0.2*N* H_2SO_4 have a thin outer layer of light-absorbing oxide. The bulk of the film is, however, nonabsorbing and homogeneous. A large part of the thickness of films formed in concentrated sulfuric acid absorbs light. The refractive index at 4358Å wavelength of films formed in dilute solution increases by about 0.3% per tenfold decrease in the current density at which they are made and by about 0.06% per 10°C rise in the temperature at which they are made. The refractive indices of films formed on niobium, on 25 a/o Ta + 75 a/o Nb, and on 25 a/o Nb + 75 a/o Ta were estimated and a preliminary study was made of films on zirconium.

In the comparative study of the growth of anodic oxide films on metals such as tantalum, niobium, tungsten, zirconium, etc., it is desirable to be able to determine the absolute thickness of the film with an accuracy of better than 1%. The spectrophotometric location of the wavelengths of the minima due to interference in the specular reflectivity at near normal incidence (1) enables this to be done if the refractive index of the oxide is known at one wavelength and if the oxide is essentially homogeneous. The present type of measurement, that is, the measurement of the intensity reflectivity as a function of angle of incidence for increasing thicknesses of oxide with monochromatic light polarized in the plane of incidence, gives the refractive index in certain cases, in particular when the oxide is homogeneous. The measurements themselves give information on whether the oxide is in fact homogeneous.

The present type of measurement therefore provides a second optical method for the investigation of these films which is complementary to the spectrophotometric method of determining the thickness. As a method of obtaining the refractive index, the present measurements have the advantage over "immersion" methods of not requiring the removal of the film from the surface of the metal, a process which is easy with films formed on tantalum surfaces prepared in certain ways but not in others, and which is never easy with films on many of the other metals concerned.

The theory of the reflectivity of metals coated with homogeneous oxide films is relatively old and is well established.[1] Reference is made to the reviews by Winterbottom (4) and by Heavens (5, 6). The present method of obtaining the refractive index is a development of a method due to Abelès (7). The first measurements on tantalum oxide films using light polarized in the plane of incidence were reported by Heavens and Kelly (8) and by Kelly (9). Their results are discussed in a later section. The method of obtaining the optical constants of the metal appears to be new.

Basic Theory of the Method

The amplitude reflectivity of the oxide coated metal is assumed to be given by

$$R = \frac{r_1 + r_2 e^{-2i\delta}}{1 + r_1 r_2 e^{-2i\delta}} \qquad [1]$$

where r_1 and r_2 are the Fresnel coefficients for light incident from the air side on the oxide/air and metal/oxide interfaces, respectively, and $\delta = [(2\pi n_1 D \cos\psi_1)/\lambda]$, where n_1 and D are the refractive index and thickness of the oxide, respectively, ψ_1 is the angle of refraction in the oxide, and λ is the wavelength. The intensity of reflection is $|R|^2$. For light polarized in the plane of incidence, that is for p-light, and for examination in air:

[1] This is despite the remarks by MacSwan (2) repeated by Miller (3). The use of Smith's charts, proposed by MacSwan, is a computational device and the theory is otherwise the same as previously developed. MacSwan is correct in that, as Heavens (6) also has indicated, the correct theory has not always been applied. It is as appropriate to describe the colors as interference colors as it is to apply this term to the colors produced when the films do not have an opaque substrate.

$$r_1 = \frac{\cos\psi_1 - \overline{n_1}\cos\psi_0}{\cos\psi_1 + \overline{n_1}\cos\psi_0}$$

$$r_2 = \frac{\overline{n_1}\cos\psi_2 - \overline{n_2}\cos\psi_1}{\overline{n_1}\cos\psi_2 + \overline{n_2}\cos\psi_1}$$

where ψ_0 = angle of incidence, $\overline{n_1} = n_1 - ik_1$ where n_1 and k_1 are the indices of refraction and absorption of the oxide, and $\overline{n_2} = n_2 - ik_2$, where n_2 and k_2 are the corresponding quantities for the metal and $i = \sqrt{-1}$. ψ_1 and the angle of refraction in the metal ψ_2 are given by Snell's law, *i.e.*, $\sin\psi_0/\sin\psi_1 = \overline{n_1}$; and $\sin\psi_1/\sin\psi_2 = \overline{n_2}/\overline{n_1}$. The modulus of the Fresnel coefficient gives the relative amplitude of the reflected ray; the argument of the Fresnel coefficient gives the phase change on reflection.

It will be seen that, particularly when the oxide absorbs ($k_1 \neq 0$), the calculations, although elementary, become very long since nearly all the quantities involved are complex (*i.e.*, of the form $x + iy$, where $i = \sqrt{-1}$). In the present work, numerical calculations were normally made using the ALWAC III E electronic digital computer of the University of British Columbia computing center. Two programs were written, one for absorbing oxide and one for nonabsorbing oxide. Both programs utilized an "algebraic compiler" program due to G. A. Bachelor and J. R. H. Dempster. "Floating point" arithmetic is used by this program. The outputs included r_1, r_2, and R for successive thicknesses of oxide and angles of incidence as controlled by the input.

There are two simple cases. These are (i) a homogeneous oxide which does not absorb light, and (ii) a homogeneous absorbing oxide. The behavior may be understood qualitatively[2] by noting that in Eq. [1] the denominator is relatively close to unity. Thus, the behavior of R is dominated by the numerator. The numerator is the vector sum of r_1 and $r_2e^{-2i\delta}$. With a nonabsorbing oxide, r_1 is real and negative for angles of incidence from zero (normal incidence) to the Brewster angle θ, defined by $\tan\theta = n_1$. It decreases in modulus as ψ_0 increases and becomes precisely zero at $\psi_0 = \theta$. Beyond the Brewster angle, r_1 is real and positive and increases rapidly with increasing ψ_0. The term $e^{-2i\delta}$ represents the effect of the phase difference due to the path length of the oxide and this causes the vector $r_2e^{-2i\delta}$ to rotate clockwise about the end of r_1. The vector sum R is a maximum when the two vectors are in line and a minimum when $r_2e^{-2i\delta}$ doubles back on r_1. The vector diagrams of Fig. 3 will be found useful in understanding these arguments. At near normal incidence with tantalum $|r_1| \simeq |r_2|$, so that the ratio of maximum to minimum reflectivity is very large: hence the brightness of the interference colors and the accuracy of the spectrophotometric method for thickness. The reflectance of nonabsorbing oxide as a function of thicknes for angles of incidence equal to the Brewster angle and just above and below the Brewster angle is shown in Fig. 1. At the Brewster angle the reflectivity (in p-light) is independent of the thickness of oxide and would be equal to that of the bare substrate. In principle, in order to determine the refractive index one need only determine the angle of incidence at which the reflectivity is independent of thickness.

[2] The full expressions were, of course, used in the calculations.

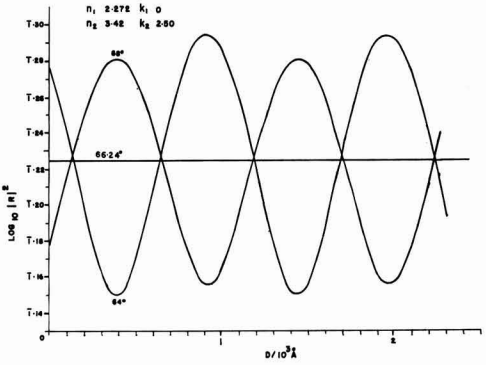

Fig. 1. Calculated plots of reflectivity vs. thickness of oxide near the Brewster angle for nonabsorbing oxide. This and later graphs all refer to p-light.

With an absorbing oxide, $|r_1|$ goes through a minimum at the Brewster angle, but does not become zero. Also, arg r_1, instead of changing discontinuously from π to 0 at $\psi_0 = \theta$, changes gradually from π to 0 over a range of angles near θ. Furthermore, δ is now complex so that $|r_2e^{-2i\delta}|$ decreases with increasing D. The reflectivity at angles of incidence near the Brewster angle changes with thickness as shown in Fig. 2. It will be seen that the "phase" of the cyclical fluctuation of the reflectivity with thickness at the Brewster angle is a little less than $\pi/2$ ahead of the phase at angles a few degrees less than the Brewster angle and a little less than $\pi/2$ behind that at angles a few degrees greater than the Brewster angle. The reflectivity decreases with increasing D till eventually $|R|^2 = |r_1|^2$.

Experimental Procedure

The tantalum specimens were cut from Fansteel Metallurgical Corporation "Capacitor Grade" sheet 0.05 in. thick. The prepared surface was ¾ x 1 in. in the earlier experiments and ½ x ¾ in. in the later experiments. The light beam (2.4 mm diameter) in-

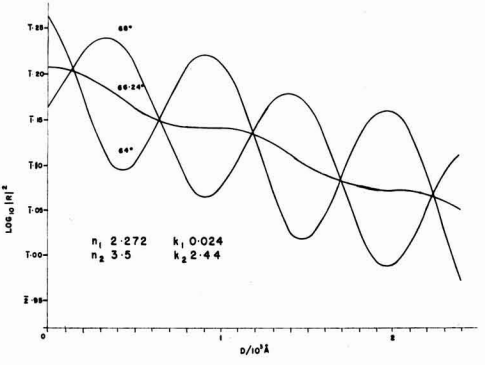

Fig. 2. As Fig. 1 except that for a homogeneous absorbing oxide.

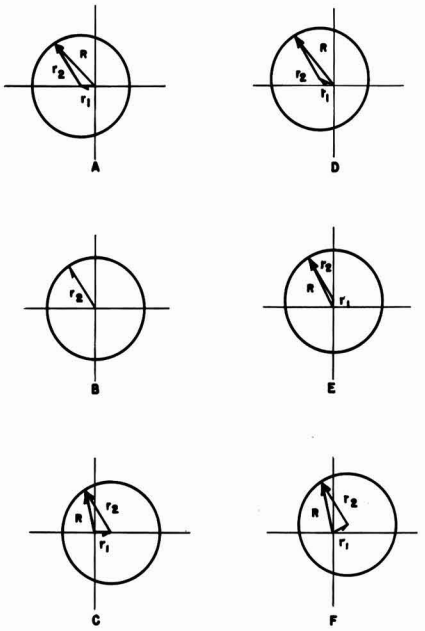

Fig. 3. $r_1 + r_2 e^{-21\delta}$ (see text). Left column: nonabsorbing oxide; right column; thin outer layer of absorbing oxide. Top row: $\psi_0 < \theta$; middle row $\psi_0 = \theta$; bottom row $\psi_0 > \theta$.

tersected only a very small fraction of this area, but it is easier to prepare a small flat area if this forms part of a larger area. The whole specimen was first chemically polished. The working surface was then taken through metallurgical papers in the usual way. In the earlier work, the surface was given a preliminary metallographic polish, but this step was omitted in later work. Finally, the surface was electropolished in a bath containing 1:9 by volume of 49% HF and 96% H_2SO_4 at an initial temperature of about 35°C. The surface was accepted if it had a sufficiently high reflectivity at a given angle of incidence (in the later work: 15.8% at 66°). The polishing electrolyte was contained in a cell machined from a block of Teflon in which a Teflon propeller impelled the solution round a rectangular circuit. The block also contained a circuit for thermostatted water. The optimum conditions depend on the shape of the specimen and its preparation. In our experiments the applied current was normally about 100 ma cm^{-2}. The quality of the surface obtained is illustrated by Fig. 4. The tab was insulated by a thick layer of anodic oxide. This layer was laid down after stopping-off with picien, since without a stopping-off compound the oxide "sparks" at the meniscus during formation. The picien was then removed by vapor degreasing with trichloroethylene. Normally, before the first formation, the specimen was also cleaned in $K_2Cr_2O_7 + H_2SO_4$ mixture, washed, immersed in 49% HF for a few seconds, washed, immersed again in the chromic mixture, and washed. The surface was usually immersed in chromic mixture before each set of measurements.

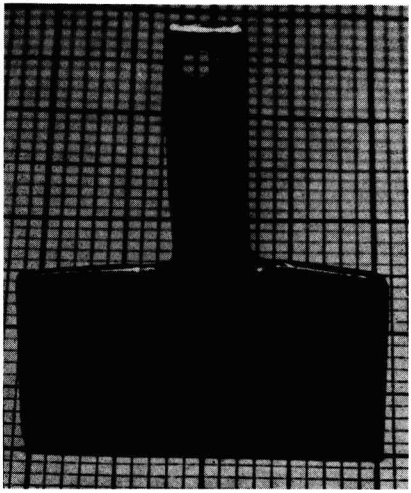

Fig. 4. Photograph of specimen reflecting squared paper.

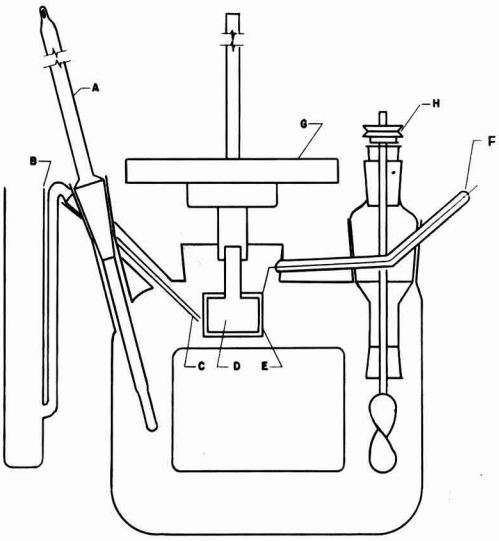

Fig. 5. Diagram of cell: A, thermometer; B, saturated calomel electrode well; C, Luggin-Haber capillary; D, specimen; E, platinum cathode plate (one only of two shown); F, cathode terminal; G, prism table and specimen mount; H, shaft of propeller.

The niobium was also Fansteel material. The alloys were melted and rolled by the staff of the Bureau of Mines, Ottawa.

The films were formed in the cell shown in Fig. 5. The electrolyte was circulated in order to avoid a local temperature rise in the oxide during polarization at the higher current densities. Formation was at constant current and was controlled using the automatic electronic equipment described previously (1).

The reflectivity in polarized light was measured as a function of angle of incidence using the equipment illustrated in Fig. 6. The 4358Å line from a 100-w mercury lamp (normally, G.E. type H4AB) was se-

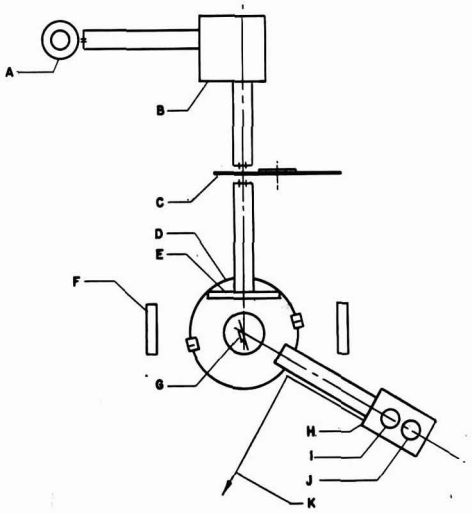

Fig. 6. Diagram of reflectometer: A, mercury lamp source and blower; B, monochromator (constant deviation prism); C, chopper (synchronous driving motor not shown); D, spectrometer; E, nicol polarizer circle and aperture plate; F, framework supporting cloth light shield; G, specimen; H, photomultiplier enclosure; I, removable eyepiece and cross-hair tube; J, photomultiplier tube; K, power and signal leads for photomultiplier.

lected using a monochromator and chopped at 1470 cps to produce an a-c signal. This is easier to amplify than a d-c signal and is less affected by stray light and by changes in the dark current through the photocell. The specimen was mounted rigidly on a bracket bolted to the prism table of a standard spectrometer. The specimen was not demounted from the prism table until the end of the experiment. The specimen and prism table were removed as one unit when it was required to form the films. This procedure was adopted in order to ensure that the same area was examined throughout. The width of the area examined depends of course on the angle of incidence. The specimen was carefully aligned so that the center of the illuminated area was at the same point on the surface independent of the angle of incidence. The collimated light was polarized with a nicol prism and reflected from the specimen. The telescope was aligned using an eyepiece with cross-hairs. The eyepiece could be removed to allow the light to strike a ground-glass plate in front of an RCA 1P21 photomultiplier. The cross-hairs were adjusted to give coincidence with the position of maximum response of the photocathode. The whole optical apparatus was mounted on a 3 ft 6 in. length of 18 in. wide channel iron. The signal from the photomultiplier was amplified by a tuned negative feedback amplifier and was measured using a null system with a potential divider and standard reference voltage. The ratio of the gain settings for direct and reflected beams gave the percentage reflectivity. The undeflected beam was measured after each measurement of the reflected beam and was plotted as a function of time. The times were recorded at which readings of the reflected beam were made,

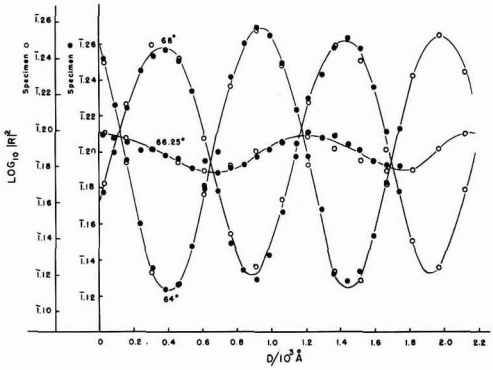

Fig. 7. Experimental reflectivity vs. thickness plot for films formed on tantalum in dilute solution at 10 ma cm^{-2} and 25°C. Two specimens O and • with vertical shift (as shown by scales) to superimpose. Different specimens from those of Fig. 13. The curves are not calculated.

and the corresponding values for the undeflected beam were read from the plot. The scatter in the percentage reflectivity readings may be judged from the experimental results given here. The accuracy of the percentage reflectivity (as obtained by assuming linearity of the response curve of the photomultiplier + amplifier) was checked by using standardized photographic and grid filters. It was believed to be better than 0.5%.

Results

Properties of Films Formed on Tantalum in Dilute Solution (0.2N H_2SO_4)

Presence of thin outer layer of absorbing oxide.— Typical experimental plots of reflectivity *vs.* thickness at angles of incidence near the Brewster angle of the oxide and at about 2° on either side of this angle are given in Fig. 7. The thicknesses were obtained by determining the final thickness using the chart of thickness *vs* wavelengths of minimum reflectivity at 11° incidence given previously (1) and by then assuming that the thicknesses of intermediate films were proportional to the oxide overpotential. Where, in this paper, the experimental curves are compared with theoretical curves calculated on a particular value of the index of the oxide the appropriate small correction has been made to the estimates of thickness. The same behavior (Fig. 7) was obtained with electropolished surfaces with and without a preliminary etch in HF to remove the invisible film left by electropolishing and also with and without an immersion in $K_2Cr_2O_7 + H_2SO_4$ after each formation. Less complete data were obtained with surfaces vapor degreased in trichloroethylene, but these were consistent with the other results.

The essential points are as follows. First, the reflectivity returns to the same value after each cycle. There is no continued decrease of the kind illustrated in Fig. 2. This point is also illustrated in Fig. 13. This shows that the bulk of the oxide does not absorb light at this wavelength. More precisely, comparison with calculated curves shows that k_1 for the bulk of the oxide is less than about 0.0004. Sec-

ond, at no angle is the reflectivity independent of the thickness. The plots of reflectivity *vs.* thickness are distorted sinusoidal waves. The amplitude of the oscillation goes through a minimum, but this is not zero as it would be if the oxide did not absorb. Third, the "phase" changes gradually through nearly π as a range of angles of incidence near the Brewster angle is traversed, instead of changing discontinuously by π at the Brewster angle.

There seems to be only one explanation of these results. This is that there is a thin outer layer of oxide which absorbs light. This layer need be only a few angstroms in thickness. This two-layer model may be treated in a good approximation by taking the absorbing layer to cause r_1 in Eq. [1] to behave like the Fresnel coefficient of an absorbing oxide, whilst δ (the path length) remains real (rather than becoming complex as it would if the whole thickness absorbed light). Furthermore, we neglect any slight reflection at the junction between the absorbing layer and the rest of the film. This model is easily seen (by considering the vector diagrams for $r_1 + r_2 e^{-2i\delta}$ on the right hand side of Fig. 3) to account qualitatively for the observations and it will be shown in a later section to account quantitatively for the results.

The thin outer layer cannot be identified with the film present before anodization since the effect of the nature of the pre-existing film on the adhesion of the anodic oxide to its substrate seems to prove that the pre-existing film must remain between the metal and the anodic oxide (10). The absorbing layer must be on the outside rather than the inside, since, if the outer layer did not absorb, $|r_1|$ would be zero at the Brewster angle, and the reflectivity at this angle would be independent of thickness.

Determination of the refractive index of the oxide. —To obtain the refractive index of a homogeneous nonabsorbing oxide, the reflectivity would be plotted against the angle of incidence for a succession of thicknesses of oxide. These plots would intersect at the Brewster angle $\theta = \tan^{-1} n_1$. In the present case, the plots must be taken at selected critical thicknesses, that is at thicknesses giving maxima or minima in the plots of reflectivity *vs.* thickness. Actually, as will be discussed later, the thicknesses giving extreme values at $\psi_0 = 64°$ are not quite the same as those giving extreme values at $\psi_0 = 68°$, but this difference is not important in the present application. Typical experimental data are given in Fig. 8. The plots in Fig. 8a and 8b are for films on two specimens, which were treated identically except that one specimen was prepared with the normal good finish, and the other deliberately prepared with a rough surface. The aim of this experiment was to find if the results could be in error due to the fact that even the best surfaces were, of course, not perfectly flat. Since the surfaces normally used were the best we could make, this point was tested by examining less flat surfaces. It was found that the angle of intersection was the same within experimental error, and, in fact, the two plots could be superimposed by a vertical shift, when plotted as the logarithm of the reflectivity. Evidently the effect of surface imperfections was to reduce the reflectivity by a factor which was constant over the limited range of angles concerned and was independent of the thickness of oxide.[8] By within experimental error we mean that the t-test applied to the data from these identical experiments with two specimens, one rough and one smooth, gave no statistically significant difference (see, however, footnote on page 433).

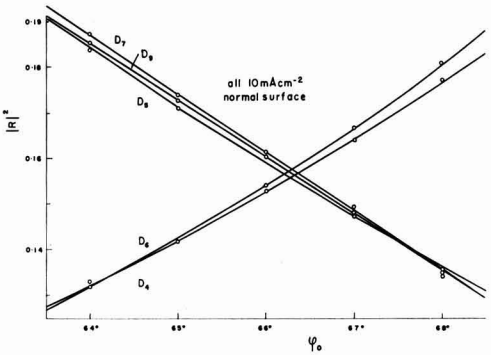

Fig. 8. Experimental plots of reflectivity vs. angle of incidence for successive film thicknesses: (a) normal surface; (b) rough surface; (c) successive pairs of films formed at 0° and 94.5°C both at 25 ma cm^{-2}.

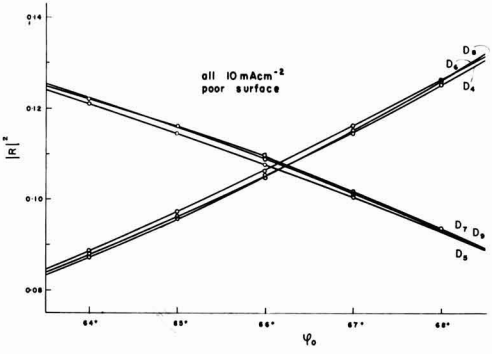

Fig. 8b

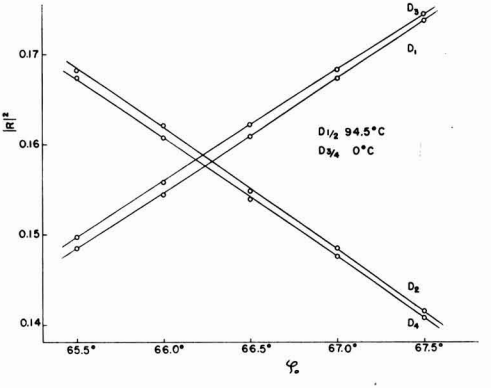

Fig. 8c

[8] The reflectivities observed were slightly higher than those reported by Heavens and Kelly (8).

The angle of intersection was always independent within experimental error of the thicknesses of the pair of films giving the intersection. (This was for "critical" thicknesses; if arbitrary thicknesses were used the intercept would fluctuate with increasing thickness.)

Strictly, the refractive index determined in this way is that of the outer layers of the oxide. However, as will be shown, a good fit is obtained with $|R|^2$ *vs.* D plots calculated with this index. Furthermore, the index obtained in this way is in good agreement with the value $n_1 = 2.26$ (3) at 4358Å calculated from the expression $n_1(\lambda) = 2.14 + 0.292/(\lambda/10^3\text{Å} - 2.305)^{1.2}$ previously reported by Young (1) (see this reference for other values previously reported). This expression for $n_1(\lambda)$ was for films formed at 25°C and 10 ma cm^{-2} and was based on (i) a value of the index of stripped films obtained in sodium light by the Becke immersion method using the standard S + Se melts of Merwyn and Larsen (11), and (ii) on information on the dispersion obtained from spectrophotometric data. The immersion method depends on the critical angle of reflection of the broken edge of the stripped oxide. The spectrophotometric data measure the average index as indicated by the path length δ. The value of $n_1(\lambda)$ was claimed to be reliable within about ±1%. Thus the agreement of this and the present values within the experimental errors confirms the previous result that the index is constant through the thickness of the film and is independent of the total thickness.

Variation of the refractive index with the current density and the temperature at which the film is made (dilute solution).—Since one of the principal reasons for determining the index is to allow accurate thickness determinations in the study of the kinetics of growth, it is important to know how the index depends on the current density and temperature at which the film is made. We consider first steady-state conditions, that is, the conditions existing when a constant current density has been applied for a sufficiently long time.

To establish the dependence on current density two specimens were formed to the first two critical thicknesses at 25 ma cm^{-2} and 25°C, and then to the second two critical thicknesses at 0.025 ma cm^{-2}. Two further specimens were formed first at 0.025 ma cm^{-2} and then at 25 ma cm^{-2}. The reflectivity at each critical thickness was measured at 0.5° intervals near the Brewster angle. The voltages required to give the critical thicknesses were calculated from the steady-state data reported by Young (12). The final thicknesses were checked by the spectrophotometric method using the chart in reference (1). The procedure was designed to eliminate the errors that could be involved in using only one current density with one specimen, and also to eliminate any variation with thickness. Results are given in Table I. The dependence on current density is very definitely statistically significant (t-test). A similar procedure was adopted to establish the dependence on temperature (Table II). A typical reflectivity plot is shown in Fig. 8c.[4] Finally, intermediate current densities and temperatures were studied. The assembled results, including the estimated standard errors of the means are shown in Fig. 9. The size of the effect in relation to the accuracy does not permit any nonlinearity of the dependence on log i or on T to be established. A nonlinear effect would be required to cancel the nonlinear Tafel slope reported elsewhere (12). We conclude that the index increases by about 0.06% per 10°C rise in the temperature of formation and decreases by about 0.3% for a tenfold increase in current density.

[4] The accuracy was higher in the later work such as Fig. 8c than in earlier work such as Fig. 8a and 8b.

Table I. Effect of current density on refractive index

Formation at 25°C. Target thicknesses 375, 900, 1425, and 1950Å. Observed final thickness is indicated to show degree of control obtained. Specimens each formed at two current densities. Specimen numbers refer to metal substrates not to sequence of films.

Spec. No.	25 ma cm^{-2}	0.025 ma cm^{-2}	Final thickness, Å
4	2.267	2.284	1963
5	2.271	2.285	1955
6	2.267	2.293	1933
7	2.270	2.280	1940
Mean	2.269	2.286	
Error of mean	0.001	0.003	

Table II. Effect of temperature on refractive index of films formed at 25 ma cm^{-2}

Specimens formed each at two temperatures.

Spec. No.	0°C	94.5°C	Final thickness, Å
4	2.266	2.275	1952
5	2.265	2.275	1946
6	2.264	2.279	1946
7	2.260	2.273	1948
Mean	2.264	2.276	
Error of mean	0.001	0.001	

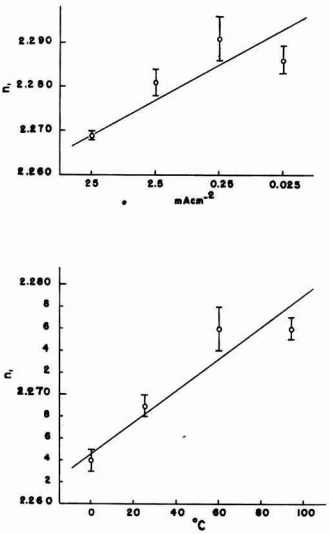

Fig. 9. Top: refractive index of oxide vs. current density of formation at 25°C (log scale); bottom: refractive index of oxide vs. temperature of formation (current density 25 ma cm^{-2}).

The field strength in the oxide that is required to give a particular ionic current depends on the history of the film. Most of this effect is believed to be due to a variation of the concentration of the mobile ions, although Vermilyea (13) has suggested that there is also some other change involving what one might call the degree of amorphousness of the oxide. Recent work shows that the oxide is brought into a state indistinguishable by kinetic measurements from the steady state by formation through only about a volt. To test whether the refractive index behaves similarly two specimens were formed to the successive critical thicknesses at 25 ma cm^{-2}. The reflectivities were measured at each critical thickness and then again after about 1.4 x 10^{-3} coulomb cm^{-2} had been passed at 0.025 ma cm^{-2}. This amount of charge corresponds to about 10Å of thickness or about 0.5 v at the lower current density. This thickness change is probably negligible. The indices obtained from the intersections of the reflectivity *vs.* angle of incidence plots are given in Table III. The results show that the index increased in statistically significant fashion during the passage of the above small amount of charge. The amount of the increase was only about ½ of that found in the steady-state conditions, but the errors must be taken into account in assessing the difference. It is concluded that a large amount of the change in index is produced by a small amount of charge passed. This result is consistent with the theory that a change in concentration of mobile ions is responsible for the change in index as well as for the change in kinetic behavoir.

Optical Constants of the Metal

The spectrophotometric method for the thickness relies on the fact that successive minima in reflectivity at a given angle of incidence and wavelength occur at thicknesses such that $(D + X) = (2r - 1)\lambda/4n_1 \cos \psi_1$ where X is a constant at a given λ and ψ_0 which takes account of the phase changes on reflection at the air/oxide and oxide/metal interfaces, and $r = 1,2,3. . .$ The increments of thickness between successive minima are $(\lambda/2n_1 \cos \psi_1)$. The method allows the identification of a film as being of a standard but not necessarily known thickness, and it also gives absolute increments of thickness. It does not give the absolute thickness unless the optical constants of the metal are known. They are not independently known for tantalum with any useful degree of accuracy. However, a nonoptical method may be used to obtain the zero point of thickness [*e.g.* (1)], and the procedure may then be reversed in order to determine the optical constants of the metal. The method adopted was to determine experimentally two quantities, which are independent of the degree of perfection of the surface finish, and which define values of n_2 and k_2 (knowing n_1), given appropriate calculated charts. The first quantity selected was the ratio of the maximum to the minimum reflectivity in plots of reflectivity *vs.* thickness (this will be called the "intensity ratio"). The second quantity selected was the "phase" of such plots as measured by the thickness to the first minimum for ψ_0 less than the Brewster angle, or to the first maximum for ψ_0 greater than the Brewster angle, divided by the thickness increment between successive minima or maxima and mutliplied by 2π. The "phase," defined in this way, is equal to arg $r_2 + (\pi - \arg r_1)$ for $\psi_0 < \theta$ and to arg $r_2 - \arg r_1$ beyond the Brewster angle. Thus, if the oxide absorbs, the phase is slightly greater than arg r_2 at $\psi_0 = 64°$, and slightly less than arg r_2 for $\psi_0 = 68°$, but unless the oxide absorbs very strongly it is almost equal to arg r_2 at $\psi_0 = 11°$. For the moment we neglect the outer absorbing layer and take the phase as giving arg r_2. Using a calculated graph, *e.g.*, Fig. 10 for $\psi_0 = 64°$, the "intensity ratio" defines a value of $|r_2|$. The effect of the absorbing layer on the estimate of $|r_2|$ is less important and will be neglected. Finally, with a chart such as Fig. 11, calculated for a given value of n_1, the values of n_2 and k_2 required to give the observed values of arg r_2 and $|r_2|$ may be read off. The result is shown in Fig. 12. From Fig. 12 and from experience in fitting calculated to experimental curves, it was concluded that $n_2 = 3.50$ and $k_2 = 2.44$ with a reliability of ± 0.1 for both n_2 and k_2.[5] Experi-

Table III. Change in refractive index on passing small amount of charge at different current density at 25°C

Spec. No.	25 ma cm^{-2} to critical thicknesses	After 1.4 x 10^{-3} coulomb cm^{-2} at 0.025 ma cm^{-2}
6	2.270	2.279
	2.271	2.274
7	2.274	2.279
	2.274	2.283
Mean	2.273	2.279
Error of mean	0.001	0.002

[5] If the oxide nearest the metal—the pre-existing film—has very different $\bar{n}_1$ from the bulk of the oxide film, this will introduce an error in the estimate of $\bar{n}_2$. However, the result did not depend detectably on which of the pretreatments listed was used. The calculations were made at an early stage in the research using $n_1 = 2.272$. This is sufficiently close to the final values obtained (Fig. 9 and Tables I and II) to obviate any need to recalculate the charts.

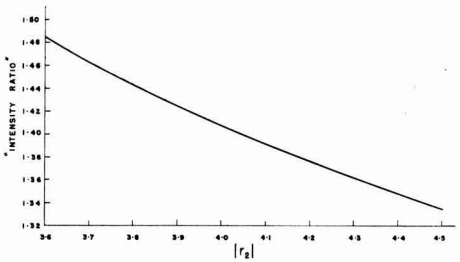

Fig. 10. Calculated "intensity ratio" (see text) vs. $|r_2|$ given $n_1 = 2.272$, and $\psi_0 = 64°$.

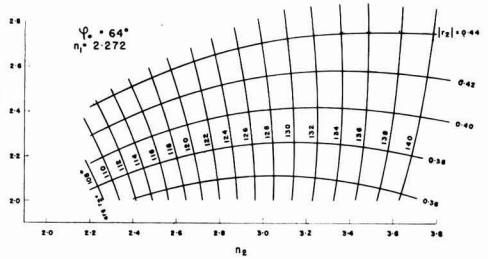

Fig. 11. Calculated chart of arg r_2 and mod r_2 as functions of n_2 and k_2 for $n_1 = 2.272$ and $\psi_0 = 64°$.

mental reflectivity data for two specimens are compared with curves calculated using these values of n_2 and k_2 in Fig. 13. The experimental data for each specimen have been shifted upward on the logarithmic reflectivity scale to allow for the imperfection of the surface. It can be seen that the fit is excellent except that, as expected, the phases of the experimental curves at 64° and 68° are slightly greater and smaller, respectively, than those of the calculated curves. Arg r_2 changes very little from $\psi_0 = 64°$ to $\psi_0 = 68°$, so that for a nonabsorbing oxide the phases of the 64° and 68° curves are very close, maxima in one curve corresponding to minima in the other. With n_2 and k_2 thus determined, the "intensity ratio" at the Brewster angle determined k_1 for the thin absorbing layer, using a calculated graph of the intensity ratio at the Brewster angle *vs.* k_1. The value found was $k_1 = 0.024 \pm 10\%$. The derived value of k_1 in turn gave arg r_1 at $\psi_0 = 64°$ and 68° (from Fig. 14), and the values found were in good agreement with the values required to explain the deviations in Fig. 12 and 13.

The values of the phase and hence of arg r_2 and of n_2 are most accurately determined at $\psi_0 = 11°$, since the minima in reflectivity are sharpest at this angle, and since the nonzero k_1 has least effect at this angle. The values used above are derived from the values of X given previously (1), and these were confirmed by further experiments. This gave arg $r_2 = 138 \pm 1°$ (at this wavelength and ψ_0).

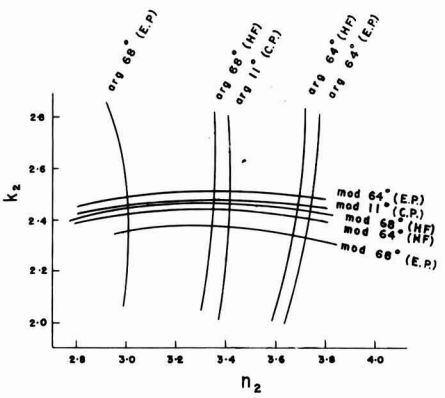

Fig. 12. Experimental data on n_2 and k_2: E.P. = electropolished; HF = E. P. followed by dip in HF; C.P. = chemically polished.

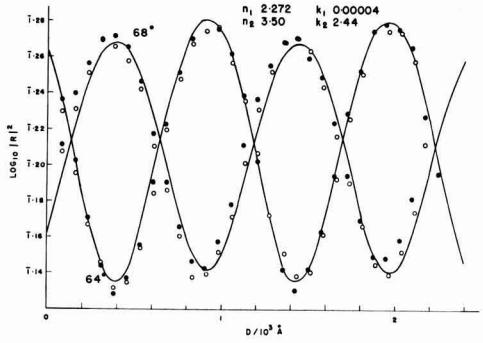

Fig. 13. Calculated reflectivity vs. thickness curves and experimental data (two specimens) with vertical shift to allow for surface imperfection 10 ma cm^{-2} and 25°C.

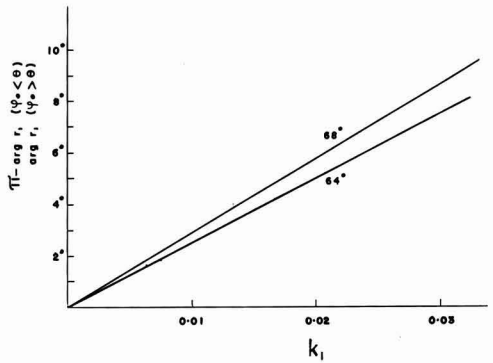

Fig. 14. Calculated (π — arg r_1) for $\psi_0 < \theta$ and arg r_1 for $\psi_0 > \theta$ as function of k_1 for $n_1 = 2.272$ and $\psi_0 = 64°$ and 68°.

The above values of n_2 and k_2 may be compared with the previous values of Wartenberg (14) published in 1910 of $n_2 = 2.05$ and $k_2 = 1.12$ x 2.05, obtained by the classical methods and with those of Heavens and Kelly (8) $n_2 = 2.04$ and $k_2 = 2.09$ (claimed to be reliable to ±1-2%) obtained by matching plots of intensity reflectivity *vs.* angle of incidence assuming that their thin evaporated layers of tantalum had the full theoretical reflectivity of a flat surface and were free of oxide.

Measurements on Unanodized Metal

The top part of Fig. 15 shows calculated reflectivity *vs.* angle of incidence plots for bare metal and

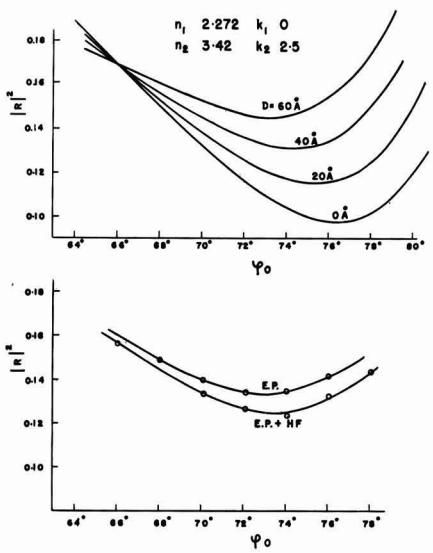

Fig. 15. Top: calculated reflectivity for bare metal and for very thin films; bottom: experimental data for unanodized electrolytically polished tantalum before and after immersion in HF.

for metal with a few tens of angstroms of oxide. The bottom part shows observed curves for electropolished metal with and without treatment in HF. This treatment will presumably remove the pre-existing film, but a film will again grow on removal from the HF and drying. The results appear to indicate 30Å or more of oxide to be present. Since the refractive and absorption indices of this pre-existing film may differ from those found for the anodic film and used in the calculation of the curves in the upper part of Fig. 15, the fit would not be expected to be exact. Furthermore the ratio in which the reflectivity is reduced by surface imperfections may not be independent of angle of incidence over this wider range of angle.

Comparison with Previous Work

Several previous researches have also indicated (with varying precision) that apart from narrow interfacial regions the films formed on tantalum in dilute aqueous solutions at a given current density and temperature are both homogeneous and invariant with total thickness. In the most recent of these (1, 12) (consult for references to the earlier work) in which the spectrophotometric method was used to determine the thickness, it was shown that this was so with high accuracy (<1%) at least with films over 200Å in thickness unless remarkably complicated and nicely balanced compensations occurred involving the capacity, the charge to form the films, the refractive index, and the field strength.[6] However, Heavens and Kelly (8) in their work using light polarized in the plane of incidence obtained results which indicated that the index varied through the thickness of the oxide by about 10%. The mean index reported was some 10% less than the value reported by Young (1) at the same wavelength 5461Å although higher values were reported in the fuller account by Kelly (9). Other results in contradiction with previous work, in particular a 2% difference between films formed on two specimens with only a 1:2 ratio of current density, and a 10% increase with increasing thickness to a few 100Å were reported by Kelly. The non-uniformity was deduced from a rather slight misfit between experimental and calculated curves of reflectivity *vs.* angle of incidence. The range of angle was small, only four experimental points were compared with theory, and only one experiment was quoted. Plots of reflectivity *vs.* thickness were not obtained. The significance of the misfit depends on the accuracy of the method (described above) which was used to obtain the optical constants of the metal. Evaporated tantalum substrates were used for most of the experiments. These were in fact extremely thin, so that only very thin oxide films could be examined before the substrate became transparent. No evidence was given that these films were not granular or otherwise different from the massive metal. It is evident from the fuller account given by Kelly that a large scatter was observed in the values of n_1 obtained by the determination of ψ_0 at which $|R|^2$ was the same for anodized and unanodized area. In view of these points, we conclude that the results obtained by Heavens and Kelly are not typical for films formed on massive tantalum. Probably, the most important source of contradiction with other work (including the present work) was the use of very thin evaporated layers of tantalum. It has often been found that thin evaporated films have properties different from those of the massive material.

[6] Heavens' statement (6) that the index was assumed to be uniform is only correct in that such compensations are only excluded on the grounds of probability.

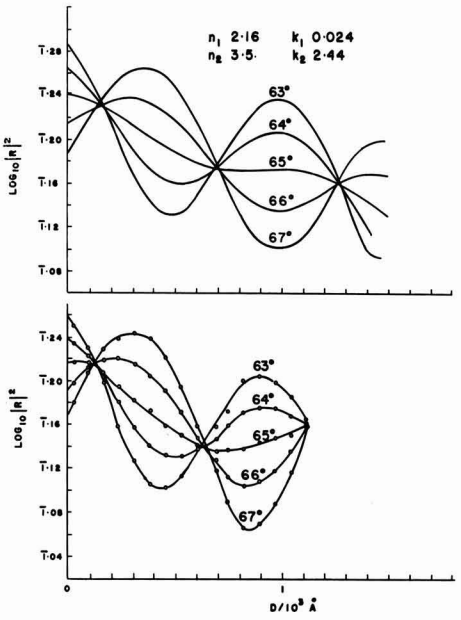

Fig. 16. Reflectivity vs. thickness. Top: calculated for homogeneous oxide; bottom: observed for films formed in 70 wt % H_2SO_4 at 100°C and 10 ma cm^{-2}.

Anodic Oxide Films Formed on Tantalum in Concentrated Sulfuric Acid

Typical experimental curves of reflectivity *vs.* thickness at several angles of incidence are shown in the lower part of Fig. 16. The shape of the curves between crossover points allows a good estimate to be made of the refractive index, and k_2 may also be estimated. Calculated curves for a homogeneous film with $n_1 = 2.16$ and $k_1 = 0.024$ are shown in the top part of the figure. The fit (on a logarithmic intensity scale) is good up to a certain thickness but not beyond. Evidently, a large fraction of the film absorbs light, but after a certain thickness is reached the films are not homogeneous. The refractive index is slightly less than that of films formed in dilute sulfuric acid, and the absorption index is about equal to that of the thin outer absorbing layer of the films formed in dilute solution. Other information on the properties of films formed in concentrated sulfuric acid has been given by Vermilyea (15) and by Young (12)

Niobium and Niobium + Tantalum Alloys

Plots of reflectivity *vs.* angle of incidence for a series of "critical" thicknesses of films formed in di-

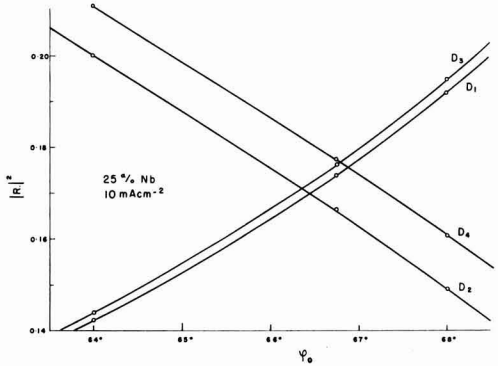

Fig. 17. Reflectivity vs. angle of incidence at "critical" thicknesses of oxide for niobium and tantalum + niobium alloys.

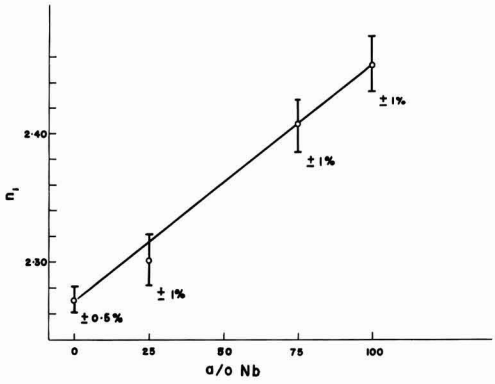

Fig. 18. Refractive index vs. composition in a/o of tantalum + niobium alloys.

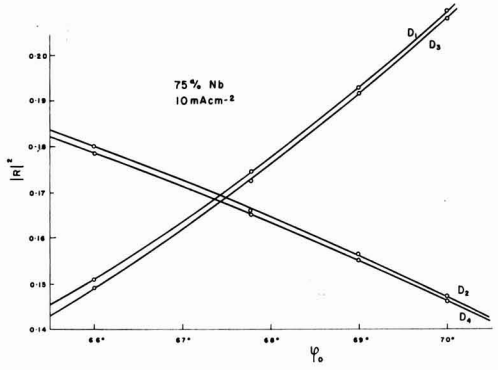

Fig. 17b

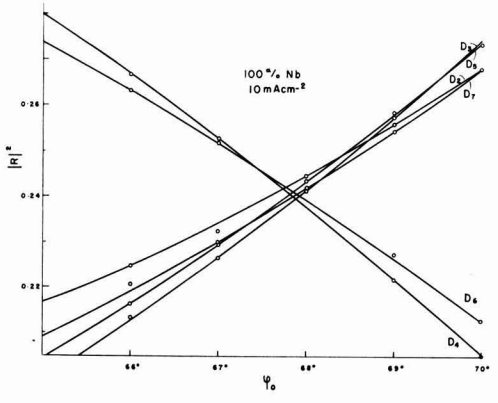

Fig. 17c

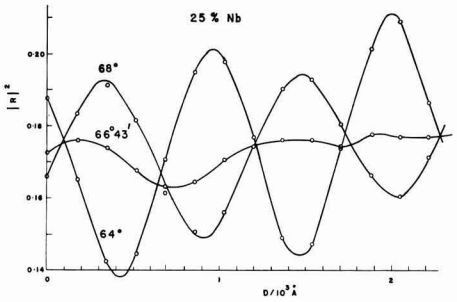

Fig. 19. Reflectivity vs. thickness of oxide for alloys.

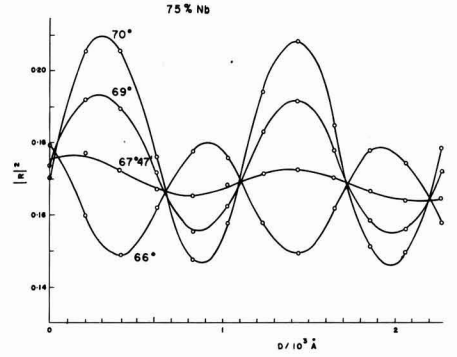

Fig. 19b

lute sulfuric acid at 10 ma cm^{-2} and 25°C on niobium, and on the two 25 a/o alloys with tantalum are given in Fig. 17. These indicate refractive indices as follows: Nb, $2.46 \pm 1\%$; 75 a/o Nb + 25 a/o Ta, $2.41 \pm 1\%$; 25 a/o Nb + 75 a/o Ta, $2.30 \pm 1\%$. As shown in Fig. 18 the index of the mixed oxide is, therefore, approximately a linear function of the composition in atomic per cent, assuming that the films have the composition of the alloy. Reflectivity *vs.* thickness plots are given in Fig. 19. There would again appear to be an outer absorbing layer. With the 25 a/o niobium alloy, $|R|^2$ increased with D. Possibly this could be due to segregation within the oxide or metal. X-ray fluorescence analysis of films dissolved in layers was used to test this possibility, but the result was inconclusive.

Zirconium

Reflectivity *vs.* thickness plots for films formed at 10 ma cm^{-2} and 25°C in 0.2*N* H_2SO_4 are given in Fig. 20. Clearly a large part of the films absorbed light at this wavelength: a surprising result. Because of this absorption, it has not been possible as yet to fit calculated curves and to determine whether the films are homogeneous.

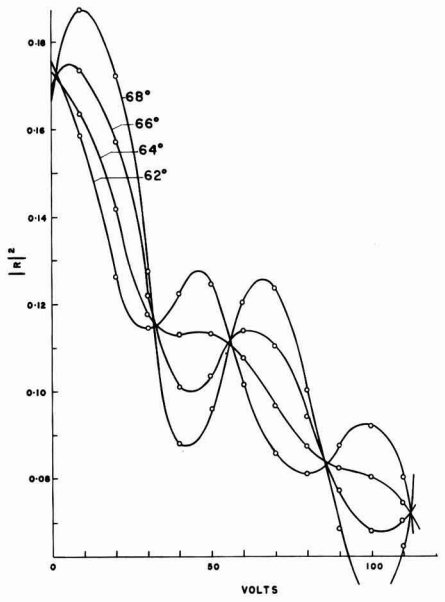

Fig. 20. Reflectivity vs. voltage of formation at 10 ma cm^{-2} and 25°C for zirconium.

Discussion

The direction of the dependence of the refractive index on the conditions of formation is somewhat surprising, since, according to present theories, it means that the index is higher the lower the concentration of mobile ions, *i.e.*, of Frenkel defects.

The explanation of the thin outer layer of absorbing oxide is at present uncertain. It certainly seems to be significant that the thin absorbing layer present in films formed in dilute solution becomes a thick layer in films formed in concentrated solution. It is tempting to assume that this layer represents a transitional layer in which the adjustment is made between the kinetics of the oxide/solution interface and those of the electrically neutral oxide in the interior of the film. However, the effect could be due to some more trivial cause, such as the adsorption of SO_4^{-2} by the outer layers of oxide. It is worth noting that to account for accurate reflectivity measurements it has usually been required to introduce the idea of transitional layers in which, for example, the refractive index varies through the outer few angstroms of the reflecting material.

Acknowledgments

This work was supported by the Defence Research Board of Canada. The authors wish to thank Dean G. M. Shrum, Director of the British Columbia Research Council, and Dr. R. H. Wright, Head of the Chemistry Division for their encouragement, and Mr. H. V. Kinsey of the Bureau of Mines, Ottawa, for the tantalum + niobium alloys.

Manuscript received Nov. 21, 1960; revised manuscript received Jan. 20, 1961. Part of this paper was prepared for delivery before the Chicago Meeting, May 1-5, 1960.

Any discussion of this paper will appear in a Discussion Section to be published in the December 1961 JOURNAL.

REFERENCES

1. L. Young, *Proc. Roy. Soc. A*, **244**, 41 (1958).
2. A. M. MacSwan, *Proc. Phys. Soc.*, **72**, 742 (1958).
3. G. L. Miller, "Tantalum and Niobium," Butterworths, London (1959).
4. A. B. Winterbottom, Apendix in "Metallic Corrosion, Passivity and Protection," U. R. Evans, 2nd ed., Arnold, London (1946).
5. O. S. Heavens, "Optical Properties of Thin Solid Films," Butterworths, London (1955).
6. O. S. Heavens, *Repts. Progr. Phys.*, **23**, 1 (1960).
7. F. Abelès, *Compt. rend.*, **228**, 553 (1949); *J. Phys. Rad.*, **11**, 310 (1950).
8. O. S. Heavens and J. C. Kelly, *Proc. Phys. Soc.*, **72**, 906 (1958).
9. J. C. Kelly, Thesis, Reading, England (1958).
10. L. Young, *Trans. Faraday Soc.*, **53**, 841 (1957).
11. H. E. Merwyn and E. S. Larsen, *Am. J. Sci.*, **34**, 42 (1912).
12. L. Young, *Proc. Roy. Soc. A*, **258**, 496 (1960).
13. D. A. Vermilyea, *This Journal*, **104**, 427 (1957).
14. H. von Wartenberg, *Ber. dtsch. phys. Ges.*, **12**, 105 (1910).
15. D. A. Vermilyea, *Acta Met.*, **2**, 482 (1954).

The Volatilization of Chromium Oxide

D. Caplan and M. Cohen

Division of Applied Chemistry, National Research Council, Ottawa, Canada

ABSTRACT

The phenomenon of evaporation of chromium oxide from chromium alloys oxidized at high temperatures was investigated by observing the loss in weight when Cr_2O_3 pellets were heated at 1000°-1200°C in various atmospheres. Appreciable volatilization occurred in oxygen, more in wet oxygen, but none in argon or wet argon. Fe_2O_3 specimens showed volatilization in none of these atmospheres. The results indicate that evaporation occurs by oxidation of Cr_2O_3 to gaseous CrO_3 which dissociates to Cr_2O_3 on redeposition. The mechanism by which moisture promotes volatilization was not established.

When Cr alloys are oxidized at high temperatures, it has sometimes been observed that Cr_2O_3 crystals deposit at cooler parts of the apparatus (1-4), indicating that Cr or its oxide somehow evolves from the specimen and is transported through the gas phase. This is surprising in that the barrier film of refractory oxide covering the specimen would be expected to prevent such an effect. Interpretation of the kinetics of oxide film thickening from weight gain/time measurements is thus complicated since

a weight loss is superimposed on the weight gain of oxygen which supposedly is being measured. In addition, it is likely that the characteristics of the film as a diffusion barrier are affected.

Neither the vapor pressure of Cr_2O_3 nor its dissociation pressure is high enough to account for the quantities of deposit observed. Because of the known high vapor pressure of Cr it was at first considered that the metal itself escaped in some manner. The authors proposed (1) that Cr_2O_3 was reduced to Cr at the outer surface by the carbon of the alloy. When volatilization was observed with essentially carbon-free alloys it seemed necessary to invoke a mechanism whereby Cr evaporation takes place because the oxide film fails to act as a proper barrier layer, perhaps by rapid diffusion of Cr along oxide grain boundaries or escape at real discontinuities in the film (5). But when it was learned that Cr_2O_3, in the absence of metal, lost weight when heated in oxygen (6) it became evident that a volatile oxide was being formed.

To investigate the effect, Cr_2O_3 was heated in flowing oxygen and argon and the weight loss measured. Parallel experiments were performed with Fe_2O_3. The loss in weight was determined also in moist oxygen and argon since moisture had previously been shown to affect the oxidation rate of Cr alloys (1, 7). In addition, Cr_2O_3 was formed from metal in the same atmospheres and examined by x-ray diffraction and infrared absorption spectroscopy to see if moisture modified the oxide structure.

Experimental

Pellets 1.2 cm in diameter and 1.2 cm high were pressed from reagent grade Cr_2O_3 and Fe_2O_3 and sintered at 1400° in air or oxygen to about 98% of theoretical density. Chromium metal was U.S. Bureau of Mines 0.015-in. sheet.

The specimens were suspended in a vertical tube furnace, 2.9 cm ID, up through which purified oxygen or argon at 1 atm flowed at rates regulated between 10 and 200 ml/min. The gases were used dry or saturated with water at 25° at which temperature the vapor pressure of water is 24 mm. Runs were at 1100° and 1200° except for one at 1000° in still air. Table I summarizes most of the runs carried out. The oxide pellets were held in a high-purity alumina crucible cut in an openwork pattern to expose them to the flowing gas. Runs were started by lowering the specimen into the hot zone slowly to avoid loss of weight by spalling. Although weight loss *vs.* time curves were obtained with a recording automatic balance only the final, total weight changes are reported since up to 40% of the evolved product condensed back on to the suspension system.

The Cr sheet samples were oxidized in similar fashion for such times, 5-100 hr, as to give oxide films 1-10μ thick. (The weight gain/time curves recorded by the automatic balance will be reported subsequently in connection with the scaling of Cr alloys.) In this range of thickness the Cr_2O_3 absorbed infrared radiation in the proper amount to yield an absorption spectrum when a method of reflection at 90° incidence was used. Spectra were also obtained by transmission through mull samples prepared from finely ground separated oxide.

In an additional experiment[1] an oxy-gas torch was directed at the surface of sintered Cr_2O_3 and the small amount of smoke evolved caught on a cold support. The surface temperature of the Cr_2O_3 was approximately 2000°C. The product was examined by reflection electron diffraction.

Results

Figure 1 shows the effect of atmosphere on the volatilization of Cr_2O_3 at 1100° and 1200° and a gas flow rate of 200 ml/min. At this flow rate moisture

[1] Suggested by discussion with R. M. Fowler of Union Carbide Metals Corp. when this work was presented at the ECS Houston meeting, October 1960.

Table I. Weight loss on heating Cr_2O_3 and Fe_2O_3 in various atmospheres

Run	Specimen	Temp, °C	Gas	Time, hr	Gas flow		Weight loss		
					ml/min	l	mg	mdd	μg/l
1	Cr_2O_3	1000	still air	72	—	—	0.3	1.5	—
2	Cr_2O_3	1100	oxygen, dry	65	10	39	0.9	5	23
3	Cr_2O_3	1100	oxygen, dry	19	200	230	0.8	15*	3.5
4	Cr_2O_3	1100	oxygen, dry	20	200	240	0.6	11	2.7
5	Cr_2O_3	1100	oxygen, wet	20	200	240	2.1	38*	8.9
6	Cr_2O_3	1200	argon, dry	66	200	792	0	0	0
7	Cr_2O_3	1200	argon, dry	115	192	1300	0	0	0
8	Cr_2O_3	1200	argon, wet	20	192	230	0	0	0
9	Cr_2O_3	1200	oxygen, dry	20	10	12	2.1	37	173
10	Cr_2O_3	1200	oxygen, dry	20	10	12	1.3	24	111
11	Cr_2O_3	1200	oxygen, dry	20	20	24	1.8	33	77
12	Cr_2O_3	1200	oxygen, dry	20	200	240	2.3	41	10
13	Cr_2O_3	1200	oxygen, dry	20	200	240	2.6	45	11
14	Cr_2O_3	1200	oxygen, dry	42	200	504	8.0	68*	16
15	Cr_2O_3	1200	oxygen, wet	20	10.2	12.2	1.9	33	152
16	Cr_2O_3	1200	oxygen, wet	20	63	76	3.3	58	43
17	Cr_2O_3	1200	oxygen, wet	20	200	240	5.6	99	23
18	Cr_2O_3	1200	oxygen, wet	20	200	240	6.0	106*	25
19	Fe_2O_3	1200	oxygen, dry	20	200	240	0	0	0
20	Fe_2O_3	1200	oxygen, wet	20	200	240	0	0	0
21	Fe_2O_3	1200	oxygen, wet	65	200	240	0	0	0

* Plotted in Fig. 1.

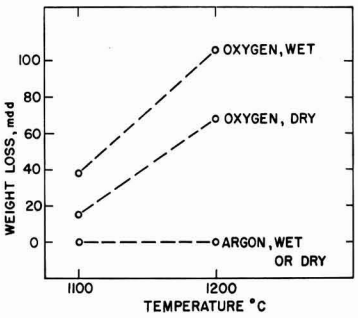

Fig. 1. Weight loss of Cr_2O_3 in wet and dry oxygen and argon at 1100° and 1200°C; Flow rate 200 ml/min.

approximately doubles the rate of weight loss in oxygen. No loss occurs in argon, either wet or dry. With Fe_2O_3 (Table I) no loss occurs in wet or dry oxygen.

The variation in evaporation rate with oxygen flow rate is shown by the results in Table I, which includes the data of Fig. 1. Expressing the weight loss in micrograms per liter of gas flowed (last column), it is seen that as the flow rate is decreased the numbers increase as they should (*e.g.*, runs 9-14, 15-18, or 2-4) but that a constant value is not obtained, as should be the case if the saturation pressure of the volatile species were to be determined (8, 9). Furthermore, nonsystematic variations appear *e.g.*, the loss in run 9 is greater than in run 10. This occurred because run 9 immediately followed four 1200° runs with Fe_2O_3 in oxygen during which the Cr_2O_3 which had been condensed in the apparatus from previous runs was evaporated away. In run 9, therefore, only the specimen itself was contributing the volatile material to the flowing gas and a higher (and more nearly correct) weight change was observed. This applies also to runs 14, 15, and 18. Otherwise some evaporation occurs from Cr_2O_3 deposits as well as from the pellet, but is not recorded as part of the weight loss. It follows that the experimental design is not satisfactory for the accurate determination of vapor pressure or that the transportation method is not applicable to the Cr_2O_3-O_2-H_2O system.

Infrared absorption spectra of adequate quality were obtained from the thin oxide films on Cr sheet by the normal incidence, single reflection method, as well as with the more conventional mull samples. Absorption maxima were observed at 680, 850, 930, 980, 1100, and 1160 cm^{-1}. No differences in the spectra could be detected between Cr_2O_3 formed in dry oxygen, wet oxygen, or argon containing 20 ppm oxygen.

X-ray diffraction of these same three Cr_2O_3 samples and also of Cr_2O_3 condensed on the suspension system from Cr_2O_3 heated at 1200° in wet oxygen (run 17) disclosed no significant difference in the interplanar spacings; the variation was no more than 1 part in 10,000.

Electron diffraction of the smoke developed by directing an oxy-gas torch onto Cr_2O_3 showed this condensate to be CrO_3. Sufficient material could not be produced to confirm this by x-ray diffraction.

Discussion

The observation that no loss of Cr_2O_3 occurs in argon confirms the fact that volatilization is not by dissociation of the oxide nor as Cr_2O_3 vapor. Since weight loss does occur in oxygen, the volatile species must be a higher oxide of chromium. Fe_2O_3 shows no volatilization, presumably because no oxide of appreciable vapor pressure forms, and none is known. CrO_3 is a known volatile oxide of Cr, but it exists normally only at lower temperatures so that, at the temperatures and oxygen pressures of the present work, oxidation of Cr_2O_3 to CrO_3 is thermodynamically unfavorable. However, the reaction to form gaseous CrO_3

$$Cr_2O_{3(s)} + 3/2\ O_{2(g)} = 2CrO_{3(g)} \qquad [1]$$

would have in its favor the increase in entropy associated with the extra half mole of gaseous product, and therefore a less unfavorable free energy change. Furthermore, in a dynamic system with a considerable flow of gas, appreciable material transport can occur even from a rather small equilibrium partial pressure.

Taking the largest experimental value of weight loss per liter of gas flowed, which is to say the most nearly correct value, run 9, a Cr_2O_3 loss of 173 $\mu g/l$ corresponds to a CrO_3 partial pressure of 5.1×10^{-5} atm. If this represented saturation, the equilibrium constant

$$K_p = \frac{(P_{CrO_3})^2}{(P_{O_2})^{3/2}} \qquad [2]$$

becomes 2.6×10^{-9}, equivalent to $\Delta F^\circ_{1473} = +29$ kcal. In fact, saturation has not been demonstrated so that K_p is too small and ΔF° too large by an unknown amount, although the error may not be very large. But the main point of the foregoing is that CrO_3 may be reasonably considered as the volatile species despite its instability. This observation of hexavalent Cr oxide is consistent with an explanation offered in a previous publication (10) to account for an anomalous sharp minimum in the cathodic reduction curves of oxide films on Cr alloys. The proposal was made that Cr_2O_3 films formed under strongly oxidizing conditions were defect oxides containing appreciable Cr^{6+} ion and would be properly described as $Cr_{2-2x}^{3+}\ Cr_x^{6+}\ \square_x\ O_3$ where $\square_x$ represents the concentration of cation vacancies. The latter would be larger the higher the oxygen pressure and the lower the temperature.

The Cr smoke experiment lends strong support to the CrO_3 hypothesis. That CrO_3 actually was condensed must be ascribed to the gas quenching that the volatilized Cr oxide receives as it is swept out of the oxy-gas flame. In all other cases the CrO_3 vapor decomposes to Cr_2O_3 and oxygen by the reverse of equation [1]. Hence, in the flow experiments only Cr_2O_3 is detected by x-ray diffraction in the sublimate on the furnace tube and suspension system. [In some work which had not appeared in print at the time that this paper received its final revision, CrO_3 had been detected mass spectrometrically as a

gaseous species when Cr_2O_3 was heated under oxidizing conditions (26).]

The accelerating effect of moisture cannot be elucidated from these experiments. The attempts by x-ray diffraction and infrared spectroscopy to demonstrate the presence of hydrogen in Cr_2O_3 heated or formed in moist gas were not successful; one can say that large quantities do not incorporate themselves in the solid oxide lattice. The vaporization of some nonvolatile oxides in the presence of moisture has been shown to be due to the formation of gaseous hydrates. This is so with Li_2O (11, 12), B_2O_3 (13), BeO (14-17), and perhaps Al_2O_3 (17), WO_2, W_4O_{11}, WO_3, MoO_3 (18) and some others (19). But the Cr_2O_3 case is different in that the wet argon experiment in which no volatilization occurred showed that a hydrate of Cr_2O_3 does not form. It may be that volatilization is enhanced by formation of a gaseous CrO_3 hydrate, but there is as yet no evidence in support of this. Where a volatile hydrate forms and no volatile oxide exists the situation appears quite straightforward. But where volatile oxides are present, U, Mo, Cr, Si, Pt, the function of water has not been demonstrated unequivocally.

Alternatively, moisture may increase volatility by stabilizing gaseous polymers. Mass spectrometric observations have shown rather surprisingly that the high-temperature volatile species over such oxides as WO_3, MoO_3, BeO, and GeO are polymers as high as pentamers (20, 21).

Third, moisture may, by changing the activation energy, act as a promoter for the surface oxidation reaction, perhaps facilitating removal of the oxidized product from the surface. The results at the slowest flow rate suggest such a catalytic effect: the weight loss in wet oxygen was not greater than in dry oxygen (run 15 *vs.* run 9). If the gaseous hydrate or polymer idea were valid, the weight loss should be greater with moisture at the slow flow rate also. But because of the aforementioned inadequacies of the transportation method for the Cr_2O_3-O_2-H_2O system, the data at low flow rates are variable and a definite conclusion cannot be drawn.

Having established the conditions under which Cr_2O_3 evaporates one can recognize instances where the effect of such evaporation should be considered. The spurious kinetic results that can arise in studies of oxide film growth on Cr alloys at high temperatures were mentioned at the beginning. A corollary is that moisture might appear to inhibit or promote high-temperature oxidation depending on whether the measurements were of gain in weight of oxygen or loss in weight after removal of oxide. For example, the weight gain/time curves of the Cr panels used to form Cr_2O_3 films show smaller parabolic rate constants in moist oxygen than in dry oxygen, in an amount that could be accounted for by the more rapid volatilization in wet oxygen rather than by a change in film growth kinetics. In alloys, where oxides of more than one metal occur, the composition of the outermost layer especially would be depleted in Cr oxide by the evaporation.

Spurious results can occur also in chemical analysis where materials containing Cr are ignited in air. In the chemical analysis of passive films separated from stainless steel, moisture contents up to 30% were deduced (22) on the basis of the decrease in weight that occurred when 100 μg or smaller samples were ignited at 1000°. A possible alternative explanation is that Cr_2O_3, not H_2O, was driven off in the ignition. If so, the suggestion that passive films have gel-like characteristics loses support. Attempts in this laboratory to confirm the presence of water in passive films prepared similarly have not succeeded. The reported permeability of Cr_2O_3 films for Cr (5) might also be explained as oxide volatilization.

In the mixed oxides that form protectively on heat resistant alloys containing Cr, the volatility of Cr oxide may be less than from Cr_2O_3, either because of a crystallographic difference (spinel instead of rhombohedral), dilution, or the valence compensation effect (23) by which, for example, the evaporation of uranium oxide is depressed by inhibiting the oxidation of UO_2 to UO_3. If this is so, a mixed oxide in some atmospheres and temperatures could be preferable to pure Cr_2O_3 in spite of a less ideal defect structure which may permit more rapid diffusion. There is some literature evidence in this direction (24), but the situation is not yet clear.

To summarize, Cr_2O_3 is shown to volatilize but only in an oxidizing atmosphere. Moisture increases the rate of evaporation in some way not yet understood. Fe_2O_3 does not volatilize. CrO_3 is thermodynamically reasonable as the gaseous species, can be gas-quenched out of hot Cr oxide smoke, and is believed to account satisfactorily for the evaporation of Cr oxide. Normally it dissociates to Cr_2O_3 on redeposition. Identification of CrO_3 in the vapor phase and an explanation of the moisture effect requires additional information: application of the Knudsen effusion method in which the high-temperature gaseous product is viewed with a mass spectrometer (13, 23) seems ideally suited to this purpose. Incorrect interpretation may be attached to high-temperature processes involving Cr oxide if its volatility is not recognized.

Manuscript received Nov. 14, 1960; revised manuscript received Jan. 13, 1961. This paper was prepared for delivery before the Houston Meeting, Oct. 9-13, 1960.

Any discussion of this paper will appear in a Discussion Section to be published in the December 1961 JOURNAL.

REFERENCES

1. D. Caplan and M. Cohen, *J. Metals*, **4**, 1057 (1952).
2. G. Bandel, *Arch. Eisenhüttenwesen*, **15**, 271 (1941).
3. G. R. Wilms and T. W. Rea, *J. Less Common Metals*, **1**, 411 (1959).
4. I. Warshaw and M. L. Keith, *J. Am. Ceram. Soc.*, **37**, 161 (1954).
5. E. A. Gulbransen and K. F. Andrew, *This Journal*, **104**, 334 (1957).
6. A. U. Seybolt, Private communication.
7. D. Caplan and M. Cohen, *Corrosion*, **15**, 141t (1959).
8. O. Kubaschewski and E. Evans, "Metallurgical Thermochemistry," p. 150, Pergamon Press, New York (1956).
9. C. B. Alcock and G. W. Hooper, *Proc. Roy. Soc.*, **A254**, 551 (1960).
10. D. Caplan, A. Harvey, and M. Cohen, *This Journal*, **108**, 134 (1961).
11. A. E. van Arkel, U. Spitsbergen, and R. D. Heyding, *Can. J. Chem.*, **33**, 446 (1955).

12. D. J. Meschi, W. A. Chupka, and J. Berkowitz, *J. Chem. Phys.*, **33**, 533 (1960).
13. D. J. Meschi, W. A. Chupka, and J. Berkowitz, *ibid.*, **33**, 530 (1960).
14. C. A. Hutchison and J. G. Malm, *J. Am. Chem. Soc.*, **71**, 1338 (1949).
15. L. I. Grossweiner and R. L. Seifert, *ibid.*, **74**, 2701 (1952).
16. W. A. Young, *J. Phys. Chem.*, **64**, 1003 (1960).
17. H. v. Wartenberg, *Z. anorg. Chem.*, **264**, 226 (1951).
18. T. Millner and J. Neugebauer, *Nature*, **163**, 601 (1949).
19. L. Brewer and G. R. B. Elliott, URCL—1831 (1952).
20. J. Berkowitz, M. G. Inghram, and W. Chupka, *J. Chem. Phys.*, **26**, 842 (1957).
21. M. G. Inghram and J. Drowart, Intern. Symp. on High Temp. Technol., McGraw-Hill Book Co. (1960).
22. T. N. Rhodin, *Ann. N. Y. Acad. Sci.*, **58**, 855 (1954).
23. W. B. Wilson, BMI—1318 (1959).
24. O. Kubaschewski and B. E. Hopkins, "Oxidation of Metals and Alloys," p. 198, Butterworths, London (1953).
25. R. T. Grimley, R. P. Burns, and M. G. Inghram, *J. Chem. Phys.*, **33**, 308 (1960).
26. R. T. Grimley, R. P. Burns, and M. G. Ingraham, *ibid.*, **34**, 664 (1961).

Electrolytic Etching of Dense Tantalum

A. L. Jenny and R. A. Ruscetta

Capacitor Department, General Electric Company, Irmo, South Carolina

ABSTRACT

A practical method of etching dense tantalum for the purpose of magnifying its effective surface area is described. The degree of surface area magnification is related to such parameters as electrolyte composition, anodic current density, temperature, and characteristics of metal specimens to be treated. The decrease in surface area magnification as a function of postetch anodizing voltage apparently signifies the filling in of certain etch pits with tantalum oxide and gives a clue to the size of these pits.

Tantalum metal of capacitor quality is a powder metallurgy product of relatively high purity. The metal in a variety of forms such as porous sintered compacts, wire, sheet, and foil is being used in substantial quantities in the manufacture of high-quality tantalum electrolytic capacitors.

The present investigation is concerned with the magnification of the capacitance value of plain tantalum foil to the greatest extent possible by a practical and economical etching treatment.

Magnification of capacitance.—The equation which characterizes the electrical capacitance of a parallel plate capacitor is equally valid for an electrolytic capacitor.

$$C = (K A)/T \qquad [1]$$

wherein C is capacity; K a dimensional constant which includes ϵ, the specific inductive capacitance; A area of electrodes; T distance between plates.

In an electrolytic capacitor, T is the thickness of the anodic oxide film which is directly proportional to the formation voltage and to the absolute temperature. Hence, we may now write

$$C = (K' A)/E \qquad [2]$$

In Eq. [2] K' is a temperature-dependent function having the units of volt microfarads per cubic centimeter when C is expressed in microfarads and the cgs system is used dimensionally. The experimental values of K' for unetched tantalum foil are approximately 25 and 21, respectively, for formation temperatures of 25° and 95°C.

As predicted by Eq. [2] when plain and etched specimens of foil are anodized (formed) to the same voltage and at the same temperature, the increase in surface area achieved by etching will be manifested by a proportional increase in the measured capacitance.

The ratio of the capacitance per unit of projected area of an etched specimen to that of a plain specimen is termed the capacitance ratio or etch ratio. To define the etch ratio completely, both the anodizing voltage and temperature must be specified. In this paper the voltage is 75 ± 1 v d.c. and the temperature is 25° ± 2°C unless otherwise specified.

Etching process-general.—Several U. S. patents have been issued relating to etching processes to increase the effective area (and therefore the capacitance) of tantalum specifically for electrolytic capacitor purposes. Kahan (1) uses aqueous solutions of concentrated HF and HCl in an electrolytic system, Houtz (2) reacts tantalum with chlorine at 350°-400°C, Jenny (3) etches electrolytically in a substantially nonaqueous system containing fluoride salts, and Ruscetta and Jenny (4) use an essentially nonaqueous electrolyte containing a variety of salts.

The inherent properties of tantalum render it generally unresponsive to the usual chemical and electrochemical etching techniques. For example, the rapid embrittlement of tantalum by hydrogen even at room temperature precludes the use of chemical etchants which liberate hydrogen such as hydrofluoric acid alone or mixed with other acids or solutions of ammonium bifluoride. This is particularly true when treating thin gauge foils which must be wound subsequently on small diameter arbors, the so-called winding process in the manufacture of electrolytic capacitors. Furthermore, the ease with which tantalum acquires an insulating film when polarized anodically in most aqueous solutions represents a distinct departure from normal electrolytic etching procedures.

The electrolyte must have adequate conductivity and be such as to promote a pit-type of corrosion to produce a significant increase in the effective surface area, while inhibiting oxide formation. To be practical, these characteristics must prevail over a reasonable range of current density, temperature, composition, and time.

Specimen Preparation and Treatment

Tantalum foil specimens 12 x 1 x 0.00127 cm were prepared by first spot welding a flattened tantalum wire, 0.05 cm in diameter and about 5 cm long, to one end of the foil. This provided a convenient handle and terminal for subsequent mechanical and electrical processing. The welded area was not immersed in the electrolyte during the etching cycle. Both foil and wire were purchased to the following purity specification: Ta 99.90 min; Fe 0.03 max; C 0.03 max; all others 0.04 max.

The foil/wire assemblies were cleaned first in C.P. acetone, then boiled gently for 15 min in a mild detergent solution to remove rolling lubricant. Specimens then were rinsed thoroughly in boiling distilled water and air-dried after a final rinse in C.P. acetone.

The power source for etching was a rectifier with a variable current limiting resistor to control current density. A regulated voltage power supply was used for forming etched specimens and unetched controls to 75 v d.c. The forming solution comprised aqueous ammonium pentaborate having a resistivity of 300 ± 15 ohm cm at 25°C. Capacity measurements were made at 120 cps on a standard capacitance bridge.

Electrolyte Composition

A great many solutions were found ultimately which satisfied the technical requirements and also met a criterion of adequate etching action. That is, to be successful, an electrolyte must produce an etch ratio of at least 1.5/1 after 10 min of etching. Although the primary solvent in most solutions consisted entirely of methanol, other organic liquids miscible with methanol also were used with it, provided the combination contained at least 6.5% methanol by weight.

Examples of such liquids used with methanol are higher molecular weight primary alcohols, polyhydric alcohols, simple and substituted ethers, amines, amides, and many aromatic compounds.

The solute comprised halides, thiocyanates, nitrates, chlorates, and many other miscellaneous compounds such as trichloroacetic acid, for example. The solvents and solutes were used individually or in combination, and all combinations exhibited to a greater or lesser degree the same general behavior. For purposes of simplicity, the following descriptions will be limited to the system methanol, ammonium bromide/water.

Effect of Water

The profound influence of the water content on etch ratio and the type of corrosion obtained was not predicted. A study was made of its effect only after the erratic behavior of solutions as a function of age was noted. The basic solution comprised 1 l absolute refined methanol in which was dissolved 30 g N.F. granular ammonium bromide. The water content as made was determined by a modified Karl Fischer method and ranged from 1000 to 3500 ppm. After etching two specimens at 1.08 amp/dc² in the electrolyte as made, small amounts of distilled water were added, thoroughly stirred in and two more specimens etched, etc. The effect of the water content on the etch ratio is shown in Table I and plotted in Fig. 1.

Table I. Effect of water content of methyl alcoholic NH_4Br on etch ratio

Wt. % added water	Capacity, μf	Etch ratio at 75 v d.c.
0	4.62	1.17
1.2	17.50	4.42
2.4	12.75	3.72
3.6	12.65	3.70
4.8	12.40	3.14
6.0	11.45	2.90
8.4	9.15	2.32
10.8	8.65	2.19
13.2	8.45	2.14

Etching cycle, 10 min @ 1.0b ASD.
Capacity unetched control 3.95 μf at 75 v d.c.

For comparison purposes the etch ratio *vs.* water content curve for methyl alcoholic fluoride solutions is plotted in Fig. 1 as curve 2. The sharp peak of this curve made it difficult, if not impossible, to maintain optimum etching conditions. Methyl alcoholic solutions of bromides followed curve 1 and the halogen appeared to be liberated briefly at a water content indicated by point A. The liberation of halogen was substantially continuous throughout the etching cycle at point B. At the same time, specimens etched at water contents in the range A to B began to show evidence of anodic polarization by acquiring the well-known interference colors of tantalum oxide.

Apparently the liberation of halogen and the incipient oxidation at high water contents decreased the coulombic efficiency of etching. This is shown in Fig. 2 wherein the milligram weight loss of specimens etched for 10 min at 0.86 ASD is plotted against the water content of the etching electrolyte. Figures 1 and 2 indicate that, at low water content, under about 1%, tantalum metal is being efficiently but uniformly removed from the surface of the

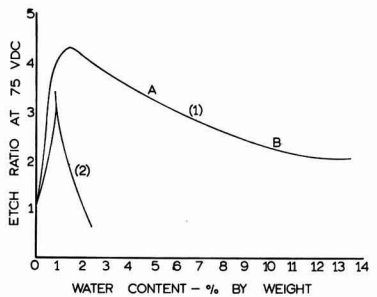

Fig. 1. Effect of composition and water content on etch ratio.

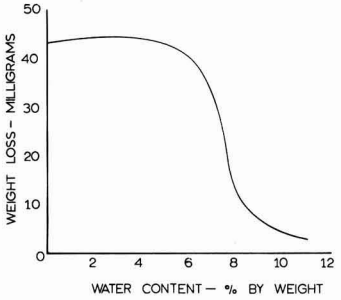

Fig. 2. Effect of water content on weight lost during etching

anode. At this point there is apparently very little pit-type corrosion so necessary to obtain a substantial increase in effective surface area. The exact mechanism involved and the role of water in this mechanism is not understood.

Anodic Current Density

A series of tantalum foil specimens was prepared and etched at anodic current densities from 0.86 to 17.2 amp/dm^2. The etching time was reduced as the current density increased, but not necessarily in such proportion as to maintain constant coulombic input. Several specimens were treated at each current density, and periodic checks of water content were made to assure adherence to near optimum water concentration. The loss in weight of each sample and the capacitance at a formation voltage of 75 v d.c., together with the etch ratio were determined. These data are summarized in Table II and plotted in Fig. 3 and 4.

The effect of increasing apparent current density on the etch ratio is seen to be analogous to the effect

Table II. Effect of apparent current density on etch ratio and weight loss of tantalum foil

Current density, ASD	Etch time, min	Weight loss, Mg/coul	Etched capacity, μf	Etch ratio
0.86	12.5	0.363	17.0	3.86
1.72	8.0	0.372	18.5	4.20
1.72	7.0	0.378	14.8	3.36
2.58	6.5	0.379	15.4	3.50
2.58	5.0	0.364	12.5	2.84
5.16	6.0	0.370	12.0	2.74
5.16	4.5	0.364	10.0	2.30
5.16	3.0	0.358	8.1	1.84
7.74	4.0	0.344	7.5	1.71
7.74	3.0	0.362	8.0	1.82
7.74	2.0	0.344	6.3	1.43
10.32	2.5	0.305	5.1	1.16
10.32	2.0	0.324	5.2	1.18
10.32	1.5	0.329	5.3	1.20
12.04	1.75	0.336	5.3	1.20
12.04	1.5	0.324	5.4	1.21
12.04	1.25	0.319	5.4	1.22
17.2	0.75	0.272	5.2	1.18
17.2	0.50	0.280	5.2	1.18

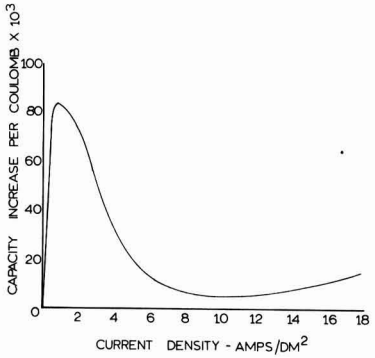

Fig. 3. Effect of anodic current density on capacitance increase per coulomb.

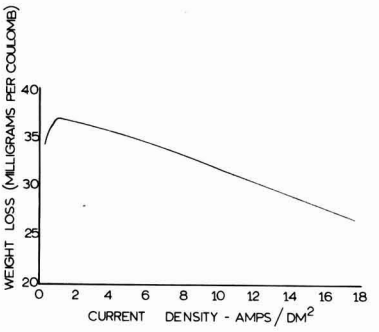

Fig. 4. Effect of anodic density on loss in weight per coulomb

of increasing water content. Both result in a reduction in etch ratio due primarily to the manner in which metal is removed rather than the absolute amount removed. In the electrolytes tested, both high water content and high apparent current density tend toward an electropolishing rather than an electroetching mechanism. Two additional points are worthy of note at this time. First, Fig. 3 indicates that in a chemical sense, that is, at zero current density, there is no observable etching action on the specimen in terms of measurable increase in capacitance. Also, because of variable coulombic input, Fig. 3 is plotted as capacity increase per coulomb *vs.* apparent current density. Second, since the current was held constant during the etching cycle, it is misleading to speak of any but a starting current density. The specimen area obviously increases with time so the current density must decrease.

Electrolyte Concentration

Foil specimens were etched in methanol containing various concentrations of N.F. granular ammonium bromide, and the etch ratio was determined as a function of the approximate water content of each solution. The variation in etch ratio over the entire range of concentrations was approximately ±5%, so apparently the salt concentration and, therefore, the resistivity are not critical, nor do they affect the optimum water content. The data are summarized in Table III.

Table III. Effect of NH_4Br concentration on etch ratio

Approx. water content, wt %	Etch ratio at 75 v d.c. for indicated g/l NH_4Br 5	15	20	60
0	1.13	1.16	1.23	1.25
0.7	3.02	2.82	3.32	2.79
1.4	3.26	3.16	3.36	3.14
2.1	3.06	3.00	3.15	3.01
2.8	2.85	—	—	—
3.5	2.82	2.60	2.87	2.88
6.6	2.49	2.54	2.72	2.68

Forming Voltage

The thickness of the anodic film is directly proportional to the formation voltage, and tantalum metal is consumed in building the oxide film. Consequently, as formation progresses and the voltage increases, peaks of metal are cut down and etch pits are filled in with oxide in a manner to reduce the effective area. For these reasons it is to be expected that the etch ratio decreases with forming voltage and this is shown in Fig. 5. The rate at which the etch ratio falls off is related to the nature of the etch structure. If the etch is fine, the curve drops rapidly, but if the etch is coarse the curve drops more gradually. For analytical purposes the etch structure has been idealized in the form of inverted right cones having a circular base located in the plane of the foil at the surface.

In Fig. 6 the capacity per unit area of plain and etched foil and the etch ratio are plotted on log-log scale against the formation voltage at 95°C. When the curves are extrapolated, the plain and etched lines converge at about 1000 v. This point is construed as that oxide thickness which presents an effective area to the test electrolyte comparable to plain foil. Using a growth rate for oxide of 20Å/v at 95°C and the fact that the oxide/metal volume ratio is 2.4/1, the maximum etch pit diameter according to the idealized model was calculated to be approximately 2.5×10^{-4} cm in diameter.

Tantalum Hardness

Annealed and unannealed tantalum sheet was etched under near optimum conditions of water content and current density to determine the effect of hardness on the etchability. The unannealed specimens showed a 70% greater surface area increase

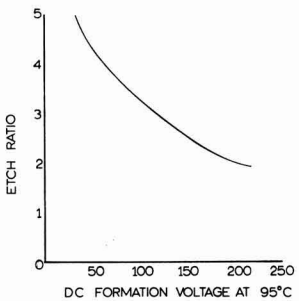

Fig. 5. Effect of d-c forming voltage on etch ratio

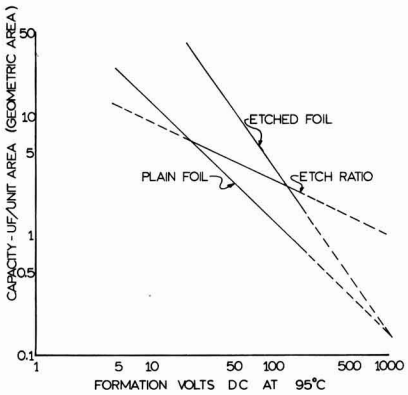

Fig. 6. Effect of d-c formation at 95°C on capacitance per unit area of plain and etched foil.

than the annealed. This was attributed to the presence of regions of high residual stress and energy and to a greater grain boundary path in the unannealed state. There was no evidence in the unetched specimens of increased surface area due to thermal etching.

Summary

Substantially nonaqueous solutions comprising basically a methanol solvent for halides, thiocyanates, nitrates, chlorates, and certain other inorganic and organic compounds may be used to etch tantalum foil electrolytically. The term etch as used here refers to an increase in effective surface area and is not to be confused with metallographic etching. The water content of the etching electrolyte is critical and must be controlled for reproducible results. The anodic current density has been shown to be important, the optimum value being in the range 0.86-2.15 ASD.

The concentration of solute has relatively little effect on etch ratio, but the condition of the metal being etched is of considerable importance. The decrease in etch ratio with forming voltage signifies the filling in of etch pits with tantalum oxide and gives a clue as to the size of these pits.

Acknowledgment

This work was done in partial fulfillment of development contracts on tantalum electrolytic capacitors supported by the Signal Corp, Fort Monmouth, New Jersey. The authors gratefully acknowledge the assistance and contributions of D. H. Stephenson and J. C. Henry in this work.

Manuscript received Nov. 15, 1960. This paper was prepared for delivery before the Chicago Meeting, May 1-5, 1960.

Any discussion of this paper will appear in a Discussion Section to be published in the December 1961 JOURNAL.

REFERENCES

1. G. Kahan, U. S. Pat. 2,775,553, Dec. 25, 1956.
2. C. Houtz, U. S. Pat. 2,756,373, July 24, 1956.
3. A. Jenny, U. S. Pat. 2,742,416, April 17, 1956.
4. R. A. Ruscetta and A. Jenny, U. S. Pat. 2,863,811, Dec. 9, 1958.

The Equivalent Series Resistance of Anodically Formed Oxide Films on Aluminum

Walter J. Bernard

Sprague Electric Company, North Adams, Massachusetts

ABSTRACT

The equivalent series resistance of an electrolytic capacitor is the sum of several resistive elements, the major contributors being the electrolyte and the dielectric film on the anode. The frequency-independent contribution of the electrolyte, R_E, is determined by the resistivity of the solution and the geometry of the capacitor. The contribution of the dielectric film, R_A, is the sum of the series resistance of the film itself and the resistance of the double layer, both of which are frequency-dependent.

R_E may be determined by measuring the series resistance at frequencies sufficiently high so as to make negligible the contribution from other sources, or by extrapolating to $1/f = 0$. The resistance of anodic oxide films on aluminum is influenced by many factors and poses difficulties in measurement; a cell has been constructed which obviates some of these problems. A plot of R_A *vs.* reciprocal frequency is nearly a straight line, the greatest deviation being shown at the higher voltages. In addition, R_A (for a fixed frequency) is directly proportional to film thickness over the range studied. The intercept at zero formation voltage has been attributed to the double layer resistance. The linearity of the plot shows that the dissipation factor of the dielectric film is independent of film thickness, since capacitance is inversely proportional to film thickness, and amounts to about 0.6% at 100 cps.

The dissipation factor, tan δ, of an electrolytic capacitor is expressed by ωRC, where R represents the equivalent series resistance and C the equivalent capacitance. However, the dependence of tan δ on frequency, temperature, and capacitor design can be attributed largely to the changes which occur in series resistance and only to a slight degree to capacitance. Under most conditions the capacitance demonstrates reasonably simple behavior and can be calculated easily. The net capacitance of an electrolytic capacitor ordinarily is due entirely to the anode since the counter-electrode is constructed commonly of material of large capacitance. This anode capacitance is inversely proportional to the thickness of the oxide film and demonstrates a frequency dependence which has only a slight effect on the change of dissipation factor with frequency up to about 10 kc. Compared to the gross effects of the change in series resistance with frequency, this dependence of C on ω may be neglected safely. For example, the average change in C for the specimens shown in Fig. 1 is less than 3% from 100 cps to 6 kc.

The series resistance, on the other hand, is not a simple function of the oxide thickness and is strongly frequency-dependent. It may be considered to be due to the sum of contributions from the electrolyte, R_E, and the resistance at the anode, R_A, due to oxide. Under many circumstances the electrolyte may be the dominant factor which controls the total resistance, but at ordinary temperatures and low frequencies the other resistive elements may be important also.

The oxide layer does not act as a simple parallel resistance. It has been observed in the case of niobium by Young (1) and for tantalum and aluminum by Winkel and de Groot (2) that the equivalent series resistance of anodic oxide is proportional to $1/\omega$ and not to $1/\omega^2$. Young has explained his observations on the basis of a theory which assumes that a resistivity gradient exists in the oxide layer, while Winkel and de Groot arrive at the same results by means of a theory of amorphous dielectrics.

Experimental

Measurements of the anodic impedance of aluminum were made in solutions of ammonium pentaborate in ethylene glycol, similar to the commonly used electrolytes of the aluminum electrolytic capacitor industry. This is advantageous since it avoids the use of aqueous solutions in which electrical measurements of anodic aluminum oxide are difficult, particularly in solutions of high conductance. Electrical characteristics of aluminum oxide films in such solutions are frequently unstable, unlike the

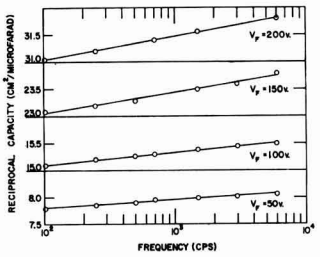

Fig. 1. Reciprocal capacity vs. frequency for anodic aluminum oxide films.

behavior of films of tantalum oxide and niobium oxide.

Solutions in ethylene glycol introduce a difficulty in measurement because of their relatively low conductance. In conventional laboratory equipment the electrolyte resistance (which is in series with the anodic resistance) may be very large and thus makes it difficult to distinguish with precision the effects of the smaller anodic resistance. A useful instrument to nullify the effects of high electrolyte resistance was constructed, similar to the design of that described by Jones and Christian (3). In our equipment a microscope stand was used, connected to a heavy base. The rack and pinion assembly, along with their controls, permitted the vertical variation of the electrodes and the accurate measurement of spacing. The bottom electrode consisted of a platinized platinum sheet sealed to a brass disk and securely encased in an epoxy resin, leaving only the platinum face exposed. The brass disk made electrical connection to the measuring equipment through an insulated sleeve in the base. An epoxy resin cup was used to contain the electrolyte. The upper electrode (removable) was the aluminum anode and consisted of a disk of high purity aluminum[1] 1 in. in diameter. It was machined flat, and one face was drilled and tapped to accommodate a threaded brass rod for making subsequent electrical contact. It then was polished mechanically and anodized to a relatively high voltage, usually in excess of 400 v, over all but the top face. The oxide on the bottom face then was removed by a mechanical polish carried out to a mirror finish, followed by a chemical polish. The disk with the connecting brass rod in place was encased then in epoxy resin, the polished face being protected during this operation by use of grease. A thorough cleaning operation followed the setting of the resin. The exposed face of aluminum then was oxidized in a conventional boric acid solution at 25°C to the desired voltage, transferred to the measuring electrolyte, and maintained at constant voltage until the current had fallen to 2.0 $\mu a/cm^2$. This ensured a uniform electric field for all samples and also helped eliminate some of the poorer specimens. Good results were obtained in this way for experiments up to 200 v. Beyond that voltage the insulating properties of the plastic were not satisfactory and erratic results were obtained. The construction of the cell was such as to keep the faces of the electrodes parallel to within a few tenths of a millimeter across the surface. The vertical separation of the electrodes was measured by means of a micrometer scale attached to the top of the cell.

The mechanical operation of the instrument was satisfactory. Figure 2 shows the values obtained with only the electrolyte and two inert electrodes. The origin is the measured contact position of the electrodes, that is, zero separation, and the plot shows that the extrapolated short-circuit position is very close to the measured contact position. In addition to this, the resistivity of the electrolyte may be calculated from the slope of the line and the measured

[1] Alcoa aluminum plate, 99.986% Al (minimum).

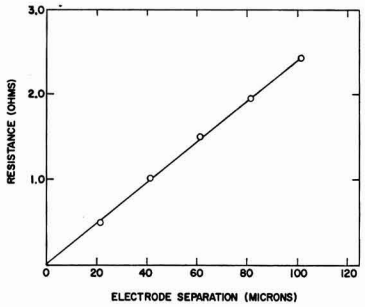

Fig. 2. Cell resistance as a function of electrode separation at 25°C and 10 kc.

cell geometry; it was found to compare with the true value to within a few per cent.

For all the results given here, the electrolyte used was a solution of 30% ammonium pentaborate in ethylene glycol. This solution corresponds to a typical capacitor electrolyte and has a resistivity of about 1000 ohm-cm.

A bridge of the series resistance-capacitance type was used for the measurements reported here.[2] The frequency range available was from 40 cps to 400 kc and the a-c signal strength was 0.2 to 0.3 v. All measurements were made without applied d-c bias.

Results and Discussion

For a given electrode the cell resistance was measured as a function of electrode spacing at several frequencies. The value extrapolated to zero in each case gives the anodic resistance, since it is that part of the total R which is not due to the electrolyte. Typical curves are shown in Fig. 3; each of the intercepts on the vertical axis represents the anodic resistance at that frequency. For most measurements it was found that the value of R for a given electrode spacing at infinite frequency when subtracted from the total resistance for any other frequency at that spacing gave a figure in agreement with the R obtained by extrapolation to zero spacing. This was true when the electrode spacing was small, *i.e.*, less than 1 mm. Data obtained in this way were used extensively. In Fig. 4 the results of formations between 50 and 200 v are given; these curves are plots

[2] Constructed by Dr. Robert P. Auty of the Sprague Electric Company.

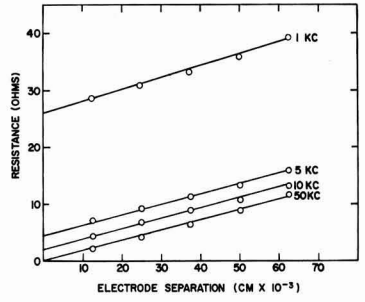

Fig. 3. Cell resistance, with formed aluminum anode, vs. electrode separation.

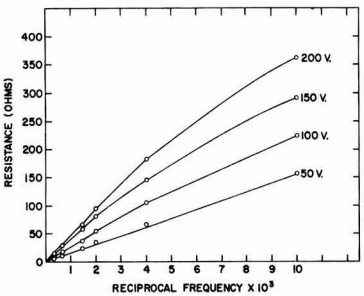

Fig. 4. Anodic resistance vs. reciprocal frequency for several formation voltages.

of the anodic resistance *vs.* the reciprocal frequency. For lower voltages quite good straight line plots are obtained but there is a pronounced deviation from a linear relationship at higher voltages. This may possibly be due to the problems in obtaining good specimens using the technique employed here, since the higher the voltage the more difficult it became to obtain reproducible results. Data above 200 v were completely unreliable. Curves of this sort have been reported also by Winkel (2), but the types of film which gave rise to his results were quite different from those described here. The films which he found gave this effect contained a large fraction of hydrated alumina and were high-resistance films. There is no reason to believe that the films studied here contained any appreciable amount of hydrated oxide. Smith (5) also has observed a pronounced curvature in plots of this type which he ascribes to geometrical effects of the measuring cell, enhanced by the relatively high resistance of the electrolyte. It is unlikely that his treatment can explain the observations reported here since the cell described in this paper obviates these conditions.

Figure 5 shows the result of a plot of anodic resistance at 100 cps *vs.* formation voltage. The resistance shows a linear dependence on oxide thickness. Capacity is, of course, inversely proportional to the oxide thickness, and the conventional $1/C$ plot is also included here. Since the resistance plot does not go through the origin it has been concluded that, if the extrapolation is valid, some part of the anodic resistance exists at zero formation voltage and is constant over the voltage range. This conclusion is compatible with the idea that an appreciable contribution to the total resistance is given by the double layer and that this layer at the oxide-electrolyte interface has an equivalent series resistance shown by the intercept on the vertical axis. This resistance would be expected to be temperature-dependent and to differ at least in magnitude with the oxide temperature dependence, but reliable data for this effect have not been obtained yet.

The actual values of R_A are lower than has been reported previously. This may be due to the better quality of the film or the manner in which it was measured. R_A is influenced by the conditions of oxidation and depends on the current density, temperature, and electrolyte composition used.

If the increments in the R_A plot are assumed to be due to the oxide, it is seen that tan δ of the oxide is independent of formation voltage, and for the conditions described here the value is about 0.6% at 100 cps. We also note that since R_A is inversely proportional to the frequency and the capacity is essentially frequency-independent, then the dissipation factor, ωRC, of the film is also frequency-independent. Electrolytic capacitors in practice do not show a dissipation factor which is independent of frequency or formation voltage; tan δ generally is increased by increasing frequency and decreasing formation voltage. This is due principally to the electrolyte resistance and the resistance which has been ascribed to the double layer. At high frequencies the entire anodic resistance is negligible and because of the constant resistance of the electrolyte the dissipation factor is proportional to the frequency at suitably high frequencies.

Figure 6, adapted from data of Robinson and Burnham (4), illustrates the effect of increased surface area of the capacitor, brought about by etching the foil. It is observed commonly that capacitors containing etched foil have higher dissipation factors than those with plain foil, but this cannot be attributed to the oxide film since the RC product of the film is independent of surface area. However, if the circuit of an electrolytic capacitor, at a fixed frequency, is considered to be a capacity in series with an anodic resistance and an electrolyte resistance, then the effect may be explained. R_A decreases

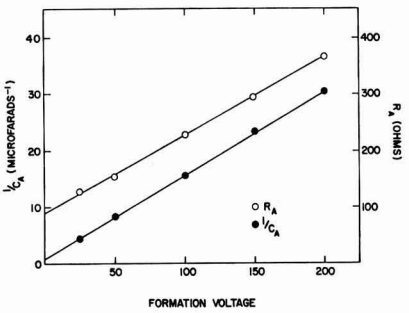

Fig. 5. Reciprocal capacitance and anodic resistance at 100 cps as a function of formation voltage.

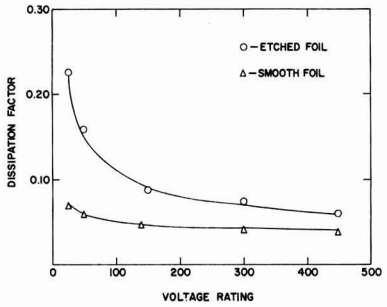

Fig. 6. Effect of surface roughness on the dissipation factor of aluminum electrolytic capacitors.

with increasing area, with a proportional increase in capacity. The other major resistive element, R_E, is unchanged, however, because the geometry of the electrolyte is unaffected by the etched foil. Since a proportional decrease in the total resistance does not occur, an increase in tan δ is observed. The effect is more pronounced at low formation voltages because the electrolyte has a correspondingly larger contribution in the presence of thinner oxide films.

Acknowledgment

The author would like to thank Mr. Stanley Szpak for his assistance in the course of this work.

Manuscript received Nov. 15, 1960. This paper was prepared for delivery before the Chicago Meeting, May 1-5, 1960.

Any discussion of this paper will appear in a Discussion Section to be published in the December 1961 JOURNAL.

REFERENCES

1. L. Young, *Trans. Faraday Soc.*, **51**, 1250 (1955).
2. P. Winkel and D. G. de Groot, *Philips Research Repts.*, **13**, 489 (1958).
3. G. Jones and S. M. Christian, *J. Am. Chem. Soc.*, **57**, 272 (1935).
4. P. Robinson and J. Burnham, *This Journal*, **83**, 261 (1943).
5. A. W. Smith, *Can. J. Phys.*, **37**, 591 (1959).

On the Mechanism of Cathodic Crystal Growth Processes

B. C. Banerjee and P. L. Walker, Jr.

Mineral Technology Division, The Pennsylvania State University, University Park, Pennsylvania

ABSTRACT

An electron diffraction and electron microscopic study on thin films of copper electrodeposited on clean 1 mil foils of copper and platinum from acid-copper and complex copper-glycine baths maintained at 25°C has been conducted. The foils of copper and platinum consist of small grained structure. Results show that for a current density of 10 ma/cm² and high acidic conditions (*p*H 0.3 or 0.9), large crystal grains of copper (10-40μ) are developed, even when the deposit thickness is very small. A limited study on the effect of current density on the orientation of nickel, electrodeposited mainly on brass disks from some common plating solutions maintained at 25°C, has also been carried out. Results are discussed in light of existing mechanisms for the cathodic crystal growth process.

Studies on the mechanism of cathodic crystal growth processes have received considerable attention in recent years as a result of successful application of electron waves in determining the structure, orientation, and, hence, the mode of growth of cathodic deposits. Electron diffraction studies on the structure of electrodeposited metals of widely varying thickness on polycrystalline substrates suggest that these deposits are initially random and polycrystalline. They possess a fine grain structure which develops preferred orientations as the film grows thicker. These orientations which determine the mode of growth of electrodeposits were found to be profoundly influenced by bath conditions such as current density, temperature, *p*H, concentrations of anions and cations, presence of trace impurities and addition agents, and mechanical agitation of plating solutions (1-6). A systematic investigation of the structure of electrodeposited metals by electron diffraction and elucidation of a tentative mechanism of their growth process was first accomplished by Finch, Wilman, and Yang (1). According to their classical mechanism (1, 2), deposition conditions which favor either the plentiful supply or impoverishment of metal ions at the immediate vicinity of the cathode are the controlling factors in determining the preferred orientations developed by the deposits and hence their mode of growth. In a f.c.c. metal, the (110) orientation was supposed to be of outgrowth type whereas the (100) or (111) orientation, lateral type. Electrodeposits, however, often develop abnormal values of internal stresses (7, 8) which cannot be understood by the above mechanism. In working with nickel electrodeposited from solutions maintained at room temperature, one of the authors found recently that the outgrowth type of deposit, as characterized by the (110) orientation of nickel, is always favored at very low (0.5-1 ma/cm²) and very high (above 100 ma/cm² depending on the *p*H or bath temperature) current densities, whereas the lateral or transitional type of growth [*i.e.*, (100) or (210) orientations, respectively] are favored at intermediate current densities. These results cannot be explained satisfactorily on the basis of the classical mechanism (1, 2).

These results on nickel prompted the study of the electrodeposition of copper which forms the main subject of the paper. In the present investigation, surface structure and morphology of copper, electrodeposited on thin foils of copper and platinum from three different baths were studied by electron diffraction and electron microscopy.

Experimental

The main experiments may be divided into three parts: (*a*) electrodeposition of copper at a current density of 10 ma/cm² from plating solutions maintained at room temperature on clean 1 mil foils of copper and platinum, (*b*) electron diffraction studies of these surfaces, and (c) electron microscopic

studies of the replicas of the surfaces of these electrodeposits.

Electrodeposition of copper on thin foils cleansed in suitable etching solutions was carried out from the following solutions:

[1] $CuSO_4 \cdot 5H_2O$, 120 g/l + H_2SO_4, 74 g/l, pH = 0.3

[2] $CuSO_4 \cdot 5H_2O$, 120 g/l + glycine, 25 g/l + H_2SO_4 added to give a pH of 0.9

[3] $CuSO_4 \cdot 5H_2O$, 120 g/l + glycine, 25 g/l, pH = 2.5

Bath [1] will be called an acid-copper bath and baths [2] and [3] will be called complex copper baths in the following discussions. All the chemicals used in the preparation of the solutions were of A. R. grade and the solutions were further purified by electrolyzing them at a low current density as described elsewhere (3). A foil area of *ca.* 4 cm^2 for deposition was available.

The copper and platinum foils, of high-purity reagent grade, were obtained from Fisher Scientific Co. (Cat. No. C-428). Before electrodeposition, the copper foils were etched for a few seconds in moderately dilute HNO_3 followed by a dip in concentrated HCl and a rinse in distilled water. An electron diffraction study of the copper and platinum foil surfaces reveal ring patterns, characteristic of polycrystalline small grained structure. The pattern for the copper foil is shown in Fig. 1. The polycrystalline structure of the copper foil can also be seen from the platinum preshadowed carbon replica of the foil surface at a magnification of 1300X (before reduction for publication) in Fig. 2.

Following electrodeposition, the deposits of copper were washed with a jet of distilled water, dried with filter paper, and immediately removed for electron diffraction studies. They were examined with a 50 kv electron beam of 25μ width at grazing incidence by the reflection technique.

For replica studies, the freshly prepared surface was covered with a few drops of a dilute collodion solution. After evaporation of the solvent, a replica of the metal surface was obtained. The collodion replica thus formed was removed from the metal surface (by attaching the collodion replica on to scotch tape), shadowed with platinum at angles varying from 15° to 35°, followed by deposition of a thin film of carbon in a vacuum evaporator. The collodion was then dissolved in amyl acetate and the carbon replica was collected on fine copper grids for an electron microscopic investigation.

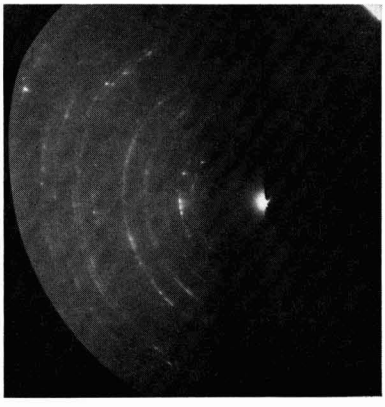

Fig. 1. Electron diffraction pattern for clean copper substrate, revealing polycrystalline and small grained structure of initial cathode surface.

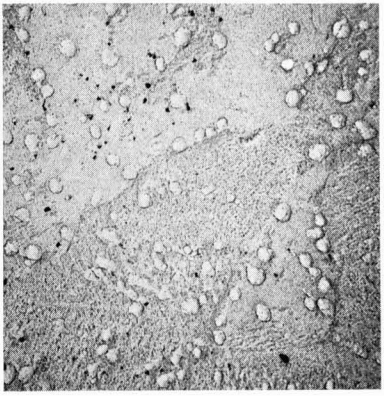

Fig. 2. Electron micrograph of the initial copper cathode, as obtained by platinum preshadowed carbon replica technique at a magnification of 1300X.

In some limited preliminary studies, nickel was electrodeposited on mechanically polished thick brass disks and 1 mil thick foils of copper and platinum from sulfate-boric acid, chloride-boric acid, and sulfate-chloride-boric acid baths maintained at room temperature (25°C). The time of deposition was adjusted so as to have a thickness of about 3-5μ of electrodeposited nickel. Bath compositions are listed in Table II.

Results and Discussion

Results of electron diffraction studies of electrodeposited copper and nickel are presented in Tables I and II, respectively; and electron microscopic

Table I. Electron diffraction studies on copper, electrodeposited at 10 ma/cm^2 and 25°C on 1 mil thick copper and platinum cathodes

Bath	Time of deposition, min	Cathode substrate	Remarks on electron diffraction patterns	Figure
1	5-10	Cu	Spot pattern showing reflection, probably from (200) face of copper	3
1	5	Pt	Nearly spot pattern showing (110), preferred orientation	4
2	8-12	Cu	Spot pattern showing reflection from (111) face	5
3	10	Cu	Ring pattern showing $(10\bar{1}0)$ + (211) preferred orientation	6
3	25	Cu	Dotted arc pattern showing $(10\bar{1}0)$ + (211) preferred orientation	7

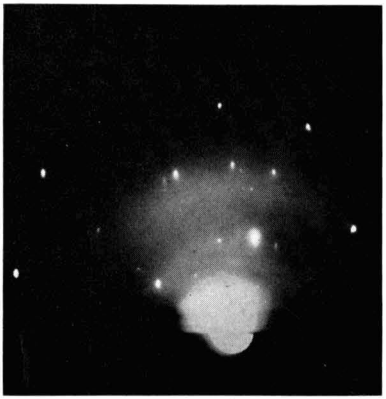

Fig. 3. Electron diffraction patterns of electrodeposited copper. See Table I for experimental details.

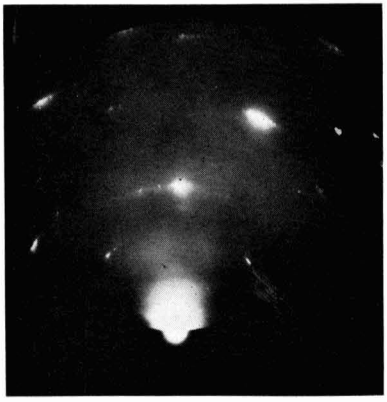

Fig. 4. Electron diffraction patterns of electrodeposited copper. See Table I for experimental details.

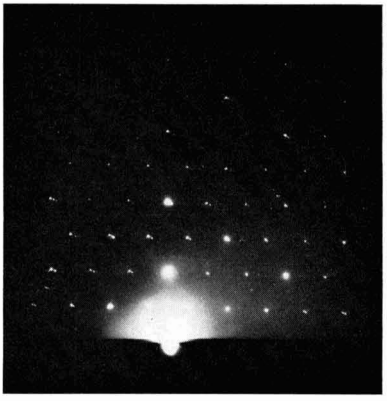

Fig. 5. Electron diffraction patterns of electrodeposited copper. See Table I for experimental details.

studies of surfaces of electrodeposited copper are presented in Table III. Table I shows that under high acidic conditions, *i.e.*, baths [1] and [2], copper electrodeposited on 1 mil thick foils of copper and platinum (as cathodes) yields spot electron diffraction patterns, indicating a larger grain size. These results can be seen by studying the appropriate

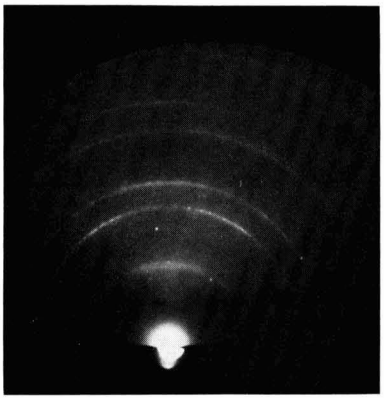

Fig. 6. Electron diffraction patterns of electrodeposited copper. See Table I for experimental details.

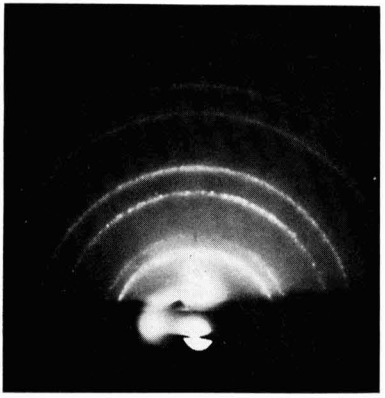

Fig. 7. Electron diffraction patterns of electrodeposited copper. See Table I for experimental details.

figures listed in Table I. Bath [3] favors the development of a $(10\bar{1}0) + (211)$ preferred orientation of electrodeposited copper on 1 mil copper foils for short deposition times. Longer deposition times generally result in dotted arc patterns having larger grain sizes, as can be seen from Fig. 6 and 7.

Table II. Effect of current density on orientations of electrodeposited nickel at 25°C

Bath	pH	Current density in ma/cm²	Orientations
$NiSO_4 \cdot 7H_2O$, 280 g/l	3.5	1	(110)
		10	(100)
+ H_3BO_3, 31 g/l		25	(210)
		45	(210) + (110)
		75, 100	(110)
$NiCl_2 \cdot 6H_2O$, 150 g/l	4.9	1	(110)
		10 to 50	$(10\bar{1}0) + (211)$
+ H_3BO_3, 31 g/l		75, 100	(210)
		200	(110)
$NiSO_4 \cdot 7H_2O$, 280 g/l	3.6	1	(110)
		10	(100)
+ $NiCl_2 \cdot 6H_2O$, 48 g/l		20	(100) + (210)
		45	(210)
+ H_3BO_3, 31 g/l		75	(210) + (110)
		100, 200	(110)

Table III. Electron microscopic studies on copper surfaces, electrodeposited from different baths at 10 ma/cm² and 25°C (Magnification, 1300X before reduction for publication)

Deposition conditions	Time of deposition, min	Average grain size, μ	Figure
Bath [1], on 1 mil Cu foil	5	~35	8a
	10	>45	8b
Bath [1], on 1 mil Pt foil	5	Elongated grains more than 35μ in length and 10μ in breadth	8c
Bath [2], on 1 mil Cu foil	5	~10	9a
	10	~23	9b
Bath [3], on 1 mil Cu foil	5	<3	10a
	15	~7	10b

It is seen from Table II that very low and high current densities always favor the development of (110) preferred orientations of nickel, electrodeposited on mechanically polished brass disks as well as on thin foils of copper and platinum at 25°C from three commonly used nickel plating solutions. The trend of the results shown in Table II is maintained for all possible *p*H conditions for any of the baths used (9).

An estimate of the grain size of electrodeposited copper, as obtained under various conditions of deposition, was made possible by an electron microscopic study of the replicas of the surface.[1] The results are presented in Table III. It is noted that deposits with grains larger than 35μ separated by well-defined grain boundaries are obtained, even in very thin deposits, from bath [1] as compared with much smaller grains, even in comparatively thicker deposits, from bath [3] under otherwise identical conditions of deposition. This may be seen by comparing electron micrographs, Fig. 8a, 8b, and 8c with Fig. 10a and 10b. Relatively large grain deposits are also evident from bath [2], as seen in micrographs, Fig. 9a and 9b.

Results on the formation of unusually large grains of electrodeposited copper, resulting in spot electron diffraction patterns, or the development of much smaller grains, depending on the bath conditions used, cannot be understood fully on the basis of the classical mechanism for cathodic crystal growth processes proposed by Finch, Wilman, and Yang (1). Other possible explanations can be considered briefly.

[1] A longer time of deposition generally gives rise to larger grain size of deposits for identical conditions of deposition. The thickness of the deposits was found to depend mostly on the time of deposition for all three baths used for copper plating.

Fig. 8a. Electron micrographs of electrodeposited copper surfaces. See Table III for experimental details.

Fig. 8b. Electron micrographs of electrodeposited copper surfaces. See Table III for experimental details.

Fig. 8c. Electron micrographs of electrodeposited copper surfaces. See Table III for experimental details.

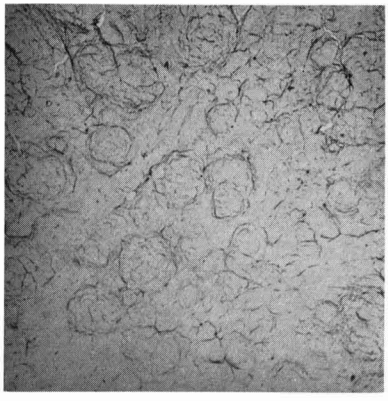

Fig. 9a. Electron micrographs of electrodeposited copper surfaces. See Table III for experimental details.

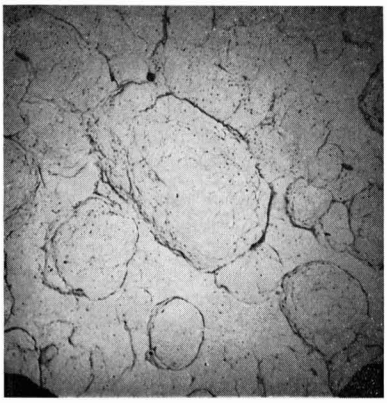

Fig. 9b. Electron micrographs of electrodeposited copper surfaces. See Table III for experimental details.

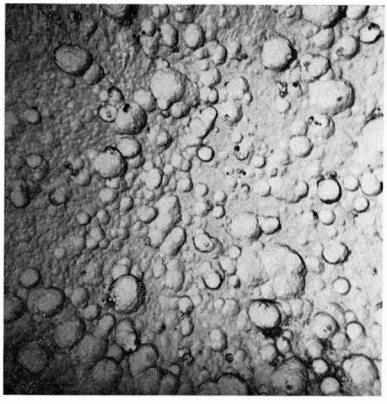

Fig. 10a. Electron micrographs of electrodeposited copper surfaces. See Table III for experimental details.

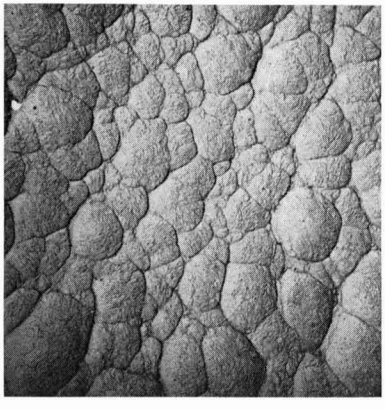

Fig. 10b. Electron micrographs of electrodeposited copper surfaces. See Table III for experimental details.

According to the dislocation theory of crystal growth, which was first proposed by Frank and his co-workers (10) and applied by Vermilyea (11), Cabrera and Vermilyea (12), and others (13) to explain various aspects of cathodic growth, a crystal can grow at a fast rate if there are present on the growing surface numerous imperfections in the form of kinks in steps of screw dislocations emerging at the surface. If atoms are deposited at kink sites or migrate there at a fast rate by a process of diffusion, a crystal grain may grow at a rapid rate resulting in large grained deposits. It is believed (12, 13) on the basis of dislocation theory that crystal growth occurs by movement of steps over close packed surfaces. When a crystal is exposed to a supersaturated medium, only those steps can advance which have a radius of curvature greater than a critical value, depending on the edge energy of a step per unit area and free energy decrease per unit volume accompanying deposition (the latter being proportional to supersaturation or overvoltage). Strongly adsorbed impurity particles such as atoms, ions, or molecules can prevent the movement of steps with which they are in contact. The larger particles by virtue of having smaller vibrational frequencies than metal atoms are likely to be embedded into the growing crystals. Dissolved oxygen from an acid-copper bath or glycine and codeposited hydrogen from a complex copper-glycine bath may thus radically alter the growth velocity at a given supersaturation of the species in the catholyte layer.[2] Since immobile, adsorbed impurities are more effective than mobile impurities in retarding and ultimately stopping the flow of growth steps and consequently growth of large crystals, we have reason to believe that dissolved oxygen is much more mobile than glycine or codeposited hydrogen so far as the advance of steps on growing cathode surfaces are concerned. The fact that abnormally large crystals showing spot electron diffraction patterns result during electrodeposition from an acid-copper bath which contains no impurity other than dissolved oxygen strongly suggests the above contention. This point has recently been thoroughly discussed by van der Meulen and Lindstrom (14). However, such impurities as H^+, OH^-, H_2O, or Cu^+ which are inherent with the bath may also be effective in producing dislocations and maintaining them on the growing surface.

Development of large grains may also take place as a result of coalescence of existing smaller grains if the temperature of the growing surface is sufficient to promote such a process. According to Wilman (7, 8) heat evolved as a result of neutralization of ions into atoms as well as metallic bond formation during electrodeposition may raise the temperature of a growing cathode surface well above its recrystallization temperature. Wilman suggests that such a temperature rise can, in part, be caused by the highly porous nature of some cathode deposits. This high porosity[3] results in a low thermal conductivity for the growing cathode and makes incorrect an estimate of rise in surface temperature if the growing cathode is assumed to have thermal conductivity values usually assigned to solid metals. Large

[2] The interference in crystal growth by colloidal copper hydroxide (or basic sulfate) present in the cathode film region, rendered more alkaline as a result of hydrogen discharge as compared with the bulk pH of the complex copper-glycine bath, is also a possibility.

[3] The porosity of electrodeposited metal generally decreases with increasing thickness (17). In fact, under certain conditions of deposit, as was observed by Ogburn and Benderly (18) in the case of nickel, an electrodeposited metal film as thin as 5μ can be formed essentially pore free. Our deposits, however, were much thinner than 5μ and may have contained considerable porosity.

amounts of internal stresses, which are developed in electrodeposits during the plating process (15), may deform surface layers of the original cathode to a considerable extent.[4] This deformation may introduce lattice defects such as vacancies, interstitials, dislocations, and stacking faults on the cathode surface contributing to a lattice disturbance, which according to Broom and Barrett (16) is responsible for a large scattering of conduction electrons resulting in lower electrical conductivities for cathode-deposit interfacial layers. Development of large grains during electrodeposition can then possibly be explained by the combination of a rapid growth rate due to the presence of imperfections on the cathode surface and a predominantly stress-activated coalescence mechanism, where the recrystallization temperature will be appreciably lowered by deformation of the electrodeposited metal (19, 20). In this connection, Boudart (21) has shown by calculations that the heat evolved as a result of metallic bond formation is considerably lowered if the work function of the metal surface is raised due to chemisorption of hydrogen. The efficiency of the complex copper-glycine bath is reduced due to evolution of hydrogen at the cathode during electrodeposition. Whatever be the temperature of the growing cathode, it is possible that this evolved hydrogen may partly be chemisorbed on the growing surface and result in inhibition of grain growth by decreasing this temperature.

The transmission of heat through a porous material containing numerous defects is a complex phenomena, and little information is available on interaction of these defects not only with phonons but also with other adsorbed species from the catholyte layer. This we feel is partly responsible for the lack of a quantitative understanding of the crystal growth process at the present time. Hoffman and co-workers (22) calculated a temperature rise of about 700°C during the evaporation of nickel on mica under high vacuum at the instant at which the energy is shared by the first and second neighbors of a site. This temperature rise can be much larger in the case of electrodeposition of nickel or copper since the energy of neutralization is six times larger (7) than the energy required to incorporate neutral metal atoms into a crystal. The important question arises whether this idealized high-temperature pulse for a particular layer of deposited atoms would disappear by thermal conductivity with a relaxation time of the order of 10^{-12} sec before the second layer of freshly deposited atoms appear on the surface. Also a full understanding of the properties of imperfections based on complete information on a variety of metal is necessary before one can arrive at a final conclusion as to the exact mechanism of the cathodic crystal growth process.

[4] We have recently observed with electron microscopy, using a platinum preshadowed carbon replica technique, the development of subgrain structure and facets on copper or aluminum cathode surfaces when a very thin film of nickel is electrodeposited at room temperature (25°C) from a Watts' type of bath of pH 3.2 and at a current density of 10 ma/cm². Since deformation of surface layers plays an important role in subgrain formation (19), although it is in general a thermally activated process (19), we believe that the cathode surface undergoes rearrangements during electrodeposition. This will be discussed in a later paper.

Acknowledgments

This work was supported by the Atomic Energy Commission, Contract No. AT(30-1)-1710. The authors are indebted to Professor J. J. Comer for some experimental suggestions and to Professor W. R. Buessem for valuable discussions.

Manuscript received Aug. 23, 1960; revised manuscript received Dec. 28, 1960.

Any discussion of this paper will appear in a Discussion Section to be published in the December 1961 JOURNAL.

REFERENCES

1. G. I. Finch, H. Wilman, and L. Yang, *Discussions Faraday Soc.*, **1**, 144 (1947).
2. G. I. Finch and D. N. Layton, *J. Electrodepositors' Tech. Soc.*, **27**, 215 (1951).
3. B. C. Banerjee and A. Goswami, *J. Sci. Ind. Research (India)*, **14B**, 322 (1955).
4. B. C. Banerjee and A. Goswami, *This Journal*, **106**, 20 (1959).
5. B. C. Banerjee and A. Goswami, *ibid.*, **106**, 590 (1959).
6. B. C. Banerjee and A. Goswami, *J. Sci. Ind. Research (India)*, **16B**, 144 (1957).
7. H. Wilman, *Proc. Phys. Soc. (London)*, **68B**, 474 (1955).
8. H. P. Murbach and H. Wilman, *ibid.*, **66B**, 905 (1953).
9. Unpublished results.
10. W. K. Burton, N. Cabrera, and F. C. Frank, *Trans. Roy. Soc. (London)*, **A243**, 299 (1951).
11. D. A. Vermilyea, *J. Chem. Phys.*, **25**, 1254 (1956).
12. N. Cabrera and D. A. Vermilyea, "Growth and Perfection of Crystals," p. 393, John Wiley & Sons, Inc., New York (1958).
13. P. B. Price, D. A. Vermilyea, and M. B. Webb, *Acta Met.*, **6**, 524 (1958).
14. P. A. van der Meulen and H. V. Lindstrom, *This Journal*, **103**, 390 (1956).
15. I. Laird Newell, *Metal Finishing*, p. 56, October 1960.
16. T. Broom and C. S. Barrett, *Acta Met.*, **1**, 305 (1953).
17. W. Blum and G. B. Hogaboom, "Principles of Electroplating and Electroforming," p. 141, McGraw Hill Book Co., New York (1949).
18. F. Ogburn and A. Benderly, *Plating*, **41**, 61, 169 (1954).
19. H. T. Lambot, *J. Inst. Metals*, **84**, 473 (1956).
20. G. E. Doan, "The Principles of Physical Metallurgy," p. 103, McGraw Hill Book Co., New York (1953).
21. M. Boudart, *J. Am. Chem. Soc.*, **74**, 3556 (1952).
22. R. W. Hoffman, R. D. Daniels, and E. C. Crittenden, Jr., *Proc. Phys. Soc. (London)*, **67B**, 497 (1954).

Transparent Luminescent Films by Solution Spraying

Russell D. Kirk and James H. Schulman

U. S. Naval Research Laboratory, Washington, D. C.

ABSTRACT

Spraying solutions of zinc chloride or cadmium iodide with activator onto preheated Pyrex or silica glass yields cathodoluminescent films by direct reaction with the glass. The activated silicate films have excellent adherence, good transparency, and, on silica, a brightness comparable to that of evaporated films on Vycor. Films on silica require refiring in air.

In recent years transparent phosphor films have been produced by various methods. Film formation by vapor phase reaction of zinc metal plus a volatile compound of the desired activator with H_2S at heated glass surface is exemplified by the work of Studer and Cusano (1). Vacuum evaporation of previously prepared phosphor powders followed by refiring has recently been used successfully by Feldman and O'Hara (2) for sulfide, fluoride, and several oxygen-containing phosphors. It is the purpose of this paper to describe yet another method of preparing phosphor films.

Transparent, electrically-conducting films of tin oxide prepared by spraying alcoholic or aqueous solutions of tin chlorides onto preheated glass have been known and used for about ten or fifteen years (3). Modification of film properties can be achieved by addition of other metal halides, and similar films can be obtained from solutions of indium (4), cadmium (5), and from $TiCl_4$ (6). Recent work at this laboratory has produced transparent luminescent films of zinc and cadmium silicate phosphors by spraying suitable zinc and cadmium halide solutions plus activator onto hot Pyrex or fused silica with an atomizer. Films on Pyrex were produced by a one-step spraying process, while those on fused silica required refiring in air at a temperature higher than that used during the atomizing process.

Transparent, cathodoluminescent films of green-emitting Zn_2SiO_4:Mn have been prepared on Pyrex and on fused silica, yellow-emitting Zn_2SiO_4:Mn on Pyrex, $CdSiO_3$:Mn on fused silica, and Zn_2SiO_4:Ti on Pyrex and on fused silica by this technique.

Experimental

Methanolic solutions of reagent grade $ZnCl_2$ (50% by weight) containing $MnCl_2$ or $TiCl_4$ were used for the Zn_2SiO_4 phosphors, CdI_2 solutions (because of the greater solubility of CdI_2 in methanol) with $MnCl_2$ for $CdSiO_3$:Mn. Although 2-5 ml of solution was the usual amount for each test run, neither the concentration nor the volume appeared to be critical.

In early trials a glass and plastic hand atomizer was used for spraying. Later, the solutions were sprayed with an all-glass gravity-fed "Chicago" atomizer (7) into the fused silica tube containing the glass samples, the silica tube placed in a tube furnace as illustrated in Fig. 1. Orifice diameters in millimeters are as follows: liquid, 1.52 ID, 2.36 OD; air, 2.80 ID. A line air pressure of 16 psi was used which gave a liquid flow rate of approximately 0.33 ml/sec for the solutions used. Total spray discharge times were thus 6-15 sec.

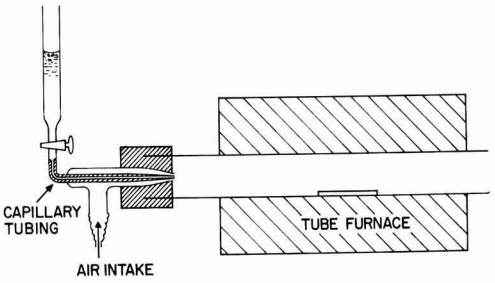

Fig. 1. Schematic view of spraying apparatus.

High-purity graphite and acid extracted porous alumina supports were used for Pyrex, since some spraying of this glass was done above its softening point. Temperatures of the glasses during exploratory test runs were varied from 500° to 1000°C. The glasses used were No. 7740 Pyrex filters, fused silica laboratory tubing, and polished fused silica microscope slides, all sawed to convenient size.

The samples were tested in a demountable cathode-ray tube (14) at 7.5 kv and about 10 $\mu a/cm^2$ beam current, with a conductive tin oxide film on the samples to prevent surface charge buildup. The tin oxide film on the samples absorbs part of the beam energy at 7.5 kv; brightness of the original phosphor films at this voltage was 1.6 times that of the same films with the conducting coating.[1] Some of the attenuation may be due to partial destruction or poisoning of the luminescent film by the process of application of the tin oxide layer. Since the films could not be evaluated nor could they have practical application without a conductive coating, all values tabulated are for films with this coating. Emission spectra were obtained with a calibrated radiometer. Brightness measurements were made with a Spectra Brightness Spotmeter[2] focused on

[1] This measurement was made with the radiometer by recording the change in photomultiplier output when coated and uncoated samples were rapidly shifted into the C. R. beam. The monochromator was set at the emission peak of the phosphor.

[2] ½° ultrasensitive model, Photo Research Corporation, Hollywood, California.

Table I. Runs producing films with good clarity and brightness

Phosphor	Substrate	Atoms activator per atom Zn or Cd, solution	Deposition temp, °C	Refiring conditions	Emission peak, Å†	Brightness, ft-L†
α-Zn_2SiO_4:Mn	Vycor		(Evaporated Film) *		5240	17
α-Zn_2SiO_4:Mn	Silica	0.01	900	1250° for 1 hr	5240	22
α-Zn_2SiO_4:Mn	Pyrex	0.01	900	None	5190	4
β-Zn_2SiO_4:Mn	Pyrex	0.01	900	None	5700	3
Zn_2SiO_4:Ti	Pyrex	0.07	850	None	3950	1
Zn_2SiO_4:Ti	Silica	0.07	850	1000° for 1 hr	3900	2
$CdSiO_3$:Mn	Silica	0.006	1000	1150° for 1 hr	5900	27

* Prepared by Feldman and O'Hara (2).
† At 7.5 kv and 10 μa/cm².

the luminescent film; readings were made directly in foot-lamberts.

Results and Discussion

Runs producing films with good clarity and brightness are summarized in Table I. The temperatures noted in column four are those measured by a thermocouple 1 mm above the surface of the glass just before spraying. Temperatures during spraying often rose 100° above these because of combustion of the methanol. Although both the spraying and refiring temperatures cited produced clear films with the equipment used, they are not necessarily optimum. The most satisfactory spraying temperature may vary with the geometry of the apparatus.

Emission spectra are shown in Fig. 2 and 3. Those of Zn_2SiO_4:Ti have a small secondary peak in the green, obviously due to traces of manganese impurity. The main emission peak is at a slightly shorter wavelength than that quoted by Leverenz (8).

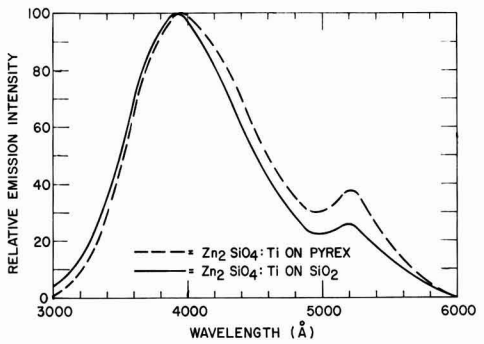

Fig. 2. Emission spectra of sprayed titanium-activated zinc silicate films.

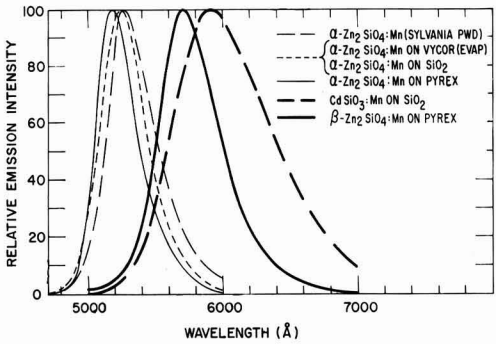

Fig. 3. Emission spectra of sprayed manganese-activated zinc and cadmium silicate films.

Emission peak positions of the various α-Zn_2SiO_4:Mn films exhibit some variation, although the spectra of the sprayed film on silica glass and that of the evaporated film on Vycor are identical. Variation of the Mn concentration may account for the differences in peak positions.

The luminescence of the sprayed β-Zn_2SiO_4:Mn film peaks at 5700Å. Leverenz (8), Feldman and O'Hara (10), Pfeiffer and Fonda (9), and Shrader (11) give peak positions ranging from 5650 to 5850Å.

The 5900Å peak of $CdSiO_3$:Mn is identical with that of reference (8).

Film adherence in general was excellent. One-step film formation on Pyrex was accompanied by a very mild but transparent etch. Quantitative measurements of the degree of fogging or frosting of a film are dependent on the angle of the transmitted light subtended by the detector. However, an idea of the transparency of the films on Pyrex may be gained from Fig. 4. All the films in the photograph are 2 in. above the background. $CdSiO_3$:Mn films on silica glass have approximately the same transparency as the illustrated films. Poorest transparency was that of α-Zn_2SiO_4:Mn on fused silica, a fact which may in part account for its superior brightness.

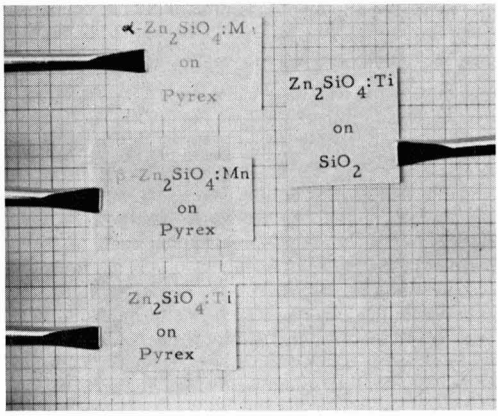

Fig. 4. Spray deposited films at a distance of 2 in. from the background.

The true physical nature of the phosphor surface on Pyrex is not known. Infrared reflection measurements made on sprayed green-emitting Zn_2SiO_4:Mn on Pyrex in the 8-14μ range show a well-defined 11.1μ peak which appears to be the 10.95μ peak found for willemite by Matossi and Kruger (13). Although peaks given for willemite by these authors at 10.66 and 11.48μ are poorly defined for the sprayed phosphor film, the correspondence is close enough to allow identification of the latter as zinc orthosilicate. On the basis of the emission spectra and the similarity of the preparative methods it is assumed that the yellow-emitting film is β-Zn_2SiO_4:Mn and that the other silicates have the composition described by the formulas given in this paper.

Attempts were made to measure film thickness by measurement of the distance between interference maxima in the absorption spectra of the films However, no interference maxima were found in the range from 1850 to 8000Å (silica substrates). Brightness *vs.* beam voltage was determined for the α-Zn_2SiO_4:Mn on Pyrex of Table I. The voltage corresponding to maximum brightness, 9 kv, yields an estimate of film thickness of 0.7 μ.[3]

$ZnCl_2$ + $TiCl_4$ solution sprayed on soft glass microscope slides gave films of very low brightness and poor clarity, while $ZnCl_2$ + $MnCl_2$ on soft glass resulted in only mixtures of α- and β-Zn_2SiO_4:Mn. Conditions for the formation of green-emitting α-Zn_2SiO_4:Mn *vs.* those for the yellow-emitting β form on Pyrex and silica were not established clearly in the present investigation. During a series of runs for the determination of the most effective spraying temperatures β-Zn_2SiO_4:Mn sometimes was formed under conditions duplicating as closely as the equipment would permit the conditions resulting in the usual green-emitting willemite. Formation of both forms in evaporated films has been noted in the earlier publication by Feldman and O'Hara (2) and later examined more closely by them (10).

Attempts to produce films of the following phosphors from solutions of the component halides resulted in either poor clarity, poor brightness, or both: $CaSiO_3$:Mn, $CaSiO_3$:Mn, Pb, $MgSiO_3$:Mn, $ZnWO_4$ and $CdSiO_3$:Ti.

The results of the present investigation are limited to the films which could be obtained with the simple apparatus described, and no attempt was made to prepare large pieces of film-coated glass or to improve control conditions or product uniformity by the use of more elaborate equipment. Many parameters await further exploration. One of these is the determination of the ratio of Zn or Cd to activator in the starting solution that results in the optimum final ratio in the film. Another is the effect of the amount of material atomized on the final film thickness. In the present study as much as 20 ml of 50% $ZnCl_2$:$MnCl_2$ solution sprayed over a 1 x 2 in. piece of Pyrex resulted in a film with transparency and brightness close to that of a sample for which only 2 ml of solution was used. Spraying into the silica tube (30 mm diameter) which held the glass samples produced a high degree of turbulence which was difficult to control. Use of a larger heated chamber may give more duplicable results. Utilization of propellant gases other than air may allow formation of other phosphor films, *e.g.*, H_2S to produce sulfides.

The phosphors described in this paper are, of course, formed by the reaction of the Zn or Cd in the solution with the SiO_2 of the supporting glass. Formation of transparent films of SiO_2 by thermal decomposition of ethyl silicate has been described by Law (12), indicating the possibility of spray deposition of silicate phosphor films on substrates not containing SiO_2 either by precoating the substrate with SiO_2 or by inclusion of ethyl silicate or silicon tetrachloride in the spray solution.

In summary, it can be stated that by direct reaction of suitable solutions with heated glass, transparent cathodoluminescent films of zinc and cadmium silicate can be made which are comparable in brightness and transparency with those prepared by the evaporation technique.

[3] Voltage *vs.* brightness measurement and thickness estimate were made by Dr. Charles Feldman. The thickness was estimated by using a plot of optimum beam voltage *vs.* thickness obtained with evaporated Zn_2SiO_4:Mn films of measured thickness.

Acknowledgments

The authors gratefully thank Dr. Ronald E. Kagarise of this laboratory for making the infrared reflection measurements, Harold W. Gandy for assistance in using the demountable cathode ray tube, and Dr. Charles Feldman for making the thickness estimate.

Manuscript received Oct. 5, 1960; revised manuscript received Jan. 27, 1961. This paper was prepared for delivery before the Indianapolis Meeting, April 30-May 3, 1961.

Any discussion of this paper will appear in a Discussion Section to be published in the December 1961 JOURNAL.

REFERENCES

1. F. J. Studer and D. A. Cusano, *J. Opt. Soc. Amer.*, **45**, 495 (1955).
2. C. Feldman and M. O'Hara, *ibid.*, **47**, 300 (1957).
3. An excellent literature survey is available from Metal and Thermit Corporation, Rahway, N. J., entitled "Use of Tin Compounds as Electroconductive Coatings on Non-Conducting Surfaces," June 1959.
4. M. J. Zunick (to General Electric X-ray Corp.), U. S. Pat. 2,516,663, July 25, 1960; J. K. Davis (to Corning Glass Works), U. S. Pat. 2,564,677, Aug. 21, 1951.
5. J. K. Davis (to Corning Glass Works), U. S. Pat. 2,564,677, Aug. 21, 1951.
6. M. A. Tanner and L. B. Lockhart, Jr., *J. Opt. Soc. Amer.*, **36**, 703 (1946).
7. T. Rosebury, Experimental Air-Borne Infection, (The Williams and Wilkins Co., 1947), p. 80; also J. C. Gage, *J. Sci. Instr.*, **30**, 25 (1953).
8. H. W. Leverenz, "An Introduction to the Luminescence of Solids," Table 5, John Wiley & Sons, Inc., New York (1950).
9. H. G. Pfeiffer and C. R. Fonda, *This Journal*, **99**, 140 (1952).
10. C. Feldman and M. O'Hara, *J. Opt. Soc. Amer.*, **48**, 816 (1958).
11. R. E. Shrader, *J. (and Trans.) Electrochem. Soc.*, **95**, 699 (1949).
12. H. B. Law, *Rev. Sci. Inst.*, **20**, 958 (1949).
13. F. Matossi and H. Kruger, *Z. Physik*, **99**, 1 (1936).
14. Designed by H. W. Gandy, Description to be submitted for publication.

Distribution Coefficient of Antimony in Silicon from Solvent Evaporation Experiments

F. A. Trumbore, P. E. Freeland, and R. A. Logan

Bell Telephone Laboratories, Incorporated, Murray Hill, New Jersey

ABSTRACT

Distribution coefficients have been calculated from Hall effect measurements on heavily doped silicon crystals grown by a solvent evaporation technique from melts containing between 2 and 8 atom per cent antimony. Nearly a twofold decrease in the distribution coefficient (from 0.02 to 0.01) was observed in this concentration range. It appears that any "facet effect," if present, was small and that near-equilibrium solid solubilities were obtained.

In connection with a study on the effect of different donor impurities on electron mobilities in heavily doped silicon (1), a number of antimony-doped silicon crystals were grown using a recently developed solvent evaporation technique (2, 3). The Hall effect measurements on these crystals have been used to calculate the variation of the distribution coefficient of antimony in silicon in the range from about 1373°C to the melting point of silicon. The purpose of this paper is to discuss the use of the solvent evaporation technique in determining distribution coefficients and to compare the present results with previous data obtained using other methods.

Experimental

Five silicon crystals were grown from melts containing between 2.0 and 8.4 atom per cent antimony. The experimental procedure involved first melting weighed amounts of antimony (Ohio Semiconductor, 99.9999% pure) and silicon (DuPont Hyperpure, Grade I) in a vitreous silica crucible under a helium atmosphere. A conventional inductively heated crystal pulling apparatus was used. A rotating silicon seed crystal was lowered into contact with the melt, and the temperature decreased until growth had started on the seed crystal. The temperature was then raised just enough to melt back the grown material, and the rotating seed crystal was left in contact with the melt at constant temperature as measured by a control thermocouple in the graphite susceptor. Growth of the antimony-doped silicon on the seed crystal then progressed as the antimony evaporated out of the melt and condensed on the cooler walls of the apparatus.

Normally, the seed crystal is not pulled. However, the thermal conditions present in our apparatus appeared to promote appreciably more rapid radial growth than vertical growth, thus limiting the size of crystal which can be grown in a crucible of a given diameter. In addition, as the crystal diameter increased there was a greater tendency for spurious nucleation and freezing over of the melt as well as an increase in the growth rate.[1] Hence, in three experiments the crystal was also pulled in an attempt to counterbalance the radial growth and thus obtain larger crystals. Two crystals grown by this combined solvent evaporation-pulling technique are shown in Fig. 1 and 2. A number of combinations of crystal orientation, rotation rate and pull rate were used. Growth times varied from about 2 to 7 hr.

[1] Recent experiments with the growth of antimony-doped germanium indicate that some cooling of the melt occurs as the crystal becomes larger and changes the thermal conditions. Such an effect would account for the larger growth rate as the crystal diameter increases since growth would take place due to both antimony evaporation and cooling of the saturated melt.

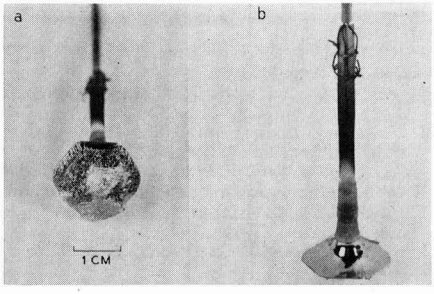

Fig. 1a. Bottom view of a <110> crystal grown by solvent evaporation and pulled at 0.15 cm/hr at a rotation rate of 75 rpm. Note the laminar structure of the growth interface. There is a small polycrystalline area in the lower section of the crystal. (The object on the center of the crystal is a drop of solidified melt). Fig. 1b. Top view of same crystal.

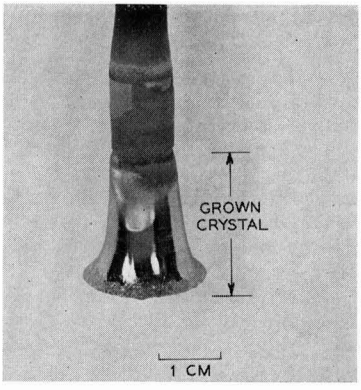

Fig. 2. <111> crystal grown by solvent evaporation and pulled at 1.1 cm/hr at a rotation rate of 60 rpm. This crystal is polycrystalline at the bottom.

Table I. Summary of data and growth parameters

x_L	$n (=1/Re)$ cm^{-3}	Orientation	Rotation rate, rpm	Pull rate, cm/hr
0.020	2.1×10^{19}	<111>	140	none
0.033	3.1×10^{19}	<111>	75	?
0.062	4.7×10^{19}	<100>	75	none
0.073	4.7×10^{19}	<111>	60	1.1
0.084	5.0×10^{19}	<110>	75	0.15

The melt composition at the end of a run was determined from weight loss measurements which, since the loss of silicon due to the SiO reaction was negligible, corresponded to the evaporated antimony. In order to minimize further loss of antimony at the end of a run the grown crystal was quickly pulled out of the melt and the induction heater turned off immediately to promote rapid freezing of the melt. The concentration of antimony in the crystal was determined from Hall effect measurements on slices cut from near the bottom of the crystal so as to correspond as closely as possible to material grown at the melt composition as determined above. For these degenerate samples the antimony concentration was assumed equal to the carrier concentration, n, determined from the Hall coefficient, R, from the relation $n = 1/Re$. The distribution coefficient, k, was calculated from the expression $k = x_s/x_L$ where x_s and x_L are the atom fractions of antimony in the solid and liquid solutions, respectively.

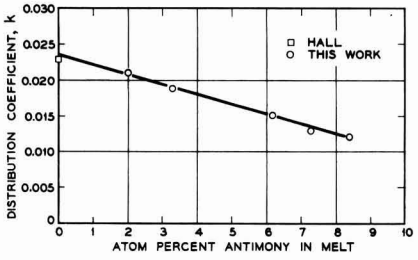

Fig. 3. Distribution coefficient of antimony in silicon as a function of melt composition.

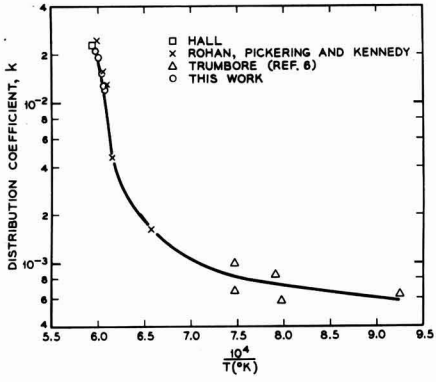

Fig. 4. Plot of log k as a function of the reciprocal of the absolute temperature.

Results and Discussion

A summary of the results is given in Table I.

In Fig. 3 distribution coefficients calculated from the data in Table I are plotted as a function of the melt composition. The value of k at the melting point of silicon, obtained by Hall (4) from crystal pulling experiments, is also plotted. A linear extrapolation of the present data to zero antimony concentration is seen to be in good agreement with Hall's value. The distribution coefficient decreases very sharply with increasing antimony concentration in the melt and with temperature as shown in Fig. 4 which is the usual plot of log k as a function of the reciprocal of the absolute temperature. Also included in Fig. 4 are values of k calculated from selected diffusion measurements of Rohan, Pickering, and Kennedy (5) and from some thermal gradient crystallization data reported earlier by one of us (6). In calculating k values from these two sets of solid solubility measurements the values of x_L at the various temperatures were taken from the liquidus curve data of Thurmond and Kowalchik (7) as were the values of temperature for various x_L values from our own data. It should be noted that the calculation of k from the diffusion data (5) near the silicon melting point is quite sensitive to small uncertainties in temperature and in the value selected for the melting point of silicon (taken as 1410°C in this work). Taking into account these and other possible sources of experimental error, the solvent evaporation data agree quite well with the diffusion data. The relatively rapid rise in k as the melting point of silicon is approached is similar to the behavior observed for tin in silicon and germanium (8) and is probably attributable in large measure to positive departures from ideal solution behavior in the Sb-Si system (7). In addition, an effect due to the influence of changes in Fermi level, as discussed for aluminum and gallium in germanium (9), is probably present.

In the above discussion it has been assumed that the distribution coefficients obtained in the various sets of experiments correspond to equilibrium values. However, the work on the facet effect in InSb by Hulme and Mullin (10) shows that a distribution coefficient determined from crystal growth experiments is subject to a considerable amount of uncertainty (3). In the present study there is some evidence to support the supposition that the observed values of k correspond closely to equilibrium conditions. First, it is evident from Table I and Fig. 3 that the use of different crystal orientations and other growth parameters appears to have little or no effect on the resulting value of k. Second, the values of k do not appear to have been influenced by the various types of growth interfaces which were laminar in some cases [see Fig. 1 and also Fig. 6, ref. (3)] and macroscopically smooth in other cases, *e.g.*, in the case of <111> crystals grown without pulling.[2]

These observations appear to indicate that if there is a facet effect in the present experiments it is less

[2] Apparently the thermal conditions present in the crystal pulling apparatus used for silicon did not permit the formation in <111> silicon crystals of the {111} facet found for <111> germanium crystals [see Fig. 2, ref. (2)].

than the precision of the experimental measurements estimated to be about ±10%. It is not known whether this argument can be applied to the thermal gradient results at lower temperatures where the grown crystals had {111} facets. Unfortunately, lack of experimental activity measurements and of a sufficiently well developed band theory for degenerate semiconductors prevents quantitative calculations which would indicate whether or not the experimental log k *vs.* $1/T$ plot corresponds to equilibrium conditions.

Conclusion

A recently developed solvent evaporation technique has been shown to be applicable to the determination of distribution coefficients. The results indicate that the method compares quite favorably with other techniques and appears capable of giving near-equilibrium values of k. Application of this method to other systems involving volatile impurities should yield interesting data bearing on equilibrium solid solubilities and the facet effect.

Acknowledgment

The authors are indebted to J. F. Gilbert for performing the Hall effect measurements.

Manuscript received Dec. 21, 1960; revised manuscript received Jan. 19, 1961. This paper was prepared for delivery before the Indianapolis Meeting, April 30-May 3, 1961.

Any discussion of this paper will appear in a Discussion Section to be published in the December 1961 JOURNAL.

REFERENCES

1. R. A. Logan, J. F. Gilbert, and F. A. Trumbore, *J. Appl. Phys.*, **32**, 131 (1961).
2. F. A. Trumbore and E. M. Porbansky, *ibid.*, **31**, 2068 (1960).
3. F. A. Trumbore, Proceedings of a Technical Conference on Metallurgy of Elemental and Compound Semiconductors, Boston, Mass., August 29, 1960, to be published.
4. R. N. Hall, Fortschritte der Hochfrequenztechnik, **4**, 129 (1958).
5. J. J. Rohan, N. E. Pickering, and J. Kennedy, *This Journal*, **106**, 705 (1959); also J. J. Rohan, personal communication.
6. F. A. Trumbore, *Bell System Tech. J.*, **39**, 205 (1960).
7. C. D. Thurmond and M. Kowalchik, *ibid.*, p. 169.
8. F. A. Trumbore, C. R. Isenberg, and E. M. Porbansky, *J. Phys. Chem. Solids*, **9**, 60 (1959).
9. F. A. Trumbore, E. M. Porbansky, and A. A. Tartaglia, *ibid.*, **11**, 239 (1959).
10. K. F. Hulme and J. B. Mullin, *Phi. Mag.*, **4**, 1286 (1959); J. B. Mullin, Electrochem. Soc. Electronics Div. Abstracts, **9**, 176 (1960).

Mass and Heat Transfer during the Chemical Vapor Deposition of Metals

J. H. Oxley and J. M. Blocher, Jr.

Battelle Memorial Institute, Columbus, Ohio

ABSTRACT

A general mathematical treatment of the mass- and heat-transfer rates in a de Boer-Van Arkel refining cell is presented. This treatment covers one of the more practical process situations wherein the change in dimensions of the deposition surface, as a result of metal deposition, significantly affects the diffusion path between the deposit and feed and the heat loss by the deposition surface. A steady-state, counter-diffusion, nonconvective system is assumed.

Although many metals can be prepared in a state of very high purity by pyrolysis of their respective halides, the relative thermodynamic stabilities of these halides generally leads to the choice of the metal iodides as the feed materials for such pyrometallurgical processes. Nevertheless, the temperatures required for appreciable decomposition of the metal iodides are frequently above 1000°C. Consequently, most published information indicates that low-pressure operation is required in order to limit the processing temperature to practical levels, since the equilibrium decomposition is more favorable at reduced pressures.

The simultaneous use of low pressures and high temperatures presents rather difficult problems in converting such iodide processes into continuous operations. Therefore, all disclosed iodide processes are batch or closed-cycle systems, as originally practiced by de Boer and Van Arkel (1). Loonam has recently presented an excellent review of the iodide process (2), and Powell, Campbell, and Gonser have published a more general description of the iodide and other vapor-deposition processes (3). These iodide processes usually are diffusion controlled and a number of analytical treatments have been reported (4-11). However, none of these treatments cover one of the more practical process situations, wherein the change in dimensions of the deposition surface, as a result of metal deposition, significantly affects the length of the diffusion path between deposit and feed.

A schematic drawing of a typical iodide diffusion cell is shown in Fig. 1. This type of cell has been used extensively at Battelle and more recently has been discussed in detail for niobium refining by Rolsten (12) and by Chizhikov and Grin'ko (13). Crude feed is charged to the outer annular section of the cell and maintained at a temperature (T_2) which is sufficiently high to assure a suitable vapor pressure of the metal iodide in the unit. The crude metal

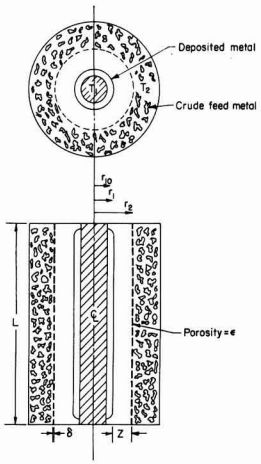

Fig. 1. Schematic drawing of iodide deposition cell

charge is held in place by a porous retaining wall of suitable porosity (ϵ) and thickness (δ). The screen is assumed to have straight and open pores, and the porosity is a direct measure of the fraction of the cross-sectional area which is available for diffusion at the radius of the cell determined by the porous retaining wall. The deposition surface is maintained at a higher temperature (T_1) than that of the feed, and since the decomposition of the metal iodide is favored by high temperatures, a net transport of metal iodide occurs between the feed and deposition surface as a result of the established concentration gradient of metal iodide. After the metal iodide decomposes at the hot surface and deposits high-purity refined metal, the iodine liberated in the reaction diffuses back to react with the feed metal.

In many systems, the size of the deposit changes appreciably during deposition, and hence the effective diffusion path between feed and the deposition surface varies appreciably. The production rate is therefore a function of not only the temperature of the feed and deposit, the porosity and thickness of the screen, the radii of the screen and the metal deposition surface, but also the amount of metal which is refined in a particular production run. In the general treatment of this iodide process which follows, it has been assumed that the reaction between iodine and feed metal is not limiting. In cases where the iodination rate is partially controlling, it can be corrected for by using an effective screen resistance. The assumptions of constant effective deposit density and the absence of all gases except atomic iodine and a single metal iodide are also implicit in the following derivation.

Mass-Transfer Analysis

The basic generalized equation for an iodide-decomposition process is

$$MI_x \rightarrow M + xI \qquad [1]$$

where x is usually >1. From the stoichiometry of the reaction, the net molar transport rates of metal iodide and iodine across a unit surface area perpendicular to the direction of diffusion are related by the equation:

$$xN_{MI_x} = -N_I \qquad [2]$$

For steady-state diffusion, the nonequal rates of counter diffusion of metal iodide and iodine can be expressed, according to Sherwood and Pigford (14):

$$N_{MI_x} + N_I = \frac{A\,D_v\,P}{RTz} \ln \frac{1 - (1 + N_I/N_{MI_x})\,(P_{MI_x}/P)_1}{1 - (1 + N_I/N_{MI_x})\,(P_{MI_x}/P)_2} \qquad [3]$$

Substitution of Eq. [2] in Eq. [3] and using mole fractions

$$N_{MI_x} = \frac{A\,D_v\,P}{(1-x)RTz} \ln \frac{1 - (1-x)\,(y_{MI_x})_1}{1 - (1-x)\,(y_{MI_x})_2} \qquad [4]$$

Defining the driving potential:

$$\Delta_{MI_x} \equiv \ln \frac{1 - (1-x)\,(y_{MI_x})_1}{1 - (1-x)\,(y_{MI_x})_2} \qquad [5]$$

And a mass-transfer coefficient:

$$k \equiv \frac{D_v\,P}{RT} \qquad [6]$$

Equation [4] becomes:

$$N_{MI_x} = \frac{A\,k\,\Delta_{MI_x}}{z(1-x)} \qquad [7]$$

The evaluation of the effective diffusion path (A/z) is complicated by possible variations in the design of a specific deposition cell. In general, the effective diffusion distance consists of two types of diffusion paths. The first path, within the porous basket wall, is related to the thickness (δ) and the porosity (ϵ) of the basket wall. Thus, for diffusion through the relatively thin wall of the feed-retaining basket:

$$N'_{MI_x} = \frac{k}{1-x} \left(\frac{2\,\pi\,r_2\,L\,\epsilon}{\delta} \right) \Delta'_{MI_x} \qquad [8]$$

The diffusion path through the annular gap between the feed-retaining basket and the hot deposition surface is in series with the diffusion path through the basket. The rate equation for annular diffusion is:

$$N''_{MI_x} = \frac{K}{1-x} \left(\frac{2\,\pi\,L}{\ln r_2/r_1} \right) \Delta''_{MI_x} \qquad [9]$$

But since the molar transport rates in the annular gap and within the wall of the porous basket are equal, since the sum of the driving potentials over both of these separate diffusion paths is equal to the total driving potential, and for the case of a multifilament cell consisting of a bundle of n cylindrical cells, combination of Eq. [8] and [9] lead to:

$$N_{MI_x} = \frac{nk\,2\,\pi\,L\,\Delta_{MI_x}}{(1-x)\,[\ln r_2/r_1 + \delta/r_2\epsilon]} \qquad [10]$$

Over a run of an arbitrary length of time (θ), the radius of the deposition filament (r_1) will normally increase considerably as a result of deposition of the metal from the iodide. Thus, the instantaneous rate of deposition will vary during the run, since the diffusion rate is related to the filament ra-

dius, as shown in Eq. [10]. The weight of metal deposited (w_M) is related to the atomic weight of the metal (A_M) and the diffusion rate of metal iodide (N_{MI_x}) by the expression:

$$d\,w_M = A_M\,N_{MI_x}\,d\theta \qquad [11]$$

Defining a new constant:

$$K \equiv \frac{A_M\,n\,k\,2\pi L\,\Delta_{MI_x}}{(1-x)} \qquad [12]$$

And substitution of Eq. [10] and [12] into Eq. [11]:

$$d\,w_M = \frac{K\,d\theta}{[\ln r_2/r_1 + \delta/r_2\epsilon]} \qquad [13]$$

An expression for the filament radius (r_1) in terms of the weight of deposited metal (w_M) can be obtained by use of the density of the deposited metal (ρ_M) in terms of the initial filament radius (r_{10}):

$$r_1 = \sqrt{\frac{w_M}{\pi L n\,\rho_M} + r_{10}^2} \qquad [14]$$

And substitution of Eq. [14] in Eq. [13]:

$$d\,w_M = \frac{K\,d\theta}{\left[\ln r_2 - \ln\sqrt{\frac{w_M}{\pi L n\,\rho_M} + r_{10}^2} + \delta/r_2\epsilon\right]} \qquad [15]$$

Separating variables and integrating Eq. [15] yields:

$$\theta = 1/K\left[w_M\left(\ln r_2 + \delta/r_2\epsilon - \ln\sqrt{\frac{w_M}{\pi L n\,\rho_M} + r_{10}^2} + \tfrac{1}{2}\right) + \pi L n\,\rho_M\,r_{10}^2\left(\ln r_{10} - \ln\sqrt{\frac{w_M}{\pi L n\,\rho_M} + r_{10}^2}\right)\right] \qquad [16]$$

Or in terms of the final deposit radius (r_{11}):

$$\theta = \frac{n\pi L\,\rho_M}{K}\left[\left(r_{11}^2 - r_{10}^2\right)\left(\ln r_2 + \delta/r_2\epsilon + \tfrac{1}{2}\right) + r_{10}^2\ln r_{10} - r_{11}^2\ln r_{11}\right] \qquad [17]$$

The average rate of deposition over an arbitrary length of time (θ) is therefore:

$$\frac{W_M}{\theta} = \frac{K(r_{11}^2 - r_{10}^2)}{[(r_{11}^2 - r_{10}^2)(\ln r_2 + \delta/r_2\epsilon + \tfrac{1}{2}) + r_{10}^2\ln r_{10} - r_{11}^2\ln r_{11}]} \qquad [18]$$

Equation [16] is used in determining the time required to produce a given weight of metal, and hence the yearly production capacity of a cell when the driving potential and mass-transfer coefficient have been calculated or experimentally determined. This equation is presented in graphical form in Fig. 2 for a deposition cell with an effective filament length of 10 ft, a feed-retaining basket radius of 5.0 cm, and for a deposited metal with a density of 4.0 g/cm³. A value of 0.01 has been used for the effective screen resistance ($\delta/r_2\epsilon$), which is fairly typical for iodide units. It is obvious from Fig. 2 that metal can be deposited more rapidly by employing larger filaments.

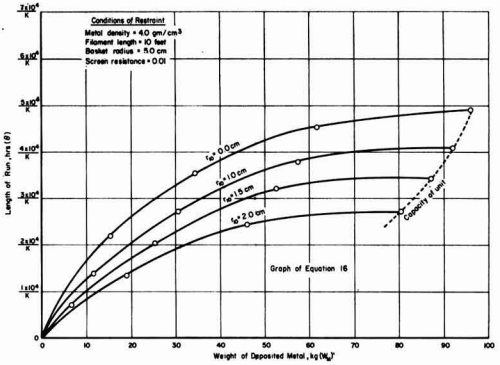

Fig. 2. Length of run as a function of weight of deposited metal.

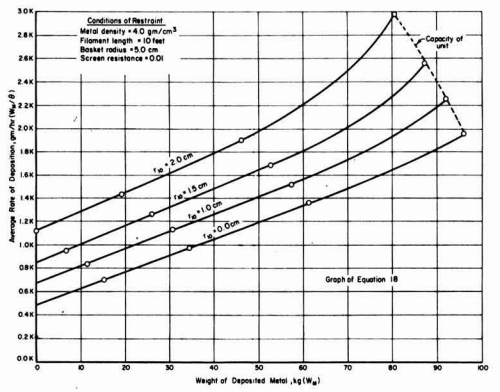

Fig. 3. Average rate of deposition as a function of weight of deposited metal.

However, larger filaments result in a lower cell capacity. A series of graphs, similar to the one presented in Fig. 2, are quite helpful at arriving at an intelligent choice of optimum design parameters.

Equation [18] is particularly valuable in analyzing data from relatively short experimental runs. Because it frequently takes a number of days to deposit the full metal capacity of an experimental unit, and since the average rate of deposition increases during the deposition process, calculation of the rate constant K by the use of Eq. [18] permits one to estimate the final average deposition rate from the measured rate in the short-term tests. This equation is presented in graphical form in Fig. 3 for the same conditions as those used in preparing Fig. 2.

Since most batch iodide processes are diffusion controlled in a pressure range where convective currents are negligible, the average deposition rates can be calculated from the preceding equations if sufficient thermodynamic information is available to evaluate the driving potential under a given applied

thermal gradient. However, the average deposition rate and rate constants can also be measured experimentally, and of course this is the preferred method of obtaining reliable data.

Heat-Transfer Analysis

The instantaneous rate of heat transfer by radiation (q_r) from the deposition surface is:

$$q_r = \sigma\, 2\pi r_1 Ln \frac{T_1^4 - T_2^4}{\frac{1}{e_1} + \frac{r_1}{r_2}\left(\frac{1}{e_2} - 1\right)} \qquad [19]$$

If the emissivity of the lower temperature surfaces in the cell is high, *i.e.*, $e_2 \approx 1$, then Eq. [19] becomes:

$$q_r = \sigma\, e_1\, 2\pi r_1 Ln\, (T_1^4 - T_2^4) \qquad [20]$$

The total heat lost by radiation during the production run is therefore:

$$Q_r = \int_0^\theta q_r d\theta = \int_0^\theta \sigma e_1\, 2\pi r_1 Ln\, (T_1^4 - T_2^4)\, d\theta \qquad [21]$$

But the radius of the metal surface varies during the run, *i.e.*, $r_1 = f(\theta)$. Differentiating Eq. [17] and substituting in Eq. [21] yields:

$$Q_r = \int_{r_{10}}^{r_{11}} \frac{4\, n^2\pi^2 L^2\, \rho_M\, \sigma e_1\, (T_1^4 - T_2^4)}{K} [\ln r_2 + \delta/r_2\epsilon - \ln r_1]\, r_1^2\, d\, r_1 \qquad [22]$$

Or

$$Q_r = \frac{4\, n^2\pi^2 L^2\, \rho_M\, \sigma e_1\, (T_1^4 - T_2^4)}{3K} [(r_{11}^3 - r_{10}^3)(\ln r_2 + \delta/r_2\epsilon + 1/3) + r_{10}^3 \ln r_{10} - r_{11}^3 \ln r_{11}] \qquad [23]$$

Equation [23] is shown in graphical form in Fig. 4 for the same conditions of restraint as used in the previous two figures, and superimposing the additional restrictions that the effective emissivity of the deposit is unity and that the difference in the fourth powers of the effective absolute temperatures of the deposit and feed is 1 x 10^{12}. It can be seen that during the initial stages of deposition, the power requirement per unit weight of metal is independent of the initial size of the deposition surface. However, if the unit is run to full capacity, it can be seen that

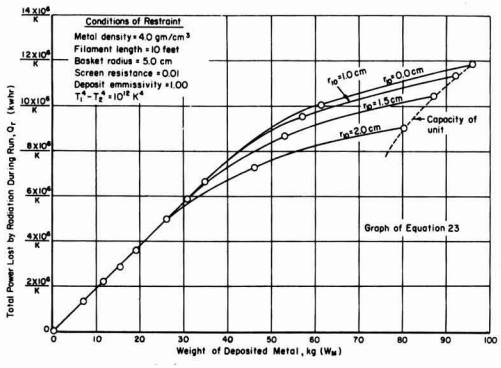

Fig. 4. Power requirements as a function of the weight of deposited metal.

the power requirements become somewhat sensitive to the choice of the radius for the initial deposition surface, with larger starting filaments resulting in lower power requirements per unit weight of deposited metal.

It can also be shown if a unit is operated at maximum capacity, *i.e.*, the deposit radius is allowed to grow until it is just short of the basket radius, and assuming the initial radius of the deposit is negligible, the power requirements per unit weight of metal increases in direct proportion to the final deposit radius. Hence, there is an economic balance at which the added heat lost by radiation tends to cancel the savings incurred by increasing the maximum cell capacity. In addition, the removal of heat in the larger size units becomes a problem of increasing severity.

In addition to the heat lost by radiation, three additional heat losses can be considered. The heat of dissociation of the metal iodide at the deposition surface is usually small compared to the radiation loss, but this loss can be included in the over-all heat balance

$$Q_T = Q_r + Q_D\, W_M \qquad [24]$$

The heat required to bring the unit up to deposition temperature is generally also minor, but can also be readily corrected for by using an additional term in the heat balance

$$Q_T = Q_r + Q_D\, W_M + C_p\, W_C\, (T - T_o) \qquad [25]$$

Heat transfer by conduction between the hot deposition surface and the feed is generally insignificant, and since a correction for this effect involves a considerable extension of the mathematics as well as an estimate of the effect of the processing variables on the conductivity of the system, this correction is usually neglected.

Summary

This general treatment of the iodide process has shown the complex relationships which exist between the rate of deposition and the driving potential for diffusion, the mass-transfer coefficient, the density of the deposited metal, the system geometry, and the amount of metal deposited. The effects of the process variables and the system geometry on the capacity and power requirement have also been treated in generalized form.

On the basis of this treatment, it is now possible to correlate metal yield, time of run, rate of deposition, and power losses in iodide refining units, a type of correlation which has not been heretofore available. In addition, these relationships permit one to extrapolate bench-scale data to pilot or semicommercial scale with a minimum of uncertainty.

Manuscript received Oct. 24, 1960; revised manuscript received Jan. 11, 1961. This paper was prepared for delivery before the Houston Meeting, Oct. 9-13, 1960.

Any discussion of this paper will appear in a Discussion Section to be published in the December 1961 JOURNAL.

REFERENCES

1. A. E. Van Arkel and J. H. de Boer, *Z. anorg. u. allgem. Chem.*, **148**, 345 (1925).
2. A. C. Loonam, *This Journal*, **106**, 238 (1959).

3. C. F. Powell, I. E. Campbell, and B. W. Gonser, "Vapor Plating," 158 pp, John Wiley & Sons, Inc., New York (1955).
4. J. M. Blocher, Jr., N. D. Veigel, I. E. Campbell, and A. C. Loonam, Paper presented at the Electrochemical Society Meeting, New York, May 1, 1958.
5. C. S. Herrick and J. G. Krieble, *This Journal*, **107**, 111 (1960).
6. G. H. Kesler, *A.I.M.E. Trans.*, **218**, 197 (1960).
7. G. H. Kesler, J. H. Oxley, and C. E. Dryden, *Trans. A.I.M.E.*, **221**, 9 (1961).
8. J. H. Oxley, J. E. Oberle, C. E. Dryden, and G. H. Kesler, Manuscript submitted for publication in A.I.M.E. Transactions.
9. B. Lustman, F. J. Kerse, and E. M. Shapiro, "The Metallurgy of Zirconium," Chap. 5, 776 pp., McGraw-Hill Book Co., New York (1955).
10. H. Schäfer, H. Jacob, and K. Etzel, *Z. anorg. u. allgem. Chem.*, **286**, 27 (1956).
11. V. S. Emel'yanov, P. D. Bystrov, and A. I. Evstyukhin, *Vesesoyuz. Sbornik Nekotorye Voprosy Inzh. Fiz. Moskov*, No. 2, 15-23 (1957).
12. R. F. Rolsten, *This Journal*, **106**, 975 (1959).
13. D. M. Chizhikov and A. M. Grin'ko, *Akad. Nauk. S.S.S.R., Doklady*, **122**, 278 (1958).
14. T. K. Sherwood and R. L. Pigford, "Absorption and Extraction," 478 pp., McGraw-Hill Book Co., Inc., New York (1952).

NOMENCLATURE

A	— cross-section area, cm²
A_M	— atomic weight of metal, g/g-mole.
C_p	— average specific heat of the deposition unit, kwh/kg-°K.
D_v	— diffusivity, cm²/hr.
d	— derivative.
e	— emissivity.
f	— an arbitrary function.
I	— iodine atom.
K	— a combined diffusion, reaction and geometric constant, $\frac{A_M\, n\, k\, 2\pi L_{MI_x}}{(1-x)}$.
k	— diffusion constant, $\frac{D_v P}{RT}$, g moles/cm.
L	— length of deposition element, cm.
M	— metal atom.
N_{MI_x}	— rate of diffusion of metal iodide, g moles/hr.
N'_{MI_x}	— rate of diffusion of metal iodide through screen, g moles/hr.
N''_{MI_x}	— rate of diffusion of metal iodide through annulus, g moles/hr.
N_I	— rate of diffusion of iodine, g atoms/hr.
n	— number of deposition elements per cell.
P	— total pressure, atm.
$(P_{MI_x})_1$	— partial pressure of metal iodide at temperature T_1, atm.
$(P_{MI_x})_2$	— partial pressure of metal iodide at temperature T_2, atm.
Q_D	— heat of dissociation, kwh/g.
Q_r	— total heat loss by radiation from deposit during deposition, kwh.
Q_t	— total heat loss from the deposit during deposition, kwh.
q_r	— rate of heat loss by radiation from deposit during deposition, kw.
R	— gas constant, atm cm³/g mole °K.
r_1	— radius of deposition surface, cm.
r_{10}	— initial radius of deposition surface, cm.
r_{11}	— radius of deposition surface after time θ, cm.
r_2	— radius of screen supporting feed, cm.
T	— average temperature in annulus, °K.
T_0	— room temperature, °K.
T_1	— temperature of deposition surface, °K.
T_2	— temperature of feed, °K.
W_C	— weight of the charged deposition cell, kg.
W_M	— weight of metal produced after time θ in deposition unit, g.
x	— atomic ratio of iodine to metal in metal iodide.
$(y_{MI_x})_1$	— mole fraction of metal iodide at temperature T_1.
$(y_{MI_x})_2$	— mole fraction of metal iodide at temperature T_2.
z	— effective diffusion distance, cm.
Δ_{MI_x}	— diffusion potential, ln $\frac{1-(1-x)(y_{MI_x})_1}{1-(1-x)(y_{MI_x})_2}$.
Δ'_{MI_x}	— diffusion potential across screen.
Δ''_{MI_x}	— diffusion potential across annulus.
δ	— thickness of screen, cm.
ϵ	— porosity of screen.
θ	— deposition time, hr.
π	— constant, 3.14.
ρ_M	— effective density of deposited metal, g/cm³.
σ	— Stefan-Boltzmann constant, 5.71 x 10^{-15} kw/cm² — °K⁴.
ln	— natural logarithm.

Vanadium by Metallic Reduction of Vanadium Trichloride

F. E. Block and M. J. Ferrante

Albany Metallurgy Research Center, Bureau of Mines, U. S. Department of the Interior, Albany, Oregon

ABSTRACT

Vanadium tetrachloride was made by chlorinating vanadium oxide with chlorine in the presence of carbon. By refluxing vanadium tetrachloride, it decomposed to nonvolatile vanadium trichloride allowing volatile oxychlorides to be separated. The trichloride was reduced with magnesium or magnesium-sodium mixtures under inert atmosphere. Excess reductant and byproduct salts were removed from the vanadium sponge by vacuum distillation. Arc-melted vanadium containing only 0.2% impurities was prepared which could be cold-rolled to thin sheets.

Vanadium has been prepared on a small scale for several years by the calcium reduction of its oxide in a sealed pressure vessel (1-4). The process is commonly termed "bomb-reduction" because the reaction is triggered inside the vessel and is allowed to proceed rapidly to completion under its own pressure and heat of reaction. It is limited in scale to relatively small batches, primarily because of the problems involved in building large pressure vessels capable of withstanding the violent reactions. Consequently, vanadium made by this practice is not only costly, but is of variable quality because each small batch of metal is the product of an uncontrolled reaction. In developing an improved process for

producing vanadium, chlorine metallurgy was selected for study because of the past success of the Kroll process in preparing other transition metals such as zirconium, and titanium (5, 6). In this process, an anhydrous metal chloride is reacted with a more active metal, usually magnesium, while under an inert atmosphere. The Kroll process is not only adaptable to large-scale processing, but it has the additional advantage of employing an intermediate metal chloride product free of oxygen or nitrogen compounds, elements which are the most damaging impurities in vanadium metal.

High-purity zirconium and titanium can be prepared readily by the Kroll process because their common tetravalent chlorides can be purified by distillation or sublimation. However, vanadium forms a considerably more complex system of chloride salts, and a direct application of the Kroll process to vanadium production was unsuccessful. Although vanadium tetrachloride is a volatile liquid, it is usually contaminated with vanadium oxytrichloride. Both compounds boil within 25°C of each other, making it impractical to separate the oxygen-containing material by a simple distillation. Normally two liquids such as these could be fractionated; however, vanadium tetrachloride decomposes when it is refluxed, forming nonvolatile, solid vanadium trichloride which would foul the packing of a fractionating column. Even though it is possible to prepare relatively pure vanadium tetrachloride by other methods, it was expedient to employ nonvolatile vanadium trichloride for metal production, because it could be prepared more nearly free of contaminants by a simple procedure.

This paper describes the development of a process for preparing vanadium by the reduction of vanadium trichloride with magnesium or sodium. In some respects it is similar to a process reported by Foley, Ward, and Hock (7), who prepared vanadium chloride by the chlorination of ferrovanadium. As a consequence, ferric chloride was a major impurity in the chlorination product and also represented a loss of chlorine. In the present work vanadium oxide was chlorinated directly yielding vanadium tetrachloride contaminated by vanadium oxytrichloride. Purification techniques, including rechlorination, eliminated oxy-compounds before the chloride was reduced to metal. Because of the emphasis on the removal of oxy-compounds, vanadium chlorides of high purity were formed which in turn led to the preparation of very pure vanadium metal.

This process differs from the previous work also in that a combination of magnesium and sodium was used as a reductant for vanadium trichloride. By using a mixed reductant, the reduction step could be conducted more smoothly with less chance for an uncontrollable, exothermic reaction.

Vanadium Chloride Preparation

CP grade vanadium pentoxide of 99.9% purity was used as a starting material. The chlorinator charge was prepared by blending approximately 1000 g of vanadium pentoxide with 500 g of gas carbon and 200 g of powdered sugar. A small amount of water was added to the charge, and it was mixed thoroughly by grinding before being extruded into small cylinders about ½ in. in diameter and 1 in. long. The extruded charge was well consolidated and could be handled without crumbling after it had been dried to remove all free moisture. It could be reacted directly with chlorine by heating to 500°C or higher. On chlorination, however, both vanadium tetrachloride and vanadium oxytrichloride were formed. It was found that chlorination at 500°C yielded principally the oxychloride and that operation at 750° C yielded vanadium tetrachloride as the principal product. The mixed chlorides could also be made richer in tetrachloride by partially reducing the charge before chlorination. By heating the charge in the absence of air, carbon dioxide and carbon monoxide were liberated and, depending on the temperature and time during which the reaction was allowed to proceed, various mixtures of the lower oxides of vanadium were formed. When the prereduced mixture was chlorinated a higher proportion of vanadium tetrachloride was formed, the exact proportion depending on the extent that the vanadium had been reduced. If the vanadium oxide-carbon mixture was heated to a high enough temperature to melt the mixture, complete reduction occurred yielding fused vanadium carbide. The carbide reacted exothermically with chlorine, forming vanadium tetrachloride free of oxychloride compounds.

Although this procedure can be used to prepare pure vanadium tetrachloride, it was not used extensively in this investigation because it was necessary to conduct the reduction step above the melting point of vanadium carbide (2810°C) to prepare material essentially free of all oxygen. Instead, a partial prereduction conducted at approximately 1000°C was employed.

Vanadium tetrachloride was prepared in the apparatus diagrammed in Fig. 1. The chlorination section, shown at the top, was a 5-in. diameter fused-quartz tube sealed at each end with nickel closures. The dried charge was packed into the chlorination section, and the reaction was initiated by heating the quartz tube externally with a resistance-heated furnace while chlorine was passed through the charge.

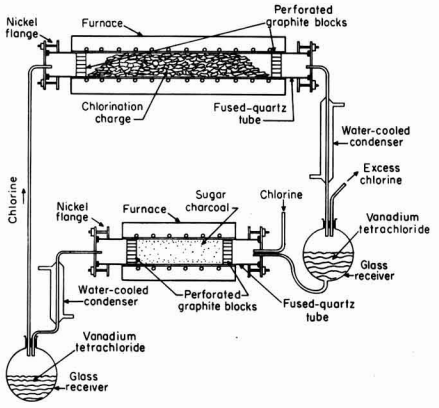

Fig. 1. Chlorination-rechlorination apparatus for preparing vanadium tetrachloride.

The reaction was continued for approximately 24 hr at 750°C and a chlorine flow-rate of 3 ft³/hr. Under these conditions 95% of the vanadium charged to the reactor was recovered as a mixture of vanadium tetrachloride together with a small amount of vanadium oxytrichloride This mixture was passed through the rechlorinator section, shown at the bottom of Fig. 1, to reduce the level of vanadium oxytrichloride. This unit also consisted of a 5-in. diameter fused quartz tube heated by a resistor furnace. The rechlorinator was packed with sugar charcoal that had been prepared by decomposing powdered sugar at 750°C. When the mixed vanadium chlorides together with chlorine were passed through the charcoal, the bulk of the contaminating oxytrichloride was further chlorinated to vanadium tetrachloride. It was difficult to determine the relative proportion of vanadium oxytrichloride present in the resulting vanadium tetrachloride since the actual amount depended on the extent that the chlorination charge had been pre-reduced as well as on the activity of the charcoal in the rechlorinator. The final product, however, usually contained less than 2% vanadium oxytrichloride.

Vanadium tetrachloride was decomposed to the trichloride simply by refluxing it at its normal boiling point. This was done conveniently in a nickel vessel heated by an external resistance furnace as depicted in Fig. 2. Attached to the top of the sealed vessel was a nickel refluxing column also heated externally by resistance heaters. Four and one-half liters of vanadium tetrachloride were charged to the nickel vessel and heated to boiling. During this time the reflux column was not heated in order that the entire charge would be totally refluxed in the air-cooled column. After 36 hr of heating, approximately 90% of the vanadium tetrachloride was converted to trichloride. At this time the temperature in the vessel was increased to 300°C, and the reflux column was heated to 250°C. By applying a vacuum of 26 in. of mercury to the vessel, the bulk of the unconverted vanadium tetrachloride and contaminating vanadium oxytrichloride was distilled away from the solid vanadium trichloride which remained inside the vessel. After cooling, the solid mass of vanadium trichloride was dug out of the nickel vessel and was crushed to approximately minus ¼-in. mesh. Because the crushed chloride contained entrapped volatile chlorides, it was heated again to 300°C *in vacuo* to remove final traces of vanadium tetrachloride and oxytrichloride as well as any lower boiling impurities such as titanium tetrachloride and silicon tetrachloride. An alternate procedure was to stir the mixed chlorides during decomposition. When this was done, a uniform vanadium trichloride powder was formed directly, and it was not necessary to crush the product or to employ the second vacuum treatment to remove entrapped volatiles.

Because all vanadium chlorides are extremely hygroscopic, it was necessary to handle and store the finished trichloride under dry argon insofar as possible. This usually was accomplished by the use of an inert atmosphere glove box.

Reduction

In the Kroll process a metal chloride is reduced by introducing it at a controlled rate into a crucible of molten magnesium. Because of the limited scale of these tests, and because the reduction reaction did not proceed violently, it was not necessary to introduce the vanadium chloride at a controlled rate as in the Kroll process. Instead, vanadium trichloride and solid magnesium were charged into a reduction crucible and were gradually heated to the reaction temperature under argon. The apparatus, as shown in Fig. 3, consisted of a type 430 stainless-steel reduction crucible approximately 7½ in. in diameter and 11 in. high, supported near the top of a stainless-steel retort. The top section of the retort, containing the charge, was heated externally by a bell-shaped resistance furnace. From 1 to 4 kg of vanadium trichloride together with an excess of magnesium were usually reacted. After the retort was evacuated and backfilled with argon to approximately 9 psig, it was heated to 825°C to melt the magnesium and promote the reaction. Heating was continued 1-4 hr to complete the reaction before the furnace section was removed to allow the retort to cool to at least 200°C At this point the retort was evacuated by a diffusion pump to approximately 5 x 10^{-3} mm Hg. While maintaining this vacuum, the furnace was replaced, and the retort was again slowly heated to 825°C. Heating was

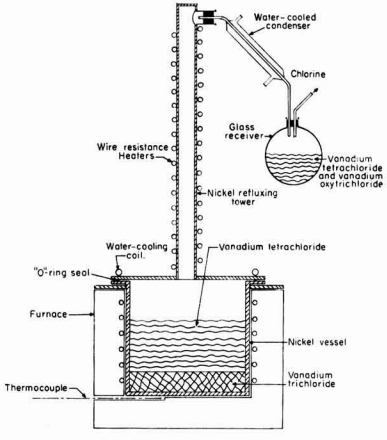

Fig. 2. Decomposition unit

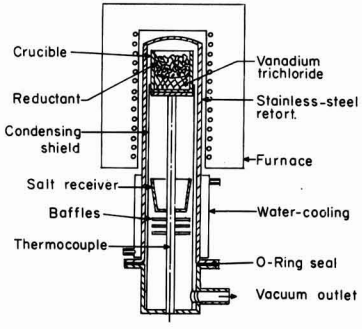

Fig. 3. High-vacuum, reduction-distillation furnace

Table I. Results of vanadium trichloride reductions

VCl_3, g	Stoichiometric % of red. Mg	Stoichiometric % of red. Na	Yield, %	Hardness, Rockwell B	Analysis, ppm O	N	C	Fe	Cr	Ni
1920	170	—	91	77	650	140	270			
2205	150	—	91	77	850	80	550			
4365	145	—	86	43	400	50	270			
1100	110	—	90	65	600	50	330			
3000	200	10	94	72	800	20	280			
1820	170	15	94	92	900	90	500			
2650	170	10	95	72	900	20	340			
1100	—	120	90	67	700	100	270			
3365	150	—	86	64	900	160	550	<100	<100	210
2080	125	1	92	67	200	40	390	<100	<100	20
3981	135	1	89	57	320	20	450	<100	<100	45
5034	125	1	82	52	600	20	400	<100	<100	56

continued for 15 to 20 hr to vaporize unreacted magnesium and byproduct magnesium chloride which were condensed in the water-cooled section at the base of the retort. After the furnace had again been removed and the retort had cooled to room temperature, the pressure had usually dropped to less than 1×10^{-4} mm Hg. Before the vanadium was removed, dry air was slowly bled into the retort to passivate the more active surfaces of the vanadium sponge. If this procedure were not employed, the vanadium would sometimes burn upon exposure to the atmosphere. Metal yields were usually over 90%, but the actual yield could not be correlated with the amount of excess reductant used.

The results of vanadium reduction tests are given in Table I which shows that interstitial impurities in vanadium sponge were usually held to low limits. Metallic impurities, principally iron and chromium, were a more serious problem in making vanadium. Metallic impurities resulted from corrosion of the reduction crucible by vanadium trichloride and its decomposition products. Because a small amount of vanadium trichloride was decomposed at the temperature of the reaction, elemental chlorine was released which readily attacked the metal crucible. It was found that metallic impurities could be controlled somewhat by substituting part or all of the magnesium reductant with sodium. Even when small amounts of sodium were used, the reaction could be started at a considerably lower temperature (approximately 550°C) than when the reductant consisted entirely of magnesium. Consequently, the tendency to form corrosion products was reduced slightly.

In the metallothermic reduction of vanadium chloride, the reaction occurs between the solid trichloride and the molten metal reductant. Because the temperature must be sufficiently high to melt the metal reductant as well as the byproduct salt of the reaction, a temperature over 800°C must be employed if magnesium is used as a reductant. However, when a combination of sodium and magnesium is employed, a low-melting mixture of magnesium and sodium chlorides is formed which allows a reaction to proceed to completion at considerably lower temperatures.

To reduce the level of metallic impurities, a titanium reduction crucible was tested in place of the type 430 stainless steel crucible which was responsible for iron and chromium contamination. Under these conditions, titanium was also subject to corrosion during the reaction. Finally, reduction crucibles constructed entirely of vanadium were used and it was possible to control metallic impurities within low levels. Table I shows the metallic impurities present in vanadium sponge prepared in vanadium reduction crucibles.

The quality of vanadium sponge varied considerably within the same batch depending on the location of the sponge in the crucible. This is not unusual to the Kroll process and is frequently made use of in controlling quality by carefully segregating the various portions of sponge. Table II shows the analysis of metal from a single batch that had been segregated into three portions. Generally a small surface layer of sponge contains a much higher proportion of impurities than the bulk of the metal in the crucible.

Metal Evaluation

Because the sponge metal usually consisted of finely divided powder lightly sintered together, it was necessary to consolidate it for evaluation. This was usually achieved by melting representative samples of sponge into small button-size melts in a cold-mold arc-melting furnace of the type usually employed to melt reactive metals. Melting the sponge also yielded a homogeneous specimen for testing. In some cases vanadium ingots were made by compressing the sponge into bars and melting them by the consumable-electrode, arc-melting technique. Button-melts weighing from 30 to 50 g were sampled for analysis by cutting lathe turnings from the inner portion of the button. Hardness values were made on a smooth surface of the button that had been prepared by wet-sanding. Arc-melted buttons were also subjected to mechanical working tests by cold-rolling the specimens directly. Vanadium with a hard-

Table II. Analysis of segregated vanadium sponge

Sponge location in crucible	Hardness, Rockwell B	Chemical analysis, ppm O	N	C
Top	95	1200	360	320
Middle	79	950	90	340
Bottom	72	800	20	280

ness of Rockwell B-85 or less usually could be cold-rolled directly to very thin sheets. Although an exact correlation between quality and workability was not obtained, oxygen and nitrogen were found to have the greatest effect on workability. Usually if the metal contained less than 0.1% oxygen it could be cold-rolled without difficulty. Nitrogen contamination in metal made in this investigation was usually well below the level affecting workability.

Conclusions

This investigation has demonstrated that high-purity, ductile vanadium metal can be made by the metallic reduction of vanadium trichloride. The success of the process depends on methods that have been developed for preparing pure vanadium trichloride free of oxygen compounds. This process is conducted in much the same manner as the Kroll process which has been operated successfully for producing titanium and zirconium on an industrial scale. Like the Kroll process, the metallic reduction of vanadium trichloride can be carried out at a controlled rate and because all reactants can be prepared in a high state of purity, the quality of the vanadium sponge can also be controlled.

Manuscript received Oct. 25, 1960. This paper was prepared for delivery before the Chicago Meeting, May 1-5, 1960.

Any discussion of this paper will appear in a Discussion Section to be published in the December 1961 JOURNAL.

REFERENCES

1. J. W. Marden and M. Rich, *Ind. Eng. Chem.*, **19**, 786 (1927).
2. R. K. McKechnie and A. U. Seybolt, *This Journal*, **97**, 311, (1950).
3. E. D. Gregory, W. C. Lilliendahl, and D. M. Wroughton, *ibid.*, **98**, 395 (1951).
4. J. R. Long and H. A. Wilhelm, Preparation of Vanadium Metal, USAEC Report, ISC-244, August (1951).
5. W. J. Kroll, C. Travis Anderson, H. P. Holmes, L. A. Yerkes, and H. L. Gilbert, *J. (and Trans.) Electrochem. Soc.*, **94**, 1, (1948).
6. W. J. Kroll, U. S. Pat. 2,205,854, June 1940.
7. E. Foley, M. Ward, and A. L. Hock, "Extraction and Refining of the Rarer Metals," p. 196, The Inst. of Mining and Metallurgy, London (1957).

Overpotential on Tellurium Cathodes in NaOH Solutions

S. A. Awad

Chemistry Department, University College of Girls, Ain-Shams University, Heliopolis, Cairo, Egypt

ABSTRACT

Overpotential on tellurium cathodes was studied on 0.005-5*N* aqueous NaOH solutions at 25°C. Dissolution of tellurium giving $Te_2^=$ ions, instead of hydrogen evolution, was suggested to explain the results. In 0.05-5*N* solutions the dissolution of tellurium is governed by a rate-determining simple electrochemical mechanism with two Tafel slopes in the linear logarithmic section. Below 0.05*N* the discharge reaction becomes rate-determining. Equations for the effect of *p*H on overpotential were deduced theoretically. The values obtained for the *p*H effect indicated the discharge of Na^+ ions. The bend-up at high current densities, observed in the Tafel lines for 1-5*N* solutions, is not due to a resistance overpotential effect. It was attributed to concentration overpotential manifesting itself by a tendency toward a limiting current. The decrease of the current density corresponding to the bend-up, by lowering the temperature, supported the above suggestion.

The major part of the experimental work on hydrogen overpotential has been concerned with metals (1). On the other hand, the literature contains but few studies on the hydrogen overpotential on metalloids and nonmetals. Thus, Bowden and Rideal (2) studied the hydrogen overpotential on carbon cathodes and obtained a value of 0.84 v for the Tafel line slope. The work of Erdey-grüz (3) on carbon cathodes also showed that the Tafel line has a lower slope which amounts to 0.1 v. Ammar and Awad (4) studied the hydrogen overpotential on tellurium in HCl solutions. The results obtained in dilute solutions indicated that the hydrogen evolution reaction is controlled by a simple electrochemical mechanism with two Tafel line slopes of 0.04 and 0.12 v at 30°C. In concentrated solutions, a rate-determining dual electrochemical catalytic mechanism, with a slope of 0.06 v at 30°C, was suggested to explain the results in the low current density range. This dual mechanism changes to a simple one at high cathodic polarization.

The aim of the present work was to study the overpotential characteristics for tellurium in NaOH solutions and to compare the results with those in acid solutions.

Experimental

The experimental technique was essentially the same as that of Bockris and co-workers (5). The electrolytic cell was constructed of arsenic-free glass and was similar to that used by Ammar and Awad (4). A sintered glass disk was inserted between the cathode compartment and the compartment used for electrolytic purification of solutions to minimize the diffusion of gaseous anodic products toward

the cathode. Water-sealed taps and ground glass joints were used to retard the diffusion of atmospheric oxygen into the cell.

The electrode was prepared from spectroscopically pure tellurium rods[1] (7 mm diameter). A thin tungsten wire was wrapped around one end of the rod. This end was squeezed inside a clean glass tubing and the glass was sealed over the tungsten wire (4). The electrode then was washed with conductance water and fitted in its position in the cell. Each electrode was used to trace one Tafel line only. Before each run, the cell was cleaned with a mixture of A.R. nitric acid and A.R. sulfuric acid. This was followed by a thorough washing with conductance water.

Sodium hydroxide solutions were prepared from the A.R. sample. The solution was pre-electrolyzed at 10^{-3}-10^{-2} amp/cm^2 for 20 hr on a platinum pre-electrolysis electrode. These conditions were satisfactory to obtain reproducible results (within ± 10 mv) in all solutions studied in the present investigation.

Cylinder hydrogen was purified from oxygen, carbon monoxide, and other impurities by passing it over hot copper (450°C), then over a mixture of MnO_2 and CuO (technically known as "Hopcalite") to oxidize CO to CO_2. CO_2 was removed by soda lime.

A saturated calomel electrode with a saturated KCl bridge was used as a reference electrode, because it was feared that any contamination from the tellurium cathode might poison the hydrogen electrode. The potential of the hydrogen electrode, in the same solution and at the same temperature as the test cathode, was measured against the calomel electrode making use of a salt bridge. In this manner errors in overpotential, due to liquid junction potentials, were minimized.

The direct method of measurements and the rapid technique (5) were employed. The current density was calculated using the apparent surface areas. The current was measured with a multirange micromilliammeter and the potential by a valve potentiometer. Temperature was kept constant with the aid of an air thermostat controlled to ± 0.5°C.

Results

All results included in this investigation are the mean of six individual results which are reproducible among themselves to within ± 10 mv.

Figures 1, 2, and 3 show the mean Tafel lines in 0.005, 0.01, 0.05, 0.1, 0.5, 1, 3, and 5*N* aqueous sodium hydroxide solutions at 25°C. It is clear from these figures that, with the exception of the results in 0.005 and 0.01*N* solutions, the Tafel lines indicate two slopes in the linear logarithmic section. In case of 0.005 and 0.01*N* solutions, Tafel lines with only one slope are obtained. At comparatively low current densities, a region of stationary potential is observed in all concentrations.

Table I contains the mean values of the slopes b_1 (at the low current density range) and b_2 (at the high current density range), together with the values of the stationary potentials, referred to the normal hydrogen electrode, for the various concentrations studied.

[1] Prepared by Johnson and Matthey, Ltd., London, England.

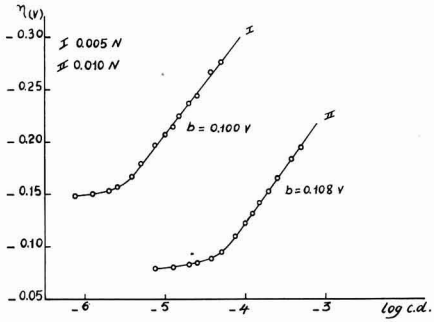

Fig. 1. Tafel lines for Te in 0.005N and 0.01N NaOH (referred to reversible hydrogen electrode).

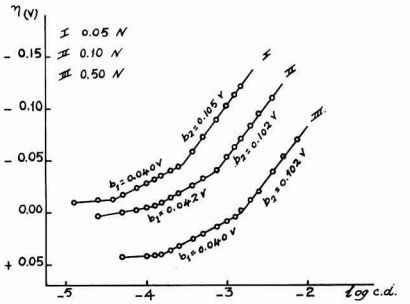

Fig. 2. Tafel lines for Te in 0.05N, 0.1N, and 0.5N NaOH (referred to reversible hydrogen electrode).

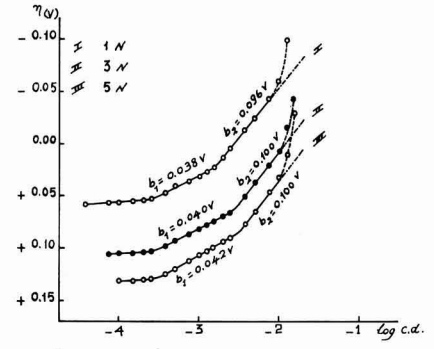

Fig. 3. Tafel lines for Te in 1N, 3N, and 5N NaOH (referred to reversible hydrogen electrode).

The values of the stationary potentials in the various solutions are assumed to represent the reversible tellurium electrode potentials. The overpotential, referred to the reversible tellurium electrode, thus is calculated at 10^{-4}, 10^{-3}, and 4 x 10^{-3} amp/cm^2, and the values for different solutions are given in Table II. This table contains also the values of $(\partial\eta/\partial_{pH})_i$, calculated for various solutions. All values in Table I and II are in millivolts.

In order to provide a support for the role of Na^+ ions in the suggested mechanism, the overpotential also was measured in 0.10 Na_2CO_3 solution. The results (referred to the normal hydrogen electrode)

Table I. Mean values

Concentration N	b_1	b_2	Stationary potential referred to the normal hydrogen electrode
0.005	—	100	−819
0.01	—	108	−782
0.05	40	105	−742
0.1	42	102	−747
0.5	40	102	−745
1	38	96	−747
3	40	100	−732
5	42	100	−724

Table II. Overpotential and pH for different solutions

Concentration N	pH	$-\eta$ (referred to tellurium electrode) at 10^{-4}	at 10^{-3}	at 4×10^{-3}	$(\partial\eta/\partial p_H)_i$
0.005	11.35	154*	.....	.....	202
0.01	11.90	43	151*	.....	118
0.05	12.40		92	.....	
0.5	13.32			78	25
1	13.60			71	18
5	14.50			55	

* These values are obtained by extrapolation.

are shown in Fig. 4, which includes also the results in 0.01 and 0.10N NaOH for comparison.

The Tafel line in 1N NaOH also is measured at 10°C. The results, together with those at 25°C for the same concentration, are shown in Fig. 5. It is clear that the bend-up of the Tafel line occurs at a lower current density as the temperature decreases.

Discussion[2]

The overpotential results on tellurium in 0.005 and 0.01N NaOH indicate the occurrence of one Tafel slope in the linear logarithmic section, which amounts to 0.1 and 0.108 v, respectively, (cf. Table I and Fig. 1). From these facts it is concluded that, if the reaction taking place at the cathode is hydrogen evolution (see below), the rate of the over-all reaction will be controlled by a slow discharge mechanism (6).

In concentrations above 0.01N NaOH, the Tafel lines showed two slopes (cf. Fig. 2 and 3). With increase of the alkali concentration, the Tafel lines also are shifted toward the reversible hydrogen electrode potential. In solutions of 0.5-5N, parts of the Tafel lines lie in the positive side with respect to the reversible potential. Such phenomenon is somewhat surprising since, for cathodic processes, η is always negative. This behavior led, therefore, to the conclusion that the reaction taking place at tellurium cathodes is not hydrogen evolution. A possible alternative reaction in case of tellurium is the dissolution of the cathode material. Tellurium, being a metalloid, can dissolve cathodically giving telluride ions. This suggestion is supported by the appearance of the deep red color, characteristic for polytellurides (7), in all the solutions during polarization.

[2] The European convention of sign of potential is used.

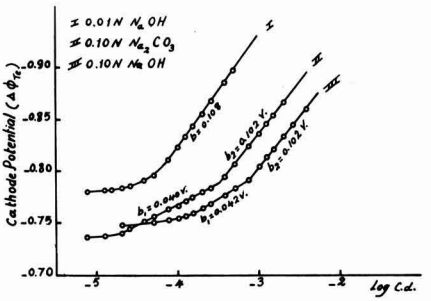

Fig. 4. Tafel lines for Te in 0.1N Na_2CO_3, 0.01N, and 0.1N NaOH (potential referred to normal hydrogen electrode).

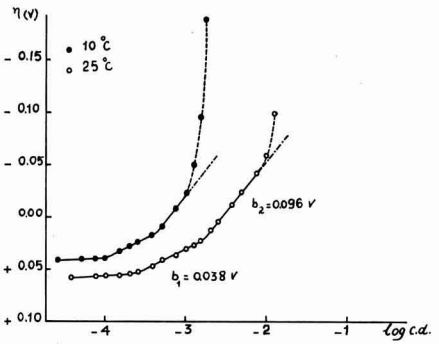

Fig. 5. Effect of temperature on overpotential in 1N NaOH

The reference electrode for overpotential measurements on tellurium in NaOH must, accordingly, be the reversible tellurium electrode and not the hydrogen electrode. The potential of the former electrode depends on the activity of telluride ions, which are formed continuously during the tracing of the Tafel line. If, however, the change in the logarithm of the telluride ions activity is negligible, the potential of the reversible tellurium electrode can be considered to remain constant over the whole current density range studied. The positive overpotential values obtained in this investigation are accounted for, therefore, by the fact that the potentials were referred to the hydrogen electrode and not to the correct reversible one.

The cathodic dissolution of tellurium in NaOH solutions can take place according to any of the following reactions:

$$Te + 2H_2O + 2e \rightarrow H_2Te + 2OH^- \quad [1]$$

$$Te + 2e \rightarrow Te^= \quad [2]$$

$$2Te + 2e \rightarrow Te_2^= \quad [3]$$

From the net free energy changes of these reactions, the corresponding standard potentials are given the values (8): −1.57, −1.14, and −0.84 v. From these values, it is obvious that tellurium dissolves according to reaction [3] since its standard potential is the least negative one.

The above conclusion finds some support in the observation of a deep red color during polarization. It is already known (7) that when H_2Te is passed

through NaOH, the liquid turns red. A colorless solution, which deposits colorless crystals, can be obtained if full precautions are taken to prevent oxidation. The red color was attributed, therefore, to some polytellurides, resulting from partial oxidation of $Te^{=}$ ions and the subsequent combination of these ions with the finely precipitated tellurium. In the present investigation, highly purified solutions were used, and numerous precautions were taken to prevent oxidation. Thus, the formation of $Te_2^{=}$ ions (or more complicated polytellurides), as indicated by the red color, through partial oxidation of $Te^{=}$ ions is unlikely to occur.

Further evidence for the direct formation of $Te_2^{=}$ ions according to reaction [3] is given by the observation that the potentials, at which the Tafel lines become parallel to log c.d. axis, are within the range −0.724 to −0.819 v (cf. Table I). Assuming, reasonably, that these are the reversible potentials in the different solutions, it is evident that Eq. [3] represents the electrode reaction, since the observed reversible potentials are within the order of magnitude of its standard potential.

The activation overpotential at tellurium cathodes may be associated with the charge reaction as represented by Eq. [3]. Thus, taking the activity of tellurium equal to unity and assuming a symmetrical energy barrier, the net cathodic current is given by

$$i = 2\,F\,V = 2\,F\,k \exp\left(-\frac{\Delta\phi\,F}{RT}\right) \qquad [4]$$

where $\Delta\phi$ is the galvanic potential difference between the electrode and the Helmholtz double layer. The Tafel line slope as indicated by Eq. [4] is equal to 0.06 v at 30°C. From the values given in Table I, it is obvious that the slow step is not the direct charge of tellurium atoms.

As an attempt to elucidate the kinetics of dissolution of tellurium cathodes in NaOH solutions, the following mechanism is suggested:

$$Te + Na^+ + e \rightarrow NaTe \qquad [5]$$

$$NaTe \rightarrow Te + Na^+ + e \qquad [6]$$

$$NaTe + Te + e \rightarrow Te_2^{=} + Na^+ \qquad [7]$$

The velocities of the above reactions are given by (6)

$$V_1 = k_1(a_{Na^+})_{d.l.}\,(1-x) \exp\left(-\frac{\Delta\phi\,F}{2RT}\right) = a_1\,(1-x) \qquad [8]$$

$$V_2 = k_2\,x\,10^{-9} \exp\left(\frac{\Delta\phi\,F}{2RT}\right) = a_2\,x \qquad [9]$$

$$V_3 = k_3\,x\,10^{-9} \exp\left(-\frac{\Delta\phi\,F}{2RT}\right) = a_3\,x \qquad [10]$$

where k_1, k_2, and k_3 are the rate constants for the discharge, the ionization and the electrochemical reactions, respectively, whereas a_1, a_2, and a_3 are the electrochemical constants. $(a_{Na^+})_{d.l.}$ is the activity of Na^+ ions in the double layer and x is the fraction of the surface covered with NaTe as intermediate telluride. The activity of tellurium in reaction [7] is taken as unity.

If it is assumed that the discharge step is fast and the electrochemical reaction is slow, the dissolution of tellurium is governed by a rate-determining electrochemical mechanism under the condition (6)

$$(a_1 + a_2) > 10\,a_3 \qquad [11]$$

At the steady state corresponding to constant surface coverage, current, and potential

$$V_1 - V_2 - V_3 = 0 \qquad [12]$$

From Eq. [8]-[12], the surface coverage becomes

$$x = \frac{a_1}{a_1 + a_2} \qquad [13]$$

The value of x can be obtained under two limiting conditions

$$a_2 > 10\,a_1 \qquad [14a]$$

and

$$a_1 > 10\,a_2 \qquad [14b]$$

From Eq. [13] and [14a]

$$x = \frac{a_1}{a_2} = \left(\frac{k_1}{k_2\,10^{-9}}\right)(a_{Na^+})_{d.l.} \exp\left(-\frac{\Delta\phi\,F}{RT}\right) \qquad [15a]$$

From Eq. [13] and [14b]

$$x = 1 \qquad [15b]$$

The net cathodic current, when x is given by [15a], becomes

$$i = 2\,F\,V_3 = 2\,F\left(\frac{k_1 k_3}{k_2}\right)(a_{Na^+})_{d.l.} \exp\left(-\frac{3\,\Delta\phi\,F}{2RT}\right) \qquad [16]$$

The Tafel line slope, as given by Eq. [16], is equal to 0.04 v at 30°C. With increase of cathodic polarization x increases and approaches unity (Eq. [15b]). The net cathodic current, therefore, becomes

$$i = 2\,F\,V_3 = 2\,F\,k_3\,10^{-9} \exp\left(-\frac{\Delta\phi\,F}{2RT}\right) \qquad [17]$$

and the Tafel line slope is 0.12 v at 30°C.

If on the other hand the electrochemical step is fast and the discharge mechanism is rate-determining, under the condition

$$a_3 > 10(a_1 + a_2) \qquad [18]$$

then, from Eq. [8], [9], [10], [12], and [18] the surface coverage becomes

$$x = \frac{a_1}{a_3} = \left(\frac{k_1}{k_3\,10^{-9}}\right)(a_{Na^+})_{d.l.} \qquad [19]$$

The net cathodic current is given the value

$$i = 2\,F\,V_3 = 2\,F\,k_1\,(a_{Na^+})_{d.l.} \exp\left(-\frac{\Delta\phi\,F}{2RT}\right) \qquad [20]$$

According to Eq. [20] the Tafel line slope is 0.12 v at 30°C.

From the above discussion and the values given in Table I, it is clear that the cathodic dissolution of tellurium in 0.05-5N NaOH is controlled by an electrochemical mechanism. At lower concentrations,

the rate-determining step is the discharge reaction. The change of mechanism from electrochemical to discharge with dilution is expected, since the electrochemical rate constant of the discharge reaction, a_1, includes the activity of Na^+ ions. Thus, by decreasing the activity of these ions, a state is reached when a_1 is far smaller than a_3 (cf. Eq. [18]) and consequently the discharge reaction is rate-determining.

The suggestion that the discharge reaction involves Na^+ ions instead of water molecules is supported by studying the effect of pH on overpotential. In the following discussion it is considered that the stationary potential, at low cathodic polarization in a given solution, is equal or at least very near to the reversible potential, so that the difference between that potential and the potential at a given current density represents the overpotential. Moreover, the reversible potential is conveniently taken as pH-independent, since, except in 0.005 and 0.01*N*, the stationary potential varies but slightly with the alkali concentration (cf. Table I).

For solutions above 0.05*N*, in which the dissolution is governed by the electrochemical mechanism, the net cathodic current corresponding to the higher slope b_2, is given by Eq. [17]. Substituting for $\Delta\phi$ by $\eta + \Delta\phi_r - \xi$, the overpotential at constant current is given by

$$\eta = \text{constant} - \Delta\phi_r + \xi \qquad [21]$$

Since $\Delta\phi_r$ is pH-independent, Eq. [21] indicates that, under conditions when $(\partial\xi/\partial \ln a_{H^+}) \simeq 0$ (in presence of excess neutral salts or when the electrode potential is very near to that of the electrocapillary maximum), η is independent of pH, whether the discharge involves Na^+ ions or water molecules.

Below 0.05*N*, when the discharge reaction is rate-determining, the net cathodic current in case of the discharge of Na^+ ions is given by Eq. [20]. Substituting for $(a_{Na^+})_{d.l.}$ by $(a_{Na^+}) \exp\left(-\frac{\xi F}{RT}\right)$, it follows that at constant current

$$\eta = \text{constant} + \frac{2RT}{F} \ln a_{Na^+} - \Delta\phi_r - \xi \qquad [22]$$

Neglecting again the change of ξ with the alkali concentration, one gets for the pH effect

$$\left(\frac{\partial\eta}{\partial \text{pH}}\right)_i = 2.303\left(\frac{2RT}{F}\right) \qquad [23]$$

Equation [23] shows that η increases by 120 mv/unit increase of pH at 30°C. If, on the other hand, the discharge involves water molecules, $(a_{Na^+})_{d.l.}$ in Eq. [20] will be replaced by the activity of water in the double layer. Assuming that the latter is equal to the activity of water in the bulk of the electrolyte, an equation similar to [21] is obtained, indicating again that η is independent of pH.

The data given in Table II show that in concentrated solutions, the overpotential increases but slightly with pH, as required by Eq. [21]. The slight increase can, however, be attributed to the variation of $\Delta\phi_r$ and ξ with concentration. Below 0.05*N*, η increases appreciably with pH, in accordance with Eq. [23]. It is evident, therefore, that the discharge reaction involves Na^+ ions but not water molecules.

A further evidence for the discharge of Na^+ ions is provided by measuring the overpotential in 0.1*N* Na_2CO_3 solution. This solution has a pH value comparable with that of 0.01*N* NaOH, whereas it contains nearly as much Na^+ ions as 0.1*N* NaOH solution, as seen from the following:

Normality of solution	Measured pH
0.01 NaOH	11.90
0.10 Na_2CO_3	11.70
0.10 NaOH	12.70

It is clear from Fig. 4 that the Tafel line in the carbonate solution nearly coincides with that obtained in the 0.1*N* NaOH solution. Moreover, it exhibits similarly two slopes in the linear logarithmic section, whereas in 0.01*N* NaOH solution only one slope is observed. The coincidence of the results depends, therefore, on the Na^+ activity and not on the pH of solutions. This conclusion points out that Na^+ ions are discharged at the cathode.

The bend-up at high current densities, observed in the Tafel lines for 1-5*N* NaOH (cf. Fig. 3), cannot be attributed to a resistance overpotential effect. This is so, since the plot of $\Delta\eta$ (difference between the actual Tafel line and the extrapolated line) against the current density does not give a straight line. The bend-up is best explained by assuming that, at current densities higher than 10^{-2} amp/cm^2, the rate of formation of $Te_2^=$ ions exceeds their rate of diffusion to the bulk of solution. The accumulation of $Te_2^=$ ions in the vicinity of the cathode leads to concentration overpotential which manifests itself as a tendency toward a limiting current. This explanation is supported by measuring the Tafel line in 1*N* NaOH solution at 10°C and comparing it with that at 25°C. Figure 5 shows that the bend-up occurs at a much lower current density, amounting to 10^{-3} amp/cm^2, as it is expected, since the decrease in temperature is accompanied by a decrease in the rate of diffusion of ions.

Manuscript received March 18, 1960; revised manuscript received Nov. 21, 1960.

Any discussion of this paper will appear in a Discussion Section to be published in the December 1961 JOURNAL.

REFERENCES

1. J. O'M. Bockris, *Chem. Rev.*, **43**, 525 (1948).
2. F. P. Bowden and E. Rideal, *Proc. Roy. Soc. London*, **A120**, 59 (1928).
3. Erdey-grüz and Wick, *Z. Physik. Chem.*, **A162**, 53 (1932).
4. Ammar and Awad, *This Journal*, **103**, 182 (1956).
5. A. Azzam, J. O'M. Bockris, B. Conway, and H. Rosenberg, *Trans. Faraday Soc.*, **46**, 918 (1950).
6. J. O'M. Bockris and E. C. Potter, *This Journal*, **99**, 169 (1952).
7. F. Ephraim, "Inorganic Chemistry," Fifth English Edition, p. 537, Gurney and Jackson (1949).
8. W. Latimer, "Oxidation Potentials," p. 85, Prentice Hall (1952).

The Kinetics of Absorption and Evolution of Hydrogen by Palladium and Palladium/Platinum Electrodes

Ted B. Flanagan[1] and F. A. Lewis

Chemistry Department, Queen's University, Belfast, North Ireland

ABSTRACT

The kinetics of absorption and desorption of hydrogen by palladium and a series of palladium/platinum alloy electrodes have been examined in hydrochloric acid solutions near their equilibrium hydrogen contents (1 atm H_2: 25°C). The kinetics have been correlated with previous studies of absorption where the desorption rate could be neglected.

The kinetics of the absorption of molecular hydrogen from acidic solutions by palladium have recently been examined (1, 2). Under conditions where the rate of desorption could be neglected, these studies showed that the rate of absorption depends on the hydrogen pressure to the first power and that the rate-determining step had an activation energy of < 2 kcal/mole H_2. Results (2) also suggested the rate-determining step was independent of the platinum content of a series of palladium/platinum alloys. It was concluded from these results that diffusion of hydrogen within the metal cannot be the rate-determining step in absorption from solution. In addition, Fallon and Castellan (1) have calculated coefficients of diffusion for hydrogen dissolved in solution from their absorption rates; these coefficients proved to be in good agreement with values previously established, indicating that diffusion of hydrogen molecules up to the surface is most probably the slow step under the experimental conditions employed. [From similar calculations based on absorption curves of palladium presented earlier (3), Von Stackelberg has also suggested this to be the slow step (4)].

The purpose of the present paper is to apply a kinetic analysis to experimental data obtained under conditions when the desorption rate cannot be neglected. It has been found possible to utilize the time dependent changes of the relative electrical resistance (R/R_o) of a 12.03% Pt alloy for this purpose. However, for hydrogen contents close to those in equilibrium with H_2 (1 atm: 25°C) small changes in the content of the majority of the electrodes under study are often difficult to follow (2, 3) from measurement of R/R_o, *e.g.* for palladium a maximum may occur (5) in the hydrogen content (H/Pd, atomic ratio)—R/R_o relationship near equilibrium. Fortunately, an alternative method of following the kinetics is available since it has been shown for palladium that the electrode potential is directly proportional to the hydrogen content in the vicinity of equilibrium (6, 7); this relationship also appears valid for certain of the Pd/Pt alloys. An equation relating absorption rate and electrode potential has therefore been derived and applied both to absorption data and to additional data reported here which was obtained during the desorption of hydrogen from supersaturated electrodes containing hydrogen in excess of the content at equilibrium.

Experimental and Procedure

The palladium and Pd/Pt specimens were in the form of wires of 0.0274 cm diameter and approximately 15 cm in length. The alloys had been prepared from specpure metals of > 99.9% purity melted under argon. Platinum contents are recorded here in atomic percentages. All measurements were made in HCl solutions continuously stirred by purified hydrogen gas at one atmosphere. Electrode potentials were recorded against a Pt/H_2 electrode in the same solution. The electrical resistance of the specimens could be measured simultaneously. Within the range studied, temperature was controlled to ± 0.2°C. The apparatus is described elsewhere in more detail (2, 3).

Before absorption of hydrogen from solution the specimens were preactivated by anodization (5 min: 2ma). Prior to studies of hydrogen desorption the specimen was allowed to attain equilibrium with H_2 in solution at the required temperature [zero volt electrode potential w.r.t. Pt/H_2 (2, 3)] and then made cathodic for at least 12 h w.r.t. a Pt anode using a current of *ca.* 0.5 ma.

Results and Discussion

Rate of absorption.—The time dependent changes of electrode potential over the range of hydrogen contents from zero to equilibrium (H/Pd = 0.69) are illustrated in Fig. 1 for absorption of hydrogen from

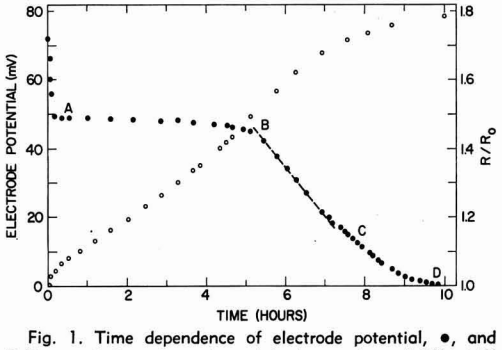

Fig. 1. Time dependence of electrode potential, ●, and R/R_o, ○, during absorption of hydrogen from 0.02N HCl by palladium (1 atm H_2: 25°C)

[1] Present address: Physics Dept., Brookhaven National Laboratory, Upton, N. Y.

0.02*N* HCl by palladium at 25°C; data for palladium/platinum alloys are shown elsewhere (2). For palladium and those alloys which undergo an $\alpha \rightarrow \beta$ transition, the electrode potential is time invariant while the transition takes place. Upon completion of the $\alpha \rightarrow \beta$ transformation, the time dependent decrease of electrode potential, when further absorption occurs in the nonstoichiometric β-phase hydride, can be represented by

$$-\frac{dE}{dt} = k \qquad [1]$$

during such time as the rate of hydrogen evolution is small enough to be neglected (B-C, Fig. 1).

For $E < ca.$ 12 mv ($p \sim 300$ mm, see Eq. [2] and [3]) the rate of hydrogen evolution becomes of sufficient significance for the potential to thereafter fall off more slowly (*e.g.*, from point C, Fig. 1) to the final equilibrium value of zero w.r.t. Pt/H_2. It has been shown (1, 2) that the time dependence (and thus the kinetics of absorption) of the sequence of changes of both E and R/R_o, and of their magnitudes, are in general independent of HCl concentration (2) within the range 0.002*N* to 1.0*N* [although coconduction of the bridge current can lead to difficulties of, and errors of measurements (2) in strongly acid solutions]. It is our purpose here to demonstrate that the rates of both absorption and evolution, for "active" electrodes, depend only on E and are virtually independent of the platinum content of the alloys.

If, for all the alloys studied, the rate-determining step in the absorption of hydrogen from solution is always dependent on the pressure of hydrogen to the first power, the net rate, considering desorption may be written as:

$$\tfrac{1}{2}d(H)/dt = k_o(P - p) \doteq k_o(1 - p) \qquad [2]$$

where the rate constant, k_o, reflects the velocity of transport of hydrogen molecules up to the metal surface (molecules cm^{-2} sec^{-1} atm^{-1}) and (H), the concentration of absorbed hydrogen atoms is, therefore, expressed as the number of hydrogen atoms in a volume corresponding to unit area of specimen; P is the external pressure of hydrogen (1 atm in the current study), and p is the effective pressure within the specimen which may be determined at any time from the measured electrode potential E (w.r.t. Pt/H_2) by the relation

$$p = \exp(-2FE/RT) \qquad [3]$$

Substitution of [3] into Eq. [2] gives

$$d(H)/dt = 2k_o[1 - \exp(-2FE/RT)] \qquad [4]$$

It has been shown (6, 7) in the case of the Pd/H system that for H/Pd > 0.58 at *ca.* 25°C

$$(H^*) \propto \ln p \propto E \qquad [5]$$

$$i.e., \quad (H^*) = E/K_2 \qquad [6]$$

where K_2 is a constant and (H^*) is the deficiency or excess of hydrogen from the content at equilibrium (H_e), *i.e.*, $(H^*) = (H_e) - (H)$. Now H/Pd = 0.69 (3) when the electrode potential of a Pd/H electrode is zero ($E = 0$) w.r.t. Pt/H_2 (25°C:1 atm H_2). It is thus permissible to substitute (H^*) and (H_e) for (H) in Eq. [4] near zero volt.

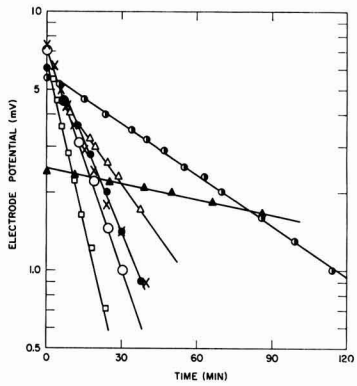

Fig. 2. Time dependent decrease of electrode potential during the final approach to equilibrium during absorption of hydrogen from 0.02N HCl (25°C:1 atm H_2). Open circle, Pure Pd; solid circle, 2.79% Pt; open triangle, 5.73% Pt; half solid circle, 8.80% Pt; solid triangle, 12.03% Pt; ×,15.42% Pt; open square, 18.99% Pt.

One obtains

$$-d(H^*)/dt = 2k_o[1 - \exp(2FE/RT)] \qquad [7]$$

Substitution of relation [6] into Eq. [7] gives upon rearrangement

$$-dE/[1 - \exp(-2FE/RT)] = 2K_2k_o dt \qquad [8]$$

Integration of Eq. [8] using as an approximation only the first two terms of the expansion of the exponential yields

$$E \simeq E_o \exp(-4FK_2k_o t/RT) \qquad [9]$$

where E_o is the initial value of the electrode potential.

Thus, provided the relationships developed above are applicable, the time dependent decrease of potential in the final decay region C-D of Fig. 1 would be expected to be described by

$$-dE/dt = k_1E \qquad [10]$$

where

$$k_1 = 4FK_2k_o/RT \qquad [10a]$$

Figure 2 shows electrode potential-time relationships for $E < ca.$ 7 mv during the final approach to

Table I. Comparison of rate constants for absorption and evolution of hydrogen for specimens with electrode potentials close to zero w.r.t. Pt/H_2 (1 atm H_2:25°C)

% Pt	$k_1 \times 10^{+2}$ min^{-1}	$k_2 \times 10^{+2}$ min^{-1}	K_2, mv/coul/cm	$k_o \times 10^{-15}$ molecules/cm^2/sec from k_1	$k_o \times 10^{-15}$ molecules/cm^2/sec from k_2
0	6.3	8.1	59.5	8.2	10.5
2.79	5.5	5.5	55.4	7.7	7.7
5.73	3.0	3.2	36.5	6.3	6.8
8.80	1.5	1.6	20.2	5.7	6.1
12.03	0.56	1.1	6.1	7.1	14.1
15.42	5.1	2.8	—	—	—
18.99	9.7	5.3	—	—	—

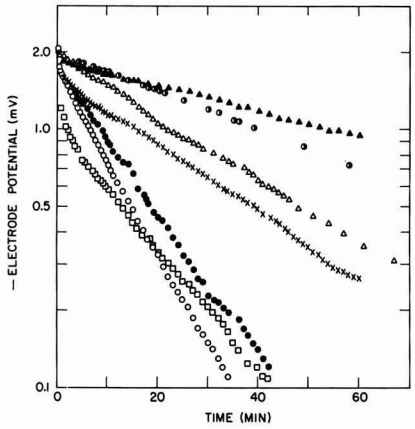

Fig. 3. Time dependent increase of the negative potential to zero following cathodic electrolysis in hydrogen saturated 0.02N HCl (25°C:1 atm H_2). Open circle, Pure Pd; solid circle, 2.79% Pt; open triangle, 5.73% Pt; half solid circle, 8.80% Pt; solid triangle, 12.03% Pt; ×, 15.42% Pt; open square, 18.99% Pt.

equilibrium by palladium and a series of palladium/platinum alloys plotted by the integrated form of Eq. [10] so as to yield straight line behavior. The agreement with Eq. [10] is seen to be reasonably good.

Values of the slopes, k_1, shown in Table I are calculated from the data of Fig. 2, but closely similar values were also obtained with other preanodized (and pre-palladized in the case of pure palladium) specimens which readily attained a final zero volt potential.

Rate of hydrogen evolution.—Electrodes which had attained a zero volt potential following absorption from solution were further charged with hydrogen electrolytically. Palladium and the alloys studied all attained approximately the same, initial negative electrode potential (ca. − 2 mv) after prolonged electrolysis at the same current density. Upon cessation of electrolysis, the spontaneous loss of hydrogen from the supersaturated electrodes, as reflected by the increase of the negative electrode potentials to zero, was measured as a function of time. The logarithmic plot shown in Fig. 3 illustrates that this time dependent increase may again be represented by

$$-dE/dt = k_2E \qquad [11]$$

where

$$k_2 = 4FK_2k_0/RT \qquad [11a]$$

Values of k_2 are again recorded in Table I. The reproducibility of the data presented in Fig. 3 is good and relatively insensitive to prolonged standing in solution between repeat determination of the rates; this stable behavior was in some contrast to the sensitivity, on standing, of the reproducibility of the rates of proton transfer between similar electrodes (8).

The deviations from Eq. [11] for the plots of the 15.42 and 18.99% Pt alloys at small times is undoubtedly due to the fact that Eq. [5] is no longer obeyed for negative electrode potentials greater than ca. 1.5 and ca. 1.0 mv, respectively. It may also be inferred from this that the electrode potential-hydrogen content relationships for these alloys are nonsymmetrical about equilibrium since Eq. [10] appears to be obeyed for these same alloys for positive potentials significantly greater than 1.5 and 1.0 mv, respectively (Fig. 2). A similar conclusion has been reached from the results of proton transfer studies (8).

Table I shows that the values of k_1 and k_2 decrease progressively from pure palladium to the 12.03% Pt alloy and increase again for alloys of higher platinum content. The magnitudes of k_1 and k_2 are comparable for palladium and the 2.79, 5.73, and 8.80% platinum alloys, but for the 12.03, 15.42, and 18.99% platinum alloys they differ appreciably, and this is again related to differences in the relationships between electrode potential and hydrogen content above and below zero volt (25°C).

Data obtained from proton transfer studies (8) for the constant K_2, which directly relates hydrogen content to electrode potential near zero volt (Eq. [5] and [6], has however, shown that K_2 also varies with the platinum content of the alloys. Thus when (so far as Eq. [5] still holds under our experimental conditions, see above) appropriate values of K_2 were combined with k_1 and k_2 in Eq. [10a] and [11a], Table I shows that the values obtained for the rate constant, k_0, are, considering the approximations used in deriving Eq. [9]and experimental uncertainties in K_2, found to be almost constant. The values of k_0 are of the order of magnitude of those previously observed in circumstances where the reverse reaction can be neglected (2) *i.e.*, 2.75 x 10^{-2} cc H_2/ cc Me/ sec or ~ 5.1 x 10^{15} molecules $H_2/cm^2/sec$.[2] [More recently, values have been obtained in closer agreement with that of Fallon and Castellan (1) *i.e.*, ~ 6.9 x 10^{15} molecules $H_2/cm^2/sec$ (under the most rapid stirring conditions employed by these workers)]. A factor which may contribute to the increase in the values of k_0 (Table I) as compared to 5.1 x 10^{15} molecules $H_2/cm^2/sec$, is that the area of the specimens may be larger at equilibrium hydrogen contents than in the two-phase region due to both an additional lattice expansion when hydrogen dissolves in the β-phase and a possible increase in surface roughness.

Kinetics of absorption of hydrogen by a 12.03% Pt alloy at 25°C.—Relationships between R/R_0 and hydrogen content (H/Me—atomic ratio) are available at 25° both for palladium and the other alloys used in these studies (2). At 25°C, alloys with < 8.80% Pt form β-phase hydrides at pressures < 1 atm. During the $\alpha \rightarrow \beta$ transition large increases of H/Me can occur, while the electrode potential is constant, which can be followed by resistance measurements (see Fig. 1). Advantage has been taken of this (1, 2, 3) to measure the rate of absorption of hydrogen over the $\alpha \rightarrow \beta$ transition regions when the constant electrode potential corresponds to pressures, p, which are sufficiently low for desorption to be unimportant in Eq. [2].

Large changes of resistance were also observed (2) during the absorption of hydrogen by the 12.03%

[2] This value was incorrectly given in ref. (2) as 8.5 × 10^{15} molecules $H_2/cm^2/sec$.

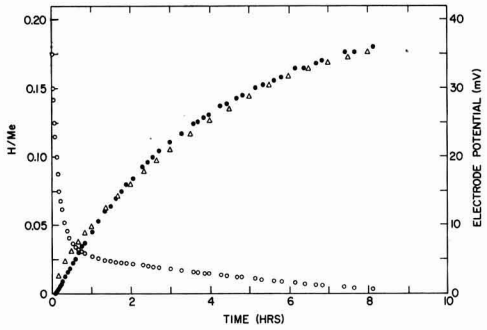

Fig. 4. Comparison of experimental and calculated rates of absorption of hydrogen from 0.02N HCl solution by a 12.03% Pt alloy (25°C:1 atm H_2). •, H/Me(exptl); △, H/Me(calc); ○, electrode potential.

Pt alloy at 25°C from which changes of H/Me have been calculated and are illustrated in Fig. 4. The accompanying electrode potentials indicate that the rate of desorption should be significant at a relatively early stage of this absorption experiment (see Eq. [1] and [2]).

If the same step is rate determining for alloys with platinum contents $\geqslant$ 12.03% as for alloys with a lesser percentage of platinum, *i.e.*, diffusion of hydrogen within the metal is still rapid compared to the rate of transport of hydrogen molecules up to the surface, then Eq. [2] is again applicable. [Also justified by the comparable rates of absorption by both pure palladium and 12.03% Pt at 0°C, where significantly larger volumes of hydrogen are absorbed (2) by the 12.03% Pt alloy than at 25°C, over values of E which corresponds to values of p sufficiently low for desorption rates to be relatively unimportant.]

The extent of absorption may be calculated at any time from

$$H(t) = 2k_0t - 2k_0\int_0^t \exp(-2FE/RT)\,dt \quad [12]$$

The integral must be evaluated graphically since the dependence of E on time is not known analytically over the whole range of hydrogen contents. Results for the 12.03% Pt alloy at 25°C are shown in Fig. 4 using a value of $k_0 = 6.3 \times 10^{15}$ molecules/cm²/sec which is in reasonable agreement with the value of k_0 measured (2) when desorption can be neglected (see above). As illustrated in Fig. 4 the agreement between the experimental and calculated values of rates of absorption based on Eq. [12] clearly demonstrates that in the case of the 12.03% Pt alloy (and also alloys with > 12% Pt) the virtual absence (2) of a period over which there is a constant rate of absorption at 25°C is due solely to the early onset of desorption.

Dependence of rates on hydrogen ion concentration and temperature.— Potential decay during the evolution of hydrogen was determined for the 2.73% Pt alloy in 1.0*N*, 0.2*N*, and 0.02*N* HCl; no significant dependence of k_2 on hydrogen ion concentration was observed in this range. This result is in accord with the relative independence of the rate of absorption on hydrogen ion concentration when desorption can be neglected (1, 2).

For the platinum alloys the H/Me-electrode potential relationships can vary significantly near zero volt in the temperature range 0°-59°C, with consequent changes in K_2 (Eq. [6]). If k_0 remains almost unaltered, changes in K_2 will be reflected by variation of k_1 and k_2 (see Eq. [10a] and [11a]). For example, for the 12.03% Pt alloy, k_2 was almost independent of temperature from 0° to 25°C, but then increased from 1.1×10^{-2} min^{-1} (25°C) to 5.9×10^{-2} min^{-1} (54°C).

Thus, it is only for palladium (where the H/Me-electrode potential relationships do not alter markedly in this temperature range) that k_2 (or k_1) can be conveniently employed for studying the temperature dependence of the rate process. It was found for pure palladium that k_2 was indeed virtually temperature independent within the range 0°-63°C, thus providing additional confirmation for the very low value previously obtained for the activation energy of the rate-controlling process from absorption studies (1, 2).

Generality of rate equation.—The analysis carried out here indicates that Eq. [2] has general application to the absorption and evolution of hydrogen by all the alloys studied. These results suggest that the equation, and the value obtained for the rate constant, k_0, are also likely to have general application to metal electrodes such as pure platinum and rhodium which absorb only very little hydrogen. This is provided the surfaces of such electrodes are sufficiently "active" for the rate of dissociation of hydrogen molecules to exceed $\sim 5.1 \times 10^{15}$ molecules/cm²/sec so that the approach of the molecules to the surface is rate controlling.

Von Stackelberg and Bischoff (7) have followed the velocity of hydrogen gas evolution as a function of the hydrogen content of palladium foil electrodes which had been supersaturated electrolytically. They concluded that the velocity of evolution depends on the square root of the pressure of hydrogen gas. This is at variance with the results obtained here and also does not agree with results based on overpotential measurements in the vicinity of the equilibrium hydrogen content (9, 10). However, von Stackelberg has suggested (4) that the square root pressure dependence can be reconciled with the present results, if the palladium foils (7) were less active than the specimens of the present study whereby the slow step would be the dissociation of hydrogen molecules at the surface rather than transport up to the surface. It would be of interest to examine the differences in the rates of hydrogen evolution from a series of such "less active" palladium/platinum alloys; the difficulties in obtaining reproducible activity amongst the alloys would, however, be considerable.

Acknowledgments

The authors wish to thank the Mond Nickel Co., Ltd. for providing the palladium/platinum alloys used in these studies.

Manuscript received July 18, 1960; revised manuscript received Feb. 3, 1961.

Any discussion of this paper will appear in a Discussion Section to be published in the December 1961 JOURNAL.

REFERENCES

1. R. J. Fallon and G. W. Castellan, *J. Phys. Chem.*, **64**, 4 (1960).
2. A. W. Carson, T. B. Flanagan, and F. A. Lewis, *Trans. Faraday Soc.*, **56**, 363, 371, (1960).
3. T. B. Flanagan and F. A. Lewis, *ibid.*, **55**, 1400, 1409 (1959).
4. M. von Stackelberg, Private communication.
5. D. P. Smith, "Hydrogen in Metals," Chicago University Press, Chicago (1948).
6. P. S. Perminov, A. A. Orlov, and A. N. Frumkin, *Doklady Akad. Nauk, S.S.S.R.*, **84**, 749 (1952).
7. M. von Stackelberg and H. Bischoff, *Z. Elektrochem.*, **59**, 467 (1955).
8. A. W. Carson, T. B. Flanagan, and F. A. Lewis, *Trans. Faraday Soc.*, **56**, 1311, 1324, 1332 (1960).
9. L. Kandler, C. A. Knorr, and M. Schwitzer, *Z. physik. Chem.*, (A) **180**, 281 (1937).
10. A. N. Frumkin and N. A. Aladjalova, *J. Physik. Chem. URSS*, **18**, 493 (1944).

Technical Notes

Photoluminescent Effects in Contact Electroluminescence

B. Morosin and F. A. Haak

Hughes Research Laboratories, A Division of Hughes Aircraft Company, Malibu, California

The emission of visible radiation by a mixture of castor oil, metal filings, and various nonelectroluminescent phosphors were reported by Lehmann (1), who named the phenomenon "contact electroluminescence." His results indicate the need of all three constituents, although various organic dielectric fillers or even air may be substituted for castor oil. More recently, Wachtel (2) reported the difference in spectral distribution of the emitted radiation for electroluminescent phosphors suspended in castor oil with and without the addition of metal particles. Lehmann explained the phenomenon of contact electroluminescence qualitatively as a result of extremely high local field strengths present in the proximity of the metal particles. His view was further supported by the fact that only metal particles of suitable size and shape (sharp edges) resulted in observable contact electroluminescence. He came to the conclusion that the only pertinent property of the metal particles is their high conductivity. The results of some experiments performed in our laboratory on various nonconductive materials with high dielectric constants appear to disagree with this conclusion and favor explanation of the observed luminescence as the result of photoluminescence induced by ultraviolet radiation generated in local glow discharges. These results are in general agreement with the experiments by Herwelly (3) regarding the luminescence of certain phosphors in strong electric fields. From his experiments, *e.g.*, the dependence of the luminescence on the degree to which gases had been removed from the phosphor particles, Herwelly concluded that the observed emission was due to photoluminescence induced by the u.v. light emitted by electrical discharges within internal voids of individual phosphor grains. In our observations of mixtures containing metal filings, emission of u.v. radiation causing visible photoluminescence was observed.

In the course of investigating the effects of ferroelectrics and other materials with high dielectric constants on the light output of various luminescent materials, emission of visible light was observed occasionally in mixtures of photoluminescent (but not electroluminescent) phosphors and ferroelectrics when suspended in organic dielectrics and subjected to alternating voltages. For example, a cell similar to that used by Lehmann, containing a suspension in castor oil[1] of equal parts (by volume) of a ZnS photoluminescent phosphor and crushed KH_2PO_4 (particle size about 100μ), exhibited several bright blue spots when operated at about 800 v (rms) and 1000 cps. Lehmann's cell consisted of an aluminum base and a thin conducting glass separated by 100μ. His observations were made between 400 and 600 v (rms) at 10,000 cps. Since we used a cell thickness of 150μ, our somewhat higher voltages correspond to about the same average applied fields. Spectral changes were observed on substitution of different phosphors; however, for any given phosphor, the same spectral emission was obtained by substitution of KH_2PO_4 with other inorganic salts ($NH_4H_2PO_4$, NaCl, anhydrous metal chlorides, etc.) or with metal particles (filings of Al, Ni, Cu, or Fe).

These experiments appear to indicate that Lehmann's contact electroluminescence is part of a class of phenomena which are probably caused by the presence of large field inhomogeneities. These strong local fields may be generated either by means of irregular particles of high conductivity (contact electroluminescence) or by the incorporation of materials with high dielectric constants (above experiments). To determine the origin of the emitted radiation, we conducted a number of experiments with aluminum filings, similar to those reported by

[1] Castor oil or other dielectric fluids used to suspend phosphors, filings and solid dielectrics were evacuated after mixing to remove any adsorbed gases.

Lehmann. In agreement with Lehmann, these experiments indicated a dependence on the shape of the aluminum or metal filings and an increase in the number of bright "dots" with the concentration of filings. On increasing the voltage from between 600-800 v to about 1000 v (10,000 cps), it was found that no phosphor particles were necessary for light emission. Bluish purple dots appeared which increased in size with increasing applied voltage until a general bluish purple glow over large areas of the cell was obtained. Similar results were obtained with other crystalline dielectrics, especially those with high dielectric constants (*e.g.*, KH_2PO_4 and $NH_4H_2PO_4$). As a matter of record, even mildly crushed NaCl in castor oil exhibited bluish purple emission under these conditions.

The difference in spectral response when the combination of aluminum and castor oil was used with and without the addition of a trace of a nonelectroluminescent phosphor suggested the investigation of the spectral distribution of the emitted radiation of the metal and castor oil system in order to ascertain whether sufficient short wave-length emission was available to cause photoluminescence.

The emission spectra of the metal and castor oil combination in the ultraviolet, visible, and infrared regions were recorded on Kodak spectroscopic film (Type 103, N, F, and O, respectively) by means of a reflex grating spectrograph. Emission bands were observed only in the short wavelength visible and near ultraviolet regions. For an aluminum and castor oil cell operated at 800 v and 9,000 cps, the observed emission bands, in microns, are: 340 (w), 355 (ms), 375 (s), 395 (s), 420-425 (m), 440 (w). The fact that no radiation with wavelengths shorter than 340μ was observed is probably due to absorption by the SnO_x conductive glass which was used.

The visible and ultraviolet radiation emitted by the metal filings and castor oil system qualitatively explains observations regarding contact electroluminescence.

The visible purple and violet bands are generally superimposed on the photoluminescent response of the phosphor and thus account for any spectral shifts occurring between regular photoluminescence and contact electroluminescent activated photoluminescence. For example, Mn-activated $MgTiO_3$, a deep red photoluminescent phosphor, mixed with aluminum in castor oil gave the usual bluish purple contact electroluminescence plus an over-all dull red. Exceptions were noted in the ZnS activated phosphors, where the yellow or greens usually masked the purple contact electroluminescent response. This may be partly accounted for by the better response of the eye to wavelengths in the vicinity of the greens.

In an evaluation of the data listed by Lehmann, only one of 17 photoluminescent phosphors gave a contact electroluminescent response that was different from its ultraviolet response. The exception was a green photoluminescent phosphor which exhibited a blue contact electroluminescent emission. This spectral shift is similar to our usual observation, such as the Mn-activated $MgTiO_3$ described above, in which the photoluminescent and contact electroluminescent emissions are combined.

It also may be noted that the spectral shift observed by Wachtel in (Zn, Cd) S:Cu, Cl electroluminescent phosphors when mixed with Cu filings is clearly in the direction of the photoluminescent response expected for that type of phosphor.

It appears that great care should be exercised in comparing the result of the two different phenomena of "contact" electroluminescence and "intrinsic" electroluminescence. The former is probably associated with photoluminescence of materials excited by the ultraviolet components of the emission of other materials present in the composite suspension, whereas the latter is associated with electroluminescent centers probably located along hexagonal to cubic faults within the crystallites of the material, as indicated by Diemer (4) and others (5, 6).

Manuscript received Dec. 27, 1960.

Any discussion of this paper will appear in a Discussion Section to be published in the December 1961 JOURNAL.

REFERENCES

1. W. Lehmann, *This Journal*, **104**, 45 (1957).
2. A. Wachtel, *ibid.*, **107**, 602 (1960).
3. A. Herwelly, *Acta Physica Austriaca*, **5**, 30 (1951-2).
4. G. Diemer, *Philips Research Repts.*, **10**, 194 (1955).
5. M. A. Short, E. G. Steward, and T. B. Tomlinson, *Nature*, **177**, 240 (1956).
6. A. H. McKeag and E. G. Steward, *This Journal*, **104**, 41 (1957).

A Diffusion Mask for Germanium

E. L. Jordan

Semiconductor and Materials Division, Radio Corporation of America, Somerville, New Jersey

The surface of silicon can be oxidized to form a coating of silicon dioxide which prevents the diffusion of specific impurities (1). This silicon dioxide mask when used in conjunction with photoengraving techniques makes it possible to prepare double diffused devices. Such techniques permit the precise control of the area of diffusion, junction depth, and level of doping.

The oxide mask may be formed readily on silicon by heating in an oxidizing atmosphere. Unfortunately, this technique does not work for germanium; although it is possible to form a coating of germanium dioxide on germanium by careful heating in an oxygen atmosphere, the germanium dioxide formed is not stable enough to act as a diffusion mask. At about 700°C in either a reducing or inert

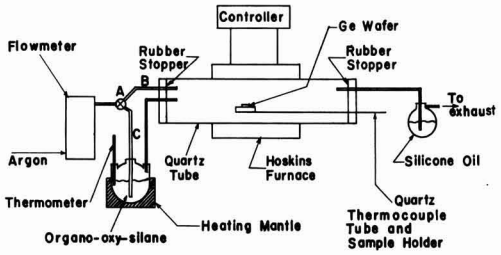

Fig. 1. Equipment for vapor deposition of silicon dioxide

atmosphere, germanium dioxide reacts with the bulk germanium as follows:

$$GeO_2 + Ge \xrightarrow[\text{heat}]{} 2GeO$$

Because the germanium monoxide formed is volatile at 700°C it is quickly removed from the surface. Heating to 700°C in an oxidizing atmosphere results in a badly pitted germanium surface, which makes its use as a diffusion mask infeasible.

Therefore, some other material must be produced on the surface of the germanium which is stable under diffusion conditions, will function as a diffusion mask, will have no effect on the electrical characteristics of the germanium, and may be removed easily from selected areas. Because silicon dioxide satisfies these requirements on silicon, its application to germanium was investigated.

The application of a silicon dioxide coating to a germanium surface was accomplished by a technique for preparing the silicon dioxide by the thermal decomposition of an alkoxysilane. This coating is easy to apply, has excellent mechanical strength, and is easily removed by etches which do not attack germanium.

Technique

The vapor deposition of silicon dioxide is accomplished in the equipment shown in Fig. 1.

The wafers to be coated are placed on the sample holder, inserted in the furnace and a 1 ft³/hr flow of argon is started to purge the furnace. While the furnace is purging, the argon flows through tube B shown in Fig. 1. After the furnace has purged for 10 min, the power is turned on. When the sample temperature is 700°C, valve A is turned to permit the argon to pass through the alkoxysilane and to enter the furnace. The mixture of argon and alkoxysilane is allowed to flow through the furnace for a period of time determined by the thickness of the coating desired. The furnace is turned off and valve A returned to the purging position. When the furnace has cooled to 200°C, the samples are removed.

Maintenance of the equipment is essentially simple, requiring only periodic cleaning of the furnace tube and sample holder by washing with 25% HF until deposits are removed. The buildup of the oxide on the furnace tube and sample holder does not affect the results, and the cleaning schedule is not a rigorous one, but is a precautionary measure to prevent a possible concentration of impurities. The oxide layer which accumulates in the furnace was checked spectrographically, and the impurities, if any, are present in quantities below the level of detection. A further indication of the purity of the materials was obtained when coatings were prepared on 15 Ω-cm germanium with no observed change taking place in the bulk resistivity after coating, thus indicating that thermal conversion due to copper contamination was not a problem. A test was also run to determine whether or not the alkoxysilane in the flask deteriorates with time. Thus far, the results of this test indicate that no deleterious changes occur over a two to three month period.

Materials

Various materials were evaluated in the course of this work as shown below:

Material	Formula	Molecular weight	Boiling point °C at a vapor pressure of: 60 mm	400 mm	760 mm
Tetraethoxysilane	$Si(OC_2H_5)_4$	208.3	—	—	167
Ethyltriethoxysilane	$(C_2H_5)Si(OC_2H_5)_3$	192.30	86.8	138.8	160.9
Amyltriethoxysilane	$C_5H_{11}Si(OC_2H_5)_3$	234.39	—	—	198
Vinyltriethoxysilane	$CH_2{=}CHSi(OC_2H_5)_3$	190.26	86.4	138.6	160.5
Phenyltriethoxysilane	$C_6H_5Si(OC_2H_5)_3$	240.35	153.2	210.5	233.5
Dimethyldiethoxysilane	$(CH_3)_2Si(OC_2H_5)_2$	148.28	—	—	111
Diphenyldiethoxysilane	$(C_6H_5)_2Si(OC_2H_5)_2$	272.40	205	251.7	296

These materials are all relatively stable liquids with boiling points ranging from 100° to 300°C, and their physical properties are typical of organic solvents. All of these materials yield coatings which appear to be the same; however, it has been found more difficult to prepare satisfactory films from materials which have less than three (3) oxygen atoms in the molecule.

Discussion

The proposed mechanism of the reaction is shown by the following equation:

$$\begin{matrix} R \\ O \\ R\text{-}O\text{-}Si\text{-}R \\ O \\ R \end{matrix} \xrightarrow{\Delta} SiO_2 + R\text{-}R + \text{SiO and C depending on the conditions}$$

where R = hydrocarbon radical. The compounds containing the most oxygen are the easiest to use since this minimizes the possibility of forming silicon monoxide, which has been found to interfere with the etching of the required pattern. In addition, while oxygen must be present to form the silicon dioxide, it must originate from the alkoxysilane. Care must be taken to exclude all external oxygen and moisture from the furnace since these will cause the film to have a cloudy appearance. The cloudy film thus formed will not etch properly and should, therefore, be avoided.

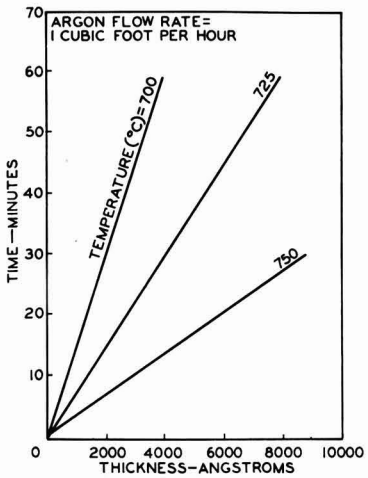

Fig. 2. Relationship between time, temperature, and film thickness.

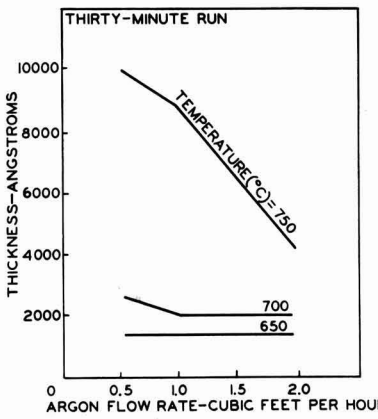

Fig. 3. Effect of varying the flow rate of the carrier gas when using ethyltriethoxysilane.

The composition of the film has been checked by the use of the infrared spectrograph. These investigations show a peak in the absorption band at 9.5μ with a shoulder at 8.5μ. These peaks correspond with the known bands for silicon dioxide as found in a hydrated, dry silica gel (2). Chemically the film is very inert showing no sign of attack after 5 min of immersion in concentrated acids such as nitric, sulfuric, hydrochloric, acetic, and aqua regia, or bases such as sodium hydroxide or potassium hydroxide. Neither hot nor cold hydrogen peroxide attack the film in concentrations up to 30%. On the other hand, hydrofluoric acid and conventional germanium and silicon etches (such as CP4, etc.) will remove the film very rapidly. It is this feature of the film that makes it very useful in device fabrication since the film may be removed readily from the required areas by photoresist masking followed by hydrofluoric acid etching to remove the oxide from the selected areas.

The effect of the carrier gas on the film formation was investigated using various gases such as argon, purified tank nitrogen containing only 8 ppm oxygen, and regular grade nitrogen. No significant difference was observed when the first two of the above gases were used. The results with regular grade nitrogen were erratic, and it was felt that this was due to the presence of varying amounts of oxygen and moisture in the gas.

The relationship between time, temperature and film thickness using ethyltriethoxysilane at 25°C in the bubbler, is shown in Fig. 2. The graph shows a linear relationship between film thickness, time, and temperature over the range investigated, and as would be expected, increasing the temperature increases the rate of deposition.

The effect of varying the flow rate of the carrier gas when using ethyltriethoxysilane, at 25°C in the bubbler, is shown in Fig. 3. It can be noted that the flow rate has a marked effect only at the higher temperatures, and it is believed that this is due primarily to the cooling of the sample by the gas stream. It was found, however, that the lower temperatures produced the desired clear coatings.

When attempts were made to prepare coatings of 20,000Å, to mask against p-type impurities, by raising the temperature to 750° to 800°C the resultant coatings were black rather than the desired clear glass. These black coatings did not etch cleanly, and it is felt that these black coatings were caused by the incorporation of carbon in the film when the organic radical cracked because of the high temperature used.

In order to produce clear coatings, 20,000Å in thickness, tetraethoxysilane was used, and the time of deposition was raised to 16 hr, while the temperature was lowered to 625°C. These conditions produced a clear glassy coating which had the desired etching characteristics.

During the development of the techniques for deposition of thick coatings, cracking of the film and germanium substrate was noticed when the above time and temperature conditions were exceeded. In order to evaluate the effect of the thick film deposition on the wafer, the following experiment was performed. Three wafers with an approximate dislocation density of 2000 etch pits/cm^2 were coated with silicon dioxide. The first wafer was coated with 2,000Å of silicon dioxide, and the second and third wafers were coated with a 20,000Å film. No signs of surface damage were observed on any of the wafers following coating. The wafer with the 2,000Å coating and one with the 20,000Å coating were heated to the same temperature, 750°C, used during diffusion processing. Upon completion of the simulated "diffusion" run, the wafers were washed in hydrofluoric acid to remove the oxide, and etch pit counts were repeated. The results of these counts are shown in Fig. 4.

Sample A shown in the figure is a wafer that had a 2,000Å coating, and sample B is a wafer with the 20,000Å coating. It is evident that slip lines have developed in sample B but not in sample A. It has been found that the dislocation density in sample A has not increased but that more than 100,000 etch pits/cm^2 were present in sample B. The wafer sur-

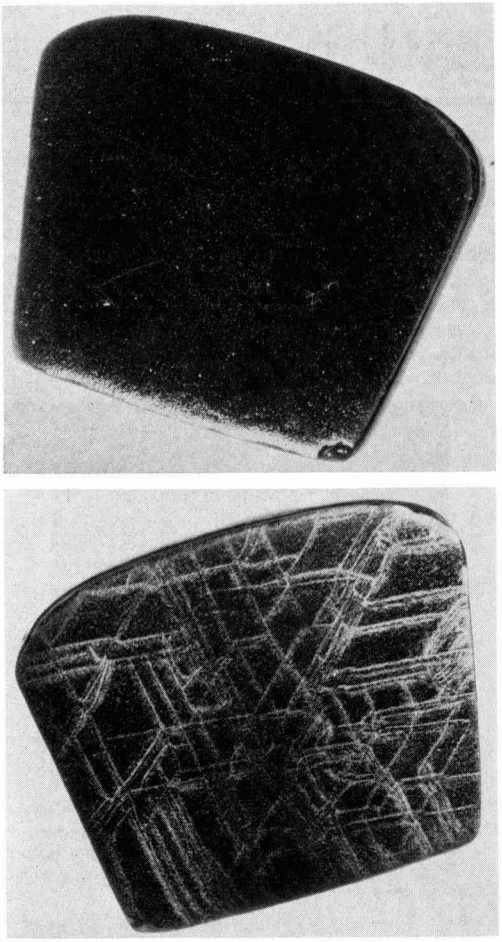

Fig. 4. Results of etch pit counts: sample A (top), a wafer with a 2,000Å coating; sample B (bottom) a wafer with a 20,000Å coating.

face also indicates that it was subjected to a strain sufficient to cause slip.

In order to determine the point in the processing where the strain originates, the second wafer with a 20,000Å coating was not subjected to the diffusion conditions, but was only washed with hydrofluoric acid to remove the oxide coating, and then subjected to standard pit counting techniques. This wafer showed the same slip lines, and high etch pit count found on sample B in Fig. 4. It is, therefore, obvious that the strain is created during the coating operation and not during subsequent processing.

Since the most useful thickness for masking against n-type impurities is approximately 2,000Å, this problem has caused no inconvenience. The use of the coating as a mask against p-type impurities is, however, greatly complicated, because of the strain induced in the base crystal, and is of only limited value.

Diffusion

The effectiveness of the coating has been proven by its successful use in many n-type diffusion runs. The coating has masked against arsenic diffusions under conditions which produce surface concentrations ranging from 10^{17} to 10^{20} at./cm^3. The diffusion runs were made using germanium-arsenic powders ranging in composition from a fraction of a per cent arsenic up to 5% arsenic by weight as a diffusion source. Diffusion with the 5% arsenic powders has been carried out at temperatures of 700°C for periods up to 2 hr with complete masking. These powders yield surface concentrations close to 10^{20} at./cm^3 on the unmasked portion of the wafer while no change in the resistivity of the masked portion was observed. Complete masking for periods up to 2 hr at temperatures up to 900°C can be made with powders yielding carrier concentrations of 10^{18} to 10^{19} at./cm^3.

Tests were run using antimony and phosphorus as the doping source with equal success. In addition, the oxide has shown promise as a diffusion mask on gallium arsenide and has been used successfully as a mask to prevent outdiffusion.

Conclusion

A diffusion mask has been developed for germanium which completely masks against the diffusion of n-type impurities (arsenic, antimony, and phosphorus) under all conditions encountered in device fabrication.

The deposition of the silicon dioxide mask by the thermal decomposition of an alkoxysilane has provided a simple and inexpensive technique for masking a double diffused germanium npn transistor (3).

Acknowledgments

The author wishes to thank J. Klerer, R. Frieser, and A. S. Rose for many helpful discussions and assistance with the preparation of the manuscript, to B. M. Upton who assisted in the gathering of the data, to S. R. Lederhandler for infrared measurements, and R. Czorny who suggested and ran the test to determine the strain induced in the crystal by thick films.

Manuscript received Nov. 8, 1960; revised manuscript received Jan. 23, 1961. This paper was prepared for delivery before the Chicago Meeting, May 1-5, 1960.

Any discussion of this paper will appear in a Discussion Section to be published in the December 1961 JOURNAL.

REFERENCES

1. C. J. Prosch and L. Derick, *This Journal*, **104**, 547 (1957).
2. Miller and Wilkins, *Anal. Chem.*, **24**, 1253 (1952).
3. H. S. Veloric, D. Rauscher, and E. L. Jordan, Paper presented at the Semiconductor Device Research Conference, Ithaca, N. Y., June 17, 1959.

Brief Communication

An Ultrastructure Study of the Corrosion of Aluminum in the Presence of Mercury

A. N. J. Heyn[1]

Virginia Institute for Scientific Research, Richmond, Virginia

It has long been known (1) that upon exposure of aluminum to mercury a remarkably destructive type of corrosion occurs in which most fantastically shaped fibrous filaments, bands, and sheets of aluminum hydroxide (1) or hydrated aluminum oxide grow rapidly from the metal surface. This particular type of corrosion is most detrimental and extremely difficult to stop, once started. It has been assumed that the aluminum hydroxide is formed in this process under dissolving of the aluminum in the fluid mercury layer covering the surface to form an aluminum-mercury alloy, which is subsequently oxidized in contact with moist air.

An ultrastructure study with the electron microscope has been carried out on the corrosion product formed during this catastrophic process. The results are briefly reported here. The material was prepared by placing a drop of mercury on a clean[2] aluminum surface in moist air. After about 30 min the white fibrous growth near the edge of the drop had reached a length of about 1 in. and was collected for study.

From the electron micrographs, one of which is reproduced here in Fig. 1 at a magnification of 23,560 times before reduction for publication, it is seen that in all cases the corrosion product has a typical ultrastructure which at first sight looks like a polycrystalline configuration. The composite structure consists of submicroscopic, uniform, elongated micellar strands or needles, which are bundled together over larger ranges in almost parallel orientation. These needles very often appear to be flattened and have an almost uniform width of about 100Å. Indications of a helical or coiling appearance is often observed. The length of the needles or strands is very difficult to determine, but is generally at least twenty times the diameter, very often much longer. Transverse ruptures are often seen across the needles. The impression is obtained that longer strands are broken at irregular places into shorter pieces to form the needles.

Sometimes consistent large patches of very high electron absorption are observed, which are probably microdroplets of mercury carried along and captured by the growing fibers. In the vicinity of these drops much finer fibers are often seen.

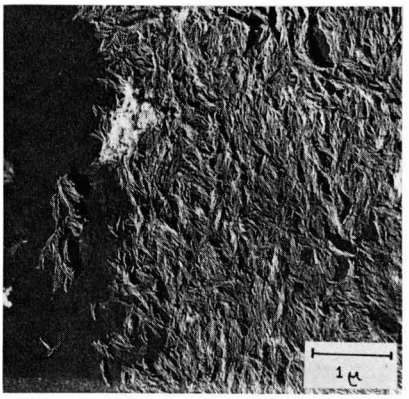

Fig. 1. Catastrophic corrosion of aluminum in the presence of pure mercury. Fibrils are almost in original arrangement. The direction of growth is perpendicular to the metal surface and along the meridian of the photograph. Magnification 23,560X before reduction for publication.

When other metals have been added to the mercury, such as lead and thallium, the shape and size of the strands is somewhat different. They are more compressed in length and more irregular in appearance and orientation.

A few electron diffraction observations were made for determining whether or not these strands have crystalline configuration; at first sight they usually give the impression of having microcrystalline nature. Since no clear electron diffraction patterns were obtained, no definite conclusion could be made, however.

The essential feature of the ultrastructure observed is the presence of elongated microfibrils of rather constant diameter, grown from the surface and packed in parallel arrangement. Similar formations have been observed in the case of so-called "metal whiskers," which are also elongated structures grown from a metal surface along one direction.

The findings on the structure of the corrosion product might be explained in the following way. If it is assumed that during this process separate ano-

[1] Present address: Department of Physics, Auburn University, Auburn, Alabama.

[2] The oxide film being removed with acid or otherwise.

dic and cathodic sites exist, the growth of separate parallel fibers could be understood. The oxidation of the aluminum alloy would take place in the anodic regions separated from each other by cathodic regions. As a result of growth pressure and maybe also shifting of the anodic regions over the surface, coiling, transverse rupture, and shifting of the fibers may occur. This would explain fully the features observed. If this hypothesis is correct, the cross section of the fibers would correspond essentially to the area of the anodic domains and the cross section of the composite fibers would be a true representation of this distribution of anodic and cathodic regions on the surface. From the cross sections of the fibers it could be concluded then that the cross section of the anodic sites would be about 100Å, and from the packing of the fibers it could be concluded that the spacing is probably not much more than twice this value. This hypothesis of alternating sites would explain nicely the main point, why a discontinuous arrangement of whiskers is formed rather than a continuous layer of oxide.

Acknowledgment

Some of the corrosion samples obtained with pure mercury were prepared by Mr. David Jackson; other samples were prepared by the author.

Manuscript received Aug. 29, 1960; revised manuscript received Sept. 29, 1960. Work on this paper was carried out under contract with the U. S. Army Chemical Corps.

Any discussion of this paper will appear in a Discussion Section to be published in the December 1961 JOURNAL.

REFERENCE

1. H. Röhrig, *Korrosion u. Metallschutz*, **3**, 1 (1927).

FUTURE MEETINGS OF
The Electrochemical Society

Detroit, Mich., October 1, 2, 3, 4, and 5, 1961
Headquarters at the Statler Hotel
Sessions probably will be scheduled on Batteries, Corrosion (including a Symposium on Surface Structure vs. Corrosion Behavior), Electrodeposition (including symposia on Addition Agents and on Electrodeposited Magnetic Films), Electronics (Semiconductors), Electro-Organics, and Electrothermics and Metallurgy

★ ★ ★

Los Angeles, Calif., May 6, 7, 8, 9, and 10, 1962
Headquarters at the Statler Hilton Hotel

★ ★ ★

Boston, Mass., September 16, 17, 18, 19, and 20, 1962
Headquarters at the Statler Hilton Hotel

★ ★ ★

Pittsburgh, Pa., April 14, 15, 16, 17, and 18, 1963
Headquarters at the Penn Sheraton Hotel

★ ★ ★

New York, N. Y., September 29, 30, and October 1, 2, and 3, 1963
Headquarters at the New Yorker Hotel

★ ★ ★

Toronto, Ont., Canada, May 3, 4, 5, 6, and 7, 1964
Headquarters at the Royal York Hotel

Papers are now being solicited for the meeting to be held in Detroit, Mich., October 1-5, 1961. Triplicate copies of each abstract (*not exceeding 75 words in length*) are due at Society Headquarters, 1860 Broadway, New York 23, N. Y., *not later than May 15, 1961* in order to be included in the program. *Please indicate on abstract for which Division's symposium the paper is to be scheduled, and underline the name of the author who will present the paper.* No paper will be placed on the program unless one of the authors, or a qualified person designated by the authors, has agreed to present it in person. An author who wishes his paper considered for publication in the JOURNAL should send triplicate copies of the manuscript to the Managing Editor of the JOURNAL, 1860 Broadway, New York 23, N.Y.

Presentation of a paper at a technical meeting of the Society does not guarantee publication in the JOURNAL. However, all papers so presented become the property of The Electrochemical Society, and may not be published elsewhere, either in whole or in part, unless permission for release is requested of and granted by the Editor. Papers already published elsewhere, or submitted for publication elsewhere, are not acceptable for oral presentation except on invitation by a Divisional program Chairman.

1961 Gordon Research Conferences

The Gordon Research Conferences for 1961 will be held from June 12 to September 1 at Colby Junior College, New London, N. H.; New Hampton School, New Hampton, N. H.; Kimball Union Academy, Meriden, N. H.; and Tilton School, Tilton, N. H.

Meetings will be held in the morning and in the evening, Monday through Friday, with the exception of Friday evening.

Requests for attendance at the Conferences, or for additional information, should be addressed to W. George Parks, Director, Dept. of Chemistry, University of Rhode Island, Kingston, R. I. From June 12 to September 1, mail for the office of the Director should be addressed to Colby Junior College, New London, N. H.

Physical Metallurgy

June 26-30, 1961
Kimball Union Academy
Meriden, N. H.
Michael Bever, Chairman
W. D. Robertson, Vice-Chairman
Imperfections, Substructure, and Microstructure

June 26

K. L. Moazed, G. M. Pound—Field Emission Microscopy of Metal Crystal Nucleation from the Vapor
C. Elbaum—Substructures in Crystals Grown from the Melt
S. Weissmann—Analysis of Substructure—Experiments and Theory
C. N. J. Wagner—Analysis of Defect Structures in Deformed Crystals

June 27

P. B. Hirsch—Dislocation Distributions, Flow Stress, and Hardening in F. C. C. Metals
U. F. Kocks—Special Arrangements of Dislocations in Deformed F. C. C. Metals
V. V. Damiano—Dislocations and Substructures in Zinc Single Crystals
L. M. Clarebrough—Short-Range Order, Point Defects, and Dislocations in Alpha Brass
J. R. Patel, A. R. Chaudhuri—Defect Structure in Dislocation-Free Crystals of Silicon and Germanium

June 28

M. J. Marcinkowski—Theory and Direct Observation of Antiphase Domain Boundaries and Dislocations in AB_3 Type Superlattices
J. S. Kirkaldy—The Thermodynamic Basis of Morphological Development
V. A. Phillips—Electron Microscopic Observations on the Role of Dislocations in Precipitation
H. I. Aaronson—The Role of Interfacial Structure in Diffusional Transformations

June 29

M. Hillert—Some Theoretical Aspects of the Formation of Proeutectoid Structures
W. L. Grube, S. R. Rouze—The Isothermal Decomposition Products of Austenite
W. S. Owen—Structures Produced by Diffusionless Transformations

June 30

J. E. Hilliard—Quantitative Electron Transmission Metallography
M. J. Fraser—Annealing Twins and Surface Topography
S. V. Radcliffe—Products of Transformations at High Pressure

Chemistry and Metallurgy of Semiconductors

July 10-14, 1961
Tilton School
Tilton, N. H.
A. Rosenberg, Chairman
P. Egli, Vice-Chairman

July 10

Epitaxial Crystal Growth

A. P. Hale—Vacuum Deposition of Silicon Layers
T. Renner—Preparation of III-V Compounds by Vapor Deposition
V. J. Lyons—Vapor Growth of Gallium Arsenide
P. I. Pollak—Vapor Phase Growth of Silicon Crystals

July 11

Crystal Growth at High Pressures

W. V. Wright—Moderately High Pressures
R. H. Wentorf—Ultra High Pressures

Thermodynamics

M. B. Bever—Properties of Compound Semiconductors
Other speaker and subject to be announced.

July 12

Chemical Bonds and Electron Energy Bands

A. J. Rosenberg—Properties of Some Ternary Systems
A. H. Cornish—Properties of Chemically Related Compounds
F. Herman—A Physicist's View
P. O. Lowdin—A Chemist's View

July 13

Organic Conductors

D. Fox—Mechanisms
M. I. Pope—Phenomena

July 14

Electroluminescence

E. E. Loebner—Mechanisms
H. F. Ivey—Phenomena

Corrosion—Oxidation of Metal Surfaces

July 24-28, 1961
Colby Junior College
New London, N. H.
Morris Cohen, Chairman
M. A. Streicher, Vice-Chairman

July 24

H. A. Liebhafsky, Discussion Leader

E. Müller—Corrosion Studies with the Field Ion Microscope
A. Dravnieks—Use of Contact Potential Measurements in Oxidation Studies
D. Pashley—Electron Optical Studies of Thin Surface Films on Metals
J. Kruger—The Use of Elliptically Polarized Light in the Study of Oxide Film Growth on Metal Surfaces Immersed in Aqueous Solutions

July 25

W. Smeltzer, Discussion Leader

J. Bernard—Nucleation and Growth of Oxide Films on Metals
T. Rhodin—Oxide Nucleation and Growth on Magnesium
A. T. Gwathmey—Some Recent Results on Oxidation of Copper and Copper-Nickel Alloy Crystals
W. Boggs—Oxide Growth on Tin and Its Alloys

July 26

A. Dravnieks, Discussion Leader

H. J. Engell—The Oxidation of Metal-Carbon Alloys
C. E. Birchenall—Some Problems in High-Temperature Oxidation of Metals
E. A. Gulbransen—The Effects of Environment, Stress, and Metal Structure on the Oxidation of Iron and Iron Alloys
J. Laukonis—Formation and Reduction of Oxide Flms on Iron Whisker Surfaces

July 27

M. A. Streicher, Discussion Leader

M. Dignam—Anodic Oxidation of Aluminum—Transient Effects and Oxide Structure
R. A. Baker—Anodic Oxidation of Lead in Sulfuric Acid
M. Cohen—A Comparison between Air-Formed and Anodic Oxide Films on Iron

July 28

M. Cohen, Discussion Leader

H. J. Engell—Breakdown of Oxide Films and Pitting. General Discussion.

Electrodeposition

July 31-August 4, 1961
Tilton School
Tilton, N. H.
W. R. Meyer and M. S. Frant, Co-Chairmen

July 31

The Mechanism of Electrodeposition
W. R. Meyer, Chairman

N. B. Hackerman—Nature and Kinetics of Discharge Species at the Electrode Surface
P. Delahay, D. Mohilner—Metal Deposition: Double Layer Effects and Investigation of Fast Discharge Processes

E. Saubestre, Chairman

J. O'M. Bockris—Rate Determining Steps and Paths in the Electrodeposition and Electrodissolution of Thin Metallic Layers
J. O'M. Bockris, D. Drazic, H. Kitz—Transient Phenomena at the Iron-Solution Interface, and the Mechanism of the Deposition and Dissolution of Iron

August 1

The Mechanism of Electrodeposition (cont'd)
N. Hackerman, Chairman

R. G. Barradas, B. E. Conway—Electrochemical Adsorption of Heterocyclic Bases and Ionic Derivatives
Late papers and general discussion on mechanisms.

Addition Agents in Electrodeposition
O. Kardos, Chairman

H. Brown—The Role and Structure of Addition Agents in Electroplating, With Special Reference to Nickel
D. Trivich—Some Aspects of Brightener Action
S. E. Beacom—Leveling in Bright Nickel Deposits

August 2

The Effect of Structure on Properties
(A) Basis Metal Structure
A. Brenner, Chairman

M. H. Jones—Effect of Substrate Metallurgy
H. Leidheiser—Nickel Plating on Copper Single Crystals
L. D. McGraw—A New Field: Surface Metallurgy

(B) Coating Metal Structure
A. Brenner, Chairman

H. J. Read—Plastic Properties of Electrodeposits
A. M. Max—Stress in Electrodeposits

August 3

Electrodeposition of Alloys
F. A. Lowenheim, Chairman

M. L. Holt—Electrodeposition of Alloys of Some of the Transition Metals
H. Koretsky—Current Research on Electrodeposited Thin Magnetic Films. A Critical Survey
I. Wolf—Factors Affecting Magnetic Properties of Iron-Nickel Films

Electrodeposition on Unusual Substrates
H. B. Linford, Chairman

D. R. Turner—Metal Deposition on Semiconductors
E. Saubestre—Plating on Unusual Metals

August 4

Current Problems in the Utilization of Plated Coatings
N. Murphy, Chairman

M. Frant—Electrodeposited Metals as Electrical Contacts
F. A. Lowenheim—Solderability of Plated Metals
C. Levy—Electrodeposited Coatings for High-Temperature Applications

Chemistry and Physics of Solids

August 14-18, 1961
Kimball Union Academy
Meriden, N. H.
Walter Kohn, Chairman
C. P. Slichter, Vice-Chairman

New Theoretical Viewpoints and Their Experimental Significance

August 14

W. Kohn, D. Pines—Introductory Session
J. M. Luttinger, B. Pippard—The Normal Metal

August 15

R. A. Ferrell, J. Friedel—The Normal Metal (Continued)
J. Bardeen, M. Tinkham—Superconductivity

August 16

F. Keffer, H. Suhl, B. Matthias—Magnetism
R. Kubo, B. Lax—Transport Phenomena

August 17

F. J. Morin and Speaker to be announced—Insulators
J. C. Phillips, C. P. Slichter—New One-Electron Theories

August 18

P. W. Anderson, C. Herring—Concluding Discussion

Section News

Philadelphia Section

The March 1, 1961 meeting of the Philadelphia Section of The Electrochemical Society, held in the Main Lecture Room of the University of Pennsylvania's Harrison Laboratory of Chemistry, took the form of a Meeting-in-Miniature.

The following program, under the Chairmanship of Robert Kunin, was presented:

3:00 P.M.—Introductory Remarks by Robert Kunin, Rohm & Haas Co.
3:05 P.M.—"Electrochemical Polarization Curves of the Corrosion of Mild Steel" by F. Donahue and R. Gaviola, Betz Labs., Inc.
3:25 P.M.—Discussion.
3:30 P.M.—"The Generation of Electrostatic Charges in Hydrocarbons" by H. Hartung, Consultant.
3:55 P.M.—Discussion.
4:00 P.M.—"Constant Potential Corrosion of Lead in Pb-Sb Alloys" by

J. Sklarchuk, Electric Storage Battery Co.

4:25 P.M.—Discussion.

4:30 P.M.—"A Laboratory Screening Procedure for the Evaluation of Corrosion Inhibitors for Uncoated Mild Steel in 10% Aqueous HCl" by J. Morrison, Rohm & Haas Co.

4:55 P.M.—Discussion.

5:00 P.M.—General Discussion.

5:30 P.M.—Social Hour, University Museum.

6:00 P.M.—Dinner, University Museum. After-dinner speaker—Dr. Henry B. Linford, Vice-President of The Electrochemical Society.

Approximately 70 people attended the program, including Dr. R. A. Schaefer and Dr. H. B. Linford, both of whom spoke to the group after dinner.

The Meeting-in-Miniature was the first attempt at this type of meeting, and the entire group was pleased with the results. Serious consideration is being given to making this a regular part of the Section's activities.

Robert Kunin,
Program Chairman

Ontario-Quebec Section

The Ontario-Quebec Section held a meeting in the Laurentien Hotel in Montreal on February 3, 1961. On this occasion, they were honored by a visit from the President of the Society, Dr. R. A. Schaefer, and also heard two interesting papers: "Some Aspects of the Chemistry and Technology of High Purity Selenium," by Dr. W. C. Cooper of Canadian Copper Refiners, Montreal, and "Exotic Semiconductor Devices" by Dr. Max Gransden of the R.C.A. Victor Co., Montreal.

Dr. Schaefer briefly reviewed the present status of the Society, pointing out that the recent increase in fees was necessary to meet steadily rising costs, particularly those for the printing of the JOURNAL.

Dr. Cooper discussed various methods for the production of high-purity selenium; recent studies of the amorphous, the red (monoclinic), and the gray (tetragonal) forms; the effects of some impurities on its electrical properties; and touched briefly on some semiconducting selenides.

Dr. Gransden briefly reviewed the theory of semiconduction, then described some lesser-known semiconducting devices such as refrigerators, power generators, infrared detectors, and alpha particle detectors. In addition, he demonstrated some of the units, such as a small, portable alpha particle detector, and a small refrigeration unit.

R. A. Campbell,
Secretary-Treasurer

San Francisco Section

The January 25, 1961 technical meeting and dinner of the San Francisco Section was held at the Men's Faculty Club, University of California, Berkeley.

After dinner, Dr. Bernard Porter, of the U. S. Bureau of Mines at Reno, Nev., spoke on the "Electrolytic Preparation of Molten Cerium Metal." He pointed out that there is available more cerium than iron, but it is harder to obtain and requires special care to remove other rare earth contaminants. By high-temperature electrolysis of fluorides in an inert atmosphere, cerium of 99.9% purity is being obtained. New applications are being found, especially since the properties are different from commercially available cerium. The high-purity material can be turned in a lathe using a steel bit, and neither the stock nor the turnings corrode rapidly as they stand around in air. The thermodynamics and the anode reactions in electrolytic preparation also were discussed.

Dr. Porter's talk was followed by a lively discussion with members involved in similar electrolytic processes with aluminum.

Worden Waring,
Vice-Chairman

Washington-Baltimore Section

The February 16, 1961 meeting of the Washington-Baltimore Section was held at Industrial Lecture Hall, National Bureau of Standards, Washington, D. C.

Dr. Kurt Stern, of the National Bureau of Standards, gave a talk on "Electrolyte-Solvent Interactions in Low Dielectric Solvents." The history of electrolytic solutions was reviewed briefly, with emphasis on the "continuum" vs. the molecular approach for the solvent. Various theories of electrolytic solutions—Debye-Hückel-Onsager, Fuoss, Bjerrum, Denison-Ramsey, Gilkerson—were discussed with particular reference to their treatment of aggregate formation.

The speaker's work on the ion pair-quadrupole equilibrium using dielectric techniques was discussed.

Manuscripts and Abstracts for Fall 1961 Meeting

Papers are now being solicited for the Fall Meeting of the Society, to be held at the Statler Hotel in Detroit, Mich., October 1, 2, 3, 4, and 5, 1961. Technical sessions probably will be scheduled on Batteries, Corrosion (including a Symposium on Surface Structure vs. Corrosion Behavior), Electrodeposition (including symposia on Addition Agents and on Electrodeposited Magnetic Films), Electronics (Semiconductors), Electro-Organics, and Electrothermics and Metallurgy.

To be considered for this meeting, triplicate copies of abstracts (*not exceeding 75 words in length*) must be received at Society Headquarters, 1860 Broadway, New York 23, N. Y., *not later than May 15, 1961. Please indicate on abstract for which Division's symposium the paper is to be scheduled and underline the name of the author who will present the paper.* No paper will be placed on the program unless one of the authors, or a qualified person designated by the authors, has agreed to present it in person. An author who wishes his paper considered for publication in the JOURNAL should send triplicate copies of the manuscript to the Managing Editor of the JOURNAL, 1860 Broadway, New York 23, N. Y.

Presentation of a paper at a technical meeting of the Society does not guarantee publication in the JOURNAL. However, all papers so presented become the property of The Electrochemical Society, and may not be published elsewhere, either in whole or in part, unless permission for release is requested of and granted by the Editor. Papers already published elsewhere, or submitted for publication elsewhere, are not acceptable for oral presentation except on invitation by a Divisional program Chairman.

This equilibrium for tetrabutylammonium bromide in benzene-methanol mixtures is very sensitive to the methanol concentration, the quadrupoles disappearing entirely when the methanol concentration exceeds approximately 10%. Comparison with simple, slightly polar solvents (e.g., toluene) shows that the effect is not due to the dielectric constant of the solvent. Entropies and enthalpies also are not in agreement with those calculated from a continuum model for the solvent.

Recent applications of infrared techniques to the above and similar systems were presented. Results were interpreted in terms of anion solvation by methanol through hydrogen bonding. The effect is most pronounced for high-charge density ions and in agreement with that predicted from a simple harmonic oscillator model for the hydroxyl group. Solvation numbers for ion pairs and quadrupoles were calculated. Thermodynamic functions for the solvation are in good agreement with values commonly encountered for hydrogen bonding.

Sigmund Schuldiner, *Secretary*

New Members

In March 1961, the following were elected to membership in The Electrochemical Society by the Admissions Committee:

Active Members

M. A. Aia, Sylvania Electric Products Inc.; Mail add: Woodside R. D. 2, Towanda, Pa. (Electronics—Luminescence)

C. E. Albertson, R. C. Ingersoll Research Center, Borg-Warner Corp.; Mail add: 240 S. Monterey Ave., Villa Park, Ill. (Electro-Organic)

W. P. Allred, Bell & Howell Research Center, 360 Sierra Madre Villa, Pasadena, Calif. (Electronics—Semiconductors)

F. J. Anderson, Jr., National Carbon Co.; Mail add: 10537 Beinhorn Rd., Houston 24, Texas (Industrial Electrolytic)

E. F. Apple, Large Lamp Dept., General Electric Co.; Mail add: 844 Cranbrook Dr., Cleveland 24, Ohio (Electronics—Luminescence)

F. P. Bacci, Allied Chemical Corp., General Chemical Div.; Mail add: Ethan Allen Dr., West Acton, Mass. (Electronics—Semiconductors)

M. L. Baig, Dept. of Electrochemistry, General Motors Technical Center, Warren, Mich. (Battery, Electrodeposition, Electrothermics & Metallurgy, Industrial Electrolytic)

Jean-Claude Balaceanu, Institut Francais du Pétrole, 4 Place Bir-Hacheim, Rueil-Malmaison (Seine et Oise), France (Battery, Electro-Organic, Theoretical Electrochemistry)

W. H. Banks, Printing, Packaging & Allied Trades Research Association, Randalls Rd., Leatherhead, Surrey, England

C. E. Benjamin, Westinghouse Electric Corp.. 7325 Penn Ave., Pittsburgh 8, Pa. (Electronics)

S. G. Berkley, Pratt & Whitney Aircraft, Connecticut Operations-Canel; Mail add: R.F.D. 1, Box 285, Mansfield Center, Conn. (Electrodeposition, Electrothermics & Metallurgy)

Daniel Bernard, Pechiney, 23 rue Balzac, Paris 8e, France (Electrothermics & Metallurgy, Industrial Electrolytic, Theoretical Electrochemistry)

W. E. Billings, Halliburton Co., Technical Center, Duncan, Okla. (Corrosion)

Odile Bloch, Institut Francais du Pétrole, 4 Ave. de Bois Préau, Rueil-Malmaison, (Seine et Oise), France (Battery, Electro-Organic, Theoretical Electrochemistry)

J. R. Booth, New Mylamaque Mining & Smelting Co., Suite 601, 11 Adelaide St. W., Toronto 1, Ont., Canada (Electrothermics & Metallurgy)

D. W. Broad, Imperial Chemical Industries Ltd., 488 Madison Ave., New York 22, N. Y. (Electronics—Semiconductors, Industrial Electrolytic)

J. T. Byrne, Dow Chemical Co.; Mail add: 2135 8th St., Boulder, Colo. (Theoretical Electrochemistry)

H. D. Childers, Nortronics Div., Northrop Corp.; Mail add: 3009 Palos Verdes Dr. N., Palos Verdes Estates, Calif. (Electronics, Electrothermics & Metallurgy)

M. A. Clark, Pacific Semiconductors, Inc.; Mail add: 5526 Via del Valle, Torrance, Calif. (Electronics—Semiconductors)

F. W. Cole, Bendix Filter Div.; Mail add: 640 E. Lincoln, Madison Heights, Mich. (Electrodeposition, Electrothermics & Metallurgy)

E. J. Colwell, Jr., Electric Storage Battery Co.; Mail add: 27352 Hollywood Dr., Westlake, Ohio (Battery)

J. A. Consiglio, General Engineering Lab., General Electric Co.; Mail add: 2040 Garden Dr., Schenectady 9, N. Y. (Battery)

W. A. Cunningham, Electric Storage Battery Co.; Mail add: 1029 Argonne Rd., South Euclid 21, Ohio (Battery)

H. A. Cook, Airpax Electronics, Inc., P. O. Box 8488, Fort Lauderdale, Fla. (Electronics)

G. R. Cronin, Central Research Labs., Texas Instruments, Inc., P. O. Box 5474, Dallas 22, Texas (Electronics—Semiconductors)

Gunther Dierssen, Harshaw Chemical Co.; Mail add: 7458 Goldenrod Dr., Mentor-on-the-Lake, Ohio (Electronics, Theoretical Electrochemistry)

Elmo Earleywine, Dow Corning Corp., Hyper-Pure Silicon Div., Midland, Mich. (Electronics—Semiconductors)

F. P. Eggers, Diamond Alkali Co.; Mail add: 7715 Oak Vista, Houston 17, Texas (Industrial Electrolytic)

Masataro Fukuda, University of Michigan; Mail add: 1678-31 Murfin St., Northwood Apts., Ann Arbor, Mich. (Battery, Theoretical Electrochemistry)

Anthony Gallaccio, Pitman-Dunn Labs., Frankford Arsenal; Mail add: 410 Covington Rd., Havertown, Pa. (Corrosion, Electrodeposition)

V. C. Garbarini, Bell Telephone Labs., Inc.; Mail add: 49 Taras Dr., Fords, N. J. (Electronics—Semiconductors)

S. J. Gaston, Yardney Electric Corp.; Mail add: 151-60 19th Ave., Whitestone, L. I., N. Y. (Battery)

R. E. Gaviola, Betz Labs., Inc., Gillingham & Worth Sts., Philadelphia 24, Pa. (Corrosion, Theoretical Electrochemistry)

P. D. George, General Engineering Lab., General Electric Co., Schenectady 5, N. Y. (Battery, Corrosion, Electric Insulation, Electrodeposition, Electronics, Electro-Organic, Electrothermics & Metallurgy, Industrial Electrolytic, Theoretical Electrochemistry)

Jean-Pierre Givry, Pechiney, St. Jean de Maurienne, Savoie, France (Industrial Electrolytic)

P. S. Gleim, Texas Instruments, Inc.; Mail add: 8631 N. Mediterranean Circle, Dallas 18, Texas (Electronics—Semiconductors)

M. H. Gottlieb, Bell Telephone Labs.,

By action of the Board of Directors of the Society, all prospective members must include first year's dues with their applications for membership.

Also, please note that, if sponsors sign the application form itself, processing can be expedited considerably.

Inc., 463 West St., New York, N. Y. (Theoretical Electrochemistry)

S. G. McGriff, Ionics, Inc., 804 Albee Bldg., 1426 6th St., N. W., Washington 5, D. C. (Battery)

Gerald Halpert, Melpar, Inc., Physical Science Lab., 3000 Arlington Blvd., Falls Church, Va. (Battery, Theoretical Electrochemistry)

E. R. Hayes, Shawinigan Chemicals Ltd., Shawinigan, Que., Canada

Louis Hoffman, Pacific Semiconductors Inc.; Mail add: 11722 John Ave., Garden Grove, Calif. (Electrodeposition, Electronics—Semiconductors, Electro-Organic, Theoretical Electrochemistry)

C. W. Hoornstra, Dow Metal Products Co., Div. of Dow Chemical Co.; Mail add: 22 Erie Court, Midland, Mich. (Corrosion)

G. N. Hoover, Electric Storge Battery Co., 1440 Chester Ave., P. O. Box 6266, Cleveland 1, Ohio (Battery)

R. N. Hyer, Frontier Chemical Co., P. O. Box 545, Wichita, Kansas (Industrial Electrolytic)

Stanley Januszkiewicz, Gould-National Batteries, Nicad Div.; Mail add: 145 Prospect St., Williamsett, Mass. (Battery)

H. J. Jordon, Electric Storage Battery Co., P. O. Box 6266, Cleveland 1, Ohio (Battery)

R. F. Justus, General Motors Research Labs.; Mail add: 5809 Arden Ave., Warren, Mich. (Battery)

L. H. Kraus, Zell Products Corp.; Mail add: 15 Drumlin Rd., Westport, Conn. (Electrodeposition)

Alois Langer, Westinghouse Research Labs.; Mail add: 600 Woodside Rd., Pittsburgh 21, Pa. (Battery, Electrodeposition)

T. S. Lee, Rocketdyne Div., North American Aviation; Mail add: 20833 Stephanie Dr., Canoga Park, Calif. (Battery, Theoretical Electrochemistry)

Kurt Lehovec, Sprague Electric Co., Marshall St., North Adams, Mass. (Battery, Corrosion, Electric Insulation, Electronics, Theoretical Electrochemistry)

C. A. Lenie, Monsanto Chemical Co.; Mail add: 1201 Port Royal Dr., St. Louis 41, Mo. (Electronics—Semiconductors)

C. W. Leung, Electro-Optical Systems, Inc., 125 N. Vinedo Ave., Pasadena, Calif. (Electronics—Semiconductors)

T. J. Lewis, Electrical Engineering Dept., Queen Mary College; Mail add: Pippins, Albany View, Buckhurst Hill, Essex, England (Electric Insulation, Electronics—Semiconductors, Theoretical Electrochemistry)

M. F. Lipworth, General Aniline & Film Corp., Linden, N. J. (Industrial Electrolytic)

Pao-Soong Lou, P. R. Mallory & Co., Inc., Mail add: 7 N. Tacoma Ave., Apt. 8, Indianapolis 1, Ind. (Battery, Industrial Electrolytic, Theoretical Electrochemistry)

C. T. McGregor, Texas Instruments, Inc.; Mail add: 6610 Chevy Chase, Dallas 25, Texas (Electronics—Semiconductors)

A. B. Middleton, Philadelphia Quartz Co.; Mail add: 336 Merion Ave., Haddonfield, N. J.

W. R. Miller, Electric Storage Battery Co., Nickel-Alkaline Battery Div.; Mail add: 113 Linden Ave., Verona, N.J. (Battery)

Zolton Nagy, Columbia Southern Chemical Co.; Mail add: 1342 Wooster Rd. W., Barberton, Ohio (Industrial Electrolytic)

G. K. Notman, Jones & Laughlin Steel Corp.; Mail add: 1838 Parkline Dr., Pittsburgh 27, Pa. (Corrosion, Electrodeposition, Theoretical Electrochemistry)

Hiroe Osafune, Nippon Electric Co., Ltd.; Mail add: 48 Shimouma 2 chome, Setagaya-Ku, Tokyo, Japan (Electronics—Semiconductors)

I. M. Pearson, National Cash Register Co., Electronics Div.; Mail add: 339 W. 218 St., Torrance, Calif. (Electrodeposition, Theoretical Electrochemistry)

H. A. Pohl, Plastics Lab., Princeton University, Princeton, N. J. (Theoretical Electrochemistry)

G. F. Pollnow, Allis-Chalmers Mfg. Co.; Mail add: 8903 W. Congress St., Milwaukee 18, Wis. (Theoretical Electrochemistry)

E. C. Rafferty, National Lead Co., Research Labs., 105 York St., Brooklyn 1, N. Y. (Electro-Organic)

R. L. Reddy, National Carbon Co., P. O. Box 6116, Cleveland 1, Ohio (Electrothermics & Metallurgy)

Notice to Members and Subscribers

(Re Changes of Address)

To insure receipt of each issue of the JOURNAL, please be sure to give us your old address, as well as your new one, when you move. Our records are filed by states and cities, not by individual names. The Post Office does not forward magazines.

We should have this information *by the 16th of the month* to avoid delays in receipt of the next issue.

F. A. Rocchi, I.B.M. Corp.; Mail add: Fenmore Dr., R.D. 2, Wappinger Falls, N. Y. (Electronics—Semiconductors)

J. E. Rome, Diotron, Inc.; Mail add: Croyden Apts., 49th & Locust Sts., Philadelphia 39, Pa. (Electronics)

R. J. Ryan, R.C.A. Semiconductor & Materials Div.; Mail add: 14 Metekunk Dr., Trenton 8, N. J. (Battery, Theoretical Electrochemistry)

M. C. Speer, Griffin Wheel Co., P. O. Box 567, Bensenville, Ill. (Electrothermics & Metallurgy)

J. H. Staub, Philco Corp., Lansdale Div., Lansdale, Pa. (Electronics—Semiconductors)

D. H. Stephenson, Transistor Electronics, Inc.; Mail add: 343 Safford St., Bennington, Vt. (Electric Insulation)

F. J. Strieter, Texas Instruments, Inc., Device Research, P. O. Box 1079, Dallas 21, Texas (Electronics—Semiconductors)

M. H. Switzer, Continental Can Co.; Mail add: 639 Hillside Ave., Glen Ellyn, Ill. (Corrosion, Theoretical Electrochemistry)

Raymond Thacker, General Motors Technical Center; Mail add: 32440 Franklin Rd., Franklin, Mich. (Battery, Theoretical Electrochemistry)

W. A. Thornton, Jr., Westinghouse Electric Corp.; Mail add: 27 Harvard Rd., Cranford, N. J. (Electronics)

Jon Van Winkle, General Electric Co., Mail add: 17 Front St., Schenectady 5, N. Y. (Battery, Industrial Electrolytic, Theoretical Electrochemistry)

S. E. Voltz, General Electric Co.; Mail add: E. Glen Circle, Media, Pa. (Battery, Theoretical Electrochemistry)

Shoji Wakayama, Sony Corp. of America; Mail add: 4035 Walnut St., Philadelphia 4, Pa. (Electronics—Semiconductors)

F. E. W. Wetmore, Electrochemistry Dept., University of Toronto, Toronto 5, Ont., Canada (Theoretical Electrochemistry)

H. J. White, National Cash Register Co.; Mail add: 2249 Carriage Dr., Rolling Hills, Calif. (Electrodeposition)

Maurice Yang, Furniture City Plating Co. & Nuclear Age Research & Mfg. Co., 743 Ottawa Ave., N.W., Grand Rapids 2, Mich. (Electronics—Semiconductors and Luminescence)

D. A. Atkinson, Allegheny Electronic Chemicals Co.; Mail add: 252 Bolivar Dr., Bradford, Pa. (Electronics—Semiconductors)

W. M. Lilker, Philco Corp., Lansdale

Tube Div.; Mail add: 4105 Barberry Dr., Lafayette Hill, Pa. (Electrodeposition, Electronics—Semiconductors)

Associate Members

J. J. Abramson, Electric Storage Battery Co.; Mail add: 26400 Parklawn Dr., Euclid 32, Ohio (Battery)

J. E. Collaton, Vapor Heating Corp.; Mail add: 8100 Niles Ave., Skokie, Ill. (Electronics—Semiconductors)

D. W. McDowell, McDonnell Aircraft Corp.; Mail add: 41 Godwin Lane, St. Louis 24, Mo. (Electronics—Semiconductors)

B. H. O'Gara, Shipley Co., Inc., Walnut St., Wellesley 81, Mass. (Electrodeposition)

Michel Prigent, Institut Francais du Pétrole, 4 Ave. de Bois Préau, Rueil-Malmaison (Seine et Oise), France (Battery, Electro-Organic, Theoretical Electrochemistry)

J. P. Sava, Massachusetts Institute of Technology; Mail add: 516 Blue Hill Ave., Dorchester 21, Mass. (Corrosion)

J. F. Shupinski, Philco Corp., Lansdale Tube Div.; Mail add: 712 Montgomery Ave., North Wales, Pa. (Electrodeposition, Electronics, Theoretical Electrochemistry)

Toshiro Yamashina, Dept. of Physics, Brown University; Mail add: 65 Charles Field St., Providence, R. I. (Corrosion)

Reinstatements to Active Membership

T. W. Blickwedel, Sylvania Electric Products Inc.; Mail add: R.D. 2, Sylvan Heights, Emporium, Pa. (Battery)

A. T. Morkel, Max Planck Institut für Physikalische Chemie; Mail add: Friedrich Ebert Str. 7, Göttingen, West Germany (Corrosion)

J. T. Porter, II, General Atomic Co.; Mail add: Box 608, San Diego 12, Calif. (Theoretical Electrochemistry)

Jesse Levine, Marlane Development Co.; Mail add:, 67-54 Burns St., Forest Hills 75, N. Y.

Transfers from Student to Active Membership

George Economy, Finishes Div., Alcoa Research Labs.; Mail add: 614 Clyde St., New Kensington, Pa. (Corrosion)

A. E. Hoover, Dept. of Chemistry, Western Michigan University, Kalamazoo, Mich. (Theoretical Electrochemistry)

M. L. Kronenberg, Union Carbide Consumer Products; Mail add: 20424 Alameda Parkway, Cleveland 28, Ohio (Battery, Electrodeposition, Theoretical Electrochemistry)

M. R. Lorenz, General Electric Co., Research Labs.; Mail add: 2239 Rosendale Rd., Schenectady 9, N. Y. (Electronics—Semiconductors and Luminescence)

Stuart Meibuhr, U. S. Steel, Applied Research Lab., Monroeville, Pa. (Corrosion, Electrodeposition, Electro-Organic, Theoretical Electrochemistry)

Deceased

F. G. McCutcheon, Henryetta, Okla.

L. R. Sheppard, Houston, Texas

Samuel Eidensohn, Riverton, N. Y.

News Items

Back Issues of ECS Journal Available from Walter J. Johnson, Inc.

The Electrochemical Society has concluded an agreement with Walter J. Johnson, Inc., of New York City, giving them reprint rights to out-of-print volumes of the JOURNAL and authorizing them to handle the sale of back volumes and single issues, with the exception of the current calendar year.

Anyone interested in obtaining back copies of volumes or single issues of the JOURNAL should correspond direct with Walter J. Johnson, Inc., 111 Fifth Ave., New York 3, N. Y.

Fifteenth Annual Power Sources Conference

The Fifteenth Annual Power Sources Conference, sponsored by the Power Sources Division, U. S. Army Signal Research and Development Laboratory, Fort Monmouth, N. J., will be held Tuesday, Wednesday, and Thursday, May 9, 10, and 11, at the Shelburne Hotel, Atlantic City, N. J.

Attendance at the conference is by invitation only. Persons who wish to attend can make the necessary arrangements by writing direct to the Power Sources Division, USASRDL.

Tentative Program

Registration—May 8-11
Primary Fuel Cell Batteries—May 9
Regenerative Fuel Cell Batteries—May 9
Secondary Batteries—May 10
Primary Batteries—May 10
Solar Energy Conversion—May 11
Thermal Energy Conversion—May 11
Cocktail Party and Banquet—May 9

First International Congress on Metallic Corrosion

The First International Congress on Metallic Corrosion was held at Imperial College, London, England, from April 10 through 15.

A total of 84 papers was presented on the following topics: Inhibitors, Fundamental Studies, Cathodic and Electrolytic Protection, Metallic Coatings, Practical Experience, Corrosion in Atomic Energy, Boiler Corrosion, Intergranular and Stress Corrosion, Experimental Methods and Laboratory Corrosion Testing, Atmospheric Corrosion, High-Temperature Oxidation, Corrosion Fatigue, Underground Corrosion, Paints.

The program also included four plenary lectures: "Chemical and Electrochemical Behavior of Metals at Passivation Ranges" by Professor Y. M. Kolotyrkin; "Radiotracers as Applied to the Study of Metallic Corrosion" by Professor P. Lacombe; "The Advancing Frontiers of Corrosion Science" by Professor H. H. Uhlig; "Factors Deciding between Active Corrosion and Protective Film Formation" by Dr. U. R. Evans.

Low-Temperature Reaction in Copper-Oxygen System

An interesting phenomenon was observed at the National Bureau of Standards, Washington, D. C., during the recent free radicals research program which it conducted for the Dept. of Defense. In experiments performed by Jerome Kruger and William Ambs of the Bureau's corrosion laboratory, no reaction occurred when oxygen was deposited at a temperature of 4°K on the surface of a copper specimen. But when the oxygen was partially dissociated by passage through a high-frequency microwave discharge before a similar deposition, a thin film formed that remained solid at room temperature. On specimens similarly treated with molecular oxygen, no film was observed.

These results—of particular significance to the Bureau's work on the fundamental mechanisms of corrosion—will be the basis for further research on other metals and gases.

G.E. Scientists Testing Thermionic Conversion Device

General Electric scientists at Pleasanton, Calif., are testing a promising thermionic conversion device for use in nuclear reactors in the next five to ten years. The device, known as a plasma diode, utilizes the heat produced in the center of nuclear reactor fuel elements for the direct generation of electricity without the use of mechanical rotating equipment.

A thermionic converter produces an electrical current by boiling electrons off a cathode, or hot metal

plate, and collecting them on an anode, a cooler plate. The plasma diode under development is a high-temperature thermionic device using cesium gas and a uranium-bearing cathode.

These diodes would be built into nuclear fuel elements, where the fissioning of the uranium in the cathode would provide the high temperatures—in the range of 4500°F—needed for efficient direct conversion. An electrical lead from the fuel element would draw off the electricity.

In addition to the directly produced electricity, lower temperature heat rejected through the walls of the fuel element would also be used to produce electricity by boiling water to make steam for the operation of turbine generator facilities.

Superconducting Wire Promises Ultrahigh Magnetic Fields

Research scientists at Bell Telephone Laboratories, Murray Hill, N. J., have demonstrated the feasibility of superconducting solenoid magnets producing extremely high magnetic fields. They utilized a superconducting compound of niobium and tin (Nb_3Sn), fabricated and reacted by special metallurgical techniques, in their latest experiment.

Although it has been realized for many years that it is possible to produce magnetic fields with superconducting solenoids, the materials that have been tried in the past would only sustain fields of a few thousand gauss. At larger magnetic fields, the superconducting properties disappear. With the new compound, steady-state magnetic fields of 88,000 gauss are possible.

Additionally, a superconducting solenoid does not require expenditure of electric energy once the field is established, whereas a solenoid of ordinary metal will use large amounts of energy. Nb_3Sn becomes superconducting at 18°K, a higher transition temperature than any other superconductor at present known. This compound was first discovered at Bell Labs. in 1954. Until the present, however, its critical field had not been measured. The material being extremely brittle, heretofore it was not possible to use the niobium-tin compound in the construction of a solenoid (coil magnet).

Indications are that the niobium-tin material will sustain fields of 100,000 gauss while carrying electrical currents of 100,000 amps/cm^2 of cross section.

This new breakthrough in the field of cryogenics (low-temperature research and development) resulted from new metallurgical arts, plus experimental and theoretical knowledge of the physics of solids. J. E. Kunzler, E. Buehler, F. S. L. Hsu, and J. H. Wernick of the Laboratories staff discussed these findings in the Feb. 1, 1961 issue of *Physical Review Letters*, a publication of the American Physical Society.

The unusual behavior of Nb_3Sn at high fields raises many questions for physicists about the nature of superconductivity.

This new material development will have important applications wherever large volumes of magnetic fields are required. Important applications in the field of communications are envisioned. Many electronic devices require magnetic fields for their operation. Among these are traveling wave tubes and masers. The availability of large magnetic fields can extend the operation of these devices to higher frequencies providing the possibility of broadband communication systems for use in earth-based radio-relay systems and active satellite repeaters for space communications.

Another attractive application is the containment of thermonuclear fusion plasmas for the production of electric power.

A third important area is in the experimental physics laboratory where the cost of producing high magnetic fields has greatly limited the experimental physicist. This new materials discovery will make high fields available to a wider community of scientists throughout the world.

To illustrate the simplification in magnet design that this new development will make possible, a superconducting electromagnet can be compared to a more conventional magnet using copper as the conductor. Such a conventional magnet at present in operation at Bell Telephone Labs. requires a power supply and cooling equipment which literally fills several rooms. While in operation, it uses thousands of gallons of cooling water per hour and consumes 1.5 megawatts of electric power; this is 25% of the total amount of power consumed at the Murray Hill facility, Bell Labs.' center of research where over 4,500 people are employed. By contrast, a superconducting solenoid magnet of Nb_3Sn, and producing a comparable field, would not consume any electric energy once the flux is established.

Electronics Division Enlarged Abstract Booklet, Spring 1961

The Electronics Division has printed an "Enlarged Abstracts" booklet containing 1000-word abstracts of papers presented before the Electronics Division's symposia during the Indianapolis Spring Meeting of the Society, April 30-May 3, 1961.

The booklet contains about 200 pages and includes approximately 18 papers on Luminescence and 36 papers on Semiconductors.

The price is $3.00 per copy with a discount of $0.50 ($2.50 net) for orders accompanied by payment and requiring no invoicing. *Orders requiring invoicing will be charged full price* even though payment accompanies the order.

Make checks payable to: Electronics Division, The Electrochemical Society.

Mail to:
Austin E. Hardy
c/o Radio Corp. of America
New Holland Pike
Lancaster, Pa.

Mallory to Establish Research Facility in Boston

P. R. Mallory & Co. Inc. has announced plans for expansion of its program of basic and applied research. Dr. Donald G. Wilson, vice-president of research, said that Mallory will establish an additional research facility in the Boston area in the near future. It will supplement the activities of the Mallory Corporate Research and Development Laboratories in Indianapolis.

The new Mallory facility will specialize in thin-film investigations and semiconductor research for application to electronic components and circuits. The Mallory Co., which has 11 operating divisions, is active in the fields of electronics, battery systems, and metallurgy.

Personals

Victor R. Erdelyi has taken a new position as senior design engineer in the Semiconductor Section of Westinghouse Electric Corp.'s Astroelectronics Lab., Newbury Park, Calif. Formerly, he was a member of the technical staff in the Advanced Devices Dept. of Hughes Aircraft Co.'s Semiconductor Div., Newport Beach, Calif.

Harris D. Hineline, of Mt. Vernon, N. Y., recently was made an Emeritus Member of The Electrochemical Society. Dr. Hineline, who was 70 years old on August 17, 1960, has been a member of the Society since April 1920. His interest in electrochemistry has continued over many years. He began his career with the Eastman Kodak Co.'s Research Lab. in 1916, working on a problem in color microscopy. From there, he went to the newly established Westinghouse Research Lab. in July 1918.

Izaak M. Kolthoff, professor and head of the Div. of Analytical Chemistry, University of Minnesota, Minneapolis, has been selected as the recipient of the 1961 Anachem Award of the Association of Analytical Chemists, Detroit. The award is made in recognition of outstanding service to the field of analytical chemistry. The presentation will take place at the Ninth Anachem Conference to be held in October 1961.

Sheldon L. Matlow has been appointed director of research and development of Intellux, Inc., Santa Barbara, Calif. Dr. Matlow is known for his work in quantum mechanics as well as for his work in the theory and practice of semiconductor device fabrication technology. He also has conducted investigations in the field of medicine. Previous to joining Intellux, Dr. Matlow was technical coordinator for the Semiconductor Div. of Hoffman Electronics.

Roy G. Post has joined the staff of the Dept. of Nuclear Engineering, University of Arizona, Tucson, Ariz. Professor Post formerly was affiliated with Texas Instruments, Inc., in Dallas.

Richard S. Robinson has been named a vice-president of Arthur D. Little, Inc., Cambridge, Mass. Mr. Robinson, who is an associate director of the ADL Research and Development Div., joined the company in 1948. Since then, he has organized and administered groups functioning in both the laboratory and management research areas of the company, working chiefly in the fields of experimental research and development, chemical sciences, corporate diversification studies, and area development programs.

Hans M. Wagner has terminated his affiliation with Shockley Transistor Corp., Palo Alto, Calif. He is now working as a research specialist in Lockheed Aircraft Corp.'s Missile and Space Div., Sunnyvale, Calif.

Sanford F. Essig

Sanford F. Essig, well-known electronic scientist of International Telephone and Telegraph Corp., Fort Wayne, Ind., died in an automobile accident on March 5. He was 64 years old.

Mr. Essig, who was an authority on image electron tubes, was manager of the photo devices development laboratory at ITT Federal Laboratories in Fort Wayne. He was the author of several papers and held several patents in the image tube field.

He graduated from Ashland College in 1928 and received an M.S. degree in physics from Ohio State University in 1929.

In addition to The Electrochemical Society, which he joined in 1945, he was a member of the Joint Electronic Devices Engineering Council and the Optical Society of America.

Announcements from Publishers

"Thin Metal Films as Corrosion Indicators," R. B. Belser and F. E. Hankinson, Engineering Experiment Station, Georgia Institute of Technology, for Wright Air Development Center, U. S. Air Force, May 1959. Report PB 151,974,* 56 pages; $1.50.

"Thin Metal Films as Corrosion Indicators," R. B. Belser and N. Engel, Engineering Experiment Station, Georgia Institute of Technology, for Wright Air Development Center, U. S. Air Force, March 1960. Report PB 161,757,* 74 pages; $2.00.

"Electrical Properties of Organic Solids: 1—Kinetics and Mechanism of Photoconductivity of Metal-Free Phthalocyanine; 2—Effects of Added Electron Acceptors and Donors," March 1960. AEC Report UCRL-9120,* 121 pages: $2.50.

"A Study of the Mechanism of Some Reactions by the Method of Hydrogen Exchange," D. N. Kursanov, V. N. Setkina, and others, *Problemy Kinetiki i Kataliza (USSR),* June 1960. Translation 60-11713,* 4 pages; 50 cents.

"Desalination of Water," OTS Selective Bibliography, July 1960. Translation OTS-SB-419,* 10 cents.

"Magnetostriction," Selective Bibliography SB-427*; 10 cents.

"Thermoelectricity," Selective Bibliography SB-432*; 10 cents.

"Semiconductors," Selective Bibliography SB-435*; 10 cents.

"A Thermogravimetric Balance for the Investigation of High-Temperature Reaction Kinetics and the Results of a Beryllium Oxidation Study," Nov. 1960. AEC Report NAA-SR-4737,* 25 pages; 50 cents.

"Fuel Cell Systems," Rome Air Development Center, U. S. Air Force, July 1960. Report PB 161972,* 17 pages; 50 cents.

"Diffuse Coatings on Iron and Steel," by N. S. Gorbunov, Academy of Sciences of the U.S.S.R., Moscow, 1958 (English translation). Volume No. 60-21148,* 170 pages; $1.75.

"Recombination of the Hydrogen Atom in an Adsorbed Layer," O. I. Leypunskiy, Oct. 1960. Translation from *Zhurnal Fizicheskoy Khimii,* Vol. VIII, No. 3 (1936). Translation 60-41586,* 28 pages; 75 cents.

"Liquid Diffusion Electrodes (On the Initial Slope of the Polarization Curves)," I. A. Zaydenman and R. M. Perskaya. Translation of an article from *Zhurnal Fizicheskoy Khimii,* Vol. 23, No. 1 (1959), U.S.S.R. Translation 60-21777,* 9 pages; 50 cents.

"Conversion of Methane to Acetylene in a High Voltage Arc—The Effect of Pressure," E. N. Eremin and others, July 1960. Translation of an article from *Zhurnal Fizicheskoy Khimii,* Vol. 32, No. 10 (1958), U.S.S.R. Translation 60-21928,* 12 pages; 50 cents.

"Metallurgical Industry in Communist China," Nov. 1960. Translation 60-41438,* 58 pages; $1.50.

"Soviet Nonferrous Metallurgy, No. 12, Selected Translations," Aug. 1960. Translation 60-41166,* 32 pages; $1.00.

"Soviet Nonferrous Metallurgy, No. 17, Selected Translations," Oct. 1960. Translation 60-41680,* 21 pages; 75 cents.

* Order from Office of Technical Services, U.S. Dept. of Commerce, Washington 25, D. C.

* Order from Office of Technical Services, U.S. Dept. of Commerce, Washington 25, D. C.

Meetings of Other Organizations

May 11-12—American Institute of Chemists, Annual Meeting, Statler Hotel, Washington, D. C.

June 22-24—American Physical Society Meeting, University of Mexico, Mexico City, Mexico.

June 25-30—American Society for Testing Materials, Annual Meeting, Chalfonte-Haddon Hall, Atlantic City, N. J.

Literature from Industry

Radioisotope Handbook, and Catalog "D." Copies are available of the Atomic Energy of Canada Ltd. Radioisotopes Handbook RP-3. There is no charge for quantities up to ten; larger quantities are available at cost price, 30 cents (whether or not a charge is levied for larger quantities depends on the ultimate use by the requisitioner). Also available, at no charge, is A.E.C.L.'s new general products Catalog "D."

Interested persons should write on company letterhead to Commercial Products Div., Atomic Energy of Canada Ltd., P. O. Box 93, Ottawa, Ont., Canada.

Electrophoresis and Chromatography. LKB Instruments, Inc., is offering a new technical bulletin describing its automatic system of semiquantitative analysis for electrophoresis and chromatography. Processes included in the system include: controlled micropumping of solvent, large-scale separation by paper partition chromatography or electrophoresis, effluent measurement and recording of u.v. absorption at 254 μ (or measurement and recording of conductivity of effluent), and controlled fractionation of liquid into test tubes.

Write for Bulletin W1-6510 to LKB Instruments, Inc., 4840 Rugby Ave., Washington 14, D. C.

Optical Maser Booklet. A booklet describing the theory and design of the recently announced solid state optical maser is available. The eight-page booklet, bearing a full-color cover picture of an operating maser emitting a pulse of coherent light, is a reprint of an article by A. L. Schawlow, of the Bell Telephone Laboratories research department, which appeared originally in the *Bell Laboratories Record.*

Copies of the booklet can be obtained by writing to H. W. Mattson, Bell Telephone Labs., Inc., Murray Hill, N. J.

Nickel Sulfamate Plating Bulletin describes Hanson-Van Winkle-Munning Co.'s Nickel Sulfamate process, a bath for heavy build-up for metal resizing, electroplating, electroforming, and other functional uses. Four important features of the process are: mechanical properties of deposits are controllable; the liquid concentrate solution is chloride free; solution is premixed, no dry chemicals to dissolve, except nickel chloride, when desired; solution is easy to control.

The bulletin is available from Hanson-Van Winkle-Munning Co., Church St., Matawan, N. J.

Nickel-Alloy-Bonded Steel Pipe and Tubing. Recently published brochure describes how NIPHOS nickel-alloy-bonded steel pipe and tubing are being used increasingly to counter corrosion and iron contamination.

The brochure is available from the "Nickel-Over-Steel" Div., M. L. Sheldon & Co., Inc. 350 Lexington Ave., New York 16, N. Y.

Automatic Determination of Chromates. New data sheet details the complete chemical methodology for the rapid determination of chromates down to parts per million using the Technicon® AutoAnalyzer®, an electronic analytical instrumentation system which requires no supervision. A flow diagram of the analytical system is included, together with the actual chart recordings derived.

Copies can be obtained by writing to Technicon Controls, Inc., Chauncey, N. Y.

Black Glass for Diodes. Information on a special black glass for encapsulating diodes is given in an eight-page brochure. The black glass, which is available as beads and cases, is said to protect diodes that are sensitive to visible and infrared wave lengths. Transmittance and other properties are detailed in a chart and a table.

The brochure is available on request on company letterhead from Receiver Bulb Sales Dept., Corning Glass Works, Corning, N. Y.

Advertiser's Index

Employment Situations

Positions Available

Consulting Physicist with thorough knowledge of single crystals, float zoning, semiconductor materials, wanted by established Western European company. Annual retainer, daily or project compensation. Work by mail. Indicate background in confidence to *Box A-287, c/o The Electrochemical Society, 1860 Broadway, New York 23, N. Y.*

Chemists and Chemical Engineers —We need physical, organic and inorganic chemists, and chemical engineers to carry out Engineering and development work in the rapidly growing power sources field. Research & Development center located in Minneapolis near University of Minnesota. Battery experience preferred but not required. Send resumés to: J. W. Baxter, Employee & Labor Relations, Gould-National Batteries, Inc., E. 1326 First National Bank Bldg., St. Paul 1, Minn.

Four challenging research positions for experienced surface chemists, in fully-equipped laboratory devoted to research and development on aluminum and copper alloys, involving: A. Electrochemical kinetics, adsorption, and oxide film structure investigations related to finishing processes. B. Studies of interfacial surface reactions between polymeric resins and metal oxide surfaces relating to strength and permanence of joints in the adhesive bonding of metals. C. Mechanisms relating to surface phenomena, associated with liquid metal-solid metal inter-action as applied to soldering and brazing. D. Surface and electrochemical reactions effecting the kinetics of general, localized, and stress corrosion processes. Pleasant living, with access to major university. Send reply to R. H. Endriss, Personnel Manager, Olin Mathieson Chemical Corp., 125 Munson St., New Haven, Conn.

The Electrochemical Society

Patron Members

Aluminum Co. of Canada, Ltd.,
Montreal, Que., Canada
International Nickel Co., Inc.,
New York, N. Y.
Olin Mathieson Chemical Corp.,
Chemicals Div., Industrial Chemicals
Development Dept., Niagara Falls, N. Y.
Union Carbide Corp.
Divisions:
Union Carbide Metals Co.,
New York, N. Y.
National Carbon Co., New York, N. Y.
Westinghouse Electric Corp., Pittsburgh, Pa.

Sustaining Members

Air Reduction Co., Inc.,
New York, N. Y.
Ajax Electro Metallurgical Corp.,
Philadelphia, Pa.
Allen-Bradley Co., Milwaukee, Wis.
Allied Chemical Corp.
Solvay Process Div., Syracuse, N. Y.
General Chemical Div., Morristown, N. J.
Alloy Steel Products Co., Inc., Linden, N. J.
Aluminum Co. of America,
New Kensington, Pa.
American Metal Climax, Inc.,
New York, N. Y.
American Potash & Chemical Corp.,
Los Angeles, Calif. (2 memberships)
American Smelting and Refining Co.,
South Plainfield, N. J.
American Zinc Co. of Illinois,
East St. Louis, Ill.
American Zinc, Lead & Smelting Co.,
St. Louis, Mo.
American Zinc Oxide Co., Columbus, Ohio
M. Ames Chemical Works, Inc.,
Glens Falls, N. Y.
Armco Steel Corp., Middletown, Ohio
Basic Inc., Maple Grove, Ohio
Bell Telephone Laboratories, Inc.,
New York, N. Y. (2 memberships)
Bethlehem Steel Co., Bethlehem, Pa.
(2 memberships)
Boeing Airplane Co., Seattle, Wash.
Burgess Battery Co., Freeport, Ill.
(4 memberships)
Canadian Industries Ltd., Montreal, Que.,
Canada
Carborundum Co., Niagara Falls, N. Y.
Catalyst Research Corp., Baltimore, Md.
Columbian Carbon Co., New York, N. Y.
Columbia-Southern Chemical Corp.,
Pittsburgh, Pa.
Consolidated Mining & Smelting Co. of
Canada, Ltd., Trail, B. C., Canada
Continental Can Co., Inc., Chicago, Ill.
Cooper Metallurgical Associates, Cleveland,
Ohio
Corning Glass Works, Corning, N. Y.
Diamond Alkali Co., Painesville, Ohio
Dow Chemical Co., Midland, Mich.
Wilbur B. Driver Co., Newark, N. J.
(2 memberships)
E. I. du Pont de Nemours & Co., Inc.,
Wilmington, Del.
Eagle-Picher Co., Chemical Div., Joplin, Mo.
Eastman Kodak Co., Rochester, N. Y.
Thomas A. Edison Research Laboratory, Div.
of McGraw-Edison Co., West Orange, N. J.
Electric Auto-Lite Co., Toledo, Ohio
C & D Division, Conshohocken, Pa.
Electric Storage Battery Co., Yardley, Pa.
Englehard Industries, Inc., Newark, N. J.
(2 memberships)
The Eppley Laboratory, Inc., Newport, R. I.
(2 memberships)
Exmet Corp., Tuckahoe, N. Y.
Fairchild Semiconductor Corp., Palo Alto,
Calif.
Food Machinery & Chemical Corp.
Becco Chemical Div., Buffalo, N. Y.
Westvaco Chlor-Alkali Div., South
Charleston, W. Va.
Foote Mineral Co., Paoli, Pa.
Ford Motor Co., Dearborn, Mich.
General Electric Co., Schenectady, N. Y.
Chemistry & Chemical Engineering
Component, General Engineering
Laboratory
Chemistry Research Dept.
General Physics Research Dept.
Metallurgy & Ceramics Research Dept.
Aircraft Accessory Turbine Dept.,
West Lynn, Mass.
General Instrument Corp., Newark, N. J.

(Sustaining Members cont'd)

General Motors Corp.
Delco-Remy Div., Anderson, Ind.
Guide Lamp Div., Anderson, Ind.
Research Laboratories Div., Detroit, Mich.
General Telephone & Electronics Laboratories Inc., Bayside, N. Y. (2 memberships)
General Transistor Corp., Jamaica, N. Y.
Gillette Safety Razor Co., Boston, Mass.
Globe-Union, Inc., Milwaukee, Wis.
Gould-National Batteries, Inc., Minneapolis, Minn.
Grace Electronic Chemicals, Inc., Baltimore, Md.
Great Lakes Carbon Corp., New York, N. Y.
Hanson-Van Winkle-Munning Co., Matawan, N. J. (2 memberships)
Harshaw Chemical Co., Cleveland, Ohio (2 memberships)
Hercules Powder Co., Wilmington, Del.
Hill Cross Co., Inc., West New York, N. J.
Hoffman Electronics Corp., Semiconductor Div., El Monte, Calif.
Hooker Chemical Corp., Niagara Falls, N. Y. (3 memberships)
Hughes Aircraft Co., Culver City, Calif.
International Business Machines Corp., Poughkeepsie, N. Y.
International Minerals & Chemical Corp., Skokie, Ill.
ITT Federal Laboratories, Div. of International Telephone & Telegraph Corp., Nutley, N. J.
Jones & Laughlin Steel Corp., Pittsburgh, Pa.
K. W. Battery Co., Skokie, Ill.
Kaiser Aluminum & Chemical Corp.
Div. of Chemical Research, Permanente, Calif.
Div. of Metallurgical Research, Spokane, Wash.
Kawecki Chemical Co., Boyertown, Pa.
Kennecott Copper Corp., New York, N. Y.
Keokuk Electro-Metals Co., Keokuk, Iowa
Libbey-Owens-Ford Glass Co., Toledo, Ohio
Mallinckrodt Chemical Works, St. Louis, Mo.
P. R. Mallory & Co., Indianapolis, Ind.
Merck & Co., Inc., Rahway, N. J.
Metal & Thermit Corp., Detroit, Mich.
Minnesota Mining & Manufacturing Co., St. Paul, Minn.
Monsanto Chemical Co., St. Louis, Mo.
Motorola, Inc., Chicago, Ill.
National Cash Register Co., Dayton, Ohio
National Lead Co., New York, N. Y.
National Research Corp., Cambridge, Mass.
National Steel Corp., Weirton, W. Va.
New York Air Brake Co., Kinney Vacuum Div., Boston, Mass.
Northern Electric Co., Montreal, Que., Canada
Norton Co., Worcester, Mass.
Ovitron Corp., Long Island City, N. Y.
Peerless Roll Leaf Co., Inc., Union City, N. J.
Pennsalt Chemicals Corp., Philadelphia, Pa.
Phelps Dodge Refining Corp., Maspeth, N. Y.
Philco Corp., Philadelphia, Pa.
Philips Laboratories, Inc., Irvington-on-Hudson, N. Y.
Potash Co. of America, Carlsbad, N. Mex.
Radio Corp. of America
Tube Div., Harrison, N. J.
RCA Victor Record Div., Indianapolis, Ind.
Ray-O-Vac Co., Madison, Wis.
Raytheon Manufacturing Co., Waltham, Mass.
Reynolds Metals Co., Richmond, Va.
Rheem Semiconductor Corp., Mountain View, Calif.
Schering Corporation, Bloomfield, N. J.
Shawinigan Chemicals Ltd., Montreal, Que., Canada
Speer Carbon Co.
International Graphite & Electrode Div., St. Marys, Pa.
Sprague Electric Co., North Adams, Mass.
Stackpole Carbon Co., St. Marys, Pa.
Stauffer Chemical Co., New York, N. Y.
Sumner Chemical Co., Div. of Miles Laboratories, Inc., Elkhart, Ind.
Tennessee Products & Chemical Corp., Nashville, Tenn.
Texas Instruments, Inc., Dallas, Texas
Metals and Controls Corp., Attleboro, Mass.
Three Point Four Corp., Yonkers, N. Y.
Titanium Metals Corp. of America, Henderson, Nev.
Tung-Sol Electric Inc., Newark, N. J.
Udylite Corp., Detroit, Mich. (4 memberships)
Universal-Cyclops Steel Corp., Bridgeville, Pa.
Upjohn Co., Kalamazoo, Mich.
Victor Chemical Works, Chicago, Ill.
Western Electric Co., Inc., Chicago, Ill.
Wyandotte Chemicals Corp., Wyandotte, Mich.
Yardney Electric Corp., New York, N. Y.